

Deposit & Copying of Thesis Declaration



UNIVERSITY OF
CAMBRIDGE

Please note that you will also need to bind a copy of this Declaration into your final, hardbound copy of thesis - this has to be the very first page of the hardbound thesis.

1	Surname (Family Name)	Forenames(s)	Title
	Ong	Lay Ping	Dr.
2	Title of Thesis as approved by the Degree Committee		
	Cell therapy for chronic heart failure: a key role for epicardial fibronectin		

In accordance with the University Regulations in *Statutes and Ordinances* for the PhD, MSc and MLitt Degrees, I agree to deposit one print copy of my thesis entitled above with the Secretary of the Postgraduate Committee who shall deposit the thesis in the University Library under the following terms and conditions:

1. THESIS AUTHOR DECLARATION

I am the author of this thesis and hereby give the University the right to make my thesis available in print form as described in 2. below.

My thesis is my original work and a product of my own research endeavours and includes nothing which is the outcome of work done in collaboration with others except as declared in the Preface and specified in the text. I hereby assert my moral right to be identified as the author of the thesis.

The deposit and dissemination of my thesis by the University does not constitute a breach of any other agreement, publishing or otherwise, including any confidentiality or publication restriction provisions in sponsorship or collaboration agreements governing my research or work at the University or elsewhere.

2. ACCESS TO DISSERTATION

I understand that one print copy of my thesis will be deposited in the University Library for archival and preservation purposes, and that, unless upon my application restricted access to my thesis for a specified period of time has been granted by the Postgraduate Committee prior to this deposit, the thesis will be made available by the University Library for consultation by readers in accordance with University Library Regulations and copies of my thesis may be provided to readers in accordance with applicable legislation.

3	Signature	Date
		29.01.2022

CORRESPONDING REGULATION

Before being admitted to a degree, a student shall deposit with the Secretary of the Postgraduate Committee one copy of his or her hard-bound thesis, in a form approved by the Committee. The Secretary shall deposit the copy of the thesis in the University Library where, subject to restricted access to the thesis for a specified period of time having been granted by the Postgraduate Committee, it shall be made available for consultation by readers in accordance with University Library Regulations and copies of the thesis provided to readers in accordance with applicable legislation.

University of Cambridge, Student Registry, New Museum Site, Cambridge CB2 3pT ·

email: student.registry@admin.cam.ac.uk · <https://www.cambridgestudents.cam.ac.uk/your-course/examinations/graduate-exam-information/after-examination/degree-approval-and-1>

Cellular therapy for chronic heart failure:

a key role for epicardial fibronectin



Lay Ping Ong

Sidney Sussex College

Department of Medicine/Wellcome-MRC Stem Cell Institute

Jeffrey Cheah Biomedical Centre/Addenbrooke's Hospital,

University of Cambridge

This degree is submitted for the degree of Doctor of Philosophy

on 20th February 2021

Declarations

This dissertation is the result of my own work and includes nothing which is the outcome of work done in collaboration except where specifically indicated in the text. It has not been previously submitted, in part or whole, to any university or institution for any degree, diploma, or other qualification.

In accordance with the Department of Clinical Medicine guidelines, this thesis does not exceed 60,000 words

Signed.....

Date.....

Lay Ping Ong (BA, MB BChir, MA, MRCS)

Cellular therapy for chronic heart failure: a key role for epicardial fibronectin by Lay Ping Ong

Abstract

Myocardial infarction (MI) results in permanent cardiomyocyte loss, frequently leading to heart failure, with a 50% 5-year mortality. At subacute time points following MI, animal studies have shown ‘remuscularization’ of the damaged heart with human embryonic stem cell (hESC)-derived cardiomyocytes. Recently, outcomes were improved by co-delivering hESC-derived epicardium. Clinically, the main challenge remains chronic heart failure. However, hESC-cardiomyocytes alone, in the chronically infarcted heart, have shown no benefit.

Here, we show that both species-matched cellular therapy and combination therapy with hESC-epicardium could attenuate cardiac dysfunction in the chronically failing heart, underpinned by sizeable cardiac grafts, cardiomyocyte proliferation and maturation, together with a host-derived vascular supply. Notably, hESC-epicardium’s augmentation of cardiomyocyte maturation within 3D-engineered heart tissues *in vitro* appeared to be underpinned by epicardial-secreted fibronectin. Thus, hESC-combination cell therapy holds clinical promise for ‘remuscularising’ chronically infarcted hearts.

Dedicated to my Papa

List of Publications

Part of the work presented in this dissertation has either been submitted or published in the following:

Ong LP, Bargehr J, Knight-Schrijver V, Colzani M, Bayraktar S, Lee J, Bernard W, Marciano S, Bertero A, Gambardella L, Sinha S. *Epicardially-secreted Fibronectin mediates epicardial-cardiomyocyte crosstalk to drive hESC-cardiomyocytes' maturation in 3D-EHTs*. Manuscript under preparation.

Ong LP, Colzani M, Gambardella L, Bertero A, Mitzelfelt K, Martinson A, Figg N, Pabon L, Reinecke H, Murry CE, Sinha S. *Regeneration of the chronically infarcted rat hearts using species-matched or human pluripotent stem cell-derived cell therapy*. Manuscript under preparation.

Bargehr J, Ong LP, Colzani M, Davaapil H, Hofsteen P, Bhandari S, Gambardella L, Le Novère N, Iyer D, Sampaziotis F, Weinberger F, Bertero A, Leonard A, Bernard WG, Martinson A, Figg N, Regnier M, Bennett MR, Murry CE, Sinha S. *Epicardial cells derived from human embryonic stem cells augment cardiomyocyte-driven heart regeneration*. *Nature Biotechnology*. 2019 Aug;37(8):895-906.

Invited Oral Presentations

Ong LP (March 2020) Cellular therapy for the chronically failing heart? *Keystone Heart Failure Conference 2020, Keystone, Colorado, USA.*

Ong LP (February 2020) Mending broken hearts? *University of Cambridge Medical Grand Rounds, Cambridge, UK.*

Ong LP (February 2020) Could cellular therapy rescue the failing heart? *Finalist, Cambridge Society for Application of Research, University of Cambridge, UK*

Ong LP (October 2019) Could cellular therapy rescue the chronically infarcted myocardium? *Wellcome-MRC Stem Cell Institute PhD Day, Cambridge UK.*

Ong LP (September 2019) Cellular therapy for heart failure. *British Society of Cardiovascular Research, Cambridge, UK.*

Ong LP (April 2019) Does cell therapy rescue the chronically infarcted myocardium? *Wellcome-MRC Stem Cell Institute Annual Retreat, Cambridge UK.*

Awards

Work arising from this dissertation has resulted in the following awards:

March 2020. Keystone Travel Award to support travel to Keystone, Colorado, US to deliver an oral presentation.

January 2020. Addenbrooke's Charitable Trust Research Grant to support a short-term extension of animal work in Cambridge, UK.

Acknowledgements

'It is not the most intellectual nor the strongest species that survives,

*but the one most able to **adapt**'- Charles Darwin*

Writing this doctoral thesis at the middle of COVID19 global pandemic has rung the above quote truer than ever. In a way, my entire scientific journey has been one of adaptation and dreams of 'What If's?' in the Tomorrowland - to have the grandest of opportunities to work on cardiac regeneration, which heralds the future.

For this, I am deeply grateful to my PhD supervisor, Dr. Sanjay Sinha, for encouraging a wide-ranging scientific inquisition and the daring imagination to finesse a therapy that is completely novel and with potentially great impact; whilst, at the same time, providing safe space to fail and try again. This was one great piece of luck for a student!

Within the Sinha Lab, I am thankful to Dr. Laure Gambardella, a senior post-doc in the lab, who taught me to observe the beautiful behaviour of the cells that we work with, whilst inspiring me with her high energy, spirit and love of science. Dr. Maria Colzani, a dear friend and confidant and also my bench supervisor, who is always patient. Dr. Johannes Bargehr, who started this work and whose name is scattered throughout this thesis, highlighting his impactful work. Semih Bayraktar and Dr. Jonathan Lee have been great sources of inspiration and enthusiasm throughout, especially reminding me during difficult times of the beauty of science. I worked closely with Alex Petchey in developing the animal model in Cambridge, and I remain deeply grateful for his steadfastness. Aishwarya, Hongorzul and Deeti, there has been insightful conversations within the lab, especially during the long TC hours. Thanks to Dr. Peter Holt and Deborah Passey for being whizzes at administrative and lab-related matters. Having moved scientific buildings once with the Sinha lab, it was a life-long bonding experience.

I was also generously 'adopted' by another lab family, the Murry lab, during our collaboration. I am deeply thankful for the insights and scientific clarity given by Professor Chuck Murry, who is a world leader in cardiac regeneration. Dr. Alessandro Bertero and Dr. Silvia Marciano, two Italian post-docs, who taught me molecular biology and continuously impressed me with their brainpower. Dr. Lil Pabon, who inspired with her love for scientific education. Dr. Hans Reinecke who taught me neonatal rat harvest, Dr. Andrea Leonard & Shiv Bandari who taught me how to make engineered heart tissues, and Amy Martinson who taught me how to perform rat myocardial infarcts; I am eternally grateful to them.

Within the cardiothoracic surgical community, I am deeply thankful to Mr. Stephen Large, a long-time mentor who prodded me away from the ‘present’ transplant and into ‘future’ cardiac regeneration for my doctoral pursuits. I also thank Aravinda Page, Jason Ali and Yan Li for sourcing difficult-to-get surgical instruments, external pacemakers and clinical items for the animal model set-up. I am deeply grateful for their support and enthusiasm for my work.

With the local animal studies, I am deeply grateful for the support and help given by the Cambridge Phenomics facility (Kate Tansley, Martin Rice, Emma Friel-Blanchard, Michiel Plugge, Olga Saunchaka), despite the animal building move. Furthermore, I am thankful for the consultations and time granted by the animal technicians in Imperial College, London (Matt Davenport, Catherine).

Throughout the PhD, I am deeply grateful to my many friends who remained supportive of my need to attend to ‘cells’ and rats, instead of birthdays, first-born births and weddings. They have been scattered around the world but namely Devin Rebello, Manpreet & Ashley, Rachel, Molly, Beth & Ahmad, and Sahitya, who provided me with a ‘home’ in Seattle. Ms.Ashvina Segaran and Dr.Vicky Snowdon, who provided me with a physical home in Cambridge.

Most importantly, I am deeply thankful to my parents, who would bravely endure the PhD with me, despite their respective illnesses during this period. In particular, I dedicate this work to my dear Papa (Mr.Ong Eng Hin) who passed away recently due to a heart attack. As well as being my biggest cheerleader, Thank you for teaching me to be fearless, to always dream and to discover.

Coming into this PhD from a surgical background, where we replace parts of the heart with off-the-shelf products daily or replace the entire heart from another dead human being, it is extremely exciting, yet humbling, to envision a future whereby we can biologically grow these replacement parts in the laboratory such that they are tailored to the individual patient and organically evolve with them, over their lifetimes. Perhaps, one day, we no longer harvest vessels from the individual patient or wait for someone’s else misfortune/death to mine for body parts, like graverobbers in the night.

Regenerative medicine offers us all this hope.

Abstract

Myocardial infarction (MI) results in permanent cardiomyocyte loss, frequently leading to heart failure, with a 50% 5-year mortality. At subacute time points following MI, animal studies have shown ‘remuscularization’ of the damaged heart with human embryonic stem cell (hESC)-derived cardiomyocytes. Recently, outcomes were improved by co-delivering hESC-derived epicardium. Clinically, the main challenge remains chronic heart failure. However, hESC-cardiomyocytes alone, in the chronically infarcted heart, have shown no benefit.

Here, we show that both species-matched cellular therapy and combination therapy with hESC-epicardium could attenuate cardiac dysfunction in the chronically failing heart, underpinned by sizeable cardiac grafts, cardiomyocyte proliferation and maturation, together with a host-derived vascular supply. Notably, hESC-epicardium’s augmentation of cardiomyocyte maturation within 3D-engineered heart tissues *in vitro* appeared to be underpinned by epicardial-secreted fibronectin. Thus, hESC-combination cell therapy holds clinical promise for ‘remuscularising’ chronically infarcted hearts.

Table of Contents

1.INTRODUCTION	25
1:1 SCALE OF CLINICAL NEED.....	25
1.2 CURRENT CLINICAL TREATMENTS FOR HEART FAILURE.....	27
1:2:1 Medical Treatment	28
1:2:2 Invasive Cardiac Interventions.....	29
1:2:3 Heart Transplant.....	31
1:2:4 LVAD (Left ventricular assist device).....	32
1:3 CARDIAC REGENERATION AS HEART FAILURE TREATMENT	34
1:3:1 Regeneration in adult zebrafish heart.....	35
1:3:2 Regeneration in the neonatal mammalian heart	38
1:4 INSIGHTS FROM CARDIAC EMBRYOGENESIS TO GUIDE CARDIAC REGENERATIVE THERAPIES.....	41
1:4:1 From epiblast to cardiomyogenic commitment.....	42
1:4:2 The epicardium in cardiac development	45
1:4:2:1 Developmental origins of epicardium- proepicardium.....	46
1:4:2:2 Epicardium undergoes epithelial-mesenchymal-transition	47
1:4:2:3 Epicardial cellular contributions to the developing heart.....	49
1:5 EPICARDIUM REACTIVATES IN RESPONSE TO CARDIAC INJURY.....	50
1:5:1 The epicardium in zebrafish cardiac regeneration	51
1:5:2 The epicardium in neonatal mouse cardiac regeneration	54
1:6 ENDOGENOUS CARDIAC REGENERATION	55
1:6:1 Cardiomyocyte formation in the adult human heart.....	56
1:6:2 Gene therapy – proliferation by pre-existing cardiomyocytes	57
1:6:3 Gene therapy - direct reprogramming of cardiac fibroblasts into cardiomyocytes	57
1:7 EXOGENOUS CARDIAC REGENERATION.....	59
1:7:1 Skeletal myoblasts.....	61
1:7:2 Adult stem cells - bone marrow mononuclear cells	62
1:7:3 Cardiac Stem Cells - c-Kit+ cells.....	64
1:7:4 hESC/IPSC – derived cardiomyocytes.....	66
1:8 CARDIOMYOCYTE-BASED CELLULAR THERAPY FOR CHRONIC HEART FAILURE	68

1:8:1 Cellular therapy with hESC/IPSC-derived cardiomyocytes alone.....	70
1:8:2 Challenges with hESC/IPSC-derived cardiomyocytes alone.....	72
1:8:2:1 Cardiomyocyte survival.....	72
1:8:2:2 Cardiomyocyte proliferation.....	73
1:8:2:3 Cardiomyocyte maturation.....	74
1:8:2:4 Cardiomyocyte’s electrical integration with the host myocardium.....	77
1:8:2:5 Cardiomyocyte-associated Immunogenicity.....	78
1:8:2:6 Cardiac graft vascularization.....	79
1:9 SPECIES-MATCHED CELLULAR THERAPY FOR CHRONIC HEART FAILURE (FOETAL/NEONATAL RAT CARDIOMYOCYTES AND A RAT MODEL)	81
1:10 COMBINATION CELLULAR THERAPY	84
1:10:1 hESC-epicardium as an adjunct for hESC/IPSC-cardiomyocytes-based cellular therapy	84
1:10:2 Tissue-engineering adjuncts to hESC/IPSC-cardiomyocytes-based cellular therapy	86
1:11 MECHANISMS UNDERLYING CELLULAR THERAPY: CONTRACTILE, PARACRINE OR BOTH?.....	89
1:12 MECHANISMS UNDERPINNING EPICARDIAL-MYOCARDIAL CROSSTALK.....	90
1:12:1 Epicardially-secreted fibronectin (epicardial-FN) as a putative key mediator of epicardial-myocardial crosstalk.....	93
1:12:2 FN form and function.....	95
1:12:3 FN-integrin signalling.....	97
1:12:4 Role of FN in development.....	98
1:12:5 Role of FN in cardiac disease.....	99
1:13 PROJECT RATIONALE.....	101
1:14 PHD AIMS	102
 2. METHODS	 103
2:1 CELL DIFFERENTIATIONS AND PREPARATIONS.....	103
2:1:1 hESC-derived epicardium	103
2:1:2 RUES2-derived epicardium	105
2:1:2 hESC-derived cardiomyocytes.....	105
THERMO FISHER CATALOGUE NUMBER: 11875101.....	106
THERMO FISHER CATALOGUE NUMBER: A1895601.....	106

2:1:3 Neonatal rat cardiomyocytes	106
2:1:4 Cellular preparation for intramyocardial injections	107
2:2 ANIMAL MODELS OF MYOCARDIAL INFARCTION (MI) AND CELL TRANSPLANTATION	108
2:2:1 Chronic MI rat model	108
2:2:2 Echocardiography, exclusion criteria, blinded assessor	111
2:2:3: Subacute MI rodent models.....	111
2:2:4 Cambridge rat cardiac regenerative model.....	112
2:3 IMMUNOCYTOCHEMISTRY AND IMMUNOHISTOCHEMISTRY	113
2:3:1 Immunostaining of paraffin-embedded heart sections	113
2:3:2 RNAscope in situ hybridisation	116
2:3:3 Infarct size, graft size quantification	117
2:3:4 Quantification of proliferation & vascularization	117
2:4 THREE-DIMENSIONAL ENGINEERED HEART TISSUES (3D-EHTs)	119
2:4:1 Generation of 3D-EHTs	119
2:4:2 Frank-Starling force measurements of 3D-EHTS	120
2:4:3 Non-ratiometric assessment of 3D-EHT calcium-handling	121
2:4:4 Histological processing of 3D-EHTs	121
2:4:4 RNA extraction from 3D-EHTs for gene expression analyses	122
2:4:5 Quantitative real-time reverse transcription PCR (RT-qPCR).....	122
2:5 SMALL PEPTIDE INHIBITOR (pUR4) OF FIBRONECTIN.....	124
2:5:1 pUR4 generation and cellular treatment.....	124
2:5:2 Western blot of pUR4-treated hESC-epicardium.....	124
2:6 GENERATION OF CRISPR-CAS9-MEDIATED KNOCKOUT FIBRONECTIN (KOFN) hESC CELL LINE	125
2:6:1 Crispr-Cas9-mediated knockout: annealing and cloning FN1- targeted sgRNA	125
2:6:2 Sequencing of transformed cells	127
2:6:3 Gene-targeting by GeneJuice-mediated transfection	127
2:6:4 Genotyping of targeted clones.....	128
2:6:5 CRISPR-Cas9-mediated knockout FN hESC cell line.....	129
2:7 GENERATION OF INDUCIBLE FIBRONECTIN KNOCKDOWN (SOPTiKD-FN) hESC CELL LINE.....	129
2:7:1 Inducible knockdown: design and annealing shRNA oligonucleotides.....	129
2:7:2 Colony PCR of transformants	132
2:7:3 Gene-targeting by GeneJuice-mediated transfection	132

2:7:4 Genotyping of targeted clones.....	133
2:7:5 Inducible FN knockdown hESC cell line.....	134
2:8 STATISTICS.....	135
3. RESULTS CHAPTER I	136
3:1: CELLULAR THERAPY AMELIORATES CARDIAC FUNCTION IN A CHRONIC MI RAT MODEL	136
3:1:1 Optimization of rodent MI studies	137
3:1:1:1 Pro-survival cocktail (PSC).....	137
3:1:1:2 NODScid gamma mouse	139
3:1:2 Cellular therapy to regenerate the chronically infarcted rat hearts	141
3:1:2:1 Experimental design of chronic MI rat studies.....	141
3:1:2:2 Cellular therapy ameliorated cardiac dysfunction in chronically infarcted rat hearts	149
3:1:2:3 Cardiac cells engrafted and formed sizable grafts in vivo.....	159
3:1:2:4 Cardiac grafts proliferated in vivo.....	167
3:1:2:5 Cardiac grafts displayed sarcomeric maturation and Cx-43 gap junction connectivity in vivo.....	172
3:1:2:6 Cardiac grafts displayed vascularization in vivo.....	179
3:2 ESTABLISHING THE CARDIAC REGENERATIVE ANIMAL MODEL IN CAMBRIDGE	185
4.RESULTS CHAPTER II	186
4:1 EPICARDIAL-FN AS A KEY MEDIATOR OF EPICARDIAL-MYOCARDIAL CROSSTALK	186
4:1:1 Increased FN deposition with Epi+CM cardiac grafts	187
4:1:2 Functional assessments of 3D-EHTs.....	190
4:1:3 Optimal ratio of Epi:CM within 3D-EHTs.....	193
4:2 FIBRONECTIN (FN) LOSS-OF-FUNCTION STUDIES	198
4:2:1 Small Peptide (pUR4) inhibition of FN	198
4:2:1:1 Effect of pUR4 inhibition of FN on 3D-EHTs force generation.....	200
4:2:1:2 Effects of pUR4 inhibition of FN on hESC-cardiomyocytes' maturation ..	207
4:2:1:4 pUR4 inhibition of FN altered downstream integrin $\alpha 5\beta 1$ signalling in 3D- EHTs	211
4:3 GENETICALLY INDUCED LOSS-OF-FN FUNCTION	213
4:3:1 Loss-of-FN function negatively affects 3D-EHTs' contractile function.....	214

4:3:1:1 Derivation of Crispr-Cas9-mediated KOFN epicardium.....	214
4:3:1:2 Crispr-Cas9-mediated KOFN epicardium decreased 3D-EHTs' contractile function	218
4:3:2 Temporal modulation of loss-of-FN function decreased 3D-EHTs' contractile function.....	227
4:3:2:1 Generation of tetracycline-induced FN knockdown in hESC-derived epicardium.....	228
4:3:2:2 Tetracycline-induced knockdown of FN in hESC-derived epicardium attenuated 3D-EHTs' contractile function	231
4:4 RECOMBINANT HUMAN FN DOES NOT COMPLETELY RESCUE THE LOSS-OF-FN FUNCTION IN 3D-EHTS	239
4:4:1 Recombinant human FN partially salvaged the 3D-EHTs' contractile function	240
5. DISCUSSION	248
5:1 CAN CELLULAR THERAPY REGENERATE THE CHRONICALLY INFARCTED RAT HEART?249	
5:1:1 Optimisation of cardiac regenerative rodent MI models.....	250
5:1:2 Cellular therapy regenerated the chronically infarcted rat hearts.....	252
5:1:2:1 Species-matched cellular therapy	252
5:1:2:2 Combination cellular therapy	257
5:1:3 Clinical challenges posed by cellular therapy	260
5:1:3:1 Cellular therapy is associated with arrhythmias	260
5:1:3:2 Cellular therapy-related arrhythmias: contractile benefits or paracrine solutions?	261
5:1:3:3 Cellular therapy is associated with immunogenicity.....	262
5:2 EPICARDIAL-FN IS NECESSARY FOR EPICARDIAL-MYOCARDIAL CROSSTALK	264
5:2:1 Ratio of Epi:CM in 3D-EHTs	265
5:2:2 Loss-of-FN function decreased hESC-CM maturation and attenuated 3D-EHTs' contractile function.....	265
5:2:3 Rescue of loss-of-FN function with human recombinant FN	267
5:3 STUDY LIMITATIONS	270
5:3:1 Chronic MI rat model.....	270
5:3:2 The 3D-Engineered Heart Tissues	272
6. FUTURE WORK AND DIRECTION	273

6:1 CELLULAR THERAPY TO SALVAGE CHRONIC HEART FAILURE	273
6:1:1 Cardiovascular imaging.....	273
6:1:2 Cardiac electrophysiological studies.....	274
6:1:3 Species-specific ESC/IPSC-derived CMs for pre-clinical studies in cardiac regeneration	275
6:1:4 Pre-clinical development of cellular therapy to regenerate the chronically infarcted heart.....	276
6:1:5 Anti-fibrotic therapies as an adjunct to cellular therapy for chronic heart failure	277
6:2 ELUCIDATION OF EPICARDIAL-FN’S ROLE IN EPICARDIAL-MYOCARDIAL CROSSTALK ..	278
6:2:1 ‘Cardiac injury’ 3D-EHT models.....	278
6:2:2 Does epicardial-FN promote angiogenesis?.....	279
6:2:3 Is the epicardial-FN secretion affected by epicardial heterogeneity?	279
6:2:4 Positioning epicardial-FN within the epicardial-myocardial crosstalk’s genetic blueprint.....	280
7. CONCLUSIONS	281
8. APPENDIX	282
8:1 CAUSES AND TIMING OF ANIMAL DEATHS WITHIN THE CHRONIC MI RODENT STUDY	282
8:2 HISTOLOGICAL AND ECHOCARDIOGRAPHIC PARAMETERS IN THE CHRONIC MI RODENT STUDY	282
8:3 PRACTICAL DETAILS OF THE CAMBRIDGE SET-UP OF CARDIAC REGENERATIVE RODENT MODEL.....	283
8:3:1 Phase 1 Rodent Studies	285
8:3:2 Phase 2 Rodent Studies	289
8:3:3 Considerations for future cardiac regenerative rat studies	294
8:4 INTERACTOME MAP OF EPICARDIAL-FN WITH CM	295
9. REFERENCES	296

LIST OF FIGURES

FIGURE 1: MYOCARDIAL INFARCTION LEADING TO ISCHAEMIC HEART FAILURE	27
FIGURE 2: SCHEMATIC OVERVIEW OF ZEBRAFISH’S CARDIAC REGENERATIVE RESPONSE	36
FIGURE 3: THE CARDIAC REGENERATIVE RESPONSE IS MODULATED BY NATURE AND EXTENT OF INJURY IN THE NEONATAL MICE.	40
FIGURE 4: OVERVIEW OF KEY CARDIAC DEVELOPMENTAL EVENTS	43
FIGURE 5: ILLUSTRATION OF EPITHELIAL-MESENCHYMAL TRANSITION BY EPICARDIUM	48
FIGURE 6: CARDIAC REGENERATIVE STRATEGIES: THEIR ADVANTAGES AND LIMITATIONS	59
FIGURE 7: OVERVIEW OF ALL CELLULAR THERAPIES CURRENTLY IN HUMAN TRIALS	61
FIGURE 8: SEQUENCES OF EVENTS AT THE CELLULAR, ECM AND TISSUE LEVEL AFTER MI	70
FIGURE 9: OVERVIEW OF TISSUE-ENGINEERING APPROACHES, IN PARALLEL WITH THE EVOLUTION OF STEM CELLS AND CELLULAR INJECTION MODELS.....	88
FIGURE 10: EPICARDIAL EMT INTO ASSOCIATED EPDCs UNDERPINNED BY EPICARDIAL- MYOCARDIAL CROSSTALK	92
FIGURE 11: FIBRONECTIN (FN) DOMAIN ORGANIZATION AND ALTERNATIVE ISOFORMS.	96
FIGURE 12: VECTOR MAP OF pSpCas9(BB)-2A-Puro (PX459) V2.0, USED FOR sgRNA FN1 KNOCKOUT.	126
FIGURE 13: VECTOR MAP OF PAAV-Puro_siKD	130
FIGURE 14: hESC-EPICARDIUM SHOWED GREATER SURVIVAL WITH A PRO-SURVIVAL COCKTAIL IN SUBACUTE MI RAT MODEL.	138
FIGURE 15: PRO-SURVIVAL COCKTAIL DID NOT IMPROVE hESC-EPICARDIUM SURVIVAL IN THE NODScid GAMMA MOUSE ACUTE MI MODEL.....	140
FIGURE 16 EXPERIMENTAL DESIGN FOR CELLULAR THERAPY IN CHRONIC MI STUDY	143
FIGURE 17 ECHOCARDIOGRAPHIC ANALYSES OF THE RAT’S CARDIAC FUNCTION (FS%)	144
FIGURE 18 BLAND-ALTMAN PLOT SHOWED THE DEGREE OF INTEROBSERVER AGREEMENT FOR FS% CALCULATIONS	146
FIGURE 19 ALL-CAUSE MORTALITY KAPLAN-MEIER SURVIVAL CURVES FOR ALL GROUPS.....	148
FIGURE 20: BOTH CELLULAR TREATMENT GROUPS HAD SIMILAR PRE-CELLULAR THERAPY CARDIAC FUNCTION	150
FIGURE 21: CELLULAR THERAPY ATTENUATED CARDIAC DYSFUNCTION IN CHRONICALLY INFARCTED RAT HEARTS	152
FIGURE 22: BETWEEN-GROUP COMPARISON OF CHANGES IN CARDIAC FUNCTION POST- CELLULAR THERAPY	154

FIGURE 23: COMPARISON OF THE INDIVIDUAL RAT’S CARDIAC FUNCTIONAL CHANGES AFTER CELLULAR THERAPY	155
FIGURE 24 GLOBAL SYSTOLIC AND DIASTOLIC CARDIAC FUNCTION CHANGES AFTER CELLULAR THERAPY.....	156
FIGURE 25: BOTH TYPES OF CELLULAR THERAPY DISPLAYED IMPROVEMENT IN SURROGATE MARKERS OF HEART FAILURE.....	158
FIGURE 26: DISTRIBUTION AND QUANTIFICATION OF FIBROSIS IN THE CHRONICALLY INFARCTED RAT HEARTS.....	160
<i>FIGURE 27: BASELINE XIST (X-INACTIVE SPECIFIC TRANSCRIPT) IN FEMALE RATS, COMPARED TO INFARCTED MALE RATS WITH CARDIAC GRAFTS.....</i>	<i>162</i>
FIGURE 28: BOTH SPECIES-MATCHED AND COMBINATION CELLULAR THERAPY ENGRAFTED AND DISPLAYED SIZEABLE GRAFTS IN CHRONICALLY INFARCTED RAT HEARTS	164
FIGURE 29: ENGRAFTED CMs HAD SIZEABLE GRAFTS DESPITE THE CHRONICALLY SCARRED MYOCARDIUM.....	166
FIGURE 30: BOTH SPECIES-MATCHED AND COMBINATION CELLULAR THERAPY’S ENGRAFTED CMs PROLIFERATED IN VIVO	168
FIGURE 31: COMBINATION THERAPY (EPI+CM) HAD A HIGHER PROLIFERATIVE RATE IN VIVO	169
FIGURE 32: BOTH TYPES OF CELLULAR THERAPY HAD SIMILAR CM DENSITIES IN THEIR RESPECTIVE CARDIAC GRAFTS	171
FIGURE 33: ENGRAFTED CMs DISPLAYED SARCOMERIC MATURATION IN VIVO	173
FIGURE 34: WITHIN-GRAFT SARCOMERES MATURED AND ALIGNED IN VIVO	175
FIGURE 35: RESPECTIVE CARDIAC GRAFT MATURITY AT ONE MONTH AFTER CELLULAR THERAPY	176
FIGURE 36: BOTH CELLULAR TREATMENT GROUPS DISPLAYED GRAFT-HOST CONNEXIN-43 GAP JUNCTION CONNECTIVITY	178
FIGURE 37: COMBINATION THERAPY (CM+EPI) PROMOTED CD31 ^{+VE} NEOVASCULARIZATION	180
FIGURE 38: CD31 ^{+VE} NEOVASCULARIZATION IN BOTH NRVM AND EPI+CM CARDIAC GRAFTS WERE DERIVED FROM THEIR CHRONICALLY INFARCTED RAT HOSTS.....	181
FIGURE 39: NRVM AND EPI+CM DISPLAYED SIMILAR SMA ^{+VE} -COATED VESSEL DENSITY WITHIN THE CARDIAC GRAFTS, INFARCTED AND REMOTE REGIONS OF THEIR HOSTS’ MYOCARDIUM.....	183
FIGURE 40: CARDIAC GRAFTS SHOWED HOST-DERIVED SMA ^{+VE} MATURE VASCULARIZATION	184

FIGURE 41: THE DIFFERENT PATTERNS OF FN DEPOSITION IN CHRONICALLY INFARCTED RAT HEARTS	188
FIGURE 42: EPI+CM ENGRAFTMENT ALTERED THE FIBRONECTIN DEPOSITION IN CHRONICALLY INFARCTED RAT HEARTS	189
FIGURE 43: 3D-EHT WORKFLOW WITH hESC-EPICARDIUM & hESC-CMs	191
FIGURE 44: FRANK-STARLING FORCE MEASUREMENT OF 3D-EHTs	192
FIGURE 45: MEASUREMENTS OF Ca^{2+} -HANDLING BY PACED 3D-EHTs	193
FIGURE 46: 3D-EHTs WITH 10% hESC-EPICARDIUM DISPLAYED THE GREATEST ACTIVE FORCE PRODUCTION	195
FIGURE 47: 3D-EHTs WITH 10% hESC-EPICARDIUM HAD GREATEST PASSIVE FORCE PRODUCTION	196
FIGURE 48: 3D-EHTs WITH 10% hESC-EPICARDIUM DISPLAYED THE MOST OPTIMAL CALCIUM KINETICS	197
FIGURE 49: INHIBITION OF FIBRONECTIN ACTIVITY BY pUR4	199
FIGURE 50: pUR4 INHIBITION OF FN DECREASED ACTIVE FORCE PRODUCTION	201
FIGURE 51: pUR4 INHIBITION OF FN CONSERVED PASSIVE FORCE PRODUCTION	202
FIGURE 52: pUR4 INHIBITION OF FN ATTENUATED Ca^{2+} -HANDLING IN 3D-EHTs	204
FIGURE 53: pUR4 INHIBITION OF FN ATTENUATED Ca^{2+} -HANDLING BY 3D-EHTs CONTAINING EPICARDIAL CELLS	205
FIGURE 54: LOSS OF EPICARDIAL-FN DECREASED hESC-CMs MATURATION	208
FIGURE 55: EFFECTS OF pUR4 INHIBITION ON THE KEY MARKERS OF hESC-CM'S MATURITY	210
FIGURE 56: pUR4 INHIBITION REDUCED INTEGRIN-SIGNALLING AND ALTERED ECM COMPOSITION	212
FIGURE 57: GENERATION OF CRISPR-Cas9 KNOCKOUT FN hESC CELL LINE (KOFN)	215
FIGURE 58: DIFFERENTIATION OF CRISPR-Cas9-MEDIATED KOFN TO THE EPICARDIUM	216
FIGURE 59: CRISPR-Cas9 KOFN EPICARDIUM DEMONSTRATES LOSS OF FN1 EXPRESSION ..	217
FIGURE 60: CRISPR-Cas9- MEDIATED KOFN hESC-EPICARDIUM DECREASED ACTIVE FORCE PRODUCTION BY 3D-EHTs	219
FIGURE 61: CRISPR-Cas9-MEDIATED KOFN IN hESC-EPICARDIUM CONSERVED PASSIVE FORCE PRODUCTION BY 3D-EHTs	220
FIGURE 62: CRISPR-Cas9-MEDIATED KOFN IN hESC-EPICARDIUM ATTENUATED Ca^{2+} HANDLING	222

FIGURE 63: CRISPR-CAS9 MEDIATED KOFN-EPI ATTENUATED CM MATURATION DUE TO DECREASED FN DEPOSITION AND REDUCED INTEGRIN 5AB1 CLUSTERING	224
FIGURE 64: CRISPR-CAS9-MEDIATED KOFN-EPICARDIUM AND KEY MARKERS OF CARDIAC MATURITY IN 3D-EHTs.....	226
FIGURE 65: SOPTiKDFN CLONES DERIVED FROM TRANSFECTION WITH THE SOPTiKD VECTOR	229
FIGURE 66: SOPTiKD CLONE 5.3 SELECTED FOR EPICARDIAL DIFFERENTIATIONS	230
FIGURE 67: SOPTiKD CLONE 5.3 DIFFERENTIATED TO EPICARDIUM	231
FIGURE 68: TETRACYCLINE-INDUCED LOSS-OF-FN FUNCTION DECREASED ACTIVE FORCE IN 3D-EHTs.....	233
FIGURE 69: TETRACYCLINE-INDUCED LOSS-OF-FN FUNCTION IN SOPTiKD- EPI CONSERVED PASSIVE FORCE IN 3D-EHTs.....	234
FIGURE 70: TETRACYCLINE-INDUCED LOSS-OF-FN FUNCTION DECREASED THE EFFICIENCY OF Ca^{2+} HANDLING BY 3D-EHTs	236
FIGURE 71: TETRACYCLINE-INDUCED LOSS-OF-FN FUNCTION IN SOPTiKD-EPI DECREASED SARCOMERIC MATURATION IN 3D-EHTs	238
FIGURE 72: RESCUE-OF-FN WITH HUMAN RECOMBINANT FN PARTIALLY SALVAGED ACTIVE FORCE PRODUCTION BY 3D-EHTs	241
FIGURE 73: RESCUE-OF-FN FUNCTION WITH HUMAN RECOMBINANT FN DID NOT AFFECT THE PASSIVE FORCE GENERATED BY 3D-EHTs.....	242
FIGURE 74: RESCUE OF EPICARDIAL-FN WITH HUMAN RECOMBINANT FN DID NOT RECOVER THE INEFFICIENT Ca^{2+} HANDLING BY 3D-EHTs	244
FIGURE 75: RESCUE-OF-FN FUNCTION WITH HUMAN RECOMBINANT FN DID NOT IMPROVE THE MATURATION OF hESC-CMs IN 3D-EHTs.....	246
FIGURE 76: OVERALL SURVIVAL WITH CAMBRIDGE SET-UP OF THE CARDIAC REGENERATIVE MODEL	284
FIGURE 77: OPTIMIZATION OF ANAESTHETIC INDUCTION AND DIRECT ENDOTRACHEAL INTUBATION IN RATS.....	286
FIGURE 78: STEP-BY-STEP PROCEDURE FOR INVOKING MYOCARDIAL INFARCTION IN RATS	289
FIGURE 79: STEP-BY-STEP PROTOCOL FOR INTRAMYOCARDIAL CELLULAR INJECTIONS IN RATS	293
FIGURE 80: MAP OF THE INTERACTOME BETWEEN EPICARDIAL-FN AND hESC-CMs.....	295

LIST OF TABLES

TABLE 1: SIGNALLING EFFECTOR PATHWAYS UTILISED DURING EPICARDIAL-MYOCARDIAL CROSSTALK.....	54
TABLE 2 LIST OF MAJOR DIFFERENCES BETWEEN IMMATURE AND MATURE CMS.	76
TABLE 3: COMPONENTS OF MEF MEDIUM.....	104
TABLE 4: COMPONENTS OF CDM-BSA, CULTURE MEDIA FOR H9 ES CELL LINE.....	104
TABLE 5: COMPONENTS OF CDM-PVA, BASAL MEDIA FOR ALL DIRECTED DIFFERENTIATIONS	104
TABLE 6: COMPONENTS OF RPMI-BASED MEDIA FOR CMS DIFFERENTIATION AND CULTURE	106
TABLE 7: SPECIFIC COMPONENTS OF PSC WITH CONCENTRATIONS.....	108
TABLE 8: LIST OF PRIMARY ANTIBODIES USED FOR ICC AND IHC	115
TABLE 9: LIST OF SECONDARY ANTIBODIES USED FOR IHC AND ICC	115
TABLE 10: PRIMERS FOR RT-QPCR ANALYSIS OF THE RNA EXPRESSION OF GENES OF INTEREST	124
TABLE 11: ANTIBODIES FOR WESTERN BLOTTING	125
TABLE 12: PCR PRIMER SEQUENCES FOR GENOTYPING CRISPR-CAS9 EDITED KOFN CLONES	129
TABLE 13: SHRNA SEQUENCES FOR PSOPTIKD VECTOR CONSTRUCTION. BGLII OVERHANG IS IN RED, TERMINATOR SEQUENCE/SALI OVERHANG IN BLUE.	131
TABLE 14: PCR PRIMER SEQUENCES FOR GENOTYPING SOPTIKD CLONES.....	134
TABLE 15: CAUSES OF ANIMAL DEATHS.....	282
TABLE 16: HISTOLOGICAL AND ECHOCARDIOGRAPHIC PARAMETERS	282
TABLE 17: CAUSE OF DEATH FOR INDIVIDUAL RATS IN PHASE 1	285
TABLE 18: INDIVIDUAL RAT’S CAUSE OF DEATH DURING PHASE 2	290

List of Abbreviations and Acronyms

3D-EHT	3D-engineered heart tissue
ACC	American College of Cardiology
ACE	Angiotensin-converting enzyme
AHA	American Heart Association
ATP	Adenosine triphosphate
AAV-prom	AAVS1 locus promoter
BMP	Bone morphogenetic protein
BNC1	Basonuclin 1
BrdU	Bromodeoxyuridine
BSA	Bovine serum albumin
bp	Base pairs
CABG	Coronary artery bypass graft
CAD	Coronary artery disease
CDM	Chemically defined medium
cDNA	Complementary DNA
CAG	CAG promoter
CF	Cardiac fibroblasts
CM	Cardiomyocytes
COL5A2	Alpha-2 type V collagen
CoSMC	Coronary smooth muscle cells
CS	Carnegie Stage
CVD	Cardiovascular disease
DAPI	4',6-diamidino-2-phenylindole
DMEM	Dulbecco/Vogt modified Eagle's minimal essential medium EC
EC	Endothelial cells
ECM	Extracellular matrix
EMT	Epithelial-to-Mesenchymal Transition
EPDC	Epicardium-derived cells
EPI	Epicardium

FN	Fibronectin
FN1	Fibronectin
FS	Fractional shortening
FGF	Fibroblast growth factor
FHF	First heart field
HH	Hamburger-Hamilton
hESC	Human embryonic stem cell
hiPSC	Human-induced pluripotent stem cell
hPSC	Human pluripotent stem cells
hPSC-epi	Human pluripotent stem cell-derived epicardium
IGF-1	Insulin-like growth factor 1
ICC	Immunocytochemistry
IHC	Immunohistochemistry
IL-1	Interleukin-1
LPM	Lateral plate mesoderm
LVAD	The left ventricular assist device
LVEDD	Left ventricular end-diastolic dimension
LVEF	Left ventricular ejection fraction
LVESD	Left ventricular end-systolic dimension
MEF	Mouse embryonic fibroblast
MEF2C	Myocyte-specific enhancer factor 2C
MI	Myocardial infarction
MMP	Matrix metalloproteinase
MSC	Mesenchymal stem cell
MYH	Myosin heavy chain
MYL	Myosin light chain
NC	Neural crest
NRVM	Neonatal rat cardiomyocytes
NYHA	New York Heart Association
OCT	Optimal controlled temperature

OFT	Outflow tract
OPTtetR	Optimised TET repressor
pA	Polyadenylation signal
PCI	Percutaneous coronary intervention
PDGF	Platelet-derived growth factor
PDMS	Polydimethylsiloxane
PEO	Proepicardial organ
PFA	Paraformaldehyde
PS	Primitive Streak
PSC	Pro-survival cocktail
PVA	Polyvinyl alcohol
qRT-PCR	Quantitative reverse transcriptase-polymerase chain reaction
RA	Retinoic acid
Puro	Puromycin resistance
qPCR	Quantitative real-time PCR
RA	Retinoic Acid
RALDH2	Retinaldehyde-dehydrogenase 2
RNAscope/ smRNA-FISH	Single-cell RNA <i>in-situ</i> hybridisation
RNAseq	RNA sequencing
SA	Splice acceptor
SD	Standard deviation
SEM	The standard error of mean
SMC	Smooth muscle cell
sOPTikd	Optimised single-step inducible knockdown vector
T2A	Self-cleaving T2A peptide
Tβ4	Thymosin beta-4
TCF21	Transcription factor 21
TET	Tetracycline
tetR	Tet repressor

TGF β	Transforming growth factor beta
TNF- α	Tumour necrosis factor- α
TNNI	Troponin I
TO	Tet operon
WNT	Wingless-integrated integration site
WT1	Wilms tumour protein
β -MHC	β -myosin heavy chain

1.INTRODUCTION

1:1 Scale of Clinical Need

A diagnosis of heart failure carries a 50% 5-year survival (McMurray et al. 2012; Jessup and Brozena 2003; Bui et al. 2012; Jones et al. 2019). This bleak 5-year survival rate is lower than most neoplasms, apart from a lung cancer diagnosis. (Jessup and Brozena 2003; Askoxylakis et al. 2010). Despite recent medical advances, cardiovascular deaths had increased by 19% over the last 10 years, globally (Naghavi et al. 2017). Thus, heart failure carries a significant mortality risk for the individual patient.

Heart failure affects 64.3 million worldwide, with an estimated 6.2 million Americans and 1 million U.K. citizens affected (Savarese and Lund 2017; James et al. 2018; Conrad et al. 2018; Virani et al. 2020). With an ageing population and concomitantly rising number of chronic heart failure patients, up to 200,000 British patients and 915,000 American patients are diagnosed with heart failure per year in the U.K. and U.S.A., respectively (Savarese and Lund 2017; Conrad et al. 2018; Groenewegen et al. 2020; Roth et al. 2015) The rising incidence and prevalence of heart failure pose a significant economic burden on the individual and society (Yancy et al. 2017; Benjamin et al. 2019). Thus, there is a dire need for new therapies to prevent or reverse heart failure.

Ischaemic heart disease is the most significant risk factor for heart failure (Jessup and Brozena 2003; Bui et al. 2012; McMurray et al. 2012; Frangogiannis and Kovacic 2020). Acute disruption of coronary blood flow due to coronary plaque rupture or

thrombosis, leads to myocardial infarction (MI) (Thygesen et al. 2007; Laflamme and Murry 2011). Up to 1 billion cardiomyocytes (CMs) die in a major infarct (Thygesen et al 2007; Jessup and Brozena 2003; Laflamme and Murry 2011). Unfortunately, this loss of CMs is irreversible. With the attendant loss of myocardium and progressive ventricular dilatation (Pfeffer et al. 1991; Jessup and Brozena 2003; Bui et al. 2012; McMurray et al. 2012), chronic heart failure ensues.

Chronic heart failure is defined as pump failure leading to end-organ congestion (Pfeffer et al. 1991; Jessup and Brozena 2003; Yancy et al. 2017; McMurray et al. 2012). This debilitating condition is often accompanied by recurrent episodes of pulmonary oedema, life-threatening arrhythmias, ischaemic mitral regurgitation, and cardio-renal syndrome, **Figure 1**. All these clinical events herald a rapidly worsening quality of life, characterized by multiple rehospitalizations. After a heart failure diagnosis, up to 25% of patients will have a hospital readmission within 30 days of discharge, 50% by a year and ~80% will readmitted within 5 years (Groenewegen et al. 2020). Apart from significant mortality risks, heart failure also poses grave morbidity on the patients.

Given the rising prevalence and severity of this clinical condition, a definitive treatment for heart failure is urgently needed. The ideal heart failure therapy would replace the loss of CMs, be easily accessible and sustainable in the long-term. Unfortunately, the current treatments for heart failure do not fulfil these requirements. In the upcoming sections, I will discuss current heart failure treatments, together with their benefits and limitations. Then, I will propose how cardiac regenerative therapies carry a huge translational potential as a definitive and accessible cure for heart failure.

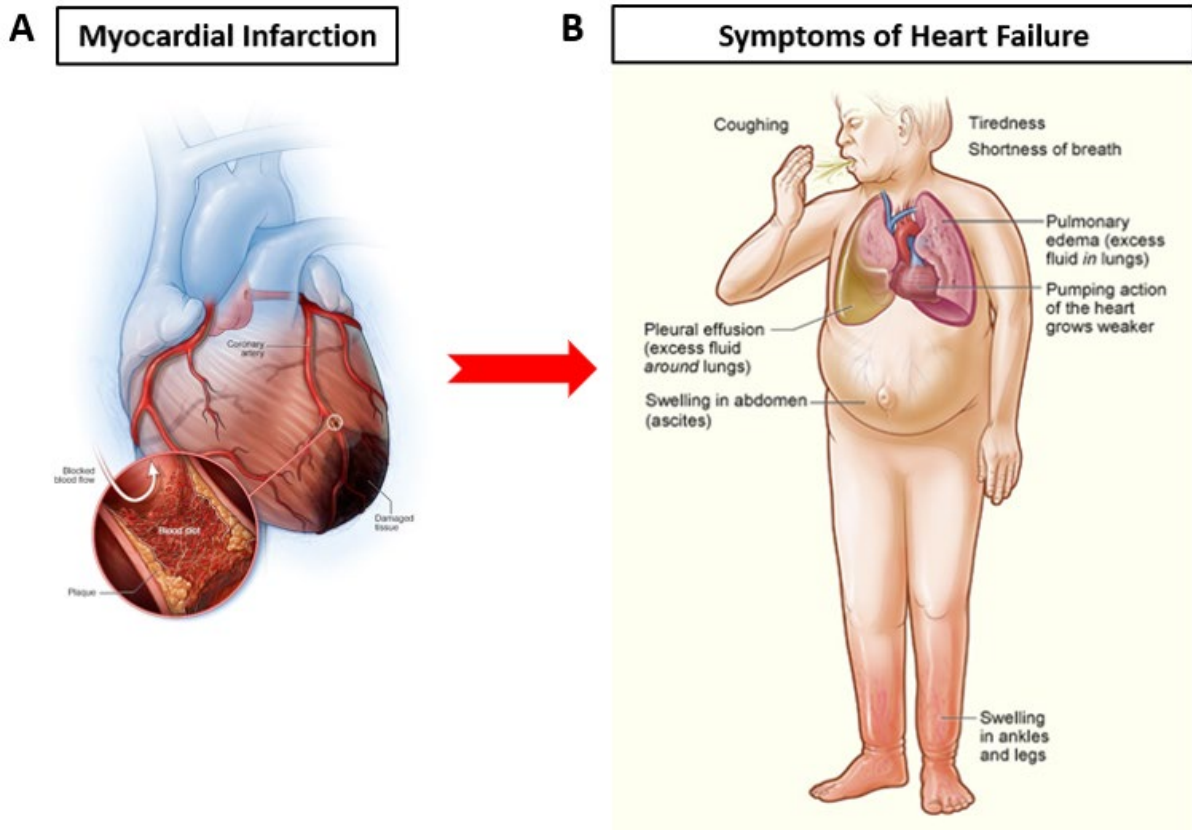


Figure 1: Myocardial infarction leading to ischaemic heart failure

A Heart schematic of atherosclerotic blockage in a coronary blood vessel, leading to myocardial infarction and subsequent tissue death (dark). Tissue death leads to dysfunctional heart contractility. **B** Heart failure is a sequela of myocardial infarction, and manifest like a constellation of signs and symptoms. (Adapted from Mayo Foundation for Medical Education and Research)

1.2 Current Clinical Treatments for Heart Failure

In the clinical setting, chronic heart failure is categorized as HFpEF (Heart Failure with preserved ejection fraction, EF%) or HFrEF (Heart Failure with reduced ejection fraction, EF%). Both categories have vastly different underlying pathologies, patient demographics and treatment strategies (McMurray et al. 2012; Yancy et al. 2017; Groenewegen et al. 2020). For the purposes of this doctoral work, I focused upon ischaemia-related chronic heart failure, therefore within the realms of HFrEF.

Drawing upon various American and European guidelines on heart failure management (McMurray et al. 2012; Yancy et al. 2017), treatment strategies for HFrEF are focused on i) optimization of remaining cardiac function and ii) prevention of further CMs death i.e. CM stress in the remodelled heart, MIs and iii) replace loss of cardiac contractile function with mechanical devices or heart transplantation. Broadly, heart failure treatment approaches are categorised as medical treatments, invasive cardiac interventions, and surgical treatments. Apart from a heart transplant, none of the treatment approaches could replace the loss of myocardium and restore contractile function to normal. However, heart transplant as a treatment strategy suffers from inaccessibility. I will elaborate on the different treatments below and detail why a more definitive cure for heart failure is required.

1:2:1 Medical Treatment

After an MI, the heart undergoes a series of pathophysiological events that involve scarring, chamber dilatation, activation of deleterious neurohormonal activation and adverse cardiac remodelling (Pfeffer et al. 1991; Jessup and Brozena 2003; Frangogiannis and Kovacic 2020). These events worsen the declining contractile function with fluid overload and pulmonary congestion. In recognition of the devastating sequelae after MI, various pharmacological treatments were discovered within the last ~50 years. These medications aimed to reduce adverse remodelling and ameliorate the symptoms of heart failure (Shah and Mann 2011; Hartupee and Mann 2016).

To minimize adverse remodelling post-MI and ameliorate heart failure symptoms, patients were prescribed medications that target deleterious neurohormonal activation, such as ACE-inhibitors (Pfeffer et al. 1991; Flather et al. 2000), angiotensin

II receptor blockers (ARB), angiotensin receptor-neprilysin inhibitors (ARNI) and beta-blockers (McMurray et al. 2012; Yancy et al. 2017). Most recently, sodium-glucose co-transporter 2 (SGLT2) inhibition was also shown to be effective in reducing heart failure-related hospitalisations and cardiovascular deaths in multi-centre trials such as DAPA-HF and EMPEROR-Reduced (Zannad et al. 2020). To further ameliorate the symptoms of heart failure, patients are also treated with diuretics, to reduce fluid overload and the cardiac workload (McMurray et al. 2012; Yancy et al. 2017). In combination, these strategies optimized the patient's declining cardiac function, with concomitant symptomatic relief.

As part of the strategy to prevent further infarcts, heart attack survivors are also prescribed anticoagulation (aspirin/clopidogrel) and cholesterol-lowering agents (statins, ezetimibe). These medications were designed to reduce further coronary thromboses and MI. Therefore, this approach is termed secondary prevention.

Combining these medications with healthy lifestyle changes significantly reduced heart failure-related hospitalizations, and improved patients' quality of life (McMurray et al. 2012; Yancy et al. 2017). However, these medications only offer symptomatic relief. They do not replace the loss of contractile function. Thus, the current medical treatments could only slow down the progression of heart failure, but neither halt nor reverse it.

1:2:2 Invasive Cardiac Interventions

Identical to medical treatment, invasive cardiac interventions are centred around optimizing the remaining cardiac function. The main invasive cardiac interventions for heart failure management are cardiac resynchronisation therapy (CRT) and

implantable cardiac defibrillators (ICD). After MI, a combination of adverse remodelling, chamber dilatation and infarct-related loss of conduction tissue may lead to disrupted normal conduction pathways and subsequent cardiac dyssynchrony (Brignole et al. 2013). Cardiac dyssynchrony compromises the remaining cardiac function and exacerbates the failing heart (Brignole et al. 2013). Both CRT and ICD were designed to improve overall cardiac contractility and hence, ameliorate the symptoms of heart failure. CARE-HF, a multi-centre trial, showed that CRT and pharmacological treatment resulted in modest reduction in cardiovascular-related mortality (Cleland et al. 2012). Nonetheless, both CRT and ICD merely slow the declining cardiac function in heart failure patients.

Coronary revascularization is usually offered as a secondary prevention to prevent further MIs and CMs death. However, heart failure is not recognised as a primary indication for coronary revascularization (Yancy et al. 2017). In the subset of patients who fit the criteria for coronary revascularization, the alleviation of coronary blockages may salvage underlying hibernating myocardium and reduce hypoxic regions within myocardium secondary to coronary obstructions. Overall, this may lead to modest improvements in cardiac function. Coronary revascularizations could be conducted as percutaneous coronary interventions or coronary artery bypass surgery (CABG), based on the patients' indication, cardiac and non-cardiac risk factors, and latest American/European guidelines (McMurray et al. 2012; Yancy et al. 2017) . Although coronary revascularizations are widely recognised to improve cardiac function and long-term survival, this approach still fails to replace the lost myocardium.

Despite the optimization of cardiac function by invasive cardiac interventions, the post-infarct heart still pumps with fewer CMs. Therefore, cardiac function will continue to

decline over time, with worsening heart failure symptoms. This approach is not a definitive cure for heart failure.

1:2:3 Heart Transplant

Despite all the innovative medical and invasive cardiac interventions over the last 50 years, there was an increasing recognition that a definitive 'cure' for heart failure is needed. Ideally, a definitive cure for heart failure needs to completely return the cardiac function to its pre-injury state. This 'cure' came in the form of human-human heart transplantation, first performed successfully by Christian Barnard in 1967 at Groote Schuur Hospital in Cape Town, South Africa (Lund et al. 2016; Stehlik et al. 2018; K. S. Shah, Kittleson, and Kobashigawa 2019). This procedure is lifesaving and dramatically improves the quality and length of the recipient's life. Heart transplantation is heralded as one of the greatest innovations in the 20th century. However, it remains challenged by its relative inaccessibility and long-term complications.

Heart transplantation is limited by the availability of organ donors. Intrinsicly, heart transplantation is reliant on the generosity of donors and a national health system (NHS) that efficiently coordinates the recipients and donor organ donation. From the NHSBT's Annual Report Cardiothoracic Organ Transplantation (2019/2020), the UK only performed between 131 to 198 adult heart transplants per year, for the past decade. However, the number of heart failure patients on the transplant waiting list has almost tripled over the last decade. Several key donor heart optimisation strategies such as utilisation of hearts from donor cardiac death (DCD) (Messer et al. 2020) and early donor management by Scouts (Barbero et al. 2019) are being developed. In May 2020, the UK changed the donor organ regulations from 'opt-in' to

'opt-out'. These strategies may translate into more donor hearts for heart failure patients. Given the rapidly rising incidence of heart failure with up to 200,000 UK patients per year, we will still fall quite short.

A heart transplant is not without significant risks, both in the short-term and long-term. The median post-transplant survival is ~12 years (Stehlik et al. 2018; Bhagra et al. 2019) . For the individual patient, the risks encompassed acute or long-term graft failure/rejection, complications secondary to long-term immunosuppression (infection, hypertension, diabetes mellitus, renal dysfunction, malignancy), and cardiac allograft vasculopathy (Lund et al. 2016; Stehlik et al. 2018). To monitor these potential risks, the individual patient is committed to life-long graft surveillance, with downstream effects on the patient's quality of life and psychological health. From some patients' viewpoints, they have exchanged one severe disease for another.

At present, heart transplantation is the only definitive treatment for advanced heart failure but remained challenged by limited healthy, donor hearts, chronic rejection states and complications associated with long-term immunosuppression (Mehra et al. 2016). Thus, heart transplantation is still far from an ideal heart failure 'cure'.

1:2:4 LVAD (Left ventricular assist device)

Cognizant of the patients' continuous deterioration whilst waiting for a heart transplant, mechanical circulatory support (MCS) devices were developed to bridge patients to successful heart transplants (Krishnamani, Denofrio, and Konstam 2010; Stehlik et al. 2018). The MCS devices comprised of the support for the right ventricle (RVAD), left ventricle (LVAD) or both ventricles (BIVAD). More specifically, LVAD (left ventricular assist device) is a mechanical heart pump implanted within the apex of the left ventricle

and connected to an external battery pack, carried by the patient. The LVAD pump utilises centrifugal force to reroute oxygenated blood from the left ventricle into the ascending aorta, and into the systemic circulation. Although quite successful in replacing the pump function of the heart, LVADs could only be used as a short-term therapy due to their severe complications.

As a heart failure treatment, LVADs served 2 main purposes as 'bridge to transplantation' for heart transplant candidates, or 'destination therapy' for patients who were refractory to maximal medical support and turned down for heart transplantation. As 'bridge to transplantation' therapy, LVADs was successful in reducing pretransplant mortality by 55% and significantly increased post-transplant 1-year survival (Frazier et al. 1995). In the USA, patients received LVADs as 'destination therapy'. MOMENTUM 3, HeartMate II and REMATCH trials showed that 'destination therapy' LVADs significantly increased survival up to 2-years, together with functional improvement and reduced hospitalizations, compared to maximum medical therapy (Rose et al. 2001; Slaughter 2018; Mehra et al. 2019). In the UK, LVADs are only used for heart transplant candidates (Parameshwar et al. 2019), thereby, obviating a large chunk of heart failure patients. In both clinical indications, LVADs improve the forward flow of the heart, leading to improved end-organ perfusion with dramatic symptomatic relief.

Unfortunately, the usage lifespan of LVADs remains short, up to ~5 years maximum. LVADS are associated with serious, life-threatening complications such as strokes, recurrent bleeding, pump thrombosis, recurrent pump or tunnel line infections, and battery pack failures (Mehra et al. 2016). We do acknowledge that LVAD technology is still at its infancy, with potential for further improvements.

Without a shadow of doubt, heart failure treatments have advanced tremendously over the 50 years. These medical treatments have been quite successful in ameliorating the symptoms of heart failure. However, they did not address the underlying pathology leading to heart failure- the irreversible loss of CMs leading to decreased cardiac pump function. Only heart transplantation and LVADs clearly recover cardiac pump function. However, only a small subset of patients are able to benefit from them. Furthermore, heart transplantation and LVADs are not without significant short-term and long-term complications. With an ageing population and the rising prevalence of heart failure patients, a definitive, accessible, and long-term therapy to prevent or reverse heart failure is crucial. Ideally, any new heart failure therapy needs to definitively address the irreversible loss of CMs.

1:3 Cardiac Regeneration as Heart Failure Treatment

Out of all the available treatments for heart failure, the LVADs came closest to the ideal heart failure therapy. LVADs could reverse the failing heart by increasing the cardiac pump function. LVADs are accessible as an off-the-shelf therapy and long-term immunosuppression is not required. Cardiac regenerative therapies could potentially offer similar functional gains and practical considerations as the LVAD, to treat the failing heart. One postulates that cardiac regenerative therapies could simulate a 'biological' LVAD, avoid the mechanical complications associated with LVADs and therefore, last longer.

Why do I propose that cardiac regenerative therapies would represent the alternative, ideal heart failure treatment? Cardiac regeneration after ventricular injury has been observed in non-mammalian species such as newts (Oberpriller et al. 1974; Bader et al. 1978; Laube et al. 2006), axolotls (Flink et al. 2002), zebrafish (Poss, Wilson, and

Keating 2002; González-Rosa, Burns, and Burns 2017) and neonatal mice (Porrello et al. 2011). However, cardiac regeneration in the face of ventricular injury seems a tall order. For complete functional heart regeneration, a series of critical processes need to occur i) clearance of dead tissue, ii) restoration of lost cardiac muscle, iii) revascularisation, iv) electrical coupling of new CMs, v) resolution of inflammation and collagen/fibrin (Poss, Wilson, and Keating 2002; Kikuchi et al. 2010; González-Rosa, Peralta, and Mercader 2012; Lai et al. 2017). The insights gained from Mother Nature's examples of cardiac regeneration, may inform us on the feasibility of cardiac regeneration therapy as a clinical therapy. Thus, I will start by examining cardiac regeneration in the adult zebrafish and the neonatal mouse.

1:3:1 Regeneration in adult zebrafish heart

A zebrafish retains the ability to regenerate its heart throughout adulthood; with complete regeneration of ~20% ventricular resection within 60 days, with no fibrotic scarring (Poss, Wilson, and Keating 2002; González-Rosa et al. 2017), **Figure 2**. Robust cardiac regeneration across different injuries was observed, such as apical resection, cryoinjury and chemical ablation (Poss, Wilson, and Keating 2002; Kikuchi et al. 2010; Wang et al. 2011; González-Rosa, Peralta, and Mercader 2012; González-Rosa, Burns, and Burns 2017; Lai et al. 2017). Even with ~60% ventricular loss and heart failure, the zebrafish could completely regenerate its heart within a week, with reversal of heart failure and minimal scarring (Wang et al. 2011). When the FGF-dependent cardiac regeneration was withheld for 60 days after cardiac injury, the zebrafish could still regenerate its heart over a chronic scar when FGF was reintroduced - simulating cardiac regeneration in chronic heart failure (Kikuchi et al.

2010). Harnessing the cardiac regenerative strategies harboured by zebrafish to aid the failing, human heart, seems pertinent.

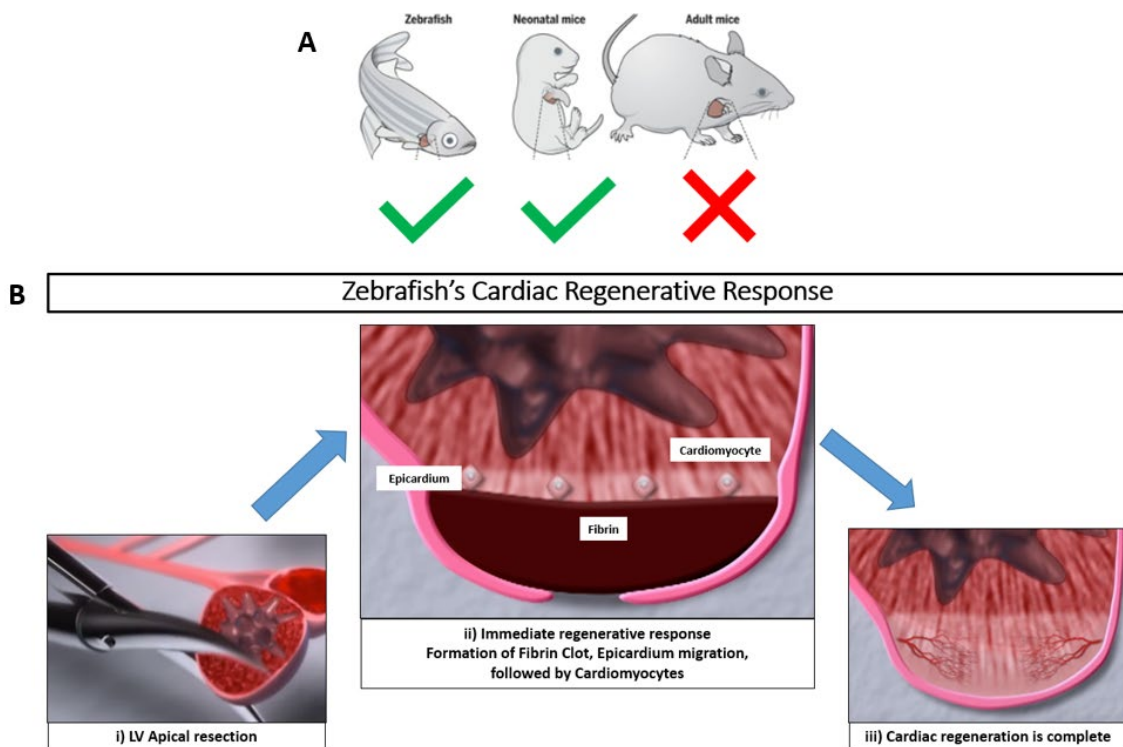


Figure 2: Schematic overview of zebrafish's cardiac regenerative response

A The adult zebrafish, neonatal and adult mice portrayed different cardiac regenerative abilities based on species and age in mammals. **B** A stepwise model outlining the cardiac regenerative response when the LV apex is amputated in the adult zebrafish. (Adapted from Cao and Poss 2018)

Production of new CMs is the lynchpin of this entire, complex process of cardiac regeneration. 'Is the zebrafish's cardiac regeneration due to dedifferentiation of pre-existing CMs with subsequent proliferation or a stem cell niche giving rise to new CMs?' Kikuchi et al. demonstrated via genetic-lineage tracing studies in zebrafish that *de novo* CMs arise from proliferating, pre-existing adult CMs post-injury; governed by Gata4 expression (Kikuchi et al. 2010; 2011; Jopling et al. 2010). Notably, zebrafish CMs remain mononucleated and diploid through their lifespan (Kikuchi et al. 2010), hinting at regular cell cycle re-entry and a continual growth model (Kishi et al. 2003).

Recent zebrafish studies illustrated the attenuation of injury-induced heart regeneration with increased myocardial polyploidisation (González-Rosa et al. 2018; Patterson et al. 2017); hinting that the adult mammalian heart's inability to regenerate may be largely due to the polypoidal adult CMs which cannot generate new CMs. For the zebrafish, its cardiac regeneration is enabled by its innate ability to generate new CMs after cardiac injury.

Non-cardiac stromal cells e.g. epicardium, endocardium and immune cells, are instrumental in promoting CM proliferation and regeneration after ventricular injury in the zebrafish (Poss, Wilson, and Keating 2002; Lepilina et al. 2006; González-Rosa, Peralta, and Mercader 2012; Jopling et al. 2010; Kikuchi et al. 2010; 2011; J. Kim et al. 2010; J. Wang et al. 2011; Choi et al. 2013). As alluded above in *Section 1:3*, successful cardiac regeneration required more than just new CMs. The epicardium emerged as the key stromal cell in orchestrating *de novo* cardiac proliferation and migration, alongside vascularization of the new cardiac tissues (Lepilina et al. 2006; Kikuchi et al. 2011; González-Rosa, Peralta, and Mercader 2012; Wang et al. 2013; Cao et al. 2017). The indispensable role of epicardium in cardiac regeneration will be further elaborated in *Section 1:6:1*.

Studying the cardiac regeneration in the zebrafish gave us two key insights, central to our cardiac regenerative efforts for heart failure patients. Firstly, new CMs are required to replace the irreversible loss of CM during injury. Secondly, non-cardiac stromal cells are instrumental in directing the new CMs towards successful cardiac regeneration. For translation to the clinical setting, we hypothesised that we could regenerate the failing human heart with new CMs and a key stromal cell.

1:3:2 Regeneration in the neonatal mammalian heart

Apart from the adult zebrafish, the neonatal mouse at P1 (day 1 post-partum) can also completely regenerate its heart, with up to 15% ventricular apical resection or left anterior descending artery (LAD) ligation (Porrello et al. 2011; 2013; Bernhard Johannes Haubner et al. 2012). Similar cardiac regeneration ability was observed in neonatal rats (Zogbi et al. 2014). Interestingly, there were anecdotal, clinical observations of complete myocardial recovery after significant MI in human neonates (Farooqi et al. 2012; Haubner et al. 2016; Ling et al. 2016). However, myocardial recovery in human neonate could be due to reversal of myocardial stunning/hibernation and further evidence would be warranted. As might be expected, the evidence is sparse due to clinical and ethical reasons. Nonetheless, the cardiac regenerative abilities observed in neonatal rodents strongly suggest that the mammalian heart has potential for cardiac regeneration.

For both neonatal mouse and the adult zebrafish, generation of new CMs and direction by non-cardiac stromal cells are instrumental in cardiac regeneration. Like the zebrafish, the proliferation of pre-existing CMs drives neonatal mice/rats' innate cardiac regeneration, rather than extracardiac or resident cardiac stem or progenitor cells (Porrello et al. 2011; Lam and Sadek 2018). Similar key transcriptional growth regulators and developmental pathways, such as Gata4, Meis1, Hippo/YAP pathway and neuregulin/ErbB pathway, had been implicated in directing CMs proliferation in the neonatal mouse (Lam and Sadek 2018; Vagnozzi, Molkenin, and Houser 2018). Furthermore, non-cardiac stromal cells, e.g. immune cells, vascular cells, and epicardium, together with ECM, play crucial roles in cardiac regeneration in neonatal mice. The epicardium's role in neonatal mice cardiac regeneration will be expanded in

Section 1:6:2. Thus, both neonatal mice and adult zebrafish share certain cardiac regenerative principles.

In contrast to the zebrafish, the regenerative ability of neonatal mice is transient, limited by the extent and type of injury (Darehzereshki et al. 2015) , **Figure 3**. Firstly, the regenerative ability in rodents is only retained until P7 (day seven post-partum) (Porrello et al. 2011). Thus, P1-7 is termed the 'regenerative window'. Secondly, a cryoinjury-mediated transmural injury within the 'regenerative window' will lead to a non-regenerative fibrotic response, identical to a ventricular injury at P8 (Darehzereshki et al. 2015; Bryant et al. 2015, Lam and Sadek 2018). These differences provoked two crucial questions; i) 'Are the extensive cardiac injuries leading to incomplete cardiac regeneration before the end of P1-7 'regenerative window'?' or ii) 'Is the degree of myocardial regeneration inherently limited in mammals?' (Lam and Sadek 2018). Understanding the principles governing the different cardiac regenerative abilities portrayed by the neonatal mouse and the adult zebrafish, will aid our cardiac regenerative efforts towards the heart failure patients.

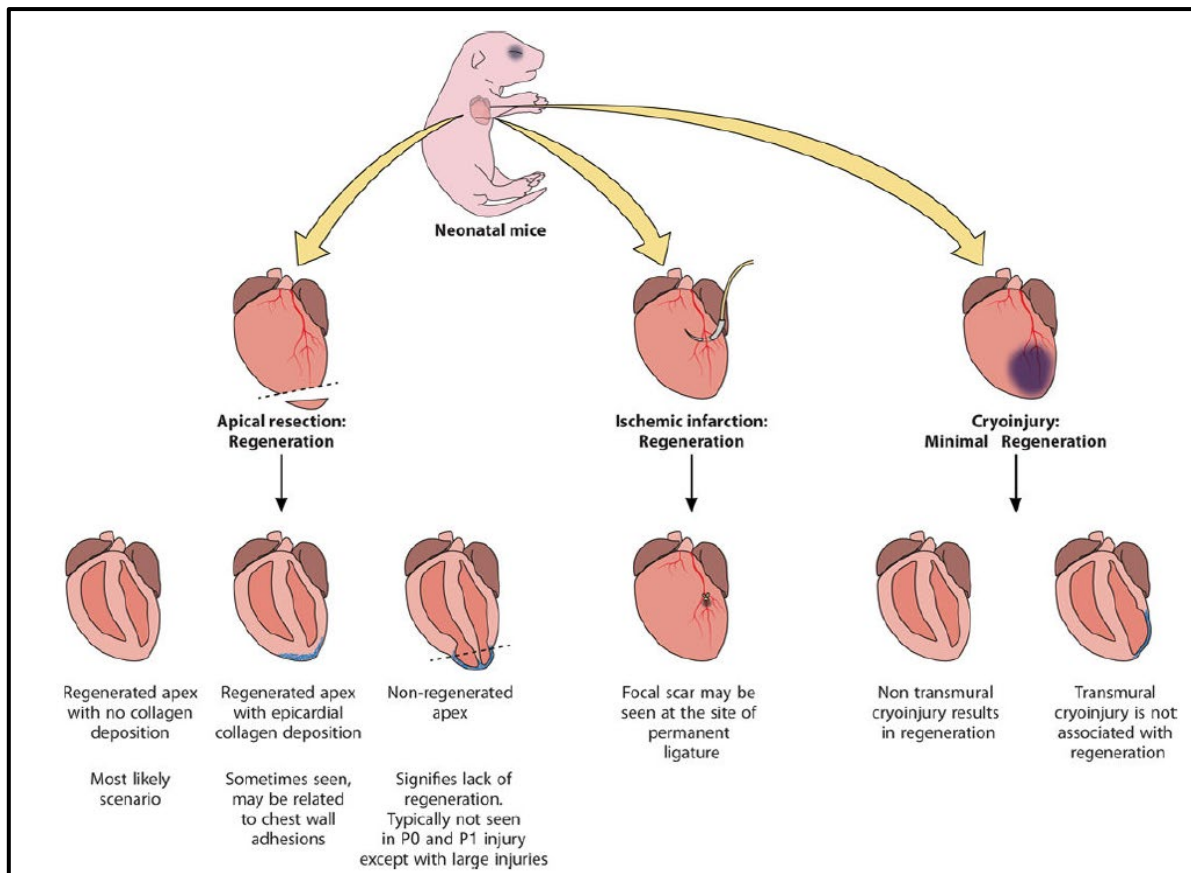


Figure 3: The cardiac regenerative response is modulated by nature and extent of injury in the neonatal mice.

The neonatal mouse's cardiac regeneration is limited by extent and type of cardiac injury. With apical resection, there are 3 possible outcomes, which are complete cardiac regeneration, regeneration with collagen deposition and non-regenerative if apical resection is >15% of LV. As for left anterior descending artery (LAD) ligation to simulate MI, the neonatal mouse would display complete cardiac regeneration. With the cryoinjury model, the neonatal mouse can only regenerate its heart if the injury is not transmural. (*Adapted from Sadek 2015*)

The transient nature of the neonatal mouse's cardiac regeneration requires further probing. Of note, most murine CMs are diploid at birth but rapidly become polyploid; conceivably linked to a postnatal burst of CM growth and uncoupling of karyokinesis from cytokinesis (Soonpaa et al. 1996; Hirai, Chen, and Evans 2016). There are further disparities between the adult zebrafish and neonatal mammal's CM proliferation, such as low pressured 2-chamber vs 4-chamber system, adult vs neonatal CM proliferation

and amount of polyploidy at the point of regeneration (Karra and Poss 2017). All factors which may govern their different cardiac proliferative abilities; based upon the plasticity of the genetic, cellular and tissue environment to enable cell cycle re-entry (Karra and Poss 2017; J. Cao and Poss 2018). Thus, ongoing complete, endogenous cardiac regeneration after injury appear to exhibit species variation.

With the goal of clinical translation, a measure of caution is recommended. Applying biological insights across huge evolutionary distances (e.g. zebrafish and/or mice to human) could prove challenging. Despite differences in injury responses and the window of cardiac regeneration, the underlying principles, such as generation of new CMs and the instructive role of non-cardiac stromal cells remain evolutionarily conserved across the adult zebrafish and neonatal mouse. Thus, these key cardiac regeneration principles will inform the development of cardiac regenerative therapies for human heart failure patients.

1:4 Insights from Cardiac Embryogenesis to guide Cardiac Regenerative therapies

Insights from cardiac embryogenesis will greatly assist in our efforts to regenerate the failing human heart. Unlike injury-induced cardiac regeneration, all species undergo cardiac embryogenesis. Broadly, cardiac embryogenesis is divided into cell specification, cardiac morphogenesis, and CM maturation (Guo and Pu 2020). Identical to injury-induced cardiac regeneration, cardiac embryogenesis requires the generation of new CMs, together with an orchestrated crosstalk with non-cardiac stromal cells to build a functional heart. Next, I will describe cardiac embryogenesis

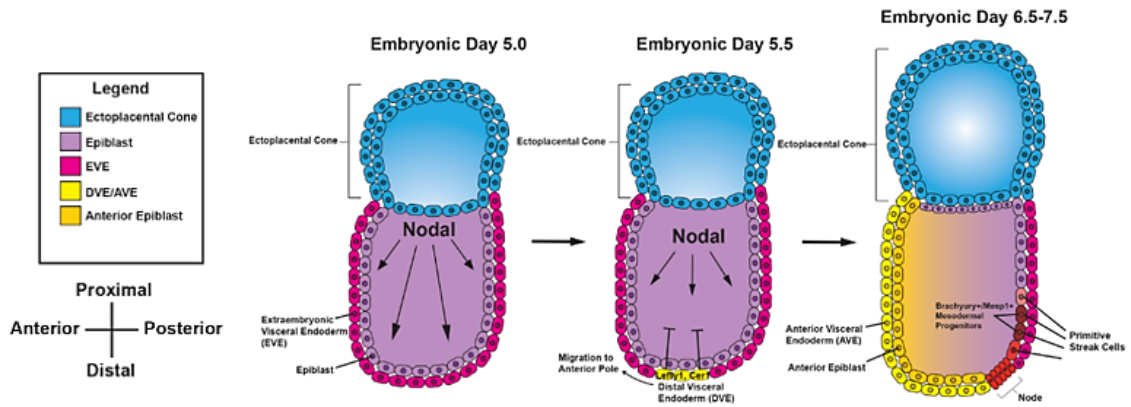
and highlight the key principles relevant to the development of our cardiac regenerative therapies.

1:4:1 From epiblast to cardiomyogenic commitment

Cardiac embryogenesis starts with mesodermal commitment from the epiblast. At embryonic day 5 (E5) in the mouse, the cylindrical shaped embryo undergoes patterning with separation into embryonic and extra-embryonic layers. Combinatorial signalling gradients of Nodal, FGF, BMP4, WNT3, across both anterior-posterior and proximal-distal axes further patterns and induces the primitive streak (PS); marked by pan-mesoderm marker, *Brachyury* (Conlon et al. 1994; P. Liu et al. 1999; Ciruna and Rossant 2001; Brennan et al. 2001; Rivera-Pérez and Magnuson 2005). PS is present by embryonic day E6.0 in mouse, corresponding to Carnegie Stage 6 in humans (2nd week of gestation). As a PS, the Nodal signalling gradient along the anterior-posterior axis patterns the epiblast into three embryonic germ layers (Arnold and Robertson 2009; Robertson 2014).

The three germ layers during gastrulation are termed as endoderm, mesoderm, and ectoderm (Xin, Olson, and Bassel-Duby 2013). High Nodal levels specify endoderm at anterior PS whilst low Nodal levels, together with BMP and Wnt3 (Winnier et al. 1995; P. Liu et al. 1999) specify mesodermal precursors in intermediate and posterior PS (Arnold and Robertson 2009; Robertson 2014), ultimately leading to cardiac mesoderm precursors arising anterior and lateral to PS (Brennan et al. 2001), **Figure 4A**. Thus, the heart is derived from the mesoderm layer.

A Specification of Mesodermal Precursors



B E7.5 Heart Fields Specification E8 Linear Heart Tube Formation

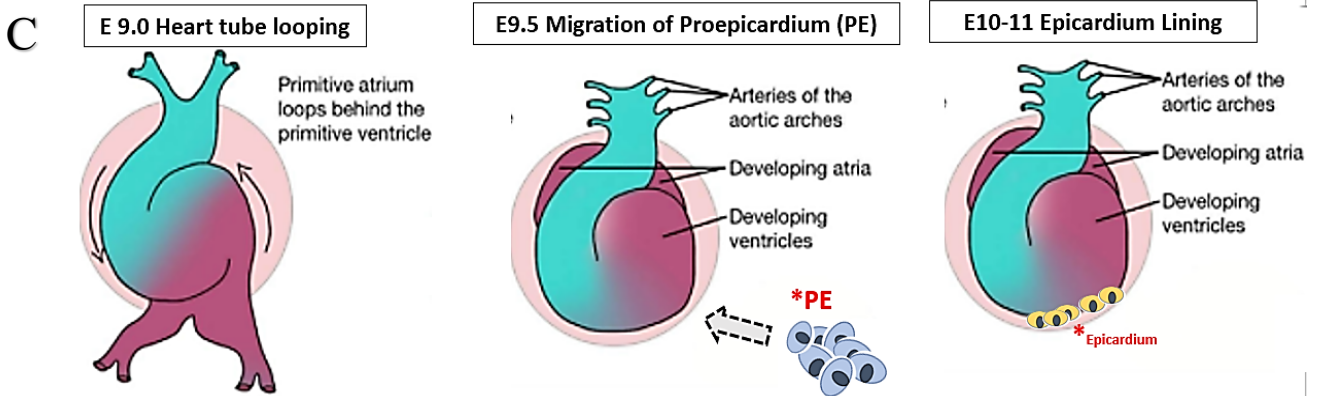
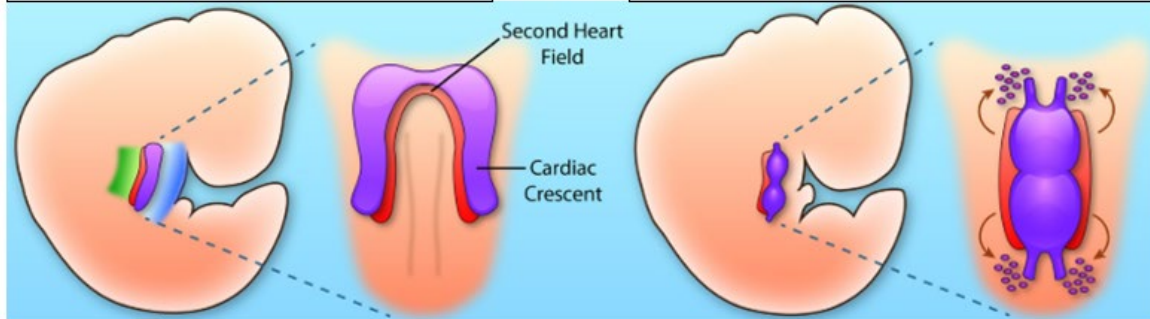


Figure 4: Overview of key cardiac developmental events

A Key combinatorial signalling events leading to the specification of mesoderm precursors over E5-7.5. **B** Schematic of formation of the cardiac crescent (FHF) with second heart field (SHF) leading to linear heart tube formation by E8. **C** Subsequently, heart tube undergoes looping to form specific chambers and outflow tracts. At E9.5, proepicardium (PE) migrates from the sinus venosus onto the left ventricle with the formation of epicardial lining over the heart on E10-11. (Adapted from Xin et al 2013, Galdos et al, 2017)

Next, the mesodermal precursors are specified into cardiac lineages. Activation of MESP1, a key transcriptional regulator of cardiovascular progenitor specification, specifies a subpopulation of mesoderm into cardiac lineages (Bondue et al. 2008; Lescroart et al. 2014). MESP1+ cells migrate anteriorly and laterally away from mesoderm, to form the anterior lateral plate mesoderm. At E7.5 in the mouse, MESP1+ cells form the first heart field (FHF) and second heart field (SHF) (Vincent and Buckingham 2010; Galdos et al. 2017). FHF constitutes the cardiac crescent with SHF lying medial and dorsal to it (Srivastava and Olson 2000; Galdos et al. 2017). Due to their position, FHF and SHF receive different combinatorial and temporally distinct signals during embryogenesis, leading to differential proliferation, migration, and terminal differentiation. The FHF receives non-canonical signalling such as *Wnts*, *Bmp2*, *Bmp4*, *Fgf8*, whilst the SHF is subjected to canonical signalling such as *Wnts/β-catenin*, *Shh* and *Fgfs* (Vincent and Buckingham 2010; Srivastava and Olson 2000; Galdos et al. 2017) **Figure 4B**. Cell fate specification into either FHF or SHF will determine the cells' role in subsequent morphogenesis, and cardiac function.

At embryonic day E8.0, FHF progenitors differentiate to form the mammalian linear heart tube (Abu-Issa and Kirby 2007). This corresponds to Carnegie Stage 9-10 in humans (3rd week of gestation). SHF progenitors remain undifferentiated, migrate to elongate the beating heart tube; eventually forming the arterial and venous poles of the heart, (Galdos et al. 2017), **Figure 4B**. At E9.0, the mammalian heart tube undergoes looping, as directed by *Lefty* and *Nodal*, with subsequent proepicardium contribution at E9.5 (Galdos et al. 2017; Abu-Issa and Kirby 2007). To achieve the final cardiac morphology, several key events subsequently ensue; looped tube rotation, the formation of inflow/outflow tracts, atrioventricular valves, cardiac

chambers specification and expansion (Xin, Olson, and Bassel-Duby 2013; Galdos et al. 2017), **Figure 4C**.

FHF and SHF progenitors are distinct. FHF progenitors first express *Nkx2.5*, which interacts with *Gata4* and *Tbx5* to activate cardiac muscle development and formation of the left ventricle. Due to the transient nature of the FHF, only *HCN4* has been reliably touted as a FHF marker with eventual confinement of *HCN4+* cells to the cardiac conduction system (Liang et al. 2013; Später et al. 2013). SHF is classically defined by sustained expression of *Is11*, which interacts with *Gata4* to sequentially activate *Mef2c* and *Hand2* (Galdos et al. 2017). After the formation of the heart tube, the SHF remains and eventually contributes towards right ventricle, inflow/outflow tract, a portion of septum and atria (Galdos et al. 2017). Although overly simplistic, FHF and SHF progenitors 'build' the entire heart, in a well-orchestrated manner.

Insights into early cardiac lineage commitment inform us that the CM's form and function are lineage specific and dependent on well-orchestrated instructions from its environment. Thus, one postulates that generation of new CMs as part of cardiac regenerative therapies, ideally needs to be lineage specific. Apart from generation of new CMs, successful cardiac embryogenesis also relies upon well-orchestrated instructions and cellular contributions by non-cardiac stromal cells.

1:4:2 The epicardium in cardiac development

After cardiac cell fate specification and morphogenesis, the CMs undergo a burst of proliferation and maturation to form a functional heart. These events are coordinated by key non-cardiac stromal cell population found within the epicardium (Carmona et

al. 2010; Chen et al. 2002; Sucov et al. 2009; Cao and Cao, 2018; Lupu, Redpath, and Smart 2020). Furthermore, the epicardium directs the vascularization of cardiac tissues (Mikawa and Gourdie 1996; Christoffels et al. 2009; Wu et al. 2013, Jing et al. 2016). Undeniably, the epicardium has an instrumental role in cardiac embryogenesis.

The epicardium is a thin layer of epithelial cells with ‘cobblestone-like’ morphology, lining the heart by E10-11, **Figure 4C**. Epicardium was initially described in 1907 (Kurkiewicz 1909), followed by a hiatus of ~60 years before its eventual rediscovery with the advent of electron microscopy (Manasek 1969, 1968). Upon that rediscovery, a stream of studies involving avian, zebrafish and quail-chick chimaera models, together with exhaustive lineage-tracing studies followed rapidly; these have widely agreed on cell markers defining the epicardium, *Wt1*, *Tbx18* and *Tcf21* (Cao and Cao, 2018), with some overlap with proepicardium as recently shown (Lupu, Redpath, and Smart 2020). Identification of these cellular markers enabled robust characterization of the epicardium’s dynamic role in cardiac development.

I shall start by discussing embryonic epicardium, epicardium’s epithelial-mesenchymal-transition, its cellular contributions and signalling pathways underpinning epicardial-myocardial crosstalk in cardiac development. Then, I will further expand on why the epicardium represents the key stromal cell for cardiac embryogenesis and by extension, cardiac regeneration.

1:4:2:1 Developmental origins of epicardium- proepicardium

The embryonic epicardium originates from the proepicardium, a primarily extracardiac primordium (Zhou et al. 2012; Liu and Stainier 2010; Smits, Dronkers, and Goumans 2018; Nesbitt et al. 2006) . At E9.5, the proepicardium consists of a transient cluster

of cells at the sinus venosus (between liver and heart), which migrate towards the ventricle, proliferate, and expand to encapsulate the heart, thereby forming the epicardium by E10-11 (Liu and Stainier 2010; Smits et al. 2018). Until this stage, the heart tube only consisted of 2 layers, endocardium and myocardium. The proepicardium's migration to the heart tube is deemed evolutionarily conserved (Cao and Poss 2018), based upon studies across various species such as zebrafish, *Xenopus*, axolotl, mouse, rat and human (Komiyama et al. 1987; Fransen and Lemanski 1990; Jahr et al. 2008; Nesbitt et al. 2006; Risebro et al. 2015; Serluca 2008). The proepicardium is the pivotal signalling node that directs epicardium and cardiac development. Disruption of the proepicardium in avian models led to failure in establishing epicardium, accompanied by lack of coronary vasculature and thin, ballooning ventricles (Gittenberger-De Groot et al. 2000); thus highlighting the importance of epicardium in orchestrating cardiac development (Carmona et al. 2010; Smits et al 2018).

1:4:2:2 Epicardium undergoes epithelial-mesenchymal-transition

During cardiac development, a subset of epicardial cells delaminates, undergoes epithelial-mesenchymal transition (EMT) at E12.5 and migrates into the subepicardial space to give rise to a variety of cells, termed epicardium-derived cells (EPDCs) (Dettman et al. 1998; Gittenberger-de Groot et al. 1998; Lie-Venema et al. 2007; Von Gise and Pu 2012; Pérez-Pomares et al. 1998), **Figure 5**. EMT is an active process, requiring the epicardial cells to reverse polarity and reorganise their actin cytoskeleton to achieve a migratory and invasive phenotype with corresponding changes in morphology, cellular markers and cell fate. (Lie-Venema et al. 2007; Wu et al. 2010; Lamouille, Xu, and Derynck 2014; Cao and Cao, 2018). EMT is triggered by reciprocal

1:4:2:3 Epicardial cellular contributions to the developing heart

The epicardium is a potent multicellular source during cardiac development. Collectively, studies in quail-chick chimaeras, transgenic mice (labelled with *Tbx18*) and transgenic zebrafish (labelled with a *Tcf21* reporter) concurred that the epicardium differentiates into EPDCs, which primarily comprise coSMCs (coronary smooth muscle cells), cardiac fibroblasts (Acharya et al. 2012; Christoffels et al. 2009; Katz et al. 2012; Grieskamp et al. 2011; Ali et al. 2014; Volz et al. 2015; Kikuchi et al. 2011; Dettman et al. 1998; Gittenberger-de Groot et al. 1998; Jing et al. 2016) and, controversially, some CMs and endothelial cells (Cai et al. 2008; Zhou et al. 2008; Perez-Pomares et al. 2002).

Classical studies characterizing epicardium and its progeny utilised quail-chick chimaeras with dye-labelling and retroviral approaches (Dettman et al. 1998; Mikawa and Fischman 1992; Mikawa and Gourdie 1996). More refined, modern studies used recombinase-based, genetic fate-mapping systems with regulatory sequences corresponding to *Wt1*, *Tbx18* and *Tcf21* (Cao and Poss 2018; Cao and Cao, 2018). However, these studies were flawed as the *Wt1*, *Tbx18* and *Tcf21* regulatory sequences also marked other non-epicardial populations, including the aberrant labelling of CMs themselves (Cai et al. 2008; Christoffels et al. 2009; Rudat and Kispert 2012). Similar aberrations were observed with epicardial differentiation to endothelial cells (Perez-Pomares et al. 2002; Carmona et al. 2020). Due to the technical limitation of fate-mapping studies specific to epicardium, various works reporting epicardial differentiation to CMs and endothelial cells were re-examined (Christoffels et al. 2009; Carmona et al. 2020; Cao and Poss 2018), with the updated conclusion that the

epicardium is unlikely to differentiate into *de novo* CMs or endothelial cells (Cao and Poss 2018).

Nonetheless, the epicardium has demonstrable cellular plasticity and plays a pro-mitogenic role in CM proliferation during cardiac development. As such, it is possible that combining epicardium, as the key stromal cells, with newly generated CMs, could successfully regenerate the failing heart. It would be important to ascertain whether the beneficial role of epicardium is diminished by cardiac injury as a precursor to testing such a hypothesis.

1:5 Epicardium Reactivates in Response to Cardiac Injury

After development, the adult epicardium is quiescent; described as early as P4 in mouse, with reciprocal myocardial quiescence (Chen et al. 2002). In the adult mammalian heart, the epicardium is reactivated organ-wide in response to myocardial injury (Smart et al. 2007; van Wijk et al. 2012; Zhou et al. 2011; Huang et al. 2012). As during development, the reactivated epicardium rapidly undergoes EMT, invades the subepicardial space and differentiates into cardiac fibroblasts (van Wijk et al. 2012; Zhou et al. 2011; Huang et al. 2012). However, this process led to scarring, dysfunctional contractility, and heart failure (Zhou et al. 2011; Cao and Poss 2018). This process is in stark contrast to the epicardium's role during development, hinting at key differences between foetal vs adult epicardium (Moerkamp et al. 2016; Wang et al. 2020). Chen and colleagues compared human foetal and adult EPDCs and found that foetal EPDCs more readily undergo EMT, suggesting a 'primed' state (Chen et al.

2002). As our hESC-derived epicardium is foetal-like (Iyer et al. 2015), this critical observation implies a more developmental-like response to hESC-derived CMs.

The reactivation of epicardium in response to cardiac injury favourably resulted in cardiac regeneration in the adult zebrafish and neonatal mice (Lepilina et al. 2006; Kikuchi et al. 2011; Wang et al. 2011; 2013; González-Rosa et al. 2012; Cao and Poss 2018); both of which are relatively rudimentary and immature cardiac models compared to the adult mammalian heart. Teasing apart the fundamental differences between foetal and adult epicardium could greatly aid our cardiac regenerative efforts. Next, I shall discuss the observations in different model systems and signalling pathways underpinning epicardial-myocardial crosstalk.

1:5:1 The epicardium in zebrafish cardiac regeneration

Adult epicardium plays a crucial role in zebrafish cardiac regeneration. Upon cardiac injury, the epicardium reactivates organ-wide with re-expression of its embryonic genes, undergoes EMT, proliferates and differentiates to EPDCs at the site of injury (Lepilina et al. 2006; Kikuchi et al. 2011; Wang et al. 2011; 2013; González-Rosa et al. 2012; Cao and Poss 2018). Genetic fate-mapping of *tcf21*⁺ cells in both larval and adult zebrafish revealed restriction of EPDCs to non-myocardial fate - EPDCs differentiated to cardiac fibroblasts and vascular cells (Kikuchi et al. 2011). This is conserved throughout development and cardiac regeneration (Kikuchi et al. 2011). A cytotoxic ablation of *tcf21*⁺ epicardial cells in adult zebrafish led to 45% epicardial loss, which rapidly repopulated within a few days (Kikuchi et al. 2011). During this transient epicardial loss, the *tcf21*-ablated zebrafish demonstrated poor cardiac regeneration

and vascularization after apical resection, which rapidly reversed upon epicardial repopulation (Kikuchi et al. 2011).

Intriguingly, the reactivated epicardium regularly migrates from ventricular base to apex (Cao et al. 2017). Cao *et al.* showed elegantly that a 'leader wave' of EPDCs marches forward by mechano-sensing the tension edge, thereby guiding the proliferating CMs to the site of injury (Cao et al. 2017). The epicardium's role in orchestrating the zebrafish's cardiac regeneration is not only critical but also displays spatiotemporal specificity (Mercer et al. 2013).

The reactivated epicardium is a potent mitogen for robust cardiomyocyte proliferation and cardiac regeneration. This process is underpinned by active epicardial-myocardial crosstalk which encompasses a wide range of signalling pathways: FGF signalling, retinoic acid signalling, TGF- β signalling, Notch signalling, NF- κ B, PDGFs, Wnt/ β -catenin, Hedgehog, BMP, Hippo/Yap, insulin-like growth factor, chemokines and Neuregulin1. Given the multimodal cellular functions of the epicardium, this broad range of signalling effectors is hardly surprising. An exhaustive summary of the effector pathways implicated in epicardial-myocardial crosstalk are listed in **Table 1**. Several effector pathways are conserved across different species such as zebrafish, neonatal mouse, and neonatal rat. Collectively, these pathways reaffirmed that the reactivated epicardium plays a wide-ranging role in orchestrating different cell types in enabling robust cardiac regeneration.

Signaling	Models	Gene induction domains upon cardiac injury and epicardial reactivation	Cell Type with Genetic Induction	Associated Functional Gains	References
Fibroblast Growth Factors (FGFs)	Zebrafish	<i>fgf17b</i>	CMs	Cardiac regeneration	Lepilina, 2006
		<i>fgfr2</i> and <i>fgfr4</i>	epicardial-derived cells		
	Rat	<i>FGF1</i>	inflammatory cells, fibroblast-like cells		Zhao et al. 2011
		<i>FGF2</i>	endothelial cells, CMs		
<i>FGFR</i>		CMs			
Retinoic Acid (RA)	Zebrafish	<i>raldh2</i>	epicardium, endocardium	CM proliferation and regeneration	Kikuchi et al., 2011; Lepilina et al., 2006
	Mouse	<i>Raldh2/RXRα</i>	epicardium		van Wijk et al. 2012; Merki et al. 2005
Transforming Growth Factor- beta (TGFβ)	Zebrafish	<i>tgfb1, 2, and 3</i>	epicardial cells, fibroblasts, CMs	ECM deposition, CM proliferation, and heart regeneration	Choi et al. 2013; Chablais and Jaźwińska 2012; Cao et al. 2016
		<i>Alk5b</i>	CMs, fibrotic cells		
		<i>pSmad3</i>	CMs, non-CMs at infarct area		
Notch	Zebrafish	<i>notch1a, notch1b, and notch2</i>	Endocardium	Reduced scar formation, CM proliferation and heart regeneration	Zhao et al. 2014; Münch et al. 2017
		<i>notch1a and notch2</i>	epicardium		
		<i>notch1b, notch2, notch3, and Dll4</i>	endocardium		
	Mouse	<i>Notch activity reporter</i>	CMs, epicardial cells/EPDCs	CM proliferation	Kratsios et al. 2010; Russell et al. 2011
		<i>NICD1</i>	CMs		
Platelet-Derived Growth Factors (PDGFs)	Zebrafish	<i>pdgfrβ</i>	Epicardium, fibrin clots	epicardial cell proliferation and coronary blood vessel formation	Kim et al. 2010
		<i>pdgfb</i>	Thrombocytes at the wound site		
	Mouse	<i>PDGFB, PDGFRα, PDGFRβ</i>	Infarct zone	Collagen deposition, vascularization maturation within infarct zone	Zymek et al. 2006
		phosphorylated PDGFRβ	Perivascular cells in the infarct zone		
Wnt	Mouse	<i>Wnt1</i>	Epicardium, cardiac fibroblasts	Epicardial EMT	Duan et al. 2012
		<i>Wnt10b</i>	CMs in the peri-infarct area	Neovascularization, fibrosis	Paik et al. 2015
BMP	Zebrafish	<i>bmp2b, bmp7</i>	Epicardium, endocardium	CM proliferation, scar attenuation	Wu et al. 2016
		<i>bmpr1aa</i>	Wound border zone		
		<i>id2b</i>	endocardium		
		pSmad1/5/8	CMs		

	Mouse	<i>Bmp4</i>	Whole heart	Reduced infarct size, increased CM survival	Pachori et al. 2010
Hippo/Yap	Mouse	<i>Yap, Taz, Tead1-3, Lats1 and Lats2</i>	epicardium	Epicardial EMT, immunomodulation	Lin and Pu 2014; Ramjee et al. 2017; Xiao et al. 2018

Table 1: Signalling effector pathways utilised during epicardial-myocardial crosstalk.

These studies covered the epicardial signalling during cardiac injury across different animal models. (Adapted from Cao et al. 2018)

Apart from signalling factors, zebrafish cardiac regeneration involves several epicardial-derived ECM proteins such as fibronectin (FN), collagen, and hyaluronic acid (HA) (Mercer et al. 2013). ECM provides signalling and mechanical cues for accurate cardiac regeneration (Mercer et al. 2013; Garcia-Puig et al. 2019). Strikingly, zebrafish heart regenerates completely without scarring, hinting at a more dynamic ECM turnover. In the zebrafish, epicardially-secreted FN (induced by *fn1* expression) upregulated integrin- β 3 in CMs to enable cardiac regeneration (Trinh and Stainier 2004; Wang et al. 2013). With *fn1* disruption, cardiac regeneration is also disrupted with resultant scarring (Wang et al. 2013; Cao and Poss 2018). Thus, epicardially-secreted FN (epicardial-FN) may underpin both CM proliferation and migration in zebrafish's cardiac regeneration. The potential of FN and integrin signalling in modulating cardiac regeneration, in the context of epicardial-myocardial crosstalk, is expanded upon in *Section 1:10:1*.

1:5:2 The epicardium in neonatal mouse cardiac regeneration

The epicardium also plays a role in the neonatal mouse's cardiac regeneration, albeit understudied compared to the zebrafish. Similar to the zebrafish, the neonatal mouse can regenerate its heart within the P1-7 'regenerative window', as discussed in

Section 1:3:2. Rui *et al.* showed that regular injections of Thymosin β 4 prolonged the regenerative window in neonatal mice and that this process was underpinned by *Wt1*+ epicardial-derived cells and *islet1* cells (Rui *et al.* 2014). Thymosin β 4 was also a potent inducer of adult EPDC migration and neovascularization of the infarcted mouse heart (Smart *et al.* 2007). Meanwhile, agrin, an extracellular matrix protein isolated from the P1 neonatal mouse heart, evoked cardiomyocyte proliferation via Yap-mediated and Erk-mediated pathways to regenerate the heart and improve cardiac function post-MI in both mouse and pig MI models (Bassat *et al.* 2017; Baehr *et al.* 2020). Recently, a preprint pinpointed agrin's role in regulating epicardial epithelial-mesenchymal transition (EMT) (Sun *et al.* 2020). The importance of epicardium in cardiac regeneration appears to be conserved across zebrafish and neonatal mammals.

Perhaps unsurprisingly, the key events and pathways implicated in cardiac development, together with cardiac regeneration in 'lower' vertebrates, mechanistically converge. A key overlapping process appeared to be epicardial-myocardial crosstalk invoked during cardiac development and injury. Thus, epicardial-myocardial crosstalk may underlie the functional benefits delivered by cardiac regenerative cellular therapies.

1:6 Endogenous Cardiac Regeneration

Based on the insights from cardiac regeneration in 'lower' vertebrates and cardiac development across all species, developing cardiac regeneration as a therapy for heart failure patients appears feasible- challenging but possible. Two key principles

stood out: i) generation of new CMs and ii) non-cardiac stromal cells required to instruct the new CMs to form functional cardiac tissue. So, how could cardiac regeneration be invoked? Broadly, either the heart could be triggered to generate new CMs (endogenous cardiac regeneration) or new exogenously derived cells could be delivered into the heart (exogenous cardiac regeneration). Both approaches still require key stromal cells. Firstly, I will discuss the feasibility of endogenous cardiac regeneration as heart failure therapy.

1:6:1 Cardiomyocyte formation in the adult human heart

In the adult mammalian heart, new CMs are generated from the replication of pre-existing CMs as part of normal, cellular homeostasis and, controversially, possibly after myocardial injury (Senyo et al. 2013). In the absence of injury, the generation of new CMs occurs at a low rate of ~1% per year at age 20, as confirmed by carbon-dating studies (Bergmann et al. 2009). Drawing upon our understanding of mammalian cardiac embryogenesis and neonatal cardiac regeneration, the key difference with adult CM proliferation appears to be the rate, and a preference for a hypertrophic response rather than hyperplasia (Vagnozzi, Molkentin, and Houser 2018). Mimicking the endogenous cardiac regeneration demonstrated by adult zebrafish and neonatal mice as a clinically relevant strategy will require altering this preference to increase the proliferation rate of pre-existing CMs.

1:6:2 Gene therapy – proliferation by pre-existing cardiomyocytes

Several genetic modifiers have enabled us to coax pre-existing CMs into proliferation, in response to myocardial injury. A cocktail of pre-selected microRNAs (miRNAs), delivered exogenously in neonatal and infarcted adult mice, promoted the proliferation of pre-existing CMs with cardiac functional recovery (Eulalio et al. 2012). The microRNAs were pre-selected from P1 neonatal rats, within the 'regenerative window', thus hinting at specific genetic modifiers downregulated with age (Eulalio et al. 2012). The delivery of a similar cocktail of miRNAs into an infarcted pig model showed cardiac functional recovery (Gabisonia et al. 2019). Unfortunately, the pigs' cardiac recovery was complicated by life-threatening tachyarrhythmias, potentially triggered by the immature, proliferating CMs (Gabisonia et al. 2019). Another group independently demonstrated that reactivation of *Myc* in adult CMs triggered a robust proliferative response (Bywater et al. 2020). Despite these breakthrough studies, the life-threatening tachyarrhythmias and the oncogenic potential of *Myc* re-expression remain significant roadblocks to safe clinical translation.

1:6:3 Gene therapy - direct reprogramming of cardiac fibroblasts into cardiomyocytes

Another approach involves reprogramming cardiac fibroblasts into CMs. Srivastava and colleagues elegantly showed that adult cardiac fibroblasts could be reprogrammed into CMs via three developmental transcription factors

(*Gata4/Mef2c/Tbx5*) (Ieda et al. 2010; Qian et al. 2012) Concomitantly, myocardial fibrosis was reduced (Muraoka and Ieda 2014). Although demonstrable in different animal models, from subacute to chronic injury models, there appears to be partial reprogramming with a low reprogramming rate (~20%) (Chen et al. 2012). Despite attempts at improving the reprogramming factors with *HAND2* and suppression of pro-fibrotic signalling, there were insufficient reprogrammed CMs to recover cardiac pump function (Song et al. 2012; Zhao et al. 2015). With this direct CM reprogramming approach, the insufficient scalability and associated risks of long-term transgenic insertion of reprogramming factors are major drawbacks for clinical translation.

A summary of the current key strategies to invoke adult cardiomyocyte proliferation and regeneration is shown below, **Figure 6**. All these strategies are based on the latest, applied understanding of endogenous regeneration in adult zebrafish and neonatal mice, together with exogenous cardiac regeneration strategies such as human embryonic-derived stem cells (hESC cells) and induced pluripotent stem cell (iPSC) therapy. hESC/iPSC-derived CM-based cellular therapy is emerging as a prominent player in translational strategies for cardiac regeneration and will be discussed next.

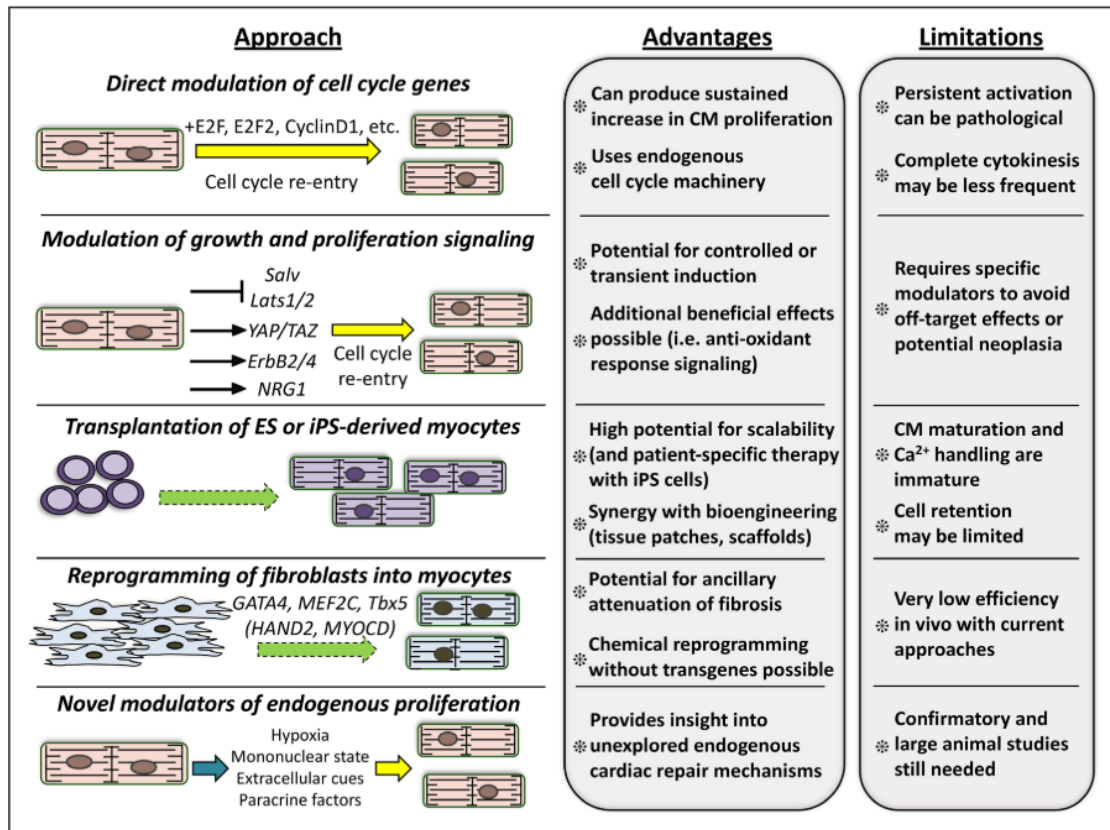


Figure 6: Cardiac regenerative strategies: Their advantages and limitations

All these strategies aim to directly replace the CMs lost after myocardial infarction. Ultimately, ‘primary remuscularization’ would improve cardiac contractile function, thereby preventing and/or attenuating heart failure. These approaches range from genetic inducers, pharmacological agents, and exogenous cellular therapy, all underpinned by our mechanistic understanding of cardiac development to date. CM indicates cardiomyocyte; ES, embryonic stem; and iPS, induced pluripotent stem. (Adapted from Vagnozzi et al., 2018)

1:7 Exogenous Cardiac Regeneration

Exogenously delivered cellular therapy is an attractive alternative, given the significant roadblocks faced by endogenous cardiac regeneration. This is broadly termed ‘exogenous cardiac regeneration’. Like endogenous cardiac regeneration, the purpose is to generate new CMs exogenously to replenish the loss of CMs after MI, thus leading

to improved cardiac pump function. Rather than relying on pre-existing CMs to proliferate, cellular therapy could be delivered as an 'off-the-shelf' clinical therapy (Fernández-Avilés et al. 2017). Thus, cellular therapy represents a safer, scalable, more convenient, and clinically relevant way to regenerate the heart (Vagnozzi, Molkenin, and Houser 2018; Bertero and Murry 2018; Murry and MacLellan 2020). With major advances over the last two decades, the full potential of exogenous cardiac regeneration is nearly realised. I will first describe the ground-breaking advances in this field, the challenges overcome and discuss how my doctoral work aims to address the next pivotal step towards clinical translation.

Initially, exogenous cardiac regeneration stemmed from the hypothesis that non-cardiac progenitors can transdifferentiate into CMs if placed within the right niche, i.e., the heart (Ptaszek et al. 2012). Based on this transdifferentiation concept and ease of access, the earliest non-cardiac progenitors trialled were skeletal myoblasts, bone-marrow derived stem cells and c-Kit⁺ cardiac progenitor cells. An overview of cellular therapies trialled to date are shown in **Figure 7**.

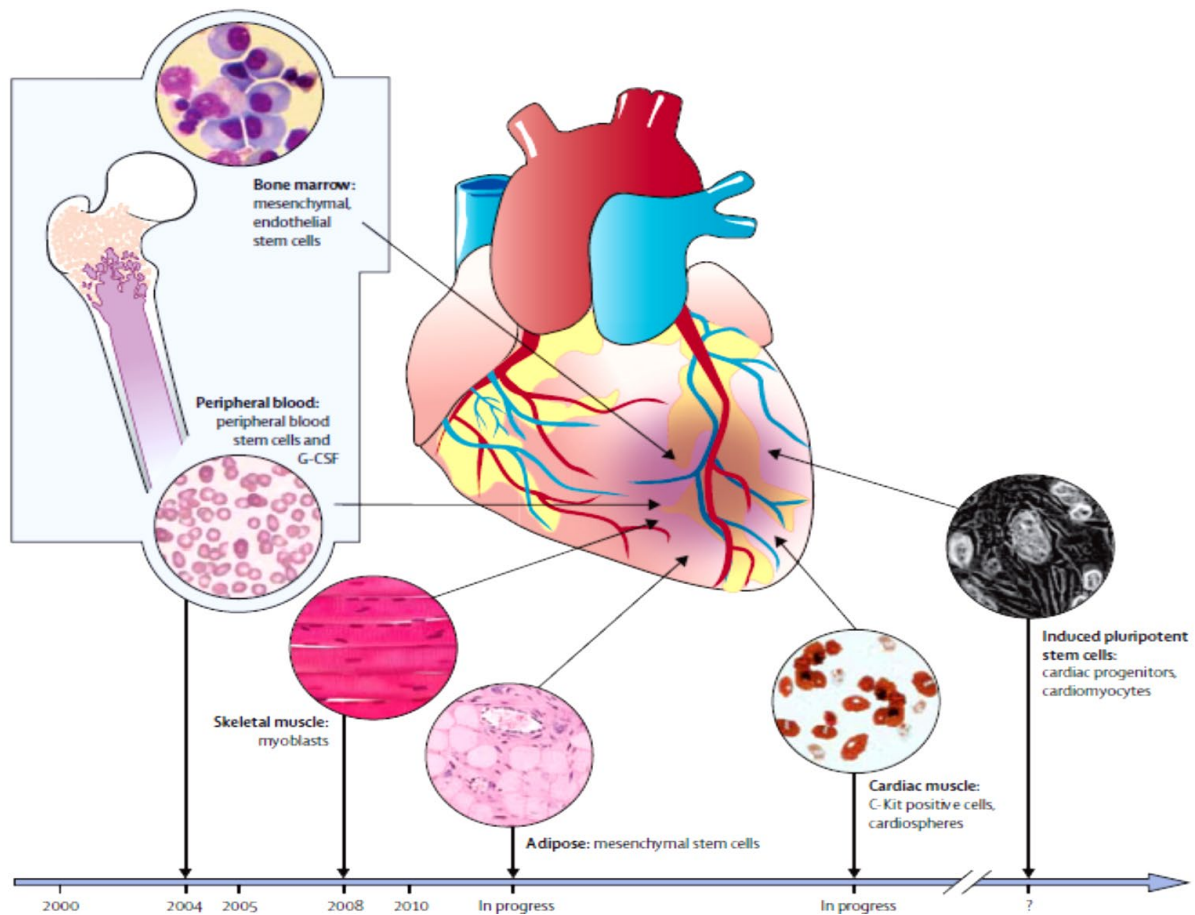


Figure 7: Overview of all cellular therapies currently in human trials

A Bone marrow-derived stem cells represent the first cells used with pleiotropic effects. **B** The field then shifted to a contractile cell type, skeletal myoblast. **C** Due to arrhythmias, the field shifted back into MSCs, a non-contractile cell type. BMMNCs, MSCs and skeletal myoblasts represent first-generation cellular therapy. **D** ‘Discovery’ of c-KIT+ cardiac stem cells proved controversial **E** Advances of hESC/IPSC technologies led to ESC/IPSC-derived CMs, a highly efficient, scalable, and lab-grown contractile cell type with clear translational potential. Second-generation cell therapy comprises other cardiac progenitor cells (CPCs), hESC-derived and IPSC-derived CMs or cardiac progenitor cells. (Adapted from Ptaszek et al, 2012)

1:7:1 Skeletal myoblasts

As skeletal myoblasts are immature ‘satellite cells’ and can regenerate new skeletal muscle, the initial hypothesis was that these cells could transdifferentiate into CMs within the heart. In 1998, Taylor and colleagues first showed that engrafted skeletal

myoblasts improved cardiac function in rabbits after MI (Taylor et al. 1998) - an outcome which was reproducible in other pre-clinical studies (Ptaszek et al. 2012). Three years later, Menasche and colleagues performed the world's first cellular therapy in a patient by injecting skeletal myoblasts into the patient's heart during cardiac surgery (Menasché et al. 2001).

Despite surfacing doubts about the ability of skeletal myoblasts to transdifferentiate into CMs (Reinecke et al. 2002), a multicentre, randomised myoblast autologous grafting in ischaemic cardiomyopathy (MAGIC) trial was conducted with over 120 patients (Menasché et al. 2008). Although a ground-breaking trial, the MAGIC trial reinforced the findings that skeletal myoblasts did not transdifferentiate into CMs when injected into the heart (Menasché et al. 2008; Ptaszek et al. 2012). These cells became skeletal myocytes instead. Skeletal myocytes' inherent lack of connexin-43 gap junctions made electrical integration with CMs difficult, thus triggering life-threatening ventricular arrhythmias (Roell et al. 2007; Menasché et al. 2008). Failure of skeletal myoblasts to transdifferentiate into CMs carried significant clinical risks and was abandoned as a potential cellular therapy.

1:7:2 Adult stem cells - bone marrow mononuclear cells

In the 1990s, scientists were quite enthusiastic about the potential of adult stem cells to regenerate the infarcted heart (Tompkins et al. 2018). Then, the scientific studies focused upon the use of adult stem cells derived from the bone marrow, which were termed as bone marrow mononuclear cells (BMMNCs) (Banerjee et al. 2018; Tompkins et al. 2018). Initially, there was wide-spread belief that adult stem cells were highly plastic and could 'transdifferentiate' into any cell type, if placed within the right

organ (Krause et al. 2001; Priller et al. 2001; Corbel et al. 2003). Furthermore, gender chimerism in transplanted hearts was observed (Quaini et al. 2001). Thus, the theory of ‘transdifferentiation’ took a stronghold in this field; circulating adult stem cells would home into the heart and ‘transdifferentiate’ into CMs (Orlic et al. 2001). A flurry of pre-clinical studies utilising adult stem cells to salvage the failing heart ensued rapidly. However, the results remained vague (Nowbar et al. 2014; Fisher et al. 2016).

In 2001, Orlic *et al.* claimed to show that injected BMMNCs ‘transdifferentiated’ into CMs in the heart (Orlic et al. 2001). Strikingly, the BMMNCs successfully made new myocardium, which occupied up to 68% of the infarcted heart (Orlic et al. 2001). Within a year, this study was translated into human clinical trials, (Strauer et al. 2001). The usage of BMMNCs to regenerate the infarcted heart escalated rapidly (Strauer et al. 2002; Wollert 2004; Assmus et al 2006). However, we would do well to remember that BMMNCs have a haematopoietic origin (Wagers et al. 2002; Chien et al. 2019). Several lineage-tracing studies showed that BMMNCs do not transdifferentiate into CMs, but rather into adult haematopoietic cells in the heart (Murry et al. 2004; Nygren et al. 2004; Balsam et al. 2004). By now, the ‘transdifferentiation’ theory as proposed by Orlic *et al.* had been mostly refuted (Murry et al. 2004; Nygren et al. 2004; Balsam et al. 2004). However, a more malignant idea has taken hold e.g. c-Kit⁺ cells (discussed in *Section 1:7:3*).

Due to the lack of BMMNCs’ ability to ‘transdifferentiate’, it is now widely believed that BMMNCs exerted benefits via paracrine signalling (Gnecchi et al. 2008). BMMNCs were postulated to have pleiotropic effects, which encompassed wide immunosuppressive activity, ECM-modulatory, antiapoptotic and pro-angiogenic effects to promote cardiac repair (Sanganalmath et al. 2013). Pre-clinical studies and Phase II & III clinical trials with BMMNCs showed modest improvements in cardiac

function (Chen et al. 2004; Lalu et al. 2018; Tompkins et al. 2018). However, exhaustive meta-analysis (Damascene Study) (Nowbar et al. 2014) and a Cochrane review (Fisher et al. 2016) showed that the BMMNC-mediated cardiac repairs were not statistically significant. The efficacy of paracrine-mediated cardiac recovery by BMMNCs remains under intense scrutiny.

BMNNCs induced the influx of macrophages to the infarcted heart which likely led to modest cardiac recovery. 20 years after the first BMMNC pre-clinical study, Vagnozzi and colleagues showed that the functional benefits of adult stem cell therapy were due to acute inflammatory responses, secondary to the accumulation of CCR2⁺ and CX3CR1⁺ macrophages which were invoked by the adult stem cells themselves (Vagnozzi et al. 2020). Similar cardiac functional gains were observed upon the delivery of zymogen, a sterile inducer of the innate immune response, within infarcted mouse hearts (Vagnozzi et al. 2020). Thus, utilising macrophages to evoke cardiac repair appears promising.

Drawing upon all the studies thus far, adult stem cell therapy is demonstrably unable to generate new CMs to repair the infarcted heart. Nonetheless, the BMNNCs' paracrine effects on the infarcted hearts warrants further study.

1:7:3 Cardiac Stem Cells - c-Kit⁺ cells

Stemming from the work by Orlic *et al.* on the ability of BMMNCs to 'transdifferentiate' to CMs, Piero Anversa's group proposed that the heart has a multi-potent cardiac stem cell population (Beltrami et al. 2003; Dawn et al. 2005; Linke et al. 2005). These cardiac stem cells carried the same c-Kit⁺ marker as bone marrow cells and were

presented as a self-renewing source of CMs in the heart (Beltrami et al. 2003; Dawn et al. 2005). As discussed in *Section 1:6:1*, the heart can self-renew via the proliferation of pre-existing CMs, albeit at a low rate ~1% per year (Bergmann et al. 2009). Pre-clinical studies reported that the transplantation of isolated human c-Kit⁺ CMs overwhelmingly regenerated the infarcted heart, with up to 70% recovery (Beltrami et al. 2003; Dawn et al. 2005; Bearzi et al. 2007). A phase I clinical trial (SCIPIO) rapidly followed (Bolli et al. 2011) with reports of similar cardiac gains. Notably, the mechanisms underlying the reported benefits of c-Kit⁺ cardiac stem cells were not elucidated prior to the clinical trials.

Meanwhile, other laboratories started demonstrating that c-Kit⁺ cells did *not* differentiate into CMs after transplantation (Pouly et al. 2008; Zaruba et al. 2010). Two independently published studies, with five novel c-Kit⁺ lineage-tracing mouse models (Sultana et al. 2015) and two c-Kit⁺ lineage-tracing mouse models (Van Berlo et al. 2014) respectively, showed exhaustively that c-Kit⁺ cells maintain endothelial identity post-infarct and contribute minimally towards *de novo* cardiomyocyte formation during development and ageing (Van Berlo et al. 2014). Instead, c-Kit⁺ cells contribute primarily to the generation of cardiac endothelial cells (Li et al. 2018), and previous reports of c-Kit⁺ CMs may have arisen from artefactually labelled leucocyte fusion with CMs (Maliken et al. 2018). The robust c-Kit⁺ lineage-tracing studies, coupled with the lack of reproducibility by other laboratories, unequivocally proved that c-Kit⁺ cells are not cardiac stem cells and cannot regenerate the heart (Van Berlo et al. 2014; Sultana et al. 2015; Maliken et al. 2018; Li et al. 2018).

Although scientific progress benefits from hindsight and many truths were later uncovered with better technology, many of Piero Anversa's scientific works were

deemed fraudulent by a 5-year investigation carried out by Brigham and Women's Hospital and Harvard University - up to 31 scientific papers were retracted (Chien et al. 2019). This rebuke remains as a cautionary tale to the cardiac regenerative scientific community; any participant of the global race to regenerate the heart needs to demonstrate scientific rigour, robustness, and reproducibility.

The interwoven lessons from BMMNCs and c-Kit⁺ cells were that our mechanistic understanding of exogenously delivered cellular therapy needs to parallel the observed cardiac functional gains. The 'transdifferentiation' theory was laid to rest. So far, the beneficial paracrine effects conferred by adult stem cells therapy remain under interrogation. However, generation of new CMs is still central to exogenous cardiac regeneration and could be fulfilled by another approach.

1:7:4 hESC/IPSC – derived cardiomyocytes

The next approach is simple - deliver new contractile CMs to replenish the irreversible loss of CMs after MI. This approach is termed as 'primary remuscularization'. Proof-of-concept studies successfully utilised foetal/neonatal rat CMs (NRVMs) via cellular injections (Etzion et al. 2001) or patches (Zimmermann et al. 2002) to evoke cardiac recovery in the acute/subacute MI setting. Obviously, we cannot translate the use of human-derived foetal/neonatal CMs into clinics. With advances in human embryonic stem cell (hESC)-derived cells (Kehat et al. 2001) and IPSC-derived cellular technologies (Takahashi and Yamanaka 2006; Yoshida and Yamanaka 2017), laboratories could generate hESC/IPSCs-derived CMs. hESC/IPSC-derived CMs are foetal-like, display classical cardiac transcription factors, e.g., *Nkx2.5*, *Gata4*, and

Mef2c, and have contractile function (Vagnozzi et al. 2018). Thus, 'primary remuscularization' with hESC/IPSC-derived CMs holds great translational potential for regenerating the infarcted heart (Leor et al. 2007; Linda W. van Laake et al. 2007).

Over the last decade, huge strides have been made by using hESC/IPSC-derived CMs in cardiac regeneration. Early studies recorded transient cardiac functional gains (Linda W. van Laake et al. 2007). With the hESC/IPSC technology then at its infancy, CMs were cultured as embryoid bodies with contamination by other stromal cells. hESC-derived CMs barely survived *in vivo* (Kehat et al. 2001). Presently, hESC/IPSC-derived CMs are regularly cultured as a monolayer. This culture method increased the efficiency of large-scale CM generation with ~90% cells displaying the cardiac troponin T protein (cTNT) (Burrige et al. 2012; Yoshida and Yamanaka 2017). Thus, hESC/IPSC-derived CMs are increasingly viewed as an accessible and highly scalable source of new CMs.

Multiple groups independently showed that injected hESC/IPSC-derived CMs survived, formed new cardiac grafts to 'remuscularize' the infarcted heart, and were accompanied by cardiac functional recovery (Laflamme et al. 2007; Shiba et al. 2013; Gerbin et al. 2015; Shiba et al. 2016; Kawamura et al. 2016; Liu et al. 2018). Specifically, hESC/IPSC-derived CMs delivered at subacute time points after MI, attenuated cardiac dysfunction post-MI (Laflamme et al. 2007; Shiba et al. 2013; Gerbin et al. 2015; Shiba et al. 2016; Kawamura et al. 2016; Liu et al. 2018). The observations of cardiac repair were reproduced by different groups in various animal models, ranging from mice, rats, guinea pigs to non-human primates (Chong et al. 2014; Shiba et al. 2013; 2016; Liu et al. 2018). The highest LVEF% improvement post-MI was ~12.4% in non-human primates (Liu et al. 2018), comparable to the LVADs

discussed in *Section 1:2:4*. Simply put, the exogenously delivered CMs contributed towards the contractile function of the infarcted heart, in the subacute MI setting.

Cellular therapy with hESC/IPSC-derived CMs resulted in sustained and reproducible cardiac recovery MI (Laflamme et al. 2007; Shiba et al. 2013; Gerbin et al. 2015; Shiba et al. 2016; Kawamura et al. 2016; Liu et al. 2018). However, several key challenges remained, *Section 1:8:2*. Strategies to overcome these challenges such as combinatorial cellular therapy and tissue-engineering adjuncts would be discussed in *Section 1:10*. Nonetheless, the avalanche of reproducible results over the last 20 years, had propelled hESC/IPSC-derived CMs forward as the major cell type to invoke exogenous cardiac regeneration (Eschenhagen et al. 2017; Bertero and Murry 2018). First-in-man trials are now imminent in various countries (Murry and MacLellan 2020).

1:8 Cardiomyocyte-based Cellular Therapy for Chronic Heart Failure

Exogenous delivery of hESC/IPSC-derived CMs to ‘remuscularize’ the infarcted heart, holds great promise as the ideal heart failure treatment. Cellular therapy with hESC/IPSC-derived CMs, would replace the loss of CMs, be universally accessible and sustainable in the long-term. Unfortunately, the cardiac regenerative community has not directly addressed chronic heart failure. In cardiac regeneration, successes with hESC/IPSC-CMs were only demonstrated at subacute time points after MI, coinciding with the healing phase post-MI (Laflamme et al. 2007; Shiba et al. 2013; Gerbin et al. 2015; Shiba et al. 2016; Kawamura et al. 2016; Liu et al. 2018). However, reversing heart failure secondary to chronic MI, represents an urgent clinical

challenge. Chronic heart failure carries a 50% 5-year mortality (Jones et al. 2019) and affects 64.3 million people, globally (James et al. 2018).

It is widely acknowledged that a chronically infarcted heart is harder to salvage than subacute infarcts in the middle of a healing phase (Jessup and Brozena 2003). The challenges are due to large areas of scarring, poor vascularisation, adverse remodelling, and the establishment of maladaptive neurohormonal activation (Pfeffer et al. 1991; Jessup and Brozena 2003; Hartupée and Mann 2016; Frangogiannis and Kovacic 2020), **Figure 8**. However, the adult zebrafish showed that they could form new cardiac muscle over a chronic, 60-day-old scar with 90% of injury sites showing histological evidence of remuscularization (Kikuchi et al. 2010). This observation hinted that cardiac regeneration within the chronic infarct environment is possible, albeit an illustration of endogenous cardiac regeneration (Kikuchi et al. 2010). Next, I will discuss the results from hESC/IPSC-derived CMs monotherapy in the chronic MI setting, together with inherent hESC/IPSC challenges that led to the negative results. Then, I would discuss how I planned to test the feasibility of cellular therapy in regenerating the chronically infarcted myocardium.

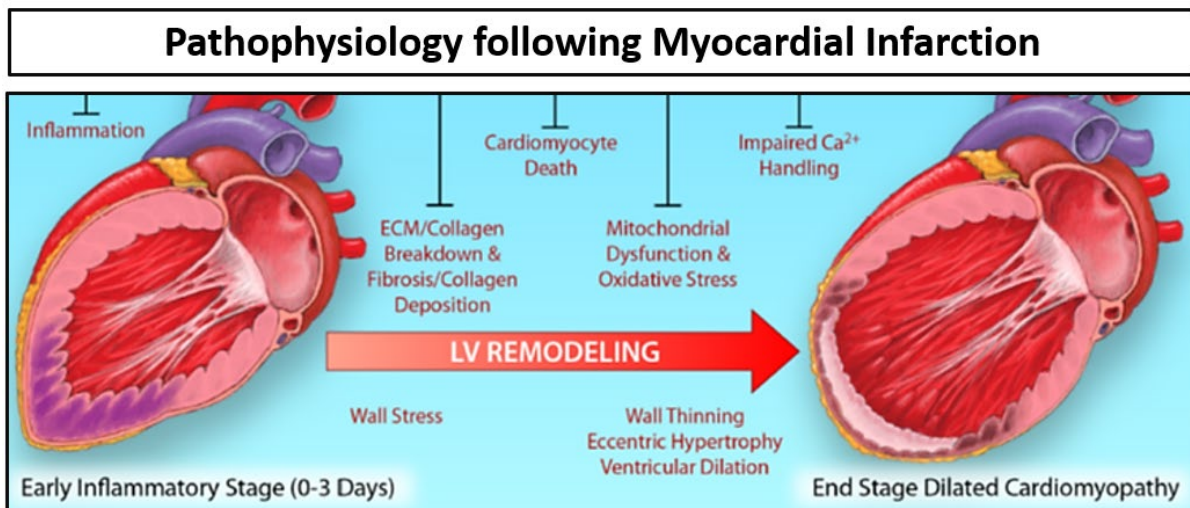


Figure 8: Sequences of events at the cellular, ECM and tissue level after MI

After MI, acute inflammation sets in over 0-3 days, followed by rapid ECM breakdown with collagen and fibrosis deposition with changes in wall stress. Ongoing CMs death led to further mitochondrial dysfunction with oxidative stress and impaired Ca²⁺ handling. At the organ level, the left ventricle (LV) extensively remodels with wall thinning, eccentric hypertrophy, and ventricular dilatation; eventually leading to end-stage dilated cardiomyopathy (chronic heart failure). (Adapted from Frangogiannis et al, 2020)

1:8:1 Cellular therapy with hESC/IPSC-derived cardiomyocytes alone

hESC/IPSCs-derived CMs successfully engrafted within the chronically infarcted myocardium but without a corresponding cardiac recovery in both rat (Fernandes et al. 2010) and guinea pig chronic MI models (Shiba et al. 2014). These studies used physiologically relevant cellular doses, cellular preconditioning with the pro-survival cocktail and measured cardiac function with MRI (Fernandes et al. 2010; Shiba et al. 2014). With direct intramyocardial injections in the chronic MI rat model, the graft sizes at 1-month post-cellular injection were reported at 0.83±0.22% of the left ventricle

(Fernandes et al. 2010), compared to $1.1 \pm 0.5\%$ of the left ventricle in the subacute MI rat model (Gerbin et al. 2015). As for the guinea pig, Shiba *et al.* showed that hESC-CM grafts at 1-month post-injection constituted $3.3 \pm 0.7\%$ of the scar area in chronic MI (Shiba et al. 2014) vs $8.4 \pm 1.5\%$ of the scar area in subacute MI (Shiba et al. 2013). Notably, all studies using primary or hESC/IPSC-derived CMs monotherapy showed minimal graft sizes in the chronic MI setting (Li et al. 1996; Sakakibara et al. 2002; Huwer et al. 2003; Fernandes et al. 2010; Shiba et al. 2014).

Compared to the subacute MI setting, is the lack of improvement cardiac function in the chronic MI setting solely due to smaller cardiac grafts? Studies reported a linear correlation between graft sizes and degree of cardiac repair in the subacute MI setting (Liu et al. 2018; Bargehr et al. 2019). Given that a chronically infarcted heart is far sicker, one reasoned that larger cardiac grafts would be required to improve cardiac function in this setting. Apart from size, the cardiac grafts also need to be mature (Karbassi et al. 2020) and electrically couple with the host tissue (Shiba et al. 2014). Thus, I hypothesized that the augmentation of these key graft-specific factors (i.e., size, maturation, electrical connectivity) would contribute a greater contractile function; capable of reversing chronic heart failure.

Regardless of subacute or chronic MI setting, achieving sizeable, mature and electrically coupled cardiac grafts are inherent challenges with using hESC/IPSC-derived CMs alone to regenerate the infarcted heart (Bertero and Murry 2018). Given the increased hostility of the chronically infarcted environment, these challenges are amplified. Next, I will discuss the specific challenges and how I aim to tackle them.

1:8:2 Challenges with hESC/IPSC-derived cardiomyocytes alone

With hESC/IPSC-derived CMs monotherapy, there are specific challenges in obtaining sizeable, mature and electrically coupled cardiac grafts. The challenges comprised of significant cell death ~80% within 24hrs of delivery (Zhang et al. 2001; Müller-Ehmsen et al. 2002; Laflamme et al. 2007), CM maturation (Kadota et al. 2017; Karbassi et al. 2020), inconsistent electrical integration with the host tissue with arrhythmias (Shiba et al. 2013; Liu et al. 2018), lack of vascularization (Bertero and Murry 2018) and immunogenicity concerns (Kawamura et al. 2016; Shiba et al. 2016). All these challenges resulted in variable cardiac graft sizes in the subacute MI setting (Laflamme et al. 2007; Shiba et al. 2013; Gerbin et al. 2015; Shiba et al. 2016; Kawamura et al. 2016; Liu et al. 2018). I will discuss the advances made to overcome these challenges and address how the challenges specific to chronic MI could be tackled.

1:8:2:1 Cardiomyocyte survival

In earlier proof-of-concept cellular therapy studies, very few hESC/IPSC-derived CMs survived or engrafted after intramyocardial injections into infarcted rats (Etzion et al. 2001; Linda W. van Laake et al. 2007; Leor et al. 2007). To enhance hESC-derived CMs' survival, LaFlamme and colleagues developed the pro-survival cocktail (PSC) to ameliorate the effects of *anoikis* and various apoptotic pathways that lead to hESC-CM's death upon injection in the post-infarct setting (Laflamme et al. 2007). PSC included Matrigel to prevent *anoikis* (Zvibel, Smets, and Soriano 2002), a cell-permeant peptide from Bcl-XL to block mitochondrial death pathways (Cao et al.

2002), cyclosporine A to attenuate cyclophilin D–dependent mitochondrial pathways (Baines et al. 2004; Nakagawa et al. 2005), a compound that opens ATP dependent K⁺ channels (pinacidil) to mimic ischemic preconditioning (Ardehali et al. 2005), IGF-1 to activate Akt pathways (Davis et al. 2006) and the caspase inhibitor ZVAD-fmk (Montolio et al. 2005). Delivery of hESC/IPSC-derived CMs in this PSC, led to greater CM survival, engraftment and cardiac recovery (Shiba et al. 2013; 2016; Gerbin et al. 2015; Bargehr et al. 2019).

Furthermore, LaFlamme and colleagues also identified that cellular delivery at four days after MI, greatly improved cell survival (Laflamme et al. 2007; Robey et al. 2009). Four days after MI constitutes the subacute MI setting, which is well-described as a pro-angiogenic, healing phase after MI (Laflamme et al. 2007; Robey et al 2009). The hESC/IPSC-derived CMs were delivered into a favourable tissue environment, thereby improving cellular survival and cardiac engraftment (Laflamme et al. 2007). To extrapolate to the hostile chronic MI setting, PSC would be required in addition to further pro-survival adjuncts. This will be discussed in *Section 1:9 and 1:10*.

1:8:2:2 Cardiomyocyte proliferation

Once engrafted, the hESC/IPSC-derived CMs could proliferate within the infarcted myocardium. Several subacute MI rodent studies confirmed that hESC/IPSC-derived CMs proliferated *in vivo*, with BrdU (5-bromo-2'-deoxyuridine) labelling of proliferating CMs (Laflamme et al. 2005, 2007; Gerbin et al. 2015; Fernandes et al. 2015). hESC/IPSC-derived CMs proliferated in the chronic MI setting, although the reported proliferation was unfortunately not quantified (Fernandes et al. 2010). In the subacute MI setting, the reported proliferative rates ranged widely from 9-15% in rodent and

non-human primate models (LaFlamme et al. 2005, 2007; Liu et al. 2018; Bargehr et al. 2019), hinting that this biological process could be enhanced.

Both CM survival and proliferation are required to form large cardiac grafts *in vivo*. Despite the ~ 80% cellular death within 24hrs of intramyocardial injections (Zhang et al. 2001; Müller-Ehmsen et al. 2002; Laflamme et al. 2007), there were sufficient CM proliferation *in vivo* to form cardiac grafts capable of invoking cardiac repair, in the subacute MI setting (Gerbin et al. 2015; Liu et al. 2018; Bargher et al. 2019). The proliferative ability of the hESC/IPSC-derived CMs reflected their foetal-like stage (Vagnozzi et al. 2018; Guo and Pu 2020). This is a unique advantage of using hESC/IPSC-derived CMs to regenerate the infarcted heart. In the context of the hostile chronic MI environment, whereby large cardiac grafts are required, further augmentation of CM proliferation is desirable.

The next challenges remain fine-tuning the hESC/IPSC-derived CM's proliferation rate and timing. Ideally, we require CM proliferation to form sizeable cardiac grafts, followed by exiting of the cell cycle to mature into efficient, contractile cardiac grafts.

1:8:2:3 Cardiomyocyte maturation

Mature, engrafted hESC/IPSC-derived CMs are needed to contract efficiently in the adult host's heart. However, the maturation of hESC/IPSC-derived CMs grown as a monolayer, is limited to a foetal-like stage (Yang et al. 2014). At the point of cellular injection, the immature ESC/IPSC-derived CMs have an inefficient excitation-contraction coupling apparatus with disorganised sarcomeres and t-tubules, and

loosely packed calcium channels on the sarcoplasmic reticulum (SR) (Karbassi et al. 2020). The CM's maturity level directly affects the efficiency of excitation-contraction coupling and, therefore, its active force generation (Bers 2002; Kane et al. 2015). Thus, more mature CMs are required to contribute a greater contractile force with a greater cardiac functional recovery.

However, immature CMs were shown to integrate better with host tissue (Reinecke et al. 1999; Kadota et al. 2017). Reinecke et al. showed that foetal and NRVMs integrated better than adult rat CMs in infarcted rat hearts, which led to better survival and cardiac engraftment *in vivo* (Reinecke et al. 1999). The efficiency of hESC/IPSC-derived CMs' integration with host myocardium also carry implications for graft: host electrical connectivity, *Section 1:8:2:4*. As the maturity of exogenously delivered CMs affects their ability to integrate with the host myocardium, the optimal balance between the CMs' ability to integrate with host myocardium and CMs' maturity must be sought (Yang et al. 2014; Karbassi et al. 2020).

Despite the recently infarcted myocardium, hESC/IPSC-derived CMs were able to mature *in vivo* (Gerbin et al. 2015; Kadota et al. 2017; Liu et al. 2018; Bargehr et al. 2019). There were histological evidence of immature ssTNI switch to the mature cTNI isoform, together with increased sarcomeric and cellular parameters over time (Gerbin et al. 2015; Kadota et al. 2017; Liu et al. 2018; Bargehr et al. 2019). **Table 2** lists the major differences between immature and mature CMs.

Parameters		Immature CMs	Adult CMs
Morphology	Cell shape	Circular	Rod Shaped
	Membrane capacitance	17.5±7.6 pF	≈150 pF
Myofibril	Sarcomere Structure	Disorganized	Highly aligned
	Sarcomere Length	≈1.6 μm	≈2.2 μm
	T-tubules	No	Yes
Isoform	Titin	N2BA	N2B
	Troponin I	ssTnI	cTnI
	MHC	β > α	β >> α
Electrophysiology and Ca²⁺-Handling	Upstroke velocity of Calcium Transients	≈50 V/s	≈250 V/s
	Resting membrane potential	≈-60 mV	≈-90 mV
	Excitation-contraction coupling	Partially developed	Mature
	Contractile force	≈nN range/cell	≈μN range/cell
	Gap junction distribution	Circumferential	Polarized to intercalated disks
	Conduction velocity	≈0.1 m/s ¹³	0.3–1.0 m/s
Metabolism	Mitochondria	Irregularly distributed, occupies a small fraction of cell volume	Regularly distributed, occupies ≈20% to 40% of cell volume
	Metabolic substrate	Glucose	Fatty Acids
Other	Multinucleation	Mononucleated	≈25% multinucleated
	Responses to β-adrenergic stimulation	Chronotropic response	Chronotropic response
		Lack of inotropic reaction	Inotropic reaction

Table 2 List of major differences between immature and mature CMs

(Adapted from Yang et al 2014, Guo and Pu 2020)

Numerous key factors were shown to augment the maturation of foetal-like hESC/IPSC-derived CMs *in vivo*, such as biophysical cues (geometric constraints, ECM viscoelasticity, electrical stimulation, mechanical strain), biochemical cues (thyroid hormone T3 i.e., triiodothyronine, glucocorticoids, insulin-like growth factor, circulating fatty acids and oxygen tension) and non-CMs stromal cells (Guo and Pu 2020). Thus, the cell type, combination cellular adjuncts and *in vivo* environment are instrumental to the maturation of the foetal-like hESC/IPSC-derived CMs (Guo and Pu 2020). As a substantial degree of CM maturation occurs *in vivo*, the relative immaturity

of hESC/IPSC-derived CMs does not hinder efforts in translating hESC/IPSC-derived CMs-based therapy into the chronic MI setting.

CM maturation is fundamental to the cardiac regenerative efforts, being intrinsically linked to both CM proliferation and electrical integration with the host myocardium.

1:8:2:4 Cardiomyocyte's electrical integration with the host myocardium

Large, mature cardiac grafts composed of hESC/IPSC-derived CMs, need to electrically integrate with the adult host heart. In pre-clinical studies of hESC/IPSC-derived CMs alone, electrical integration with the host tissue was demonstrated by histological evidence of connexin-43 gap junctions between neighbouring engrafted CMs and host CMs (Laflamme et al. 2007). In the subacute MI setting, *ex vivo* calcium-mapping studies showed efficient, 1:1 graft: host electrical coupling in both rat and guinea pig model (Shiba et al. 2013; Gerbin et al. 2015). Efficient host-graft electrical integration would contribute towards a greater cardiac contractile function and whilst poor integration would predispose towards arrhythmias.

The close relationship between host-graft electrical integration and CM maturation was recently illustrated by observations of self-terminating arrhythmic events in non-human primate subacute MI studies (Chong et al. 2014; Liu et al. 2018; Romagnuolo et al. 2019). Electrophysiology studies showed that these arrhythmic events were due to the immaturity of the engrafted CMs (Liu et al. 2018). As the cardiac grafts mature *in vivo*, the arrhythmic events resolved over time (Liu et al. 2018). These arrhythmic events represent a sizeable hurdle to clinical translation. Thus, characterization of the optimal

maturity of pre-injected hESC/IPSC-derived CMs and acceleration of CM maturation *in vivo*, warrant further work.

The chronic MI setting poses a greater challenge to hESC/IPSC-derived CMs monotherapy. Using *ex vivo* calcium-mapping studies, hESC/IPSC-derived CMs monotherapy demonstrated inefficient graft: host electrical coupling with no observable cardiac functional recovery in the chronic MI setting (Shiba et al. 2014). Given the increased hostility of the chronic MI environment, other adjuncts for hESC/IPSC-CMs such as the co-delivery with a key non-cardiac stromal cell, or even a different cell type, may be required, *Section 1:9 and 1:10*.

1:8:2:5 Cardiomyocyte-associated Immunogenicity

Exogenously delivered hESC/IPSC-derived CMs are immunogenic - a major contributing factor influencing cell survival *in vivo*. Allogeneic donor CMs can activate the host immune system via three pathways: Directly via intact allogeneic MHC molecules, indirectly via peptides derived from polymorphic sequences of allogeneic MHC molecules, or in a semi-direct pathway in which recipient dendritic cells acquire intact MHC molecules from donor cells (Zheng, Wang, and Xu 2016). Thus, the attacks on hESC/IPSC-derived CMs are predominantly driven by the adaptive immune system.

This immunogenicity of hESC/IPSC-derived CMs poses a significant challenge to clinical translation. In larger animal models, such as non-human primates, a triple immunosuppression regimen (methylprednisolone, cyclosporine and abatacept), administered throughout the animals' lifespan has been required (Chong et al. 2014;

Liu et al. 2018). Only with this substantial immunosuppression regimen have allogeneic hESC-derived cardiac grafts been reported to survive. To counteract opportunistic infections, hefty doses of antibiotics (Ceftazidime, cefazolin, vancomycin, gentamycin, fluconazole, and acyclovir) were then required (Chong et al. 2014; Liu et al. 2018).

Non-cardiac stromal cells are highly involved in modulating the immune response after cardiac injury (Forte et al. 2018). In the zebrafish, the cardiac regenerative response involves an influx of immune cells to clear the initial fibrin for subsequent cardiomyocyte proliferation (Cao and Poss 2018). In the murine, the epicardium was shown to modulate the adaptive immune response of T-regulatory cells (Tregs), a subset of CD4+ T cells via the Yap/Taz pathway (Ramjee et al. 2017). Modulating the immune response with a key non-cardiac stromal cell e.g. epicardium, may preclude immunosuppression with CM-based cellular therapy. In the context of chronic MI, whereby sizeable cardiac grafts are required, maximising cell survival is a priority. To achieve this, modulating the host's immune response by using adjunctive pharmacological or cellular therapy and/or using immune 'naïve' or species-matched cell type may be required.

1:8:2:6 Cardiac graft vascularization

Engrafted hESC/IPSC-derived CMs require an adequate and mature vascularization to ensure cell survival, CM maturation and efficient contractile function. A mature vascular supply is necessary to bring oxygenated blood and metabolites to the highly active, contractile cardiac grafts (Bertero and Murry 2018). This vascular supply needs to connect effectively with the host's vascular network. However, delivering hESC/IPSC-derived CMs alone clearly lacks vascular cells. Nonetheless, histological

evidence of neovascularization within hESC/IPSC-derived cardiac grafts was observed across a range of pre-clinical studies (Chong et al. 2014; Gerbin et al. 2015; Liu et al. 2018). The neovascularization appeared to be host-derived and its function remains unquantified (Chong et al. 2014; Gerbin et al. 2015; Liu et al. 2018). Thus, the extent and efficacy of the observed graft neovascularization warrants further interrogation.

Lack of vascularization was postulated as a key factor, for the failure of hESC/IPSC-derived CMs alone, in regenerating chronically infarcted hearts (Fernandes et al. 2010). In contrast to the subacute MI setting, the chronic MI environment is scarred, with depleted vascularization (Jessup and Brozena 2003). To rescue the chronically failing heart, pro-angiogenic adjuncts to hESC/IPSC-derived CMs monotherapy might be required, as a mature, interconnected graft-host vascular supply is a prerequisite for successful cardiac regeneration.

Pre-clinical studies with hESC/IPSC-derived CMs alone demonstrated significant promise for clinical translation. However, certain hurdles remain. These hurdles are particularly magnified in the context of chronic heart failure. Two cellular therapeutic strategies that may surmount such hurdles are effective species-matching of exogenous cells and the use of combinations of cell types, such as epicardial cells alongside CMs.

1:9 Species-matched Cellular Therapy for Chronic Heart Failure (foetal/neonatal rat cardiomyocytes and a rat model)

Species-matching of cellular graft: host has proved to be a pertinent factor for successful cardiac regeneration. A closer evolutionary distance between the species of graft cells and host (i.e., human cells in non-human primate) tremendously improved functional benefits in the subacute MI setting (Chong et al. 2014; Liu et al. 2018). When using NRVMs in a rat model, matching the heartbeat, signalling pathways for cellular maturation, proliferation and integration with the host would be considerably enhanced. Within the subacute MI setting, using species-matched cellular therapy i.e. NRVM, resulted in superior cardiac recovery in infarcted rat hearts (Etzion et al. 2001; Zimmermann et al. 2006; Kadota et al. 2017; Maass et al. 2017). Furthermore, species-matched cellular therapy would reduce immunogenicity concerns. All these factors contribute towards the augmentation of CM survival and maturation *in vivo*, thereby leading to large and mature cardiac grafts. Given the increased hostility of the chronic MI environment, the augmented cardiac grafts secondary to species-matched therapy, could potentially optimize cardiac repair and reverse heart failure.

Noting the challenges involved in salvaging the chronically infarcted heart with hESC/IPSC-derived CMs alone, the feasibility of exogenously delivered, CM-based therapy for chronic heart failure using NRVM was considered. NRVM represented the optimal CM for proof-of-concept studies of cardiac regeneration in rats; due to its species-compatibility, accessibility, cellular plasticity, and resilience in the infarcted rat

myocardium (Reinecke et al. 1999; Etzion et al. 2001; Zimmermann et al. 2006; Kadota et al. 2017). NRVMs represent the optimal cell type for testing the efficacy of cellular therapy in repairing chronically infarcted rat hearts.

However, early studies utilizing foetal rat CMs or NRVMs via intramyocardial cellular injections in chronic MI rat models showed inconsistent results (Li et al. 1996; Sakakibara et al. 2002; Huwer et al. 2003). Li *et al.* showed long-term cardiac engraftment with improvement in cardiac function, whilst Huwer *et al.* showed no cardiac improvement- both studies utilised cryoinjury and measured cardiac function via *ex vivo* Langendorff preparations (Li et al. 1996; Huwer et al. 2003). A key difference was that Li *et al.* utilised cryoinjury on the left ventricular free wall, whilst Huwer *et al.*'s cryoinjury site was at the obtuse marginal, resulting in different extents of myocardial injury (Li et al. 1996; Huwer et al. 2003). Meanwhile, Sakakibara *et al.* used a permanent LAD ligation rat MI model and echocardiography to measure cardiac function, which was reported as no cardiac recovery (Sakakibara et al. 2002). Notably, a P1 neonatal mouse could regenerate its heart after non-transmural cryoinjury, but not with transmural cryoinjury (Darehzereshki et al. 2015). The extent and nature of the cardiac injury likely affect the potential for cardiac recovery in mammals (Darehzereshki et al. 2015; Lam and Sadek 2018). Drawing upon the observations in endogenous cardiac regeneration, the variable results reported by the earlier chronic MI rat studies were likely underpinned by inconsistencies in the mode of cardiac injury (Li et al. 1996; Sakakibara et al. 2002; Huwer et al. 2003).

Minimal cellular engraftment was also noted throughout the early chronic MI rat studies (Li et al. 1996; Sakakibara et al. 2002; Huwer et al. 2003). These chronic MI rat studies delivered NRVM without PSC, a recent advancement that has been pivotal to cell

survival (Laflamme et al. 2007). The dose of transplanted cells delivered into the chronically infarcted rat heart was ~2-fold less (Li et al. 1996; Sakakibara et al. 2002; Huwer et al. 2003) than was reported to be therapeutically efficient in the subacute setting (Laflamme et al. 2005, 2007; Gerbin et al. 2015; Bargehr et al. 2019). Several subacute MI studies demonstrated that cardiac graft sizes were directly correlated to the degree of cardiac repair (Maass et al. 2017; Liu et al. 2018; Bargehr et al. 2019). Cellular adjuncts to improve NRVM's survival and engraftment in the chronically infarcted myocardium may increase the potential of cardiac recovery.

Thus far, the inconsistent cardiac repair with NRVM as reported by earlier chronic MI rat studies were likely due to key variations in the study design. The critical variables consisted of the type and extent of cardiac injury (Darehzereshki et al. 2015), the cellular dosages (Laflamme et al. 2005; Maass et al. 2017), the lack of cellular preconditioning (Laflamme et al. 2007) and different modes to measure and evaluate cardiac function; all factors shown to be pivotal for the success of endogenous and exogenous cardiac regeneration in the subacute MI setting. Despite the earlier chronic MI rat studies, the question of whether species-matched cellular therapy could rescue the chronically infarcted heart remains unanswered.

Given the benefits associated with species-matched cellular therapy in the subacute MI setting and the inconsistent results from earlier chronic MI rat studies, NRVM still represented the optimal cell type to test the potential of species-matched cellular therapy in salvaging chronically infarcted rat hearts. However, the chronic MI rat study design needs to be optimised. Thus, the first aim of my doctoral work is to optimize the chronic MI rat studies and examine whether species-matched cellular therapy

(NRVM) could regenerate chronically infarcted rat hearts. This experiment will offer fresh insights and represents a crucial step towards translating exogenously delivered, CMs-based cellular therapy into clinics.

1:10 Combination Cellular Therapy

Combination cellular therapy represents the next approach to salvage the chronically infarcted heart. Cardiac embryogenesis requires well-orchestrated signalling cues from various cell types during CM specification, development, and maturation (Galdos et al. 2017). Furthermore, non-cardiac stromal cells are integral to cardiac regeneration in adult zebrafish (Kikuchi et al. 2011; Cao et al. 2017) and neonatal mice (Wang et al. 2020a). Considering all the challenges involved (*Section 1:8:2*), the delivery of hESC/IPSC-derived CMs alone appears insufficient in overcoming the hostility of the chronic MI environment. Combining hESC/IPSC-derived CMs with a key non-cardiac stromal cell that augments CM survival, proliferation, maturation, electrical integration, and vascularization *in vivo*, is a highly feasible approach to improve cellular treatment of chronic heart failure. Testing this hypothesis forms the second aim of my doctoral work.

1:10:1 hESC-epicardium as an adjunct for hESC/IPSC-cardiomyocytes-based cellular therapy

The epicardium is an attractive source of non-cardiac stromal cells for combination cell therapy. The synergistic relationship between epicardium and myocardium is integral to mammalian cardiac embryogenesis (Lie-Venema et al. 2007; Carmona et

al. 2010; Smits et al. 2018), endogenous cardiac regeneration in adult zebrafish (Lepilina et al. 2006; Kikuchi et al. 2011; Wang et al. 2011) and neonatal mice (Rui et al. 2014; Wang et al. 2020) - as the epicardium instructs the newly generated CMs and also acts as a multicellular source of cardiac fibroblasts (CFs) and smooth muscle cells (SMCs) to build and vascularize the heart (Masters and Riley 2014; Cao and Poss 2018). Thus, co-delivering epicardial cells with hESC/IPSC-derived CMs could augment CM survival, proliferation, maturation, and vascularization *in vivo*.

Winter *et al.* showed that transplantation of human-derived epicardium-derived cells (EPDCs) preserved ventricular function and attenuated adverse remodelling post-infarction in NODScid Gamma mice, despite minimal cell survival *in vivo* (Winter et al. 2007; 2009). Human foetal-derived EPDCs also promoted CM proliferation and maturation *in vitro* (Weeke-Klimp et al. 2010). FSTL1, a protein isolated from epicardial secretome, was reported to promote the proliferation of pre-existing CM, which lead to the regeneration of the injured mammalian heart (Wei et al. 2015). However, human foetal-derived EPDCs are notoriously difficult to harvest and maintain in culture; they undergo EMT rapidly (Winter et al. 2007; 2009). Nonetheless, exogenously delivered human-derived epicardium showed tremendous potential in regeneration of the infarcted heart (Winter et al 2009).

Recent advances demonstrated that hESC-derived epicardium represented the key stromal cell for combination cell therapy with hESC/IPSC-derived CMs. In 2015, the Sinha lab developed a robust, chemically defined protocol for deriving hESC-epicardium (Iyer et al. 2015). This protocol enabled a stable, scalable, off-the-shelf source of foetal-like hESC-epicardium (Iyer et al. 2015). Next, we showed that co-injection of hESC-epicardium and hESC-CMs resulted in larger cardiac grafts

($3.9\pm 1.6\%$ vs $1.5\pm 0.9\%$), a greater proliferative index of β -MHC positive CMs ($8\%\pm 1.4\%$ vs $4\%\pm 0.9\%$), improved cardiac function and vascularization compared to hESC-CMs only, in the subacute MI setting (Bargehr et al. 2019). hESC-epicardium also augmented hESC-CM maturation and cell-cell electrical connectivity in 3D-engineered heart tissues (EHTs), compared to other stromal cells e.g., primary MSCs and hESC-MSCs (Bargehr et al. 2019). Overall, hESC-epicardium emerged as the key 'partner' stromal cell for hESC-CMs to achieve cardiac regeneration.

Thus, I postulated that the benefits conferred by the co-delivery of hESC-epicardium with hESC-CMs in a subacute MI setting could be extended to the chronic MI setting. The epicardial-augmentation of hESC-CMs' form and function *in vivo*, may be a crucial factor to overcome the amplified challenges within the hostile, chronically infarcted myocardium.

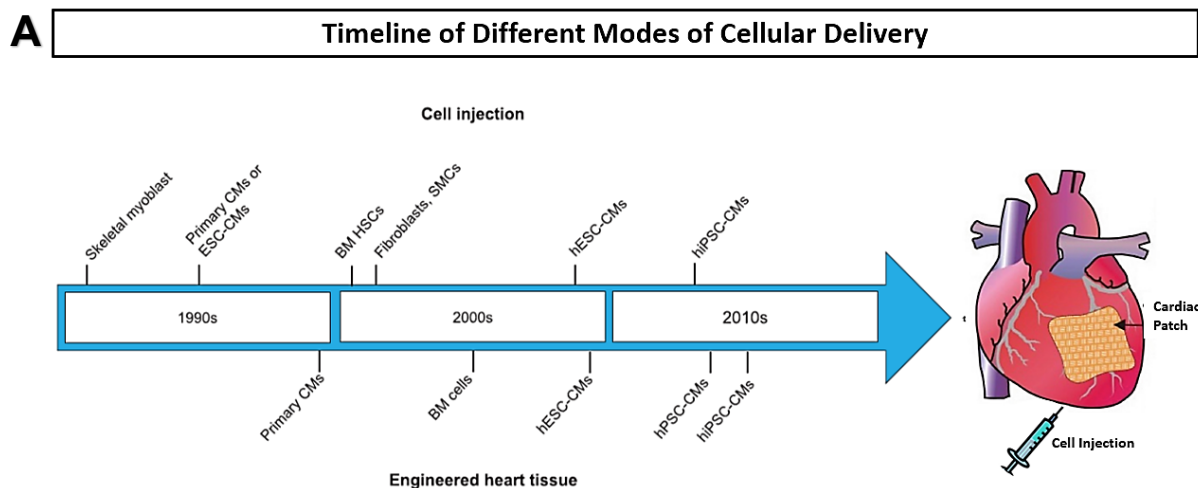
1:10:2 Tissue-engineering adjuncts to hESC/IPSC-cardiomyocytes-based cellular therapy

Apart from combination cell therapy, tissue-engineering based methods of cellular delivery could enhance hESC/IPSC-CM survival, proliferation, maturation, and vascularization *in vivo*. Tissue engineering approaches reported include using patches (scaffold vs non-scaffold) and biomaterials (gelatin, hydrogels, matrigel, collagen) to deliver hESC-CMs (Tompkins et al. 2018; Zhang et al. 2018). Engineered patches have been described as offering 3D-structural support, various CM-binding peptides, an anisotropy-enabled microenvironment, pre-vascularised networks, and pro-survival factors such as IGF-1 (Ye et al. 2014), exosomes (Khan et al. 2015), microRNAs and

pro-angiogenic factors (Madden et al. 2010; Redd et al. 2019; Zhang et al. 2016). These tissue-engineering based adjuncts aimed to enhance the survival and function of ES/IPSC-derived CMs *in vivo*.

3D-EHTs led to a 10-fold increase in cell engraftment compared to intramyocardial cell delivery (Riegler et al. 2015). Initially, Zimmerman and colleagues showed that large NRVM enriched-patches (thickness=1-4mm, diameter=15 mm) recovered cardiac function when implanted 2-weeks after MI in a rat model (Zimmermann et al. 2006). Implantation of 3D-EHTs promoted long-term engraftment of hESC/IPSCs-CMs and CM maturation in rodent MI models (Tulloch et al. 2011; Riegler et al. 2015). Newer CM patches with pre-vascularised networks to promote CM survival and angiogenesis *in vivo* have been described (Redd et al. 2019; Zhang et al. 2016). Tissue-engineering approaches in cardiac regeneration have advanced greatly over the last decade,

Figure 9.



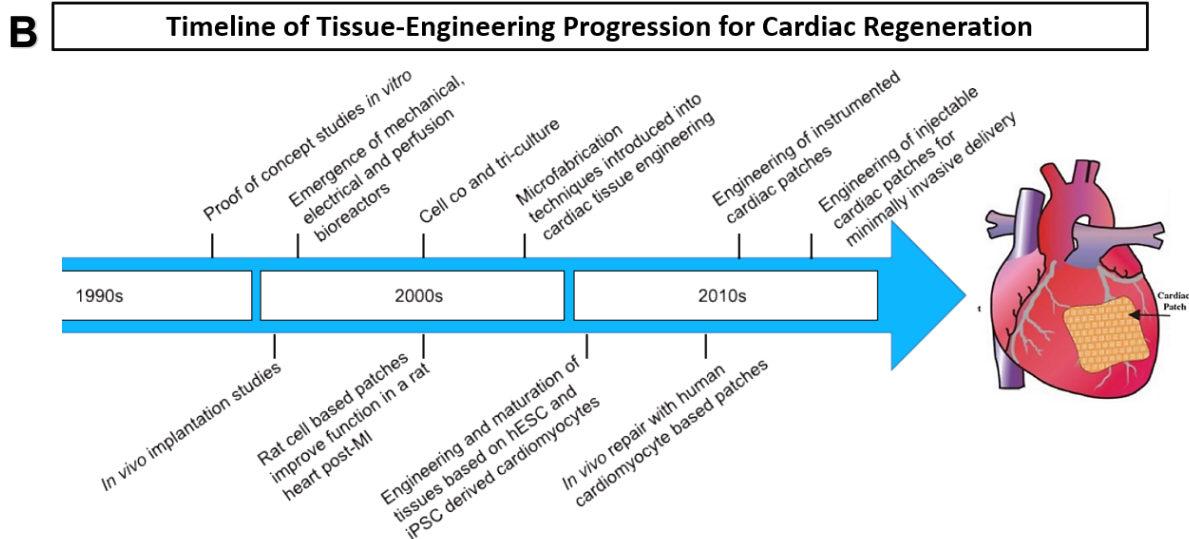


Figure 9: Overview of tissue-engineering approaches, in parallel with the evolution of stem cells and cellular injection models

A Parallel viewpoint of the advances made in intramyocardial cellular injections and tissue engineering approaches as an adjunct to cell therapy **B** Detailed timeline of key events and innovations in the tissue engineering field, eventually leading to ‘cardiac patch’ therapy for the heart.

Recent studies with hESC/IPSC-CM patches have shown mixed results. Epicardial-placed hESC/IPSC-CM patches were reported to form a scar border with the host tissue with subsequent impairment of electrical integration with host tissue (Gerbin et al. 2015; Fernández-Avilés et al. 2017). Meanwhile, endocardial placement of hESC/IPSC-CM patches may invoke cardiac thrombosis and embolization (Zhang et al. 2018). Cognizant of the limitations of hESC/IPSC-CM patches, other studies utilised cardiac progenitor cell patches (Menasché et al. 2015), clinical implantation of which resulted in minimal arrhythmic events (Menasché et al. 2018). Other non-cardiomyocyte cellular patches had also shown improved cardiac function post-infarction (Xiong et al. 2011; Zhu et al. 2018). Thus, these cardiac patches likely exerted benefits via paracrine effects and potentially ‘primary remuscularization’ – both

areas of intense scrutiny (Gerbin et al. 2015; Fernández-Avilés et al. 2017; Menasché et al. 2018).

As my doctoral work aimed to investigate whether cellular therapy could salvage the chronically infarcted rat heart, I chose to deliver my cells via intramyocardial injections instead of tissue-engineered patches. The main reason is to assess whether CM-based cellular therapy could lead to ‘primary remuscularization’ of the chronically infarcted heart and reverse heart failure. Using tissue-engineered patches at this stage would affect the clarity of my experimental results. Thus, I moved forward with using intramyocardial injections of species-matched cellular therapy and combination therapy with hESC-epicardium, in chronically infarcted rat hearts.

1:11 Mechanisms underlying Cellular Therapy: Contractile, Paracrine or Both?

Given recent advances in cardiac regeneration, the fundamental mechanistic question remains unanswered. ‘Is cardiac recovery due to paracrine signalling, cardiac remuscularization-mediated contractility, or both?’

Riegler *et al.* showed that 3D-EHTs enriched with hESC-CMs failed to recover cardiac function in chronically infarcted rats, despite a 5-fold increase in cell engraftment and retention up to 220 days post-implantation (Riegler et al. 2015). As alluded to above, cardiac patches might only generate benefits via paracrine signalling. In a comparative study of hESC-CMs vs. other non-contractile cell types (cardiac progenitor cells, bone

marrow mononuclear cells), intramyocardial injections of hESC-CMs achieved greater cardiac recovery due to 'primary remuscularization' (Fernandes et al. 2015). Although using a subacute MI setting, this study illustrated the importance of primary 'remuscularization' compared to paracrine signalling alone. In the chronic MI setting with extensive scarring, a cellular approach capable of invoking both i) primary 'remuscularization' with ample cardiac engraftment and ii) paracrine signalling, would be necessary for maximum clinical therapeutic impact.

As a step forward, I hypothesized that chronic MI rodent studies with streamlined cellular injections and mode of MI injury, utilising optimal primary cell type or novel combination cell therapy with a key supportive, stromal cell type (hESC-epicardium), would offer new therapeutic insights. Could exogenously delivered, hESC/IPSC-derived CMs and epicardial-based cellular therapy represent the ideal heart failure treatment?

1:12 Mechanisms underpinning Epicardial-myocardial Crosstalk

Our mechanistic understanding of our 'chosen' cell therapy should parallel our successes in establishing functional gains. Without such mechanistic insights, we may be pursuing an ineffective treatment. Although the benefits of hESC-epicardium upon cardiomyocyte function were demonstrated in 3D-EHTs and subacute MI rat models (Bargehr et al. 2019), the underlying mechanism has not been clearly elucidated.

However, we could certainly draw some insights based upon the role of epicardium during cardiac embryogenesis and cardiac regeneration in 'lower' vertebrate species (*Section 1.5* and *Section 1.6*). One such key insight is the need for highly active and extensive epicardial-myocardial crosstalk. A pictorial summary of the signalling pathways underpinning extensive epicardial-myocardial crosstalk is shown in **Figure 10**.

It is possible that the mechanism underlying the benefit of hESC-epicardium was stimulated by paracrine signals underpinning epicardial-myocardial crosstalk. Initially, we postulated that hESC-epicardium might be a potent cardiovascular cell progenitor source for CM vascularization and stromal support, within the combination cell therapy setting. However, our injected hESC-epicardium adopted a cardiac fibroblast-like state *in vivo* and, furthermore, the graft vascularization was derived from the host (Bargehr et al. 2019). All the evidence suggested that our hESC-epicardium delivered beneficial paracrine signals to augment hESC-CM's survival, proliferation, engraftment and maturation *in vivo*.

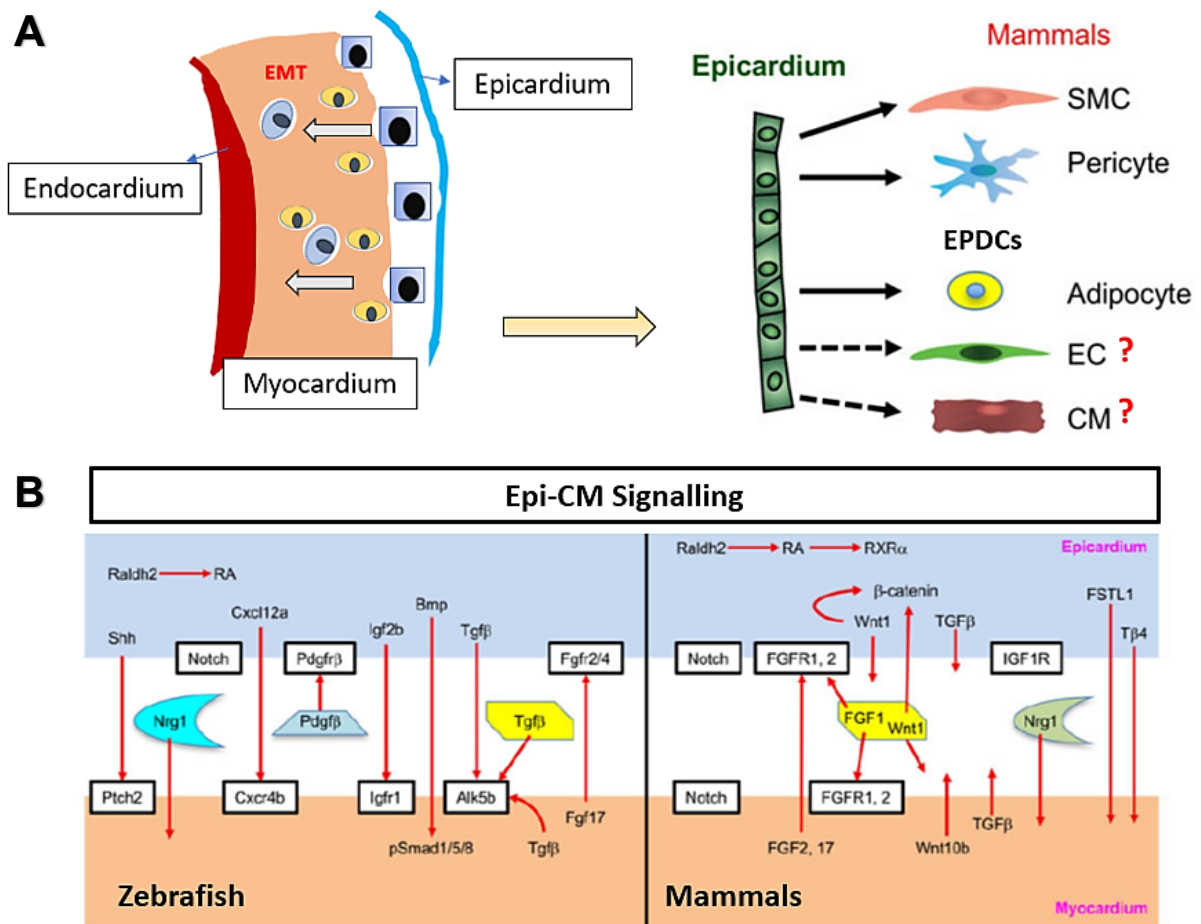


Figure 10: Epicardial EMT into associated EPDCs underpinned by epicardial-myocardial crosstalk

A A schematic representation of epicardium's hallmark process of epithelial-mesenchymal transition (EMT), which subsequently leads to the production of different cell types (EPDCs). However, the derivation of CMs and endothelial cells (EC) from the epicardium is still under debate. **B** An overview of the extensive epicardial-myocardial crosstalk that underpins EMT. The key pathways in this crosstalk share some similarities across different species such as zebrafish and mammals. (Adapted from Cao and Cao 2018)

1:12:1 Epicardially-secreted fibronectin (epicardial-FN) as a putative key mediator of epicardial-myocardial crosstalk

Epicardial-myocardial crosstalk is underpinned by active paracrine-mediated signalling via soluble factors, exosomes, cell-cell contact and extracellular matrix (ECM) (Masters and Riley 2014; Cao and Poss 2018). Paracrine signalling is an 'umbrella' term, thus raising the question, 'which paracrine signal(s) is foremost and central to hESC-epicardium's function?'

The zebrafish generates an ECM-rich zone near the injury site but completely regenerates without scarring, hinting at a unique and dynamic ECM turnover (Mercer et al. 2013, Garcia-Puig et al 2019). Similar dynamic ECM turnover were recorded in the neonatal mouse, albeit guided by the extent of cardiac injury (Lam and Sadek 2018). ECM upregulation and ECM-modifying proteases in the injured adult zebrafish heart are distinctly different to the adult mammalian heart, notably with respect to spatiotemporal changes in tenascin-C, hyaluronic acid, and fibronectin (Mercer et al. 2013; Garcia-Puig et al. 2019). Furthermore, decellularized zebrafish ECM from both injury and normal hearts could induce mammalian heart regeneration (Chen et al. 2016). These observations warranted a closer interrogation of the zebrafish ECM.

Epicardial-FN is crucial for the zebrafish's cardiac regeneration (Wang et al. 2013). The injured zebrafish hearts upregulated epicardial-FN with two paralogues, *fn1* and *fn1b*, which signalled via integrin β 3 receptors to guide the CMs towards the injury site, thereby resulting in successful cardiac regeneration (Wang et al. 2013). *fn1* loss-of-function mutations led to incomplete zebrafish heart regeneration (Wang et al. 2013).

Thus, epicardial-FN is integral to the epicardial-myocardial crosstalk which leads to cardiac regeneration in the zebrafish.

As for hESC/IPSC-CMs, FN was reported to be vital for several key cellular processes e.g. CM migration and proliferation (Ieda et al. 2009; Nosedá et al. 2009; Moyes et al. 2013). hESC/IPSC-CM migrated along an increasing FN gradient *in vitro* (Moyes et al. 2013). Meanwhile, embryonic cardiac fibroblasts promoted CM proliferation via FN and integrin- β 1 signalling (Ieda et al. 2009). As our hESC-epicardium is foetal-like (Iyer et al. 2015), it is likely to recapitulate signalling behaviours during embryogenesis and cardiac regeneration in adult zebrafish and neonatal mouse.

Thus, could epicardial-FN underpin the epicardial-myocardial crosstalk that enables superior hESC/IPSC-derived cardiomyocyte survival and maturation? In our bulk-RNA sequencing data, *FN1* was upregulated in hESC-epicardium compared hESC-neural crest cells (Bargehr et al. 2019). Moreover, increased FN deposition in 3D-EHTs and in subacute MI rat hearts were only observed in the combined presence of hESC-epicardium and hESC-CMs (Bargehr et al. 2019). The role of hESC-epicardium-secreted FN warrants further elucidation. This question forms the third aim of my doctoral work.

1:12:2 FN form and function

FN was first isolated from blood, as plasma FN, in 1978 (Edsall 1978). Subsequently, extracellular FN was discovered and usually secreted as a large dimeric glycoprotein with subunits ranging from 230-270kDa, created by alternatively spliced forms (Mosher 1989, Hynes 1990, Schwarzbauer and DeSimone 2011). Structurally, FN is composed of 3 modules: I, II and III repeats with different conformational changes and three alternative splicing sites (Pankov and Yamada 2002; Schwarzbauer and DeSimone 2011), **Figure 11**. FN displays a broad diversity in binding domains, enabling FN binding to various cell surface receptors e.g. integrins, syndecans (Pierschbacher and Ruoslahti 1984; Hynes 2002; Woods and Couchman 1998), FN-FN self-association, e.g. fibrillogenesis (McDonald et al. 1987; Mosher 1989; Schwarzbauer 1991; Singh et al. 2010) and binding to other ECM components e.g. collagens, proteoglycan, thrombospondin, tenascin-c (Hynes 1990; Ingham et al 1988, 2004) and to extra-cellular enzymes (Fogelgren et al. 2005; Hynes 2009). Sequestration or exposure of FN binding sites within the ECM further broadens its binding range (Schwarzbauer and DeSimone 2011). Furthermore, the *FN1* gene can be alternatively spliced with up to 20 isoforms in humans (Pankov and Yamada 2002). The FN protein is bestowed with multi-tasking abilities with varied roles in cell-matrix, matrix-matrix regulation, and signalling.

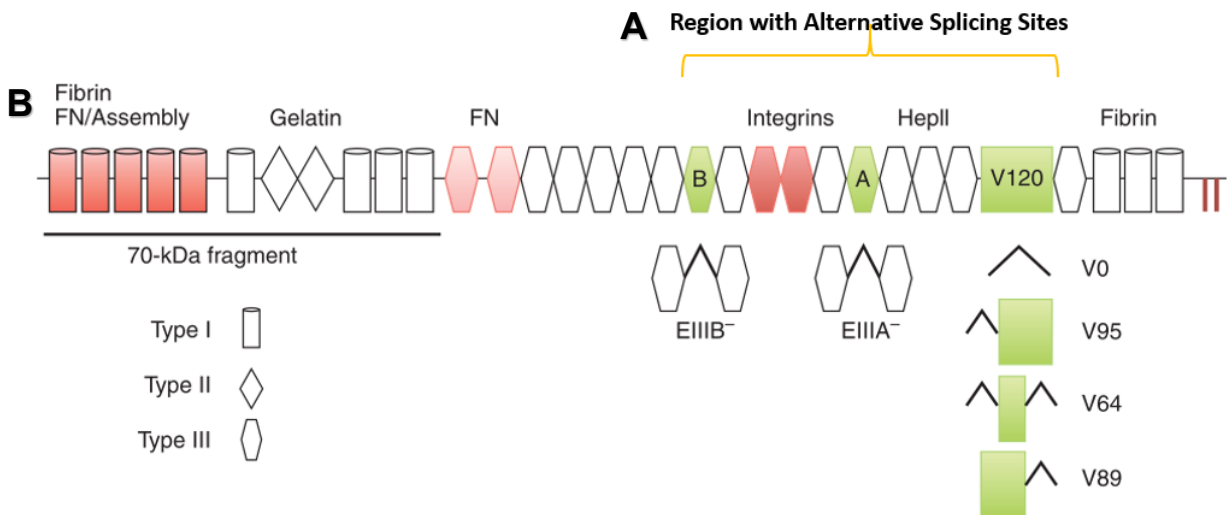


Figure 11: Fibronectin (FN) domain organization and alternative isoforms.

Each FN monomer has a modular structure consisting of 12 type I repeats (cylinders), two types II repeats (diamonds), and 15 constitutive types III repeats (hexagons). **A** Two additional type III repeats (EIIIA and EIIIB, green) are included or omitted by alternative splicing. The third region of alternative splicing, the V region (green box), is included (V120), excluded (V0), or partially included (V95, V64, V89). **B** Domains required for fibrillogenesis (matrix assembly) are in red: the assembly domain (repeats I1-5) binds FN. III9-10 contains the tripeptide Arg-Gly-Asp (RGD) and synergy sequences for integrin binding, and the carboxy-terminal cysteines form the disulfide-bonded FN dimer (k). The III1-2 domain (light red) has two FN binding sites that are important for fibrillogenesis. (*Adapted from Schwarzbauer and DeSimone 2011*)

1:12:3 FN-integrin signalling

Soluble FN primarily binds to integrin- $\alpha 5\beta 1$, a cell membrane receptor, to initiate FN matrix assembly, i.e., fibrillogenesis (Hynes 2002; Huvencers et al. 2008). FN and integrin- $\alpha 5\beta 1$ binding occurs via the RGD and synergy sites in the III₉₋₁₀ modules (Pierschbacher and Ruoslahti 1984), inducing integrin- $\alpha 5\beta 1$ clustering to bring FN dimers together, thus forming compact FN fibrils (Schwarzbauer and DeSimone 2011). Interestingly, syndecan can use glycosamino-glycan (GAG) chains to interact with FN and act as a coreceptor with integrin binding, further strengthening matrix assembly (Woods and Couchman 1998; Morgan, Humphries, and Bass 2007). Over time, FN matrix conformation and solubility can change, with some irreversible dissolved organic carbon (DOC) insolubility as a precursor to certain diseases (Schwarzbauer and DeSimone 2011).

FN can transduce environmental cues intracellularly through integrin- $\alpha 5\beta 1$ binding. The messages are subsequently relayed via the actin cytoskeleton and activation of the Focal Adhesion Kinase (FAK) pathway to influence cellular functions - '*outside-in signalling*' (Schlaepfer and Hunter 1998; Hynes 2002; Wickström et al. 2011). Correspondingly, cells could undergo actin cytoskeleton reorganisation to alter membrane tension and integrin clustering, thereby altering the FN matrix to sequester or reveal different binding sites to affect the 3D environment - '*inside-out signalling*' (Wickström et al. 2011). Dzamba *et al.* demonstrated that this could be modulated by non-canonical Wnt/PCP (planar cell polarity) signalling (Dzamba et al. 2009). Apart from integrin- $\alpha 5\beta 1$, FN can interact with other integrins, e.g. $\alpha 4\beta 1$, $\alpha v\beta 1$, $\alpha v\beta 3$, and $\alpha 11\beta 3$ to influence downstream cellular functions (Sechler et al. 2000; Schwarzbauer

and DeSimone 2011). Propagation of FN-mediated signalling affects many cellular functions such as cell survival, proliferation, adhesion, migration, and angiogenesis (Ieda et al. 2009; Itou et al. 2012; Astrof and Hynes, 2009; Schwarzbauer and DeSimone 2011). Collectively, FN-cell, FN-FN and FN-matrix interactions contribute to optimal cellular, organ and systemic functions.

1:12:4 Role of FN in development

Global FN null mouse embryos die during development, between E9-10.5, with a broad range of genetic defects, implying FN's pivotal role in development (George et al. 1993; Magnusson and Mosher 1998; Pulina et al. 2011; Astrof et al. 2007). Early studies showed that FN expression affects propulsion and convergence events in embryogenesis (Schwarzbauer and DeSimone 2011). However, a host of subsequent studies demonstrated that FN's was *not* required during certain key embryogenic events, such as i) germ layer specification, e.g. ectoderm, mesoderm and endoderm, during gastrulation (Davidson et al. 2002; Trinh and Stainier 2004), ii) cell fate specification into axial, paraxial and lateral mesoderm, iii) differentiation of mesodermal precursors into somitic or cardiac lineages (George et al. 1997; Georges-Labouesse et al. 1996; Trinh and Stainier 2004), and iv) migration of cardiac neural crest cells (Mittal et al. 2010). Despite this, some specific FN developmental roles have started to emerge.

FN has a necessary but subtle role in embryonic development. Namely, FN is integral to left-right embryonic specification, via modulation of *Lefty* and *Smads* at the floor plate (Pulina et al. 2011), alongside mediation of meso-endodermal cell fate decisions

(Cheng et al. 2013), survival and proliferation of cardiac neural crest (Mittal et al. 2010) and formation of cardiac outflow tract (Mittal et al. 2013). A study of 42 human foetal hearts from 8-26 weeks gestation, revealed that FN was constitutively expressed at endocardium, epicardium, and blood vessels until 24 weeks gestation, beyond which FN expression is confined to blood vessels (Kim et al. 1999). Collectively, FN displays a wide-ranging role in embryonic development. In particular, the role of FN in cardiac embryogenesis warrants further work.

1:12:5 Role of FN in cardiac disease

Within the cardiac injury setting, FN deposition in adult mammals has been associated with detrimental effects (Van Dijk et al. 2008; Valiente-Alandi et al. 2018). FN was implicated in fibrotic heart failure models (Dobaczewski et al. 2006; Heling et al. 2000; Konstandin et al. 2013). Valiente-Alandi *et al.* showed that inhibition of extracellular FN polymerization attenuated cardiac dysfunction and cardiac fibrosis in a mouse acute MI model (Valiente-Alandi et al. 2018). Loss of alternatively spliced fibronectin ED-A (EIIIA; EDA) similarly attenuated cardiac dysfunction in a mice MI model (Arslan et al. 2011). Fibronectin ED-A was reported to interact with TGF- β signalling for myofibroblast induction (Serini et al. 1998; Klingberg et al. 2018), together with proinflammatory effects *in vitro* and *in vivo* (Gondokaryono et al. 2007). However, the ECM environment in heart disease is more extensive than FN alone, including fibrillar collagens, elastin, basement membrane proteins, hyaluronan, and newly secreted matricellular macromolecules (Frangogiannis and Kovacic 2020). Teasing out the exact role of epicardial-FN in injured adult mammal hearts would be highly desired but

outside the scope of this thesis. Based upon FN's opposing effects in cardiac development and disease, FN appear to possess a Janus-like duality.

In the context of epicardial-myocardial crosstalk, FN-integrin signalling shows potential in modulating cardiac regeneration. The promiscuity of FN-integrin binding, together with reports of embryonic lethality require the design of multimodal loss-of-function FN studies *in vitro*. This approach offers a novel characterization of epicardial-FN's role in human cells, whilst conferring insights on epicardial-myocardial crosstalk to fine-tune cellular therapy and contribute towards successful cardiac regeneration.

1:13 Project Rationale

Heart failure carries a 50% mortality over 5 years without any sustainable therapies currently. Cellular therapy carries great potential as an ideal heart failure treatment due to its accessible and scalable generation of new CMs. 'Primary remuscularization' with hESC-CMs alone showed cardiac recovery in the subacute MI setting. Co-delivery of hESC-epicardium doubled the cardiac graft sizes with greater cardiac functional recovery at subacute timepoints post-MI. However, hESC-CMs alone resulted in small grafts without cardiac recovery in the chronic MI setting. **Thus, I hypothesized that an optimal cell type, singularly or in combination, could form sufficiently sizable and mature grafts in the hostile chronic MI environment and reverse heart failure.** To examine whether cellular therapy could salvage the chronically failing heart, I proposed two cellular strategies: i) species-matched, contractile cell therapy and ii) combination therapy of hESC-CMs with hESC-epicardium.

Epicardial-myocardial crosstalk underpins our combination cellular therapy which augmented hESC-CM's survival, maturation, and proliferation *in vivo*. Epicardial-FN was pivotal for the zebrafish's cardiac regeneration. Co-delivery of hESC-epicardium promoted both cardiac recovery and FN deposition in infarcted rat hearts. Furthermore, our hESC-epicardium displayed upregulated *FN1* expression in our bulk RNA-sequencing dataset. **Based on this collective evidence, I hypothesized whether epicardial-FN is a key mediator of the epicardial-myocardial crosstalk.** Thus, the loss-of-function (FN) studies will offer mechanistic insights to refine cellular therapy for clinical translation.

1:14 PhD Aims

1. To determine whether species-matched cellular therapy could salvage the chronically infarcted heart.
2. To investigate whether combination cellular therapy could rescue the chronically infarcted heart.
3. To interrogate whether fibronectin is a key mediator for epicardial-myocardial crosstalk.

2. METHODS

2:1 Cell Differentiations and Preparations

2:1:1 hESC-derived epicardium

Epicardial cells were differentiated from GFP-transgenic hESCs (H9, WiCell, Madison) as previously described (Iyer et al. 2015). hESCs were maintained in a chemically defined medium containing bovine serum albumin fraction A (CDM-BSA), supplemented with Activin-A (10 ng/mL, R&D Systems) and FGF2 (12 ng/ml, R&D Systems) on gelatin-coated plates with colony passaging when ~70% confluent. The chemically defined medium consisted of IMDM (250 ml, Life Technologies), Ham's F12 (250 ml, Life Technologies), penicillin-streptomycin (Sigma, added to a final volume of 1%), Insulin (7 µg/ml, Roche), transferrin (15 µg/ml, Roche), chemically defined lipid concentrate (Life Technologies) and monothioglycerol (450 µM, Sigma). Differentiation to lateral mesoderm was performed in CDM-PVA, containing polyvinyl alcohol (PVA, 1 mg/ml, Sigma) instead of BSA (Cheung et al. 2012). Early mesoderm differentiation was started with a combination of CDM-PVA, FGF2 (20 ng/ml), LY294002 (10 µM, Sigma) and BMP4 (10 ng/ml, R&D) for 1.5 days. Then, lateral mesoderm differentiation was initiated in CDM-PVA, FGF2 (20 ng/ml) and BMP4 (50 ng/ml) for 3.5 days. To direct differentiate into epicardium, cells were resuspended as single cells in CDM-PVA, WNT3A (25 ng/ml, R&D), BMP4 (50 ng/ml) and RA (4 µM, Sigma) at a seeding density of 2.5×10^4 cells/cm² and replated for exactly ten days with a full medium change every five days. Media components are as listed below.

MEF-Medium	500ml	Company information
FBS	50ml	Life Technologies, Catalogue number 10500064
Advanced DMEM-F12	450ml	Life Technologies, Catalogue number 12634028
Glutamine	5ml	Life Technologies, Catalogue number 25030024
β -Mercaptoethanol	3.5 μ l	Sigma, Catalogue number M6250-100ML
Pen/Strep	5ml	Life Technologies, Catalogue number 15140122

Table 3: Components of MEF Medium

CDM-BSA	500ml	Company information
BSA	2.5g	CCK
IMDM	250ml	Life Technologies, Catalogue number 21980065
Ham's F12	250ml	Life Technologies, Catalogue number 31765068
Pen/Strep	5ml	Life Technologies, Catalogue number 15140122
Insulin	0.35ml	Roche, Catalogue number 11376497001
Transferrin	0.25ml	Roche, Catalogue number 10652202001
Lipids	5ml	Life Technologies, Catalogue number 11905031
Monothioglycerol	20 μ l	Sigma, Catalogue number M6145-100ML

Table 4: Components of CDM-BSA, culture media for H9 ES cell line

CDM-PVA	500ml	Company information
PVA	0.5g	Sigma
IMDM	250ml	Life Technologies, Catalogue number 21980065
Ham's F12	250ml	Life Technologies, Catalogue number 31765068
Pen/Strep	5ml	Life Technologies, Catalogue number 15140122
Insulin	0.35ml	Roche, Catalogue number 11376497001
Transferrin	0.25ml	Roche, Catalogue number 10652202001
Lipids	5ml	Life Technologies, Catalogue number 11905031
Monothioglycerol	20 μ l	Sigma, Catalogue number M6145-100ML

Table 5: Components of CDM-PVA, basal media for all directed differentiations

2:1:2 RUES2-derived epicardium

For the derivation of epicardial cells from a different cell line (RUES2, female line, Rockefeller University, NIH registry number 0013), a few modifications to the step above was undertaken. The RUES2 cell line was maintained in feeder-free, irradiated mouse embryonic fibroblast (MEF)-conditioned medium containing bFGF (4 ng/ml, Peprotech) with single-cell passaging when ~70% confluent. Lateral mesoderm differentiation was initiated in CDM-PVA, FGF2 (20 ng/ml) and BMP4 (50 ng/ml) for a maximum of 2.5 days. To direct differentiation into epicardium, cells were resuspended as single cells in CDM-PVA, WNT3A (25 ng/ml, R&D), BMP4 (50 ng/ml) and RA (4 μ M, Sigma) at a seeding density of 1.5×10^4 cells/cm² and replated for exactly ten days with a full medium change every five days. All re-plating of the cells included Rock inhibitor (10 μ M, Y-27632) in addition to the cytokines described above. Additionally, SB431542 (2 μ M) was introduced into the culture medium on Day 3 after epicardium differentiation.

2:1:2 hESC-derived cardiomyocytes

hESC-derived CMs were generated with the ABCX method, utilising a Matrigel sandwich (Palpant et al. 2015). As above, hESCs (RUES2, female line, Rockefeller University, NIH registry number 0013) were maintained in feeder-free, irradiated mouse embryonic fibroblast (MEF)-conditioned medium containing bFGF (4 ng/ml, Peprotech) with single-cell passaging when ~70% confluent. Cells were seeded as single cells (1×10^5 /cm²) on Matrigel-coated (BD 449) plates with conditioned medium including Chiron 99021 (1 μ M, Cayman Chemical) and ROCK inhibitor (10 μ M, Y-

27632). On Day 0, the medium was replaced with RPMI medium supplemented with 1X B27 minus insulin (Invitrogen) containing Activin A (100 ng/ml) for 18 hours. On day 1, cells were fed with RPMI media plus B27 containing BMP4 (5 ng/ml) and Chiron 99021 (1 μ M) for 48 hours. On day 3, medium was replaced with RPMI medium plus B27 containing Xav 939 (1 μ M, Tocris). On day 5, the medium was replaced with RPMI medium plus B27. On day 7, the medium was replaced with RPMI containing B27 with insulin (Invitrogen) and was consequently replaced every other day until D28 and harvested for intramyocardial injections.

Components	Volume	Company information
RPMI 1640	500ml	Thermo Fisher Catalogue number: 11875101
B27 Supplement	10ml	Thermo Fisher Catalogue number: 17504044
B27 minus Insulin Supplement	10ml	Thermo Fisher Catalogue number: A1895601
Pen/Strep	5ml	Life Technologies, Catalogue number 15140122

Table 6: Components of RPMI-based media for CMs differentiation and culture

2:1:3 Neonatal rat cardiomyocytes

As previously described, NRVMs were harvested as previously described (Reinecke et al. 1999). All studies were approved by the University of Washington Animal Care and Use Committee (IACUC protocol number 2225-04) and were conducted in accordance with the US NIH Policy on Humane Care and Use of Laboratory Animals. At postnatal day one or day two, rat pups were separated from their mothers, sedated on ice, and euthanized by decapitation. Their hearts were rapidly removed and placed

into an ice-cold buffer (in mmol/L: NaCl 116.4, HEPES 20, NaH₂PO₄ 1, glucose 5.5, KCl 5.4, MgSO₄ 0.8; pH 7.4).

Both atria and the great vessels were trimmed and discarded. The ventricles were cut into 2 to 3 mm³ pieces and serially incubated (37°C, 25 minutes) six times, in buffer supplemented with collagenase type II (95 U/mL; Worthington) and pancreatin (0.6 mg/mL; Gibco BRL). After each round of digestion, the supernatant was centrifuged (800g, 5 minutes) and the resulting cell pellet was resuspended in DMEM/M199 (4:1) supplemented with 50% fetal bovine serum (Gibco) and Penicillin/Streptomycin (Sigma, added to a final volume of 1%). Cells were pre-plated onto gelatin-coated plates for 60 minutes to reduce the number of contaminating non-CMs. CMs were then pooled, counted, and incubated in the medium until further processing. The cell yield was ~1.5 x 10⁶ per neonatal heart, and the preparations averaged ~80% CMs, as determined by antibody staining for cTnT+ (Abcam) (Fernandes et al. 2010).

2:1:4 Cellular preparation for intramyocardial injections

All cells were heat-shocked for 30 min at 42.5°C, on the day before cell transplantation. On the day of cell transplantation, all cells were enzymatically dispersed with Trypsin-EDTA (0.05%), counted and resuspended in 100 µl volume per rat of matrigel and pro-survival cocktail (PSC). PSC consisted of 50% (vol/vol) matrigel and ZVAD-FMK (100 µM, Calbiochem), Bcl-XL (50 nM, Calbiochem), Cyclosporin A (200 nM, Wako Pure Chemicals), Pinacidil (50 µM, Sigma) and IGF-1 (100 ng ml⁻¹, Peprotech), **Table 7**. Cell preparations were delivered in a combination of Matrigel and PSC.

Constituents of PSC	Final cell/gel concentration	Supplier
Matrigel	50% (vol/vol)	Corning, Catalogue no. 354277
ZVAD-FMK	100 μ M	Calbiochem, Catalogue no. 627610-1MG
Bcl-xl BH-44-23	50 nM	Calbiochem, Catalogue no.197217-1MG
Cyclosporin A	200 nM	Wako Pure Chemicals, Catalogue no. 035-16303- 100MG
Pinacidil monohydrate	50 μ M	Sigma Aldrich, Catalogue No. P154-100mg
IGF-1	100 ng/ml	PeptoTech, Catalogue no. 100-11-100 μ g

Table 7: Specific components of PSC with concentrations

2:2 Animal Models of Myocardial infarction (MI) and Cell Transplantation

2:2:1 Chronic MI rat model

All studies were approved by the University of Washington Animal Care and Use Committee (IACUC protocol number 2225-04) and were conducted in accordance with the US NIH Policy on Humane Care and Use of Laboratory Animals. The study design consisted of the chronic myocardial infarction model (Fernandes et al. 2010) to assess the survival and fate of NRVMs or hESC-derived CMs. An *a priori* sample size calculation was undertaken to determine whether the addition of CM-based cellular therapy (NRVM or hESC-Epi+CM) is better than PSC alone (Sham) for attenuating FS% dysfunction in rats with chronic heart failure.

For simple comparison between CM-based cellular therapy versus no cells (PSC alone), number of animals/group is estimated by $n = 2 \times [z(1-\alpha/2) + z(1-\beta)]^2$ divided by standardised difference (the treatment difference/standard deviation) squared. For 5% significance, $z(1-\alpha/2) = 1.96$. While for a power of 80% $z(1-\beta) = 0.8416$.

Fernandes *et al* previously showed that rats without heart failure recorded FS% > 40% which declined to 18.8±2.6% (SEM, n=15), at 3 months after cellular therapy in the PSC alone group (Sham) (Fernandes et al. 2010). With CM-based cellular therapy, we accept that getting halfway to FS% =40% as a clinically significant improvement, then we would want to detect an improvement of $(40 - 18.8)/2 = 10.6\%$. Thus, standardised difference (treatment difference /standard deviation) = $10.6/10.07 = 1.05$. So, number/group = $2 \times [1.96 + 0.8416]^2/1.05^2 = 15.7/1.1 = \sim 14$ animals per group. To allow for deaths and incomplete infarction, we estimated at 16 animals per group.

To aid the transfer of surgical expertise to University of Cambridge, the study was structured as 2 phases with n=8 animals/group in each phase. The first phase was conducted in collaboration with University of Washington. There were 3 study arms: 10×10^6 NRVMs (n = 8), 5×10^6 hESC-epicardial cells plus 10×10^6 hESC-CMs (n = 8) and PSC vehicle control (n = 8). Number and causes of animal deaths are presented in *the Appendix 8.1*. Challenges with the second phase of the study was detailed in *Appendix 8:3*.

To induce experimental MI in rats, ischaemia-reperfusion injury instead of permanent LAD ligation was utilised. Ischaemia-reperfusion injury most closely aligns with the clinical presentation of a heart attack whereby the blocked coronary vessel is

reopened within hours to enable reperfusion (Riehle and Bauersachs 2019). The effects of reperfusion injury involving the release of ROS and oxidative stress would also be studied. The permanent LAD ligation model mimics a chronic total occlusion (CTO) of a coronary vessel which not the focus of my doctoral aims. The protocols for experimental MI and intra-myocardial cell injections have been previously detailed (LaFlamme et al. 2007; Gerbin et al. 2015).

Nine week old male athymic Sprague Daley rats (Harlan/Envigo) underwent anaesthesia through intraperitoneal injection of 68.2 mg/kg Ketamine and 4.4 mg/kg Xylazine, intubated and mechanically ventilated with room air and supplemented oxygen. A second dose of Ketamine and Xylazine was administered 20 minutes later. Animals were placed on a heating pad connected with a rectal temperature probe, which ensured the maintenance of body temperature at 37°C. A thoracotomy was subsequently performed, the anterior surface of the heart was exposed, and the left anterior descending (LAD) coronary artery was visualized. The LAD was consequently ligated for 60 minutes after which the ligation was removed, the animals reperfused and the chest closed aseptically.

At day 28 post-MI, the animals were anaesthetized with Isoflurane before undergoing a second thoracotomy for intra-myocardial cell transplantations. Animals were serially assigned to each of the experimental groups, and cells or vehicle were subsequently injected into the infarct and border zones. The chest was subsequently closed, and the animals were monitored postoperatively. To optimize graft retention animals received a subcutaneous injection of 5 mg/kg Cyclosporine A on the day before surgery and daily until seven days after the surgery. To quantify cell proliferation within

the grafts, animals were injected with 50 mg kg⁻¹ BrdU on Days one, four, seven and 14 post-cell injection.

2:2:2 Echocardiography, exclusion criteria, blinded assessor

All animals underwent echocardiography to assess cardiac function before myocardial infarction (baseline), day 21 after the infarct, and days 28, 56 and 84 after cell transplantation. Briefly, animals were lightly anaesthetized with inhaled 1% isoflurane (Novaplus), whilst echocardiography was performed with a Vevo 2100 (VisualSonics). Images were recorded and analysed using the Vevo LAB software 3.1.0 (VisualSonics). The primary endpoint was LV fractional shortening (FS%) at day 84 post-cell transplantation. Secondary endpoints included left ventricular end-systolic diameter (LVESD, mm) and end-diastolic diameter (LVEDD, mm). At day 21 post-MI, any animal with FS% $\geq 40\%$ was excluded from the study as they were not in chronic heart failure, as previously described (Fernandes et al. 2010). A subset of animals died before the day 84 endpoint. Images were anonymized and a primary, trained analyser made measurements in a blinded manner. Details of histologic and echocardiographic parameters are presented in **Appendix 9.2**.

2:2:3: Subacute MI rodent models

The pilot studies in subacute MI rodent models were similarly approved by the University of Washington Animal Care and Use Committee (IACUC protocol number 2225-04) and were conducted in accordance with US NIH Policy on Humane Care and Use of Laboratory Animals. The study design comprised two different animal

model studies to assess the survival and fate of hESC-derived epicardial cells with or without PSC and heat shock (HS). For the pilot athymic rat study, animals either received 5×10^6 ($n=4$) epicardial cells with PSC & HS or 5×10^6 ($n=4$) epicardial cells only. For the pilot NODScid Gamma Mice study, animals received either 5×10^5 ($n=4$) epicardial cells with PSC & HS or 5×10^5 ($n=4$) epicardial cells only.

A key modification from the chronic MI rat model is the timing of intramyocardial cellular injections after myocardial infarctions (MI). For the NODScid Gamma mice, the intra-myocardial cellular injections were delivered after permanent LAD ligation. As for the subacute MI rat model, the animals underwent a second thoracotomy for intra-myocardial cell transplantations at Day 4 post-MI. Animals were subsequently randomly assigned to one of the treatment groups, and cells were injected into the infarct zone. The chest was subsequently closed, and the animals were monitored postoperatively. To optimize graft retention, all animals received a subcutaneous injection of 5 mg/kg Cyclosporine A on the day before surgery until seven days after the surgery. Due to the pilot nature of these studies, these animals were followed-up for one month for histological analyses of cell survival.

2:2:4 Cambridge rat cardiac regenerative model

All studies were carried out in accordance to the UK Animals (Scientific Procedures) Act of 1986 and the University of Cambridge Animal Welfare Policy, reviewed by the University of Cambridge Animal Welfare Ethical Review Board. As adapted from the US protocol, a series of studies were performed:

i) MI as non-survival surgery

- ii) MI as survival surgery
- iii) MI with 2nd re-opening for cellular injections as non-survival surgery
- iv) MI with 2nd re-opening for cellular injections as survival surgery

Nine-week-old male wild-type Sprague Daley rats (Harlan/Envigo) underwent anaesthesia through intraperitoneal injection of 100 mg/kg Ketamine and 4.4 mg/kg Xylazine, intubated and mechanically ventilated with room air and supplemented oxygen. A second dose of Ketamine was administered 20 minutes later. Animals were placed on a heating pad connected with a rectal temperature probe, which ensured the maintenance of body temperature at 37°C. A thoracotomy was subsequently performed, the anterior surface of the heart was exposed, and the left anterior descending (LAD) coronary artery was visualized. The LAD was consequently ligated for 60 minutes after which the ligation was removed, the animals reperfused and the chest aseptically closed. At day four post-MI, the animals were anaesthetized with Isoflurane before undergoing a second thoracotomy for Vehicle (Matrigel only) injections. The chest was subsequently closed, and the animals were monitored postoperatively for seven days, one month and two months, to analyse their cardiac function.

2:3 Immunocytochemistry and Immunohistochemistry

2:3:1 Immunostaining of paraffin-embedded heart sections

For immunohistochemistry (IHC), hearts were excised post-mortem and prepared as described (Bargehr et al. 2019; Gerbin et al. 2015). The hearts were washed in PBS,

submerged in hypertonic KCl (140 mM) for 20 minutes and fixed in 4% PFA for paraffin-sectioning (4 μ m). For IHC, slides were initially de-paraffinized, followed by heat-mediated antigen retrieval at 100°C for 20 minutes and blocked with 5% BSA/PBS containing 0.5% Triton X-100 for one hour at room temperature (RT). Then, the slides were incubated with primary antibodies at 4°C overnight, and fluorescent secondary antibodies were applied at room temperature for 60 minutes the next day. All immunostainings with subsequent imaging were performed with simultaneous negative and positive controls, as available. Antibodies used for IHC and ICC were as listed in **Tables 8 & 9**.

Antibody	Species	Dilution	Manufacturer (Cat#)
WT1	rabbit	1/250	Abcam (AB89910)
Vimentin, Clone Vim 3B4	Mouse	1:100	Dako (M7020)
GFP	Goat	1:500	Novus (NB-100-1770)
Human Mitochondria, Clone 113-1	Mouse	1:100	Millipore (MAB1273)
Fibronectin	Rabbit	1:250	Abcam (ab2413)
Fibronectin (human specific)	Rabbit	1:250	Abcam (ab32419)
Alpha-Actinin	Rabbit	1:800	Abcam (ab68167)
Cardiac Troponin I	Rabbit	1:200	Abcam (ab47003)
Cardiac Troponin T	Goat	1:200	Abcam (ab64623)
Cardiac Troponin T	Mouse	1:200	Abcam (ab8295)
Cardiac Troponin T	Mouse	1:100	Thermo Fisher MC-295-P
Connexin 43	Mouse	1:500	Millipore (MAB3067)
Connexin 43	Rabbit	1:500	Abcam (ab11370)
Beta-Myosin Heavy Chain, Clone A4.951	Mouse	1:1	Human Hybridoma Bank
CD31/ PECAM-1	Rabbit	1:100	Novus (NB100-2284)

Biotinylated human Lectin		1:1000	Vector (B-1065)
Smooth Muscle Alpha Actin	Mouse	1:200	Dako (M0851)
Smooth Muscle Alpha Actin	Goat	1:200	Abcam (ab21027)
Anti-BrdU-POD, Clone BMG-6H8	Mouse	1:40	Roche (11 585 860 001)
Troponin I type 1 (slow skeletal)	Rabbit	1:200	Novus (NBP1-56641)
Wheat Germ Agglutinin, Alexa Fluor 594 Conjugate	/	1:200	Thermo Fisher (W11262)

Table 8: List of primary antibodies used for ICC and IHC

Antibody	Species	Dilution	Supplier (Cat No.)
Alexa Fluor 488	Donkey anti-rabbit IgG	1/100	Invitrogen A21206
Alexa Fluor 488	Goat anti-rabbit IgG	1/100	Invitrogen A110034
Alexa Fluor 568	Goat anti-mouse IgG	1/100	Invitrogen A11031
Alexa Fluor 568	Donkey anti-mouse IgG	1/100	Invitrogen A10037
Alexa Fluor 568	Rabbit anti-mouse IgG	1/100	Invitrogen A11061
Alexa Fluor 568	Donkey anti-rabbit IgG	1/100	Invitrogen A10042
Alexa Fluor 568	Donkey anti-goat IgG	1/100	Invitrogen A21432
Alexa Fluor 488	Donkey anti-goat IgG	1/100	Invitrogen A11055
Alexa Fluor 488	Rabbit anti-mouse IgG	1/100	Invitrogen A11054
Alexa Fluor 488	Goat anti-mouse IgG	1:100	Invitrogen A11001
Alexa Fluor 647	Chicken anti-rabbit IgG	1/200	Invitrogen A21443
Alexa Fluor 647	Donkey anti-mouse IgG	1/100	Invitrogen A21202
Alexa Fluor 647	Chicken anti-goat IgG	1/100	Invitrogen A17045

Table 9: List of secondary antibodies used for IHC and ICC

2:3:2 RNAscope *in situ* hybridisation

For identification of transplanted female NRVMs into the male rat recipient, we detected rat Xist (X-inactive specific transcript) on FFPE sections using Advanced Cell Diagnostics (ACD) RNAscope® 2.5 LS Reagent Kit-RED (Cat No. 322150) and RNAscope® 2.5 LS Probe- Rn-LOC100911498-No-XMm (Cat No. 454218). RNA quality within the tissue sections was assessed using RNAscope® 2.5 LS Probe- Rn-PPIB (Cat No. 313928; ACD, Hayward, CA, USA). Negative controls were performed using the RNAscope® 2.5 LS Negative Control Probe - DapB (Cat No. 312038).

Briefly, sections were cut at 4 µm thick, baked for 1 hour at 60°C before loading onto a Bond RX instrument (Leica Biosystems). Slides were deparaffinised and rehydrated on board before pre-treatments using Epitope Retrieval Solution 2 (Cat No. AR9640, Leica Biosystems) at 95°C for 15 minutes, and ACD Enzyme from the LS Reagent kit at 40°C for 15 minutes. Probe hybridisation and signal amplification were performed according to the manufacturer's instructions. Fast red detection of rat Xist, PPIB and DapB were performed on the Bond Rx using the Bond Polymer Refine Red Detection Kit (Leica Biosystems, Cat No. DS9390) according to the ACD protocol. Slides were then removed from the Bond Rx and were heated at 60°C for 1 hour, dipped in Xylene and mounted using EcoMount Mounting Medium (Biocare Medical, CA, USA. Cat No. EM897L).

2:3:3 Infarct size, graft size quantification

Slides were stained with picosirius red/ fast-green stain to assess total fibrotic content and scar size. Whole slide sections were scanned with the Hamamatsu Nanozoomer and the images were exported with NDP software (NDP view 2.6.13) for further analyses. In the infarcted sections, picosirius red positive areas were quantified and normalized to the left ventricular area in each section, in a blinded and automated manner, via Image J. To assess the survival of cardiac grafts, anti-human Mitochondria (Novus) antibodies were used for the Epi+CM group whilst Xist RNAScope was used to identify engrafted NRVM. Baseline quantification of Xist expression was first performed on female rat hearts. All animals were used for analysis except one animal in the CM+Epi study arm, which did not exhibit a detectable graft. Graft sizes were then normalized to the size of the corresponding infarct area. To detect hESC-cardiac grafts, antibodies directed against either human mitochondria and α -Actinin (Abcam) or β -MHC (Developmental Studies Hybridoma Bank) were used. NRVM were detected by co-staining with Xist RNAScope (ACDBio) and either cTnI (cardiac troponin I, Abcam) or α -Actinin (Abcam). For calculation of individual sarcomeric and cellular calculations, similar antibody strategies were undertaken, and the resulting images analysed via Image J software, in a blinded fashion.

2:3:4 Quantification of proliferation & vascularization

The proliferation rate of CMs was determined from sections stained for BrdU and either α -actinin (Abcam) or β -MHC (Developmental Studies Hybridoma Bank). A well-defined grid was overlaid over the whole-slide image of entire heart sections, and 9X high-

powered images were taken per graft section (Liu et al. 2018). Sections of grafts were delineated from host myocardium for the calculation. For quantification of proliferation rate (%), %BrdU+ve CMs = (BrdU+ve Graft CMs/Total Graft CMs) X 100. As for graft CM number and density of CM per mm³, several assumptions were similarly made as other reported studies (Liu et al. 2018). Firstly, we assumed that nuclei were isotropically packed, and each CM was mononucleated due to relative graft immaturity. Hence, nuclear density = CM density. Each heart was serially sliced at 1mm thickness from apex to the base. Then, each heart slice was sectioned at 4μm thickness and graft CMs were identified by immunostaining. Thus, each 1mm heart slice was composed of 250 X 4μm sections. From our immunostaining, we noted that our average CM nucleus size was 8μm in diameter, thus we assumed that each CM nucleus would traverse two (4μm) sections. Based on these assumptions, Graft CMs density (per mm³) = (Average number of Graft CMs per mm² x 250)/2. Total graft CMs per animal = Graft CM density per mm³ x Total Graft Size (mm²) x 1 mm thickness.

To quantify microvascular density, slides were stained with CD31/PECAM (Novus) and either anti-human mitochondria (Novus) or Xist RNAScope (ACDBio). To quantify mature vessel density, slides were stained for smooth muscle cells (Smooth Muscle α-Actin, Dako) and either anti-human mitochondria (Novus) or Xist RNAScope (ACDBio). For quantification of both microvascular and mature vessel density in cardiac grafts, the infarct zone and the non-injured border zone, 9x high-power images were taken in each of the three areas of interest. The number of lumens was counted and expressed as the number of vessels per mm². To determine the fate of epicardial cells, slides were co-stained with antibodies directed against anti-GFP (Novus), anti-human mitochondria (Novus), β-MHC (Developmental Studies Hybridoma Bank),

endothelial cells (CD31/PECAM, Novus) or smooth muscle cells (Smooth Muscle α -Actin, Dako). All images were acquired in technical replicates per whole-heart slide section using 3.1 ZEN Blue Lite software and subsequently analysed using Image J software, in a blinded fashion.

2:4 Three-Dimensional Engineered Heart Tissues (3D-EHTs)

2:4:1 Generation of 3D-EHTs

The tissue construct wells were fabricated using polydimethylsiloxane (PDMS) (PDMS, Sylgard 184; Dow Corning, Midland, MI). PDMS linker and base were mixed in a 1:10 mass-ratio and poured into laser-etched acrylic negative templates featuring four wells measuring 3x8x2 mm and containing 2x1mm diameter posts positioned 3mm from each other. The PDMS was baked at 65°C overnight, removed from the negatives, and then autoclaved. The PDMS wells were treated with 5% pluronic acid F127 solution (Sigma, P2443) for 1 hour prior to casting the constructs.

CMs frozen down on day 28 were thawed and cultured for 17-24 days before construct casting. Flow cytometry was performed on thawed cells using cTnT antibody (Thermo, MS-295-P) on a BD FACSCanto II instrument (Beckton Dickinson, San Jose, CA) and analysed using FACSDiva software (BD Biosciences), revealing a purity of 96.5% \pm 0.5 (i.e., cTnT+). For construct casting, CMs and epicardial cells were trypsinized and mixed in a collagen-based gel containing 10x RPMI-1640 medium (Sigma), NaOH, geltrex (Invitrogen, A1413202), collagen I Rat Protein (Gibco Life Technologies,

A1048301) and water. The cell-gel mixture was poured into the PDMS wells and allowed to solidify for 30 minutes at 37°C. Each construct contained either 5×10^5 CMs alone or 5×10^5 CMs plus 5×10^4 supportive cells. Constructs were then fed with 7ml of RPMI media with B27 plus insulin every other day, and spontaneous contractions were observed within five days. All constructs were cultured for 14-21 days and immediately snap-frozen after measurements in liquid nitrogen for further RNA analyses via RT-qPCR.

2:4:2 Frank-Starling force measurements of 3D-EHTS

Force measurement of constructs was performed after two weeks in culture as previously described (Ruan et al. 2015, Bargehr et al. 2019). In brief, constructs were removed from the PDMS wells and suspended between a force transducer (Aurora Scientific, model 400A) and length controller (Aurora Scientific, model 312B). To assess the Frank-Starling relationship, constructs were stretched from their resting length to an additional 25% strain in 6 steps while being bathed in a HEPES-buffered Tyrode solution held at 37°C. Force traces were first recorded without electrical stimulation and subsequently with 1, 1.5, 2.5Hz at 5V and 50ms pulse duration. Passive tension and active force traces were recorded and analysed using customized LabView and MATLAB software.

2:4:3 Non-ratiometric assessment of 3D-EHT calcium-handling

As for the Ca²⁺-handling by 3D-EHTs, all two-week-old constructs were incubated with Fluo-4 AM (Molecular Probes, Invitrogen) for 30 min at 37.5°C. Videos of constructs were taken at intrinsic beating rates and when paced at 1Hz, 1.5Hz and 2Hz with a Sony Handycam (Vixia HFS20) attached to a fluorescence microscope (Nikon Eclipse TS100). All videos were taken at 60 frames per second (fps), subsequently converted to frames, imported, and analysed for fluorescence intensity per frame using Image J software. All videos were normalized to the background Ca²⁺ signal.

2:4:4 Histological processing of 3D-EHTs

Constructs were washed in PBS, fixed in 4% PFA for 60 minutes and embedded in 30% sucrose overnight at 4°C to reduce the tissue water content and improve tissue preservation during subsequent cryo-embedding. Tissues were washed in PBS and allowed to equilibrate in a small amount of optimal cutting temperature compound (OCT) before being transferred to new tissue holders where they were fully embedded in OCT. The embedded constructs were subsequently transferred onto an ice bath composed of 100% ethanol on dry ice. Cryo-embedded blocks were serially sliced on a cryotome producing sections with a 10µm thickness.

2:4:4 RNA extraction from 3D-EHTs for gene expression analyses

EHTs were dissociated for gene expression analysis one day after the 2-week *in situ* contractile analyses were performed. Total cellular RNA was extracted with ARCTURUS PicoPure RNA Isolation Kit (KIT0103, Applied Biosystems) with the following modifications. EHTs were dissociated with Lysing Matrix D beads (116913050, MP Biomedicals) and 200 μ l Extraction Buffer and homogenized using a FastPrep-24 5G Instrument (MP Biomedicals) for 30s. The lysate was transferred to a fresh tube and incubated at 42 °C for 30 min. Subsequently, 70% ethanol was added to the RNA lysate and loaded into a preconditioned column. All the following steps were performed according to the supplier's recommendations, including DNase I treatment. Next, 10 μ l eluted RNA (corresponding to 75–150 ng) was subjected to reverse transcription using Maxima First Strand kit (K1641, Thermo) according to the manufacturer's protocol.

2:4:5 Quantitative real-time reverse transcription PCR (RT-qPCR)

RT-qPCR was performed with SYBR Select Master Mix (Applied Biosystems, 4472913) using 2 ng of cDNA and 400 nM each of forward and reverse primers. Reactions were run on a 7900HT Fast Real-Time PCR System (Applied Biosystem, 4329001), and data were analyzed using the $\Delta\Delta$ Ct method using *HPRT1* or *GAPDH*

as the housekeeping gene. Primers were designed using PrimerBlast and confirmed to amplify a single product. Primers sequences are listed below in **Table 10**.

Gene	Species	Forward Primer	Reverse Primer
MYH6	<i>Homo Sapiens</i>	GCCCTTTGACATTGCACTG	GGTTTCAGCAATGACCTTGCC
MYH7	<i>Homo Sapiens</i>	ACTGCCGAGACCGAGTATG	GCGATCCTTGAGGTTGTAGAGC
TNNI3	<i>Homo Sapiens</i>	TTTGACCTTCGAGGCAAGTTT	CCCGGTTTTCTTCTCGGTG
TNNI1	<i>Homo Sapiens</i>	CCGGAAGTCGAGAGAAAACCC	TCAATGTCGTATCGCTCCTCA
TNNT2	<i>Homo Sapiens</i>	CCGGAAGTCGAGAGAAAACCC	TCAATGTCGTATCGCTCCTCA
TBX18	<i>Homo Sapiens</i>	ACTCCGGGCGCAACAGAATGG	TGGGCCCCAGATGGAAGGCA
WT1	<i>Homo Sapiens</i>	CACAGCACAGGGTACGAGAG	CAAGAGTCGGGGCTACTCCA
TCF21	<i>Homo Sapiens</i>	TCCTGGCTAACGACAAATACGA	TTTCCCGGCCACCATAAAGG
BNC1	<i>Homo Sapiens</i>	GGCCGAGGCTATCAGCTGTACT	GCCTGGGTCCCATAGAGCAT
NANOG	<i>Homo Sapiens</i>	TCCTGAACCTCAGCTACAAACA	GGTAGGTGCTGAGGCCTTCT
SOX2	<i>Homo Sapiens</i>	TGGACAGTTACGCGCACAT	CGAGTAGGACATGCTGTAGGT
FN1	<i>Homo Sapiens</i>	AGCAAGCCCGGTTGTTATGA	CCCACTCGGTAAGTGTTC
POSTN	<i>Homo Sapiens</i>	TGAGGCTTGGGACAACCTTGG	AACAGTGACAACCCATTAGGA
COL5A2	<i>Homo Sapiens</i>	CCCACAGCTGACTTCATGGT	CACCATATCCTTCATCCTCGTC
TFAM	<i>Homo Sapiens</i>	CGCTCCCCCTTCAGTTTTGT	CCAACGCTGGGCAATTCTTC
CKMT2	<i>Homo Sapiens</i>	GCCAGGGGAATCTGGCATAA	CCCAGCCTCGTTCTTGGATT
CPT1B	<i>Homo Sapiens</i>	ACATCTCTGCCCAAGCTTCC	ACCATGACTTGAGCACCAGG
GLUT4	<i>Homo Sapiens</i>	ACTGGCCATTGTTATCGGCA	GTCAGGCGCTTCAGACTCTT
CASQ2	<i>Homo Sapiens</i>	TTGCCATCCCCAACAAACCT	AGAGTGGGTCTTTGGTGTTC
CACNA1 C	<i>Homo Sapiens</i>	GCCGCTGCAGGAGAGTTTTA	CCCACATGTGCAAGACCACA
SCN5A	<i>Homo Sapiens</i>	GGAGAGCGGCTGTGAAGATT	CGGTGAAGGTGTACTIONGACA
RYR2	<i>Homo Sapiens</i>	ACAACAGAAGCTATGCTTGGC	GAGGAGTGTTTCGATGACCACC

SLC8A1	<i>Homo Sapiens</i>	AGACCTGGCTTCCCACCTTTG	TGGCAAATGTGTCTGGCACT
HPRT	<i>Homo Sapiens</i>	TGACACTGGCAAAACAATGCA	GGTCCTTTTCACCAGCAAGCT
GAPDH	<i>Homo Sapiens</i>	AACAGCCTCAAGATCATCAGC	GGATGATGTTCTGGAGAGCC

Table 10: Primers for RT-qPCR analysis of the RNA expression of genes of interest

2:5 Small Peptide Inhibitor (pUR4) of Fibronectin

2:5:1 pUR4 generation and cellular treatment

pUR4 is a small peptide derived from a surface protein of *Streptococcus pyogenes* termed F1 adhesin and is a well-described inhibitor of FN polymerization (Valiente-Alandi et al. 2018). pUR4 at ~99% purity was obtained commercially from Genscript. At day seven after epicardium directed differentiation, hESC-epicardium received pUR4 (500 nM) for 72h. During 3D-EHT generation, 10 uL of pUR4 (500nM) was included in the gel mixture, and similar concentration of pUR4 was added to the 3D-EHTs during alternative day media changes, for a total of 14 days.

2:5:2 Western blot of pUR4-treated hESC-epicardium

After 72 hours of pUR4 treatment, FN protein content was assessed by immunoblotting. Lysate from one confluent well of hESC-epi cells from a six-well plate was separated by SDS PAGE on an 8% acrylamide gel, using 10 ul of Precision Plus Protein All Blue as standards. Protein was then transferred overnight onto a polyvinylidene difluoride (PVDF) membrane (Merck Millipore, IPVH00010). Membranes were blocked with 5% fat-free milk in Tris-buffered saline and 0.05%

Tween 20 (TBS-T) for 1 hour at room temperature, followed by incubation overnight at 4°C. Membranes were washed with TBS-T three times for 5 minutes at RT before incubation with secondary anti-rabbit or anti-mouse HRP-conjugated antibody (Sigma) for 1 hour at RT. Membranes were washed with TBS-T, and protein was detected with ECL western blotting detection reagents (Pierce). If necessary, the blot was stripped with mild stripping buffer for 1 hour and probed again. Antibodies used in western blot are outlined in **Table 11**.

Antibody type	Protein	Species	Dilution	Supplier
Primary	FN	Rabbit	1:250	Abcam (ab2413)
Primary	β -actin	Mouse	1:1000	CST (2148S)
Secondary	/	Anti-rabbit HRP	1:10,000	NEB (7074S)
Secondary	/	Anti-mouse HRP	1:10,000	NEB (7076S)

Table 11: Antibodies for western blotting

2:6 Generation of CRISPR-Cas9-mediated Knockout Fibronectin (KOFN) hESC cell Line

2:6:1 Crispr-Cas9-mediated knockout: annealing and cloning *FN1*- targeted sgRNA

Oligonucleotides were designed using *homo sapiens FN1* sequences from Genscript (<https://www.genscript.com/gRNA-database.html>) and modified according to a Zhang Lab protocol (<https://www.addgene.org/crispr/zhang/PX459-SpCas9+sgRNA>), **Table 12**. Oligonucleotides were annealed according to the protocol supplied by Zhang and colleagues (Ran et al. 2013), and then ligated into the cut vector pSpCas9(BB)-2A-Puro (PX459) V2.0 (a kind gift from Feng Zhang) using T4 ligase for one hour at room temperature, **Figure 12**. Subsequently, the ligation mix was transformed into alpha-select competent cells (BioLine) according to the manufacturers' directions. The

transformed cells were plated onto LB agar plates containing ampicillin and incubated overnight before colony picking and sequencing.

sgRNA ID	Oligo (5' to 3')	Oligo (3' to 5')
sgRNA 1	CACCGGACCTACCTAGGCAATGC GT	CCTGGATGGATCCGTTACGCACA AA
sgRNA 2	CACCGTACAAACCAACGCATTGC CT	CATGTTTGGTTGCGTAACGGACA AA
sgRNA 3	CACCGGCTCATAAGTGTACCCCA CT	CCGAGTATTCACAGTGGGTGACA AA
sgRNA 4	CACCGGAATGGACCTGCAAGCCC AT	CCTTACCTGGACGTTCTGGGTACA AA
sgRNA 5	CACCGTCACACACCTATGGGCTT GC	CAGTGTGTGGATACCCGAACGC AAA
sgRNA 6	CACCGGACTGTACCTGCATCGGG GC	CCTGACATGGACGTAGCCCCGC AAA

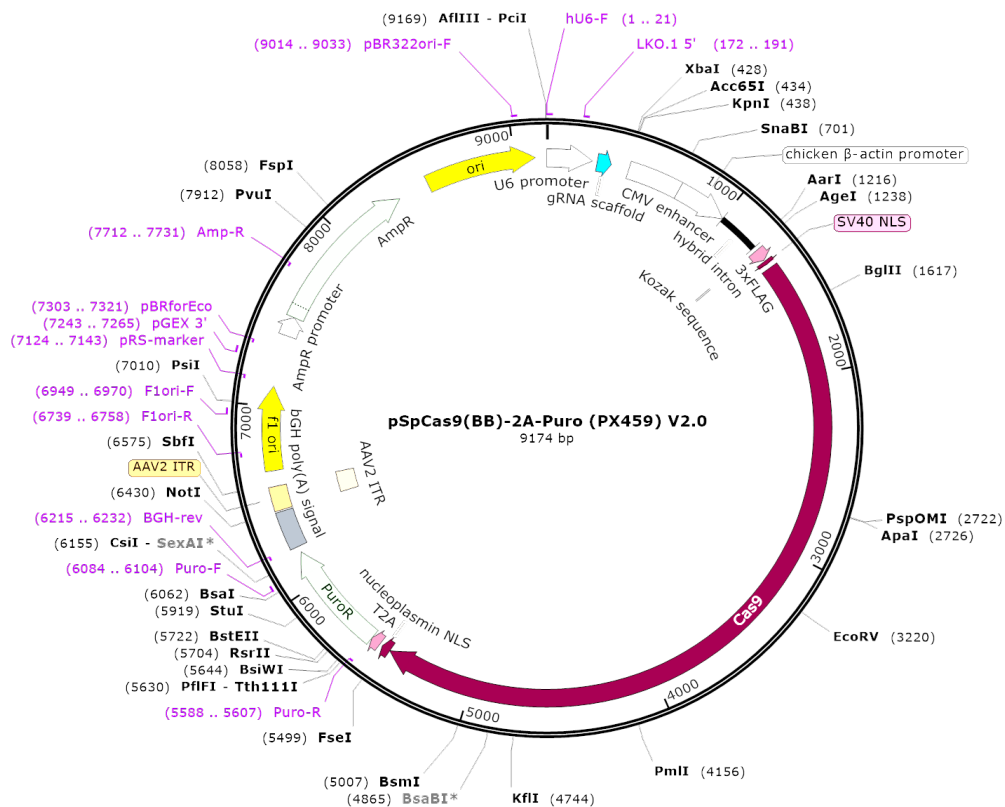


Figure 12: Vector map of pSpCas9(BB)-2A-Puro (PX459) V2.0, used for sgRNA *FN1* knockout. A kind gift from Zhang lab (Addgene plasmid #62988; <http://n2t.net/addgene:62988>; RRID: Addgene_62988). Insert for sgRNA scaffold is as shown. Successfully targeted cells were selected via ampicillin resistance.

2:6:2 Sequencing of transformed cells

Colonies of transformed cells grown on LB agar plates overnight were picked in the morning and further expanded in LB broth overnight at 37°C. Each colony was then digested using the restriction enzyme BbsI, which cuts in unmodified plasmid but not in plasmid with insert, to select out the cloned plasmids with sgRNA. Unmodified PX459V2 plasmid was used as a control. Colony digests were analysed by agarose gel (1%) electrophoresis (1.30 hour at 100V). Uncut plasmids, i.e., those with the desired insert, showed a size of 580bp. Positive colonies were plasmid mini-prepped (Qiagen, miniprep kit, used according to manufacturers' directions) before UW sequencing via Source BioScience. Mini-prepped plasmids which showed the correct insertion of the sgRNA sequence were selected for midiprep (Qiagen).

2:6:3 Gene-targeting by GeneJuice-mediated transfection

To generate the *FN1* knockout hESC cell line, individual wells of hESCs were transfected with five different cloned plasmids using GeneJuice. Following cell passaging, hESCs were incubated with 4 µg of DNA and 10 µl per well of GeneJuice in Opti-MEM medium (Gibco) for 24 hours. Briefly, cells were washed in PBS before incubation with DNA-OptiMEM mixtures. The DNA-OptiMEM mixtures were:

- i) Mixture 1 comprised 4 µg DNA in 250 µl OptiMEM per well of a six-well plate.
- ii) Mixture 2 consisted of 10 µl GeneJuice in 250 µl OptiMEM per well.

Mixtures 1 and 2 were prepared and mixed gently before incubation at room temperature for 5 minutes. 250 µl of Mixture 2 was then added to 250 µl Mixture 1 before incubation at room temperature for 20 minutes.

500 µl transfection mix of 1:1 of Mixture 1 & Mixture 2, respectively, was added dropwise to each well of hESCs. After 24 hours of incubation with DNA-OptiMEM mixtures, the cells were washed with PBS and culture medium (mTeSR) was added. After 1-2 days, 1 µg/ml puromycin-enriched culture media was added to the cells. After seven days, puromycin-resistant colonies were picked and expanded.

2:6:4 Genotyping of targeted clones

Genomic PCR was used to screen genetically targeted clones to verify site-specific targeting, determine whether allele targeting was heterozygous or homozygous, and to check for off-target integrations of the targeting plasmid. (See **Table 12** for PCR primers). Briefly, confluent colonies were used for genomic DNA extraction (Qiagen kit DNeasy, used according to manufacturer's instructions) and genomic PCR with *FN1*-specific primers were done. All PCRs were performed using 100 ng of genomic DNA as a template in a 25 µl reaction volume using LongAmp Taq DNA Polymerase (NEB) according to manufacturers' instructions, including 2.5% (v:v) dimethyl sulphoxide (DMSO). sgRNA clones with correct amplicon size were purified with a PCR purification kit (Qiagen DNeasy kit) according to the manufacturer's instructions). The genomic DNA was sent for Sanger sequencing with either FWD or RVS *FN1*-specific primers.

<i>FN1</i> Primer name	FWD Sequence (5' to 3')	RVS Sequence (5' to 3')
<i>FN1_exon2_1</i>	ATGTGACTTCAATTGTCTGCCTT C	CTCGCAGTTAAAACCTCGGCT
<i>FN1_exon2_2</i>	TGGGAAAAGGAGAAATGCAAAT GTA	AACTATGGGGCTTGTTGTCAC
<i>FN1_exon3_1</i>	GTGGGTTTTCTTTAGAGGGGAT T	CCTTACTTGCGATGGTACAGC
<i>FN1_exon3_2</i>	ACCGAGTGGGTGACACTTATG	GGCAAACCTCAAAGTTCGGA
<i>FN1_exon4_1</i>	CATGAAGGGGGTCAGTCCTAC	TGTAGATGTGATTCTGGTCCAA CC
<i>FN1_exon4_2</i>	CGTTGTATCTTCAACAGACCGC	CTGGTCCAACCCACATTAGAA

Table 12: PCR primer sequences for genotyping Crispr-Cas9-edited KOFN clones

2:6:5 CRISPR-Cas9-mediated knockout FN hESC cell line

One homozygous-targeted clone for each vector transfection was selected for subsequent differentiation into hESC-epicardium.

2:7 Generation of Inducible Fibronectin Knockdown (sOPTiKD-FN) hESC cell line

2:7:1 Inducible knockdown: design and annealing shRNA oligonucleotides

Oligonucleotides were designed using TRC sequences from Sigma and are shown in **Table 13**. Hairpin A was selected as a validating hairpin as it downregulated B2M expression. Oligonucleotides were annealed according to the protocol supplied by Bertero and colleagues (Bertero et al. 2016), and then ligated into the linearised, optimised inducible knockdown sOPTiKD vector (a gift from the Vallier Group,

shRNA ID	Top oligonucleotide (5' to 3')	Bottom oligonucleotide (5' to 3')
FN1_1	GATCCCGCGTGGTTGTATCAGG ACTTATCTCGAGATAAGTCCTGA TACAACCACGTTTTTTG	TCGACAAAAAAGCTGGTTGTATCAGG ACTTATCTCGAGATAAGTCCTGATACA ACCACGCGG
FN1_2	GATCCCGCCTGCTCCAAGAATTG GTTTCTCGAGAAACCAATTCTTG GAGCAGGCTTTTTTG	TCGACAAAAAAGCCTGCTCCAAGAAT TGGTTTCTCGAGAAACCAATTCTTGG AGCAGGCGG
FN1_3	GATCCCGTGAACCGGGAACCG AATATACTCGAGTATATTCGGTT CCCGGTTCCATTTTTTG	TCGACAAAAAAGTGAACCGGGAACCG AATATACTCGAGTATATTCGGTTCCC GGTTCACGG
FN1_4	GATCCCGAATTTGGTTTGGGATC AATACTCGAGTATTGATCCCAA CAAATCTTTTTTTG	TCGACAAAAAAGAATTTGGTTTGGGA TCAATACTCGAGTATTGATCCCAAAC CAAATTCGG
FN1_5	GATCCCGTGCAGCACAACCTCGA ATTATCTCGAGATAATTCGAAGTT GTGCTGCATTTTTTTG	TCGACAAAAAAGTCAGCACAACCTCG AATTATCTCGAGATAATTCGAAGTTGT GCTGCACGG

Table 13: shRNA sequences for psOPTIkd vector construction. BglII overhang is in red, terminator sequence/Sall overhang in blue.

2:7:2 Colony PCR of transformants

After overnight incubation, transformants grown on LB agar plates were picked in the morning for colony PCR to check for transformation. AAVs-KD forward (CGAACGCTGACGTCATCAACC) and reverse (GGGCTATGAACTAATGACCCCG) primers were used; thermocycling conditions were as follows: 95°C for five minutes, then 35 cycles of 95°C for 30 seconds, 63°C for 30 seconds and 72°C for 1 minute. These PCR reactions were analysed by agarose gel (1.5%) electrophoresis; vectors with the desired insert showed a size of 520bp. Miniprep of transformed colonies (Qiagen, miniprep kit, used according to manufacturers' directions) were conducted for genomic DNA extraction before Sanger sequencing. Sequencing was done via Source BioScience with the protocol specified for strong hairpin structures. Plasmid vectors with a correctly inserted shRNA sequence were expanded and selected for Midiprep (Qiagen), in preparation for cell transfection.

2:7:3 Gene-targeting by GeneJuice-mediated transfection

To generate an inducible *FN1* knockdown hESC cell line, AAVS1 locus targeting was performed by GeneJuice-mediated transfection. Individual wells of hESCs were transfected with five different cloned plasmids using GeneJuice. Following cell passaging, hESC cells were incubated with 4 µg of DNA and 10 µl per well of GeneJuice in Opti-MEM media (Gibco) for 24 hours. Briefly, cells were washed in PBS before incubation with DNA-OptiMEM mixtures. To make DNA-OptiMEM mixtures:

i) Mix 1 (equally divided between the two AAVS1 ZFN plasmids, also received from Ludovic Vallier's laboratory, and our shRNA targeting vector) comprised 4µg DNA in 250 µl OptiMEM per well of a six-well plate.

ii) Mixture 2 consisted of 10 µl GeneJuice in 250 µl OptiMEM per well.

Mixtures 1 and 2 were prepared and mixed gently before incubation at room temperature for 5 minutes. 250 µl of Mixture 2 was then added to 250 µl Mixture 1 before incubation at room temperature for 20 minutes.

500 µl of a transfection mix of the 1:1 of Mixture 1 & Mixture 2 was added dropwise to each well of hESCs. After 24 hours of incubation with DNA-OptiMEM mixtures, the cells were washed with PBS and culture media (CDM-BSA II) was added. After 1-2 days, 1 µg/ml puromycin-enriched culture media was added to the cells. After seven days in culture, puromycin-resistant colonies were picked and expanded.

2:7:4 Genotyping of targeted clones

Genomic PCR was used to screen genetically targeted clones to verify site-specific targeting and determine whether allele targeting was heterozygous or homozygous. (See **Table 14** for PCR primers). Locus PCR ('PCR 1') for wild-type AAVS1 locus indicates a non-targeted allele. 'PCR 2' is a locus PCR/loss-of-allele PCR. 'PCR 2' and 'PCR 3' refer to 5'INT/3'INT PCR respectively, which are PCR reactions for vector backbone 5'-end and 3'-end genomic integration region, indicative of specific transgene targeting. This will also detail homozygous or heterozygous targeting.

Firstly, DNA was extracted from all targeted clones using a genomic DNA extraction kit (Sigma-Aldrich). All PCRs were performed using 100 ng of genomic DNA as a

template in a 25 µl reaction volume, LongAmp Taq DNA Polymerase (NEB), and including 2.5% (v:v) dimethyl sulphoxide (DMSO).

Primer name	PCR Type	Primer Sequence
AAVS1_Genomic_FWD	Locus ('1')	CTGTTTCCCCTTCCCAGG CAGGTCC
AAVS1_Genomic_REV	Locus ('1')	TGCAGGGGAACGGGGCT CAGTCTGA
AAVS1_Genomic_FWD	5' Integration into AAVS1 ('2')	CTGTTTCCCCTTCCCAGG CAGGTCC
AAV_Pur_REV	5' Integration into AAVS1 ('2')	TCGCGCGGGTGGCGAGG CGACCG
OPT_tetR_FWD	3' Integration into AAVS1 ('3')	CCACCGAGAAGCAGTACG AG
AAVS_Genomic_REV	3' Integration into AAVS1 ('3')	TGCAGGGGAACGGGGCTC AGTCTGA

Table 14: PCR primer sequences for genotyping sOPTIkd clones

2:7:5 Inducible FN knockdown hESC cell line

One homozygous-targeted clone for each vector transfection was selected for subsequent differentiation into hESC-epicardium with or without the addition of 1 µg/ml tetracycline (Sigma) to culture media with the aim of mediating *FN1* knockdown. hESC-epicardium was differentiated in the presence and absence of tetracycline.

2:8 Statistics

All *in vitro* studies were performed as three biological replicates (independent experiments) from different cellular differentiations. For *in vivo* experiments, the animals were selected by a blinded animal technician for intra-myocardial injections. Cardiac function of a specific animal prior to intra-myocardial injections or echocardiography was not known to the technician. Due to logistical and technical challenges, the study groups were performed in a serial manner. Death and FS% $\geq 40\%$ at D28 post-MI (Fernandes et al. 2010) were the only exclusion criteria for further histologic analysis. All *in vivo* data included the exact number of animals analysed for each parameter and each endpoint.

Statistical testing was performed using an unpaired t-test for two-group comparisons and a paired t-test for comparison of two paired groups. One-way ANOVA was used for the statistical comparison of more than two groups, and a post-hoc Tukey test was used if the group variance was equal. As for groups with unequal variance, a post-hoc Kruskal–Wallis test with Dunn’s correction for multiple comparisons was applied. Measuring two-sided significance, a *P*-value of 0.05 was considered statistically significant. All results are presented as mean \pm s.e.m unless otherwise stated. All analyses were performed using GraphPad Prism 8.0 software.

3. RESULTS CHAPTER I

3:1: Cellular Therapy Ameliorates Cardiac Function in a Chronic MI Rat Model

Cellular therapy is an attractive, alternative therapy for chronic heart failure patients. However, mixed results had been reported for the delivery of NRVMs into a chronic MI rat model (Li et al.1996; Sakakibara et al. 2002; Huwer et al. 2003). Moreover, delivery of hESC-CMs alone in a chronically infarcted rat heart showed no benefits (Fernandes 2010 et al.; Shiba et al. 2014). However, I noted huge variability in the chronic MI rat studies; differences in cell dosage, cellular pre-conditioning (PSC) and the type & extent of cardiac injury (Li et al.1996; Sakakibara et al. 2002; Huwer et al. 2003). These key variables might explain the mixed results in the earlier chronic MI studies.

Thus, I proposed to streamline my chronic MI rat studies by using exact cellular doses with cellular preconditioning (pro-survival cocktail), a physiological MI animal model with ischaemic-reperfusion(I/R) injury, and with a novel cellular adjunct via co-delivery with hESC-epicardium. Streamlining studies in this manner should offer fresh insights and address whether hESC/IPSC-derived cellular therapy could salvage the chronically infarcted myocardium.

3:1:1 Optimization of rodent MI studies

3:1:1:1 Pro-survival cocktail (PSC)

Prior to launching into chronic MI animal studies, I ascertained that the PSC improved the survival of hESC-epicardium, *in vivo*. PSC was designed to ameliorate the effects of the three inter-linked pathways that lead to cell death post-injection: ischaemia, *anoikis* and inflammation (LaFlamme et al. 2007). However, the benefit of PSC has only been widely described for the delivery of hESC/IPSC-CMs (Chong et al. 2014; Gerbin et al. 2015; Liu et al. 2018). Although unlikely, one of the potential reasons for the functional decline with the delivery of hESC-epicardium alone, as reported by Bargehr *et al.*, could be that the PSC' has detrimental effects specific to hESC-epicardium alone (Bargehr et al. 2019).

To address this question, a set of pilot animal studies were carried out. Athymic nude rats received intramyocardial injections of hESC-epicardium (5×10^6 cells) delivered in Matrigel with PSC and heat-shock (n=4) or in Matrigel without either PSC or heat-shock (n=4) at four days after MI. All animals were followed up for 28 days; the study schematic is shown in **Figure 14A**. Infarct sizes across both groups were similar, and all animals survived till endpoint. The subacute MI timepoint was chosen as it is the most favourable timepoint for cellular therapy, corresponding to the angiogenic phase of wound repair (LaFlamme et al. 2007) This experimental decision enabled the focus to be on the effects of PSC on hESC-epicardial cell viability. Our study showed greater cell survival when hESC-epicardial cells were subjected to heat-shock and delivered with the pro-survival cocktail four days after myocardial infarct (MI), **Figure 14B**. Thus,

PSC and heat-shock enhanced broad cellular survival, unrestricted to hESC/IPSCs-CMs alone.

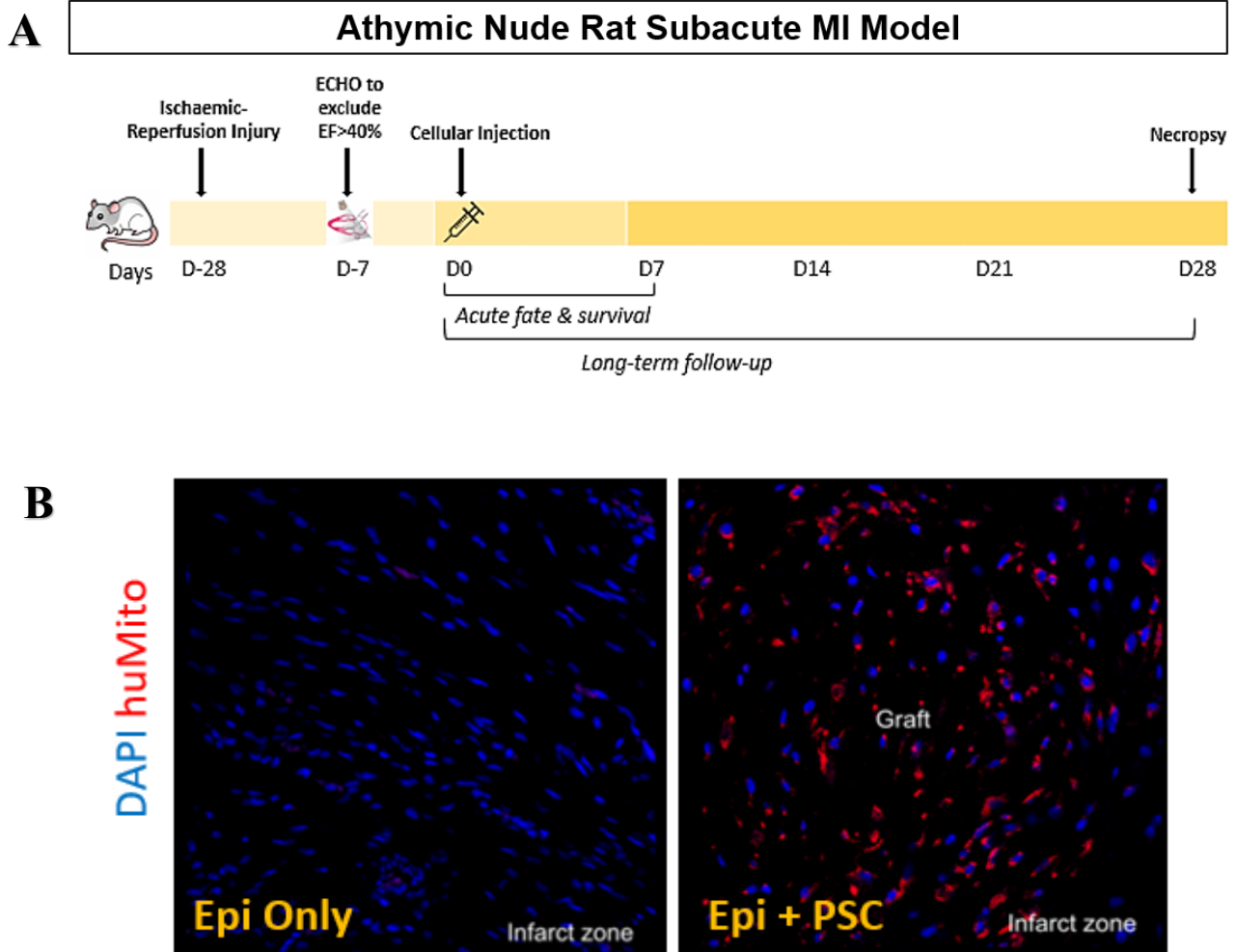


Figure 14: hESC-Epicardium showed greater survival with a pro-survival cocktail in subacute MI rat model.

A Schematic overview of subacute MI animal model with cellular delivery four days after MI with 60 min ischaemic-reperfusion injury. Two groups: i) hESC-epicardium (5×10^6 cells) with PCS & HS and ii) hESC-epicardium only (5×10^6 cells) were injected four days post-infarction. $N=4$ in each group. **B** Immunofluorescence of infarcted heart sections showed greater hESC-epicardium (huMito, red) survival with PSC & HS. (Immunofluorescence images captured with thanks to Bargehr et al.)

3:1:1:2 NODScid gamma mouse

Having ascertained that PSC enhanced cellular survival, I next interrogated the feasibility of different rodent models for the chronic MI study. From a purely practical perspective, mice were more accessible than rats, with more mouse-focused surgical experience locally. Moreover, studies with human-derived epicardial cell were first reported in the mouse MI model (Winter et al. 2007, 2010). Thus, I investigated the survival of hESC-derived epicardium in the NODScid Gamma mouse model. NODScid Gamma mouse was chosen as an initial model as it is one of the most immunodeficient strains of mice, with no T cells, B cells or NK cells, thus reducing the effects of the immune system on cell survival. As such, the effects of the PSC and heat shock should be readily apparent. Due to technical challenges and reduced resilience in mice to MI and ischaemia-reperfusion injury (I/R), this was carried out as permanent LAD ligation with direct intramyocardial injections. NODScid Gamma mouse received intramyocardial injections of hESC-epicardium (5×10^5 cells) delivered in matrigel with PSC and heat-shock (n=4) or matrigel alone without PSC or heat-shock (n=4) immediately after MI. All animals were followed up for 28 days; the study schematic is shown in **Figure 15A**.

Although infarct sizes across both groups were similar, there was minimal/no cell survival in the NODScid Gamma mouse MI model for cellular injection with or without heat-shock and pro-survival cocktail, **Figure 15B**. Also, we had two animal deaths in the NODScid Gamma mouse acute MI model, compared to none in the subacute MI rat model. The acute MI model used with the mice creates a local micro-environment that is exceptionally hostile to the newly injected cells, far more so than the sub-acute model used the rats. The mouse is also a smaller species with a greatly accelerated

heart rate. Collectively, due to the acute MI setting, technical challenges, and increased animal deaths with no cellular survival with PSC, the NODScid Gamma mouse MI model was not chosen for further cellular therapy experiments.

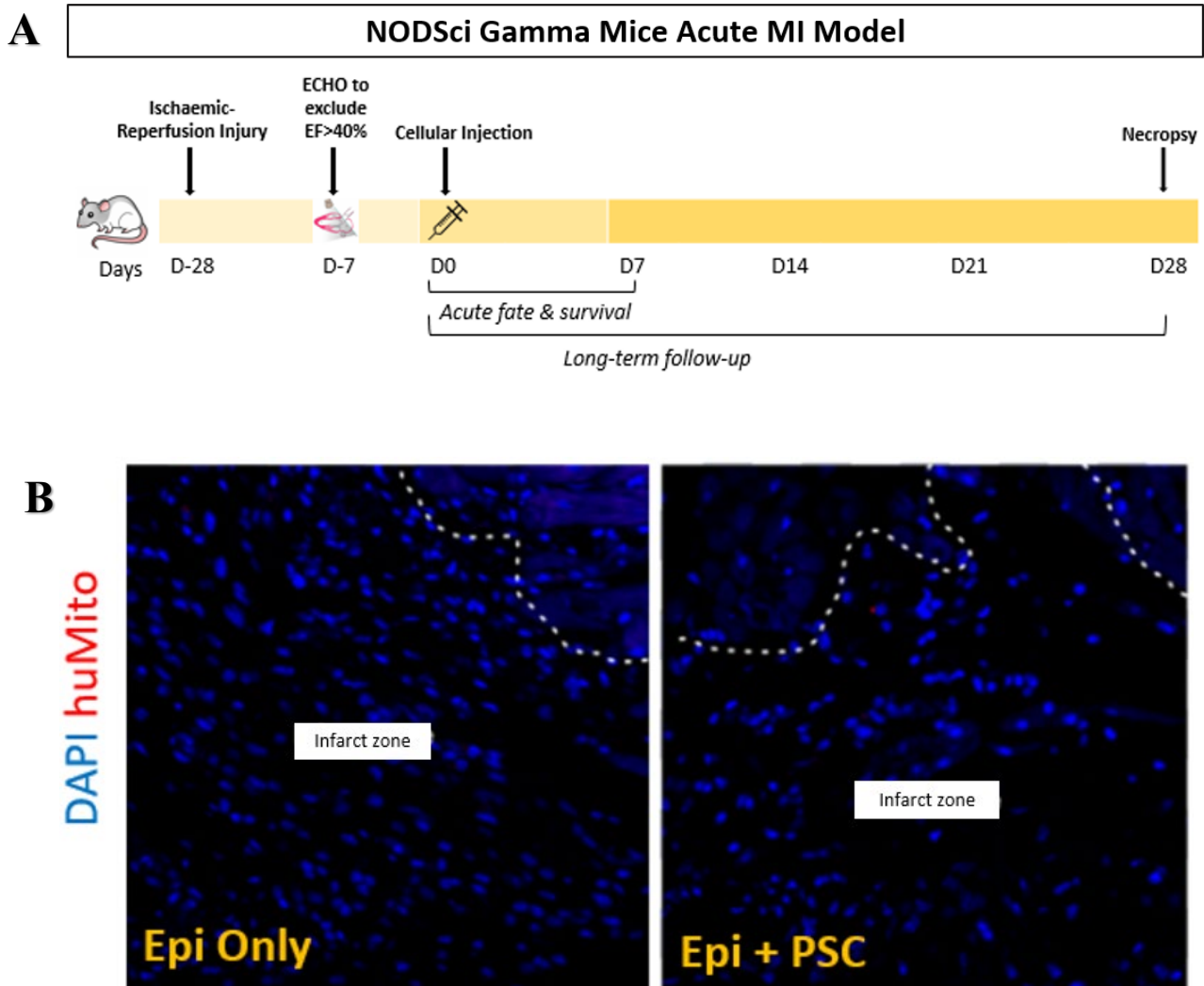


Figure 15: Pro-survival cocktail did not improve hESC-epicardium survival in the NODScid gamma mouse acute MI model.

A Schematic overview of NODScid Gamma mouse acute MI, invoked by permanent left anterior descending artery (LAD) ligation, with cellular delivery immediately after MI. Two groups: i) hESC-epicardium (5×10^5 cells) with PCS & HS and ii) hESC-epicardium only (5×10^5 cells), were injected four days post-infarction. N=4 in each group. **B** Immunofluorescence of infarcted heart sections showed no hESC-epicardium (huMito) survival with or without PSC and heat-shock. (Immunofluorescence images captured with thanks to Dr. Bargehr et al)

3:1:2 Cellular therapy to regenerate the chronically infarcted rat hearts

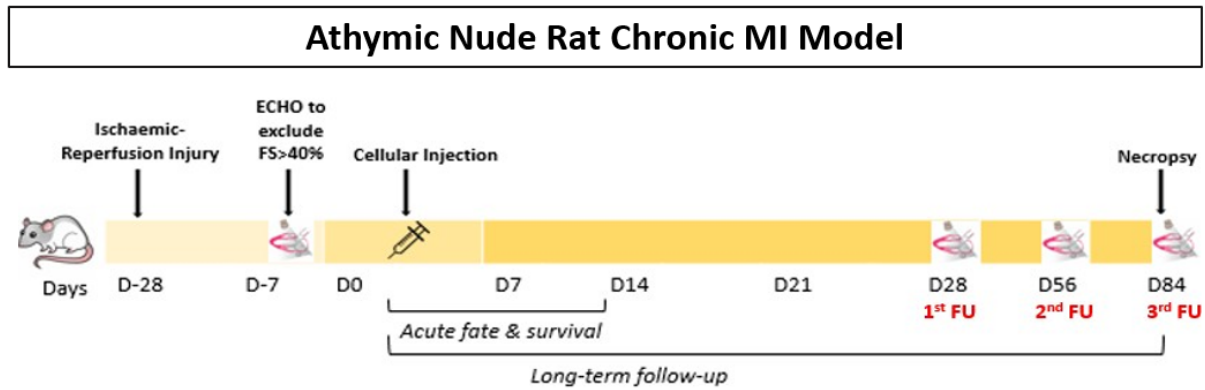
Based on the findings of the pilot studies, all subsequent cells were delivered in matrigel with PSC and heat-shock, using an athymic nude rat model for the chronic MI animal studies. As for the type of cardiac injury, proximal LAD ligation for 60 min with ischaemic-reperfusion injury (I/R) would better mimic the clinical sequelae of MI (Riehle et al. 2019). Moreover, the athymic nude rat MI I/R model had been used successfully for both subacute and chronic MI settings (Fernandes et al. 2010; Gerbin et al. 2015; Bargehr et al. 2019). The following set of studies were carried out in the University of Washington, Seattle with the help of Amy Martinson (A.M.), an experienced animal technician. Due to my surgical background, I was trained in the surgical animal model during these experiments to subsequently set up the model in Cambridge for future studies.

3:1:2:1 Experimental design of chronic MI rat studies

To overcome the hostile chronic MI environment, I rationalised that only optimal cell types, singularly or in combination, would form sufficiently sizable cardiac grafts to reverse heart failure. Notably, neonatal rat pups at P1/2 retain the endogenous potential to regenerate their hearts after cardiac injury (Porrello et al. 2011). Firstly, I hypothesised that species-matched cellular therapy with NRVMs delivered at the right dosage with PSC would represent the optimal donor cell type. Secondly, I hypothesised that despite the species-mismatch, co-delivering hESC-epicardium and hESC-CMs, a cell combination proven to augment cardiac graft sizes in the subacute MI setting, may lead to the regeneration of the chronically infarcted heart.

To test these hypotheses, I carried out a modestly sized study (n=24) in which animals were placed in one of three treatment arms following myocardial infarction. Study animals received an intramyocardial injection of either: i) 10×10^6 P1/2 NRVM, ii) a combination of hESC-CMs (10×10^6) and hESC-epicardial cells (5×10^6) [Epi+CM] or iii) PSC/Matrigel alone (a vehicle control) [Sham]. Each treatment arm consisted of 8 animals and all cells received PSC and heat-shock. A schematic of the study design is shown in **Figure 16**. The CM cell number was kept constant for both NRVM and hESC-CMs, whilst hESC-epicardium was delivered at 5×10^6 cells, as previously reported (Bargehr et al. 2019). CM cell number was kept constant to assess the degree of 'primary remuscularization'; hESC-epicardium is not known to give rise to *de novo* CMs (Cao and Cao 2018).

Next, the chronic heart failure rat model was optimised. As above, each animal received a proximal LAD ligation for 60 min. The rat's cardiac function was assessed as left ventricular (LV) function by echocardiography (VisualSonics 2.0) and expressed as fractional shortening (FS%). FS% was calculated via echocardiography-derived M-MODE images of the left ventricle at the short-axis view (SAX), **Figure 17**. Short axis views gave cross-sectional views of the left ventricle contracting, thus capturing overall contractile function.

A**B**

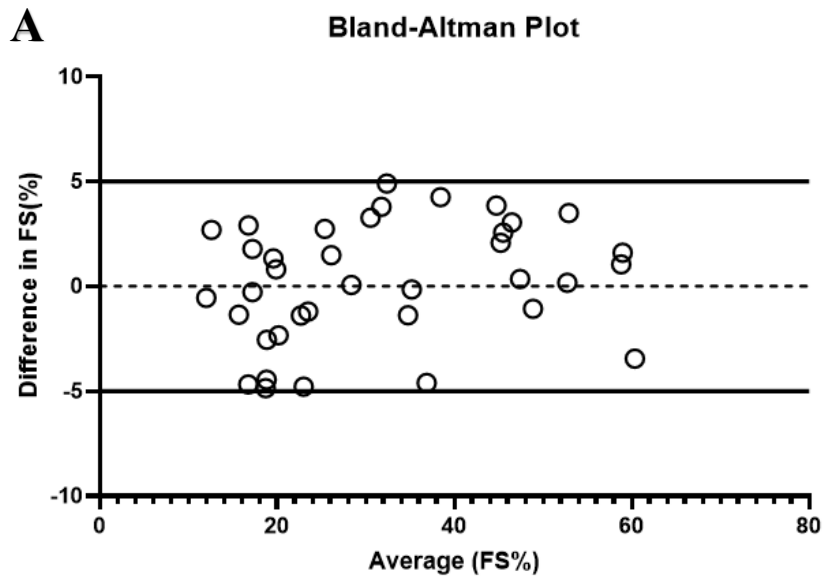
N-8 per group	Cells	
Sham	/	PSC Only
Species-Match	NRVM- 10×10^6	PSC & H/S
Combination Therapy	CM- 10×10^6 Epi- 5×10^6	PSC & H/S

Figure 16 Experimental design for Cellular therapy in Chronic MI study

A Study schematic with timing of cellular therapy and echocardiographic follow-up (FU) in the chronic MI rodent model. The rats received myocardial infarction with ischaemic-reperfusion injury. 21 days later, the infarcted rats underwent an echocardiogram (ECHO) to evaluate their respective cardiac functions. Cardiac function was calculated as FS (Fractional Shortening; %). As per *a priori* exclusion criteria, rats with FS >40% were excluded from the study. The remaining rats received intramyocardial cellular injections. All rats were followed up with serial monthly echocardiography up until 3 months post-cellular injection. **B** There were 3 different study arms with cell types and numbers as shown. Both species-matched and combination therapy groups received pre-conditioning with PSC and heat-shock. *NRVM*: neonatal rat CMs, *Epi+CM*: hESC-epicardium & hESC-CMs, *PSC*: pro-survival cocktail, *H/S*: heat-shock.

All animals received echocardiography at i) Baseline: prior to injury ii) Screening: D21 post-cardiac injury iii) 1st-month follow-up: D28 post-injection iv) 2nd-month follow-up: D56 post-injection and v) 3rd-month follow-up: D84 post-injection. An *a priori* exclusion criterion was made, whereby animals were excluded if their FS $\geq 40\%$ at D21 post-injury (Fernandes et al. 2010), **Figure 18A**. Only animals with FS $\leq 40\%$ qualified as having chronic heart failure and proceeded to cellular injections. All echocardiographic results are as shown in the **Appendix 9.2**.

Prior to study analyses, we validated interobserver ECHO analyses with the Bland-Altman plot. Interobserver agreement on echocardiographic analyses between 2 independent investigators was undertaken in a test sample, with *a priori* agreement on deviation in measurements. Our Bland-Altman plots showed an acceptable range of the average FS% difference (x-axis) and the difference between the measurements of the two different investigators (y-axis), **Figure 18**.



B

	Baseline N-8	Pre-injection N-8	1st Follow-up N-8	2nd Follow-up N-7	3rd Follow-up N-7	Total N-38
Interobserver Agreement	0.94 (0.7-0.98)	0.96 (0.82-0.99)	0.85 (0.66-0.99)	0.93 (0.61-0.99)	0.96 (0.78-0.99)	0.98 (0.96-0.99)

Figure 18 Bland-Altman plot showed the degree of interobserver agreement for FS% calculations

To evaluate whether cellular therapy could invoke functional recovery in the chronic MI setting, chronically infarcted rodents received intramyocardial injections, with subsequent monthly echocardiographic analyses of their cardiac function. **A** An interobserver agreement on the echocardiographic analyses of infarcted rats was undertaken in our chronic MI rodent study. Bland-Altman plots show the average FS% difference (x-axis) and the difference between the measurements of two different investigators (y-axis). The continuous lines exhibit *a priori* agreed deviation in measurements. For the baseline, pre-injection and 1st follow-up, there were N=8 per group. For 2nd and 3rd follow-up, there were N=7 per group. Total animals N=38. **B** Intraclass correlation coefficients (ICCs) were shown for all measurements with 95%CI.

After the exclusion criteria of $FS \leq 40\%$ at D21 post-MI, there were 6 animals in Sham, 5 animals in NRVM and 8 animals in the Epi+CM study arms, respectively. These remaining animals underwent a second thoracotomy followed by three separate intramyocardial cellular injections into the infarct and border zones at 4 weeks post-MI. This timepoint correlated with chronic heart failure in rats whilst any later timepoints precipitated scar expansion resembling LV aneurysm (Li et al. 2001; Houser 2012; Riehle and Bauersachs 2019). All animals were followed up to 3 months post-injection. This length of follow-up was chosen as cardiac grafts matured *in vivo*, with significant histological changes over three months (Kadota et al. 2017). Due to the hostility of a chronic infarct environment, a longer follow-up period for observable engraftment and functional improvement might be required. Given the pathophysiology of heart failure and associated LV remodelling, the longer timeframe (i.e. 3 months post-cellular injection) was also chosen so that long-term trends in functional changes would be revealed.

Due to the severity of the chronic heart failure model, I accepted the study's overall attrition rate of 17%. This was comparable to other rodent MI studies, reporting ~21% mortality rates (Chen et al. 2011). There was one intra-operative death during intramyocardial injections due to severe and mature adhesions of chronic infarcts, **Appendix 9.1**. Aside from the intraoperative death, some animals died prior to the 3-month timepoint from sudden cardiac death during echocardiography (n=1), presumed sudden cardiac death with overnight deaths (n=2) and euthanised secondary to drastic weight loss (n=1). Overall survival curves between groups were not significantly different, **Figure 19**. Due to the small number of animals and several non-cardiac deaths, the limited conclusion was that the severity of heart failure model was equal across groups.

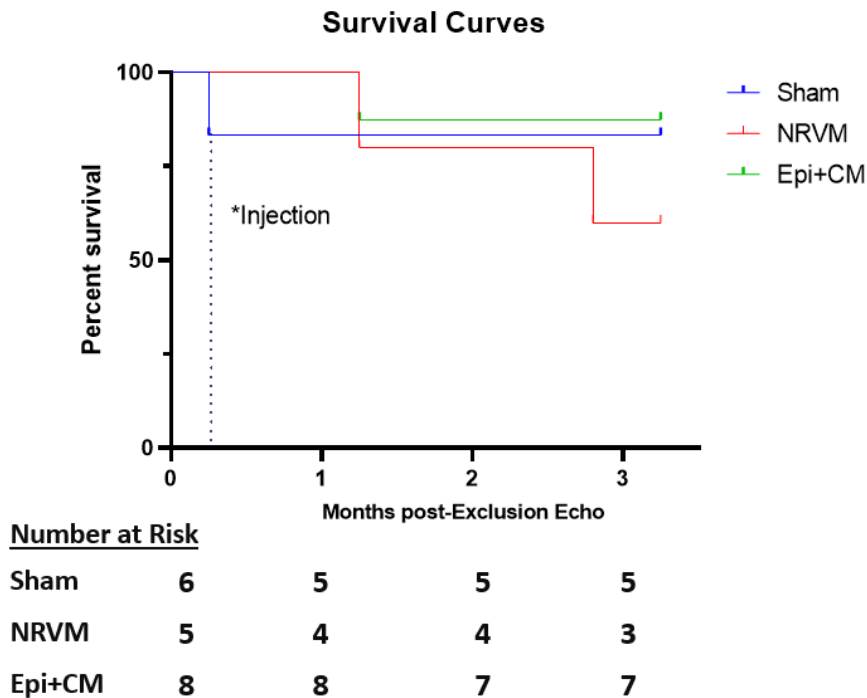


Figure 19 All-cause mortality Kaplan-Meier survival curves for all groups

All chronically infarcted rodents received intramyocardial injections, with subsequent monthly echocardiographic analyses of their cardiac function. This study aimed to investigate whether cellular therapy could invoke cardiac repair in the chronic MI setting. There were 3 groups - Sham (Vehicle-control), NRVM (species-matched cellular therapy) and Epi+CM (combination cellular therapy). After applying the exclusion criterion of FS \leq 40% at D21 post-MI, there were n=6 in Sham, n=5 in NRVM and n=8 in the Epi+CM groups which received intramyocardial cellular injections. Due to the severity of the heart failure model, the animals were followed-up for their overall survival following cellular injections. There was no significant difference between overall survival for each group, as calculated using the log-rank Mantel-Cox test. The cause of deaths is listed in the **Appendix 9.1**.

3:1:2:2 Cellular therapy ameliorated cardiac dysfunction in chronically infarcted rat hearts

All chronically infarcted animals received echocardiographic follow-up at 1 month, 2 months and 3 months after intramyocardial cellular injections to assess the effects of cellular therapy on their cardiac function. For the animals which survived beyond one month post-cellular therapy, their respective pre-injection FS% were Sham (28.1±3.59%) vs NRVM (19.2±1.2%) vs Epi+CM (21±1.2%). Sham's pre-injection FS% was significantly higher than NRVM ($p - 0.046$), denoting a less damaged heart. Meanwhile, there were no significant differences between the other groups, **Figure 20**. These results indicated that our animals in the cellular treatment groups were equally ill prior to cellular intervention.

Pre-Cellular therapy FS%

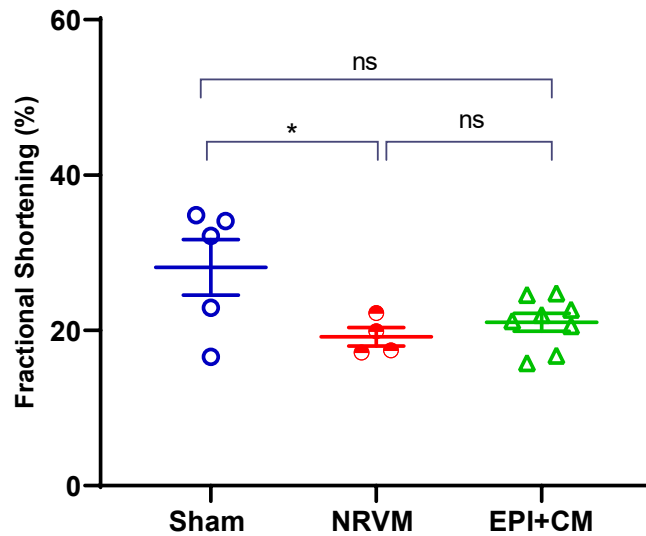


Figure 20: Both cellular treatment groups had similar pre-cellular therapy cardiac function

At D21 after MI, the cardiac functions (fractional shortening, FS%) for all rats were measured. All animals with FS $\geq 40\%$ were excluded. Only the animals with FS $\leq 40\%$ were in heart failure and eligible to continue with the study, under either the Sham, NRVM or EPI+CM study arms. All eligible animals received intramyocardial injections at D28 post-MI. Thus, cardiac function measured at D21 constituted pre-injection FS%. Sham had significantly higher pre-injection FS% than either of the cellular treatment groups. All panels, mean \pm s.e.m.; * $P < 0.05$ ** $P < 0.005$. Two-sided P values were calculated using a paired t-test for comparison of cardiac function within groups between baseline and one month follow-up. If more than two groups were compared, a one-way ANOVA with post-hoc correction for multiple comparisons was used. N=17 in total for functional analysis after 1 month; Sham, NRVM, Epi+CM, n=5, 4 and 8 animals.

The preliminary data suggested that both cell therapy groups showed potential to improve long-term cardiac function compared to sham, *despite of the chronic infarct environment*, **Figure 21-23**. Unfortunately, we cannot draw any definitive conclusions from this study as there were insufficient number of animals for an adequately-powered statistical analysis. For this thesis, we will discuss the preliminary work and how current results inform the future adequately-powered definitive rat study.

In this preliminary work, the cardiac function of the Sham group declined persistently to $\Delta\text{FS}=9.9\pm 2.9\%$ ($p=0.117$) at three months follow-up, **Figure 21**, despite better cardiac function prior to intramyocardial injections. The trend demonstrated by the Sham group represented the clinical course of heart failure after MI (Jessup et al. 2003).

By the third month of follow-up, the NRVM group demonstrated sustained cardiac functional recovery after receiving cellular therapy. Cardiac function for the NRVM group recorded an improvement of $\Delta\text{FS}=4.2\pm 2.8\%$ from pre-injection FS% ($p=0.78$), **Figure 21**. In contrast to previous studies (Huyer et al. 2003; Sakakibara et al. 2002), I observed cardiac functional recovery with the use of NRVMs in a chronic MI (I/R) model. This observation might be due to our usage of PSC and increased cell number. Surprisingly, EPI+CM was able to overcome the initial decline to recover by the 2nd month and attenuated further cardiac dysfunction by three months, with a smaller decline of $2.7\pm 0.7\%$ in FS%, ($p=0.126$), **Figure 21**. However, the degree of cardiac repair was less pronounced than species-matched therapy. These results further emphasised the need to streamline animal studies, in terms of their mode and extent of cardiac injury, cellular pre-conditioning methods and cellular doses. Otherwise, a pertinent result might be missed.

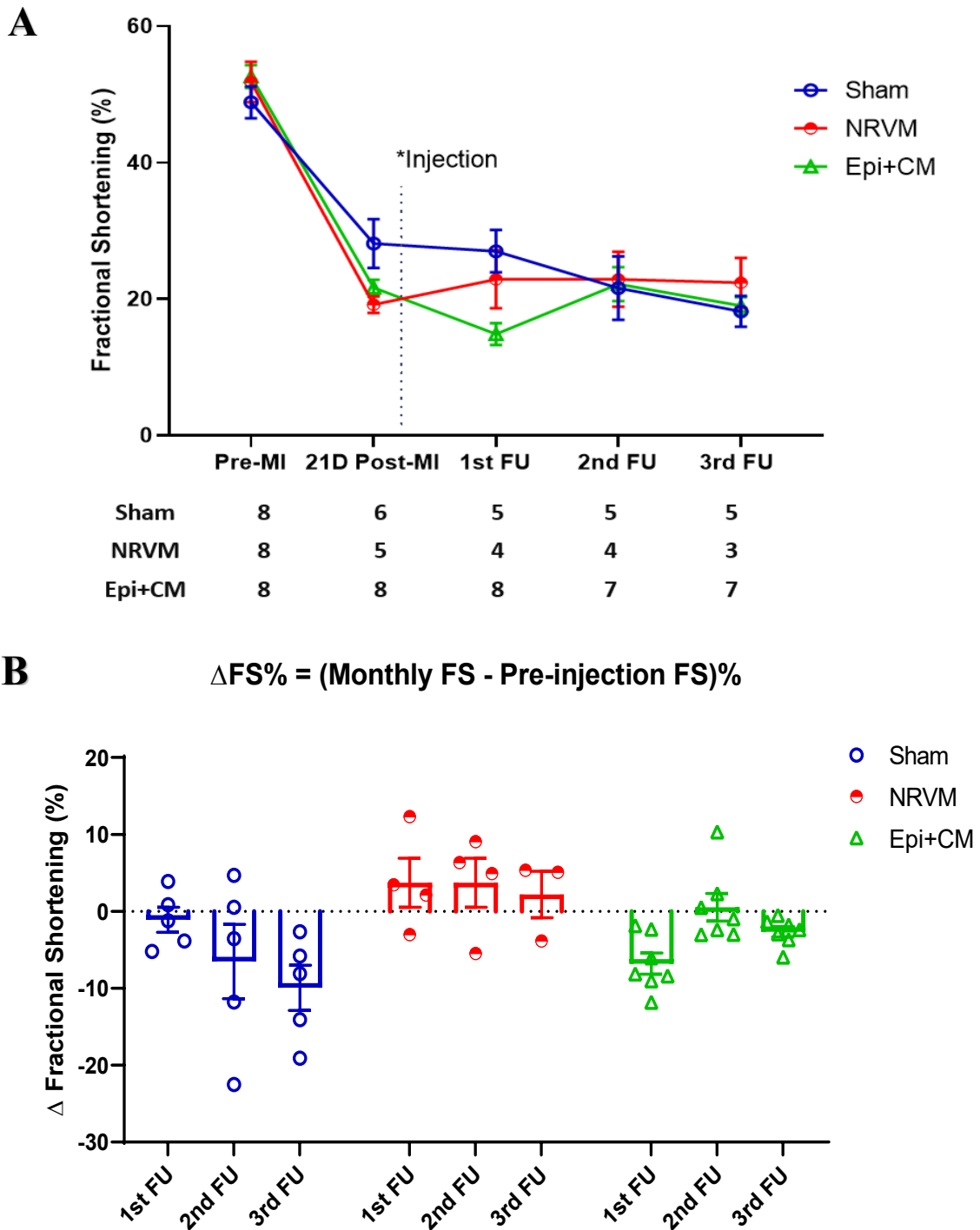


Figure 21: Cellular therapy attenuated cardiac dysfunction in chronically infarcted rat hearts

A Respective trend of the cardiac functional changes throughout the entire chronic MI rat study. Key timepoints include pre-myocardial infarction (MI), D21 after MI, intramyocardial injections and followed by monthly echocardiographic analyses until 3 months post-cellular therapy. The groups were Sham, species-matched cellular therapy (NRVM) and combination cellular therapy (Epi+CM). Cardiac function was measured as fractional shortening (FS%), FU=

echocardiographic follow-up **B** Changes in FS% from pre-cellular therapy FS% at 1 month, 2 months and 3 months, in each group. Pre-cellular therapy FS% was measured at D21 after MI. All echocardiographic measurements were analysed by a blinded, trained assessor. All panels, mean±s.e.m.; N=17 in total for functional analyses after 1 month; Sham, NRVM, Epi+CM, N=5, 4 and 8 animals.

On further comparison of the Δ FS% from pre-injection values between groups at one month, two months, and three months, we observed significant differences reflecting the different contractile profiles following cellular therapy, **Figure 22**. However, the within-group analyses were not significantly different, **Figure 23**. This finding may be explained by the change in the echocardiogram operator during the 2nd month of follow-up and the non-parallel nature of the experiment. Significant differences within- or between-groups were not observed for global left ventricular systolic or diastolic end-dimensions, **Figure 24**. However, NRVM had an overall, consistent trend for reduction in left ventricular systolic (0.63 ± 0.43 mm) and diastolic (0.37 ± 0.43 mm) end-dimensions, **Figure 24**. With great caution due to the low number of animals in this preliminary study, this observation might reflect the greater contractile contribution with cellular therapy compared to Sham. Further histological evidence will be required to explain the cardiac functional observations.

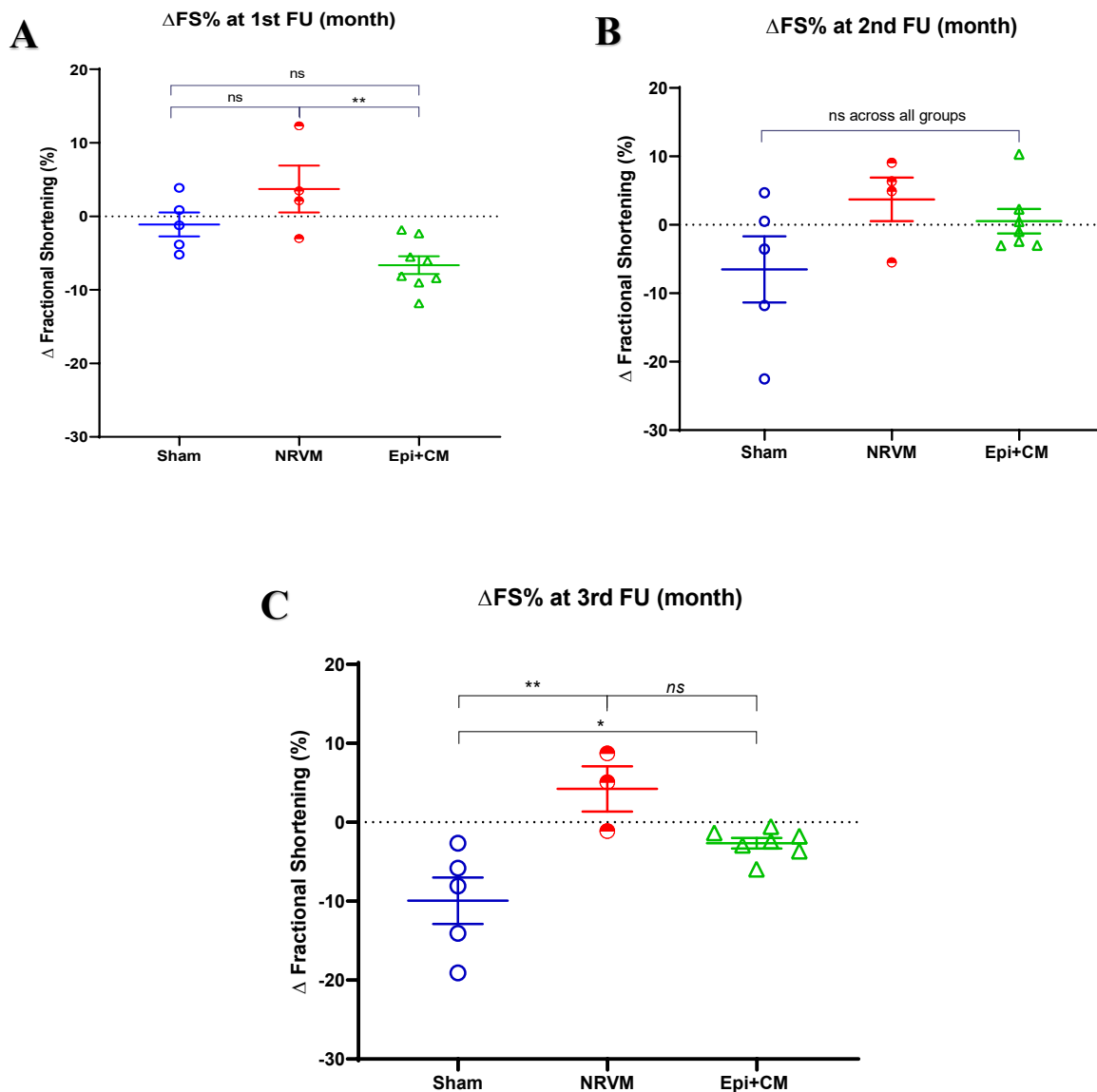


Figure 22: Between-group comparison of changes in cardiac function post-cellular therapy

To investigate whether cellular therapy could invoke cardiac repair in the chronic MI setting, all chronically infarcted rodents received intramyocardial injections, with subsequent monthly echocardiographic analyses of their cardiac function. Three groups: Sham (Vehicle-control), NRVM (species-matched cellular therapy) and Epi+CM (combination cellular therapy). Between-groups differences in cardiac functional changes (Δ FS%) at **A**) 1 month, **B**) 2 months and **C**) 3 months after cellular therapy. All echocardiographic measurements were analysed by a blinded, trained assessor. All panels, mean \pm s.e.m.; * P <0.05 ** P <0.005. $N = 17$ in total for functional analyses after 1 month; Sham, NRVM, Epi+CM, $n = 5, 4$ and 8 animals.

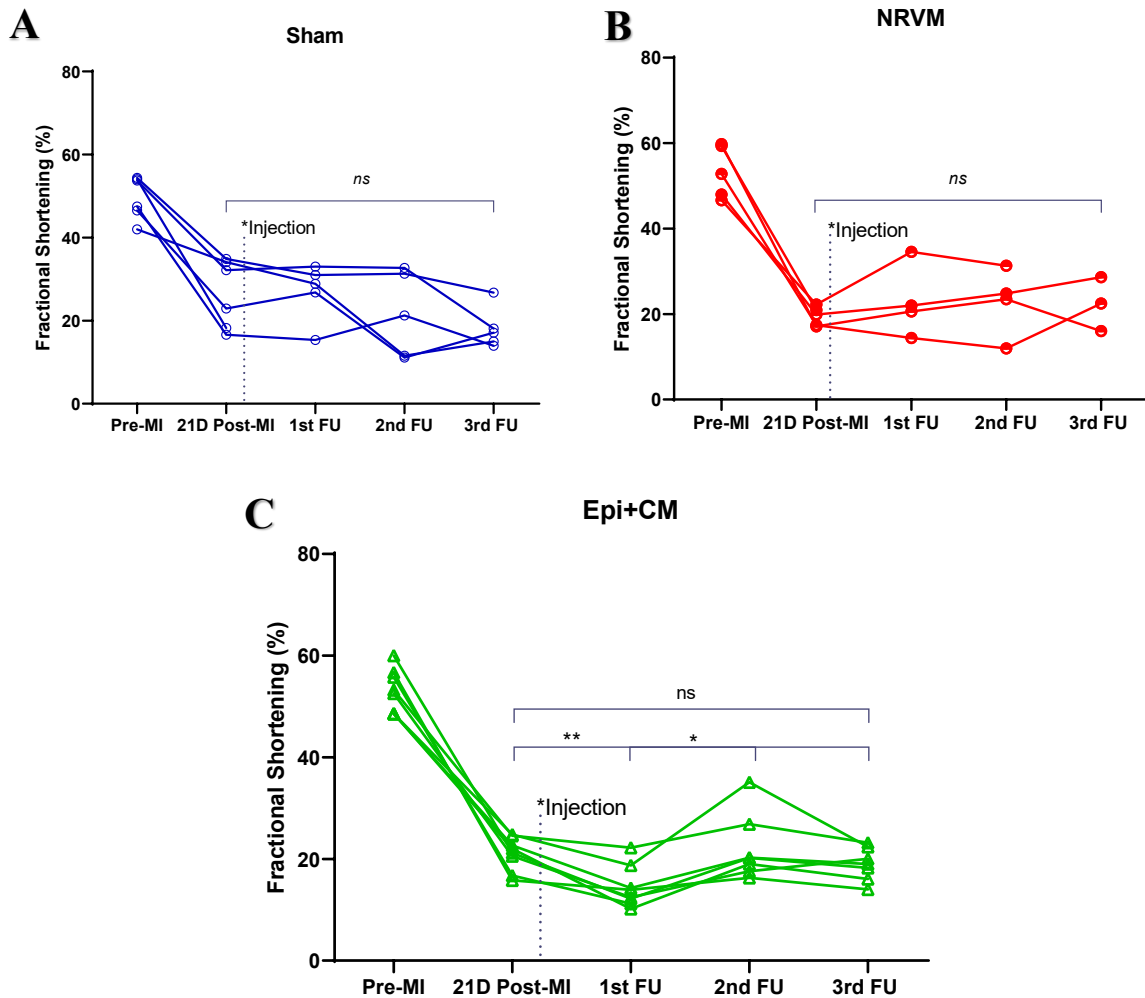


Figure 23: Comparison of the individual rat's cardiac functional changes after cellular therapy

To interrogate whether cellular therapy could invoke cardiac repair in the chronic MI setting, all chronically infarcted rodents received intramyocardial injections, with subsequent monthly echocardiographic analyses of their cardiac function. Three groups: Sham (Vehicle-control), NRVM (species-matched cellular therapy) and Epi+CM (combination cellular therapy). The trend of each individual rat's cardiac functional changes from pre-myocardial infarction (MI) until completion of 3 months follow-up for **A)** Sham, **B)** NRVM and **C)** Epi+CM, respectively. All panels, mean \pm s.e.m.; * P <0.05 ** P <0.005. N= 7 in total for functional analyses after 1 month; Sham, NRVM, Epi+CM, n = 5, 4 and 8 animals.

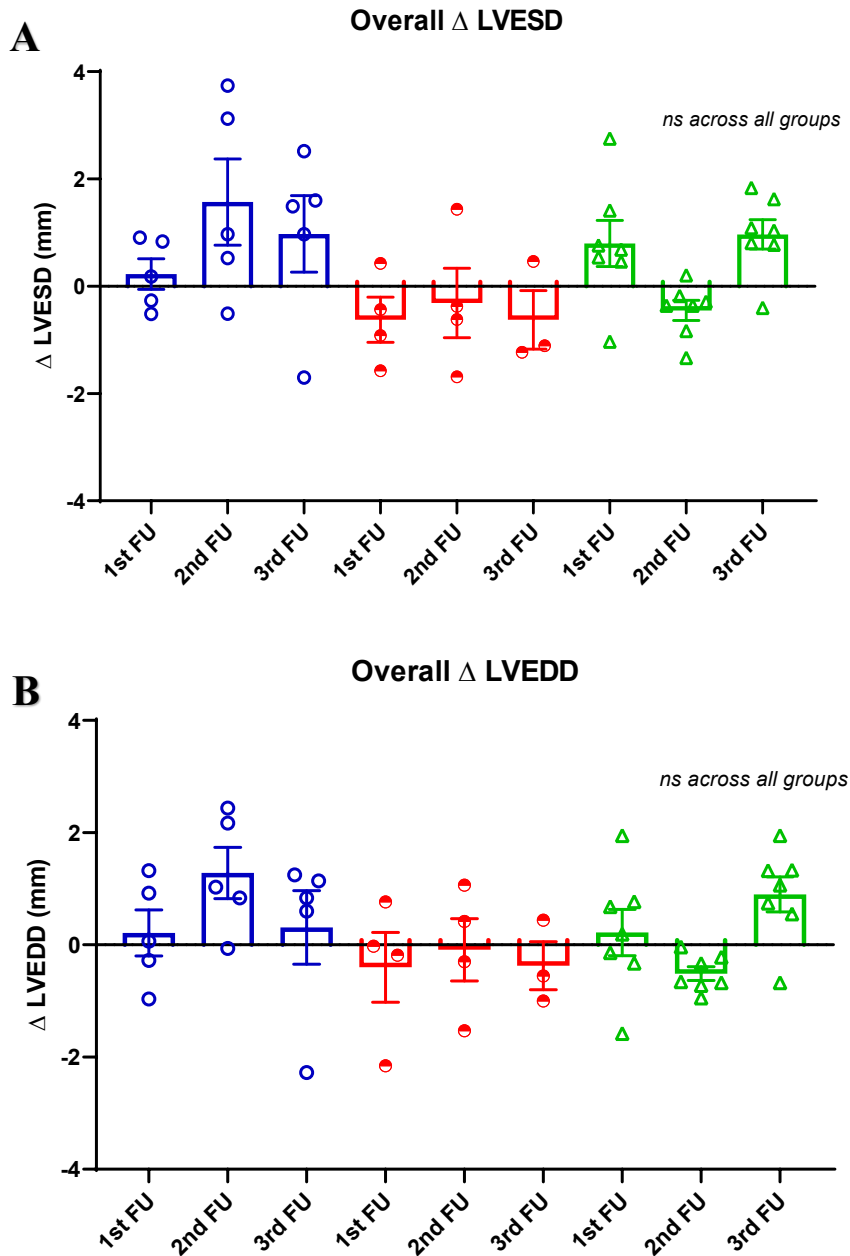


Figure 24 Global systolic and diastolic cardiac function changes after cellular therapy

To interrogate whether cellular therapy could invoke cardiac repair in the chronic MI setting, all chronic MI rodents received intramyocardial injections and was follow-up with monthly ECHO for up to three months after cellular injections. Three groups: Sham (Vehicle-control), NRVM (species-matched cellular therapy) and Epi+CM (combination cellular therapy). FU= ECHO follow-up. **A** Overall changes in left ventricular end-systolic diameter (Δ LVESD) and **B**, left ventricle end-diastolic diameter (Δ LVEDD) between groups at 1-month, 2-month and 3-month post-cellular therapy. All echocardiographic measurements were analysed by blinded, trained assessor. All panels, mean \pm s.e.m. N=17 in total for functional analyses after 1 month; Sham, NRVM, Epi+CM, n=5, 4 and 8 animals.

Due to the complex physiology of the chronically infarcted heart and the underlying remodelling over time, we interrogated surrogate markers of myocardial functional recovery, such as lung/body, heart/body and heart/lung weight ratios at the three-month endpoint for each animal, **Figure 25**. Both NRVM and Epi+CM had significantly greater heart/lung ratios than Sham, **Figure 25D**; suggesting that cellular therapy led to less lung congestion and better myocardial recovery in the chronically failing heart state. Overall, these results highlight that both species-matched and combination therapies salvaged cardiac dysfunction in the chronic MI setting, but to different extents.

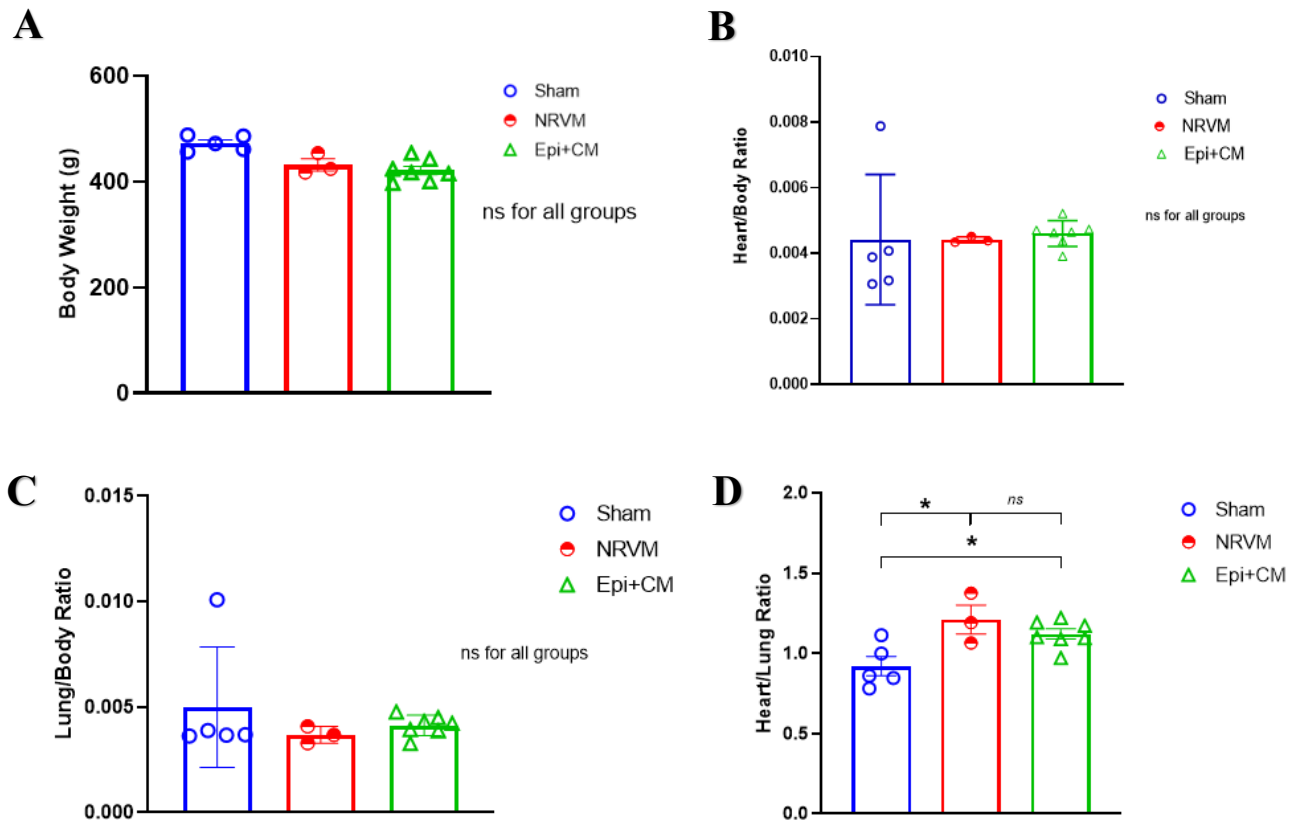


Figure 25: Both types of cellular therapy displayed improvement in surrogate markers of heart failure

To interrogate whether cellular therapy could invoke cardiac repair in the chronic MI setting, all chronic MI rodents received intramyocardial injections and was follow-up with monthly ECHO for up to 3 months after cellular injections. Three groups: Sham (Vehicle-control), NRVM (species-matched cellular therapy) and Epi+CM (combination cellular therapy). At study endpoint, the body, lung, and heart of each rat were measured. **A)** No differences in body weight between experimental groups. Then, surrogate markers of heart failure were quantified as: **B)** heart/body weight ratio, **C)** lung/body weight ratio and **D)** heart/lung weight ratios. Cellular therapies had greater heart/lung weight ratios than Sham. All panels, mean±s.e.m.; *P<0.05 **P<0.005. N=15 in total for weight analyses at 3 months after cellular injections; Sham, NRVM, Epi+CM, N=5, 3 and 7 animals, respectively.

3:1:2:3 Cardiac cells engrafted and formed sizable grafts in vivo

To understand the reasons behind the observed positive trends in cardiac functional recovery after cellular therapy, I interrogated the behaviour of the cells post-injection by analysing their engraftment, proliferation, and maturation *in vivo*.

Prior to assessing cardiac engraftment, we looked for any differences in infarct size or intramyocardial fibrosis, as infarct size or fibrotic burden could affect the quantification of cardiac engraftment. At three months post-cellular therapy, all hearts had large areas of scarring near the infarcted LAD zone and remotely in distant myocardium, with chamber dilatation and adverse myocardial remodelling, as expected in a chronically failing heart, **Figure 26A**. For quantification of fibrosis, an automated PCFG software based on intensity/area were utilised in a blinded and randomised manner. For all animals, the intramyocardial fibrosis and perivascular fibrosis were widespread throughout the entire LV. Due to our long follow-up as well, the fibrotic myocardium was analysed at 5 months after the initial MI. As such, the overall fibrotic burden could be much higher than expected. There were no differences in infarct size, remote intramyocardial and perivascular, or total fibrosis content between experimental groups, **Figure 26B, C & D**. Thus, these observations denote the consistency of MI and I/R injury and similarities in injury healing across the animals.

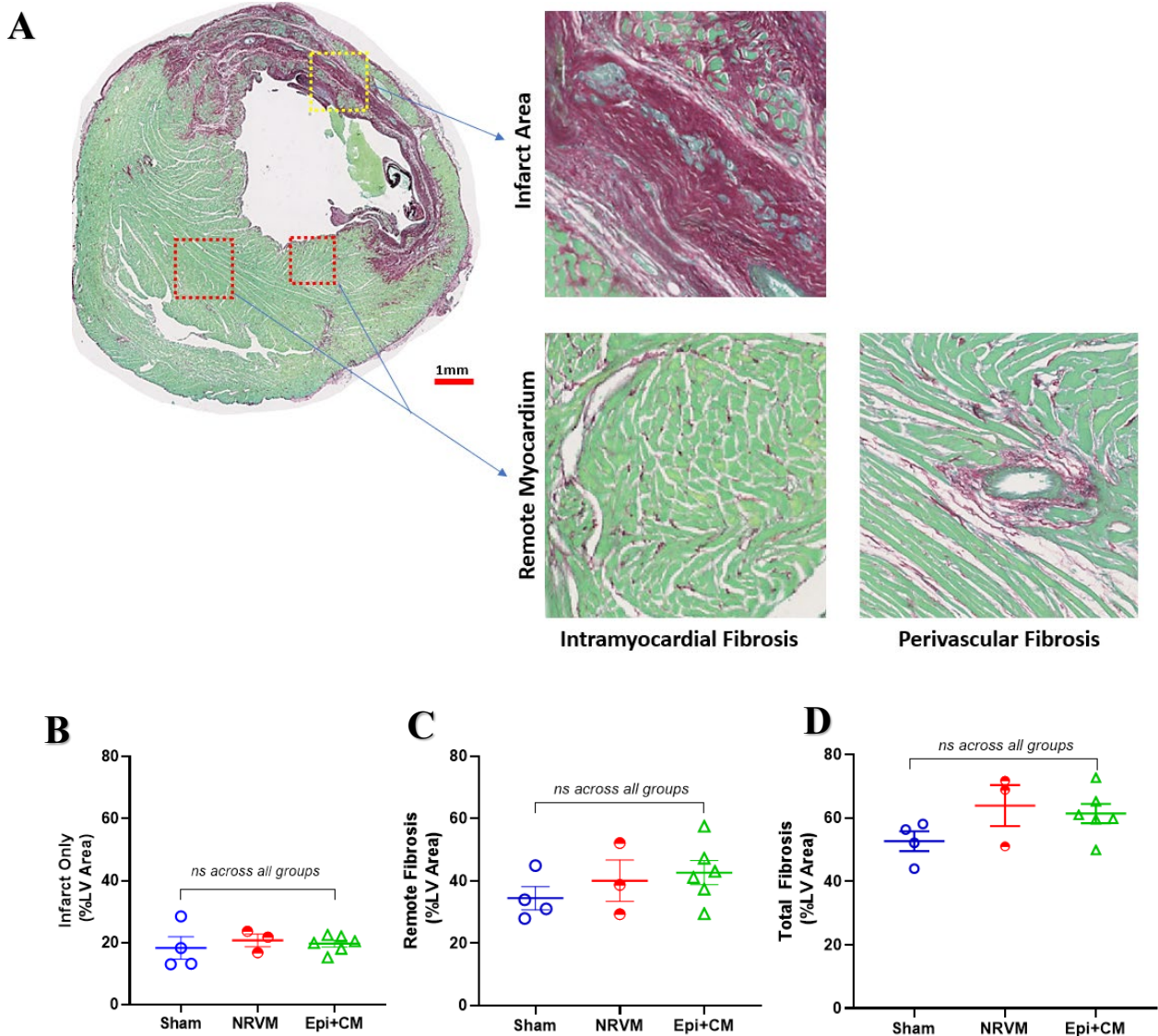


Figure 26: Distribution and quantification of fibrosis in the chronically infarcted rat hearts

A A representative transverse section of infarcted rodent heart stained for collagen with Picrosirius Fast-green (PCFG). Collagen, Red. Scale, 1mm. Quantification of **B**) infarct area, **C**) remote fibrosis and **D**) total fibrosis for Sham, NRVM and Epi+CM. PCFG staining of heart sections was performed on all animals. N=13 in total for histologic analyses at 3 months after cellular injections; Sham, NRVM and Epi+CM, N=4, 3 and 6 animals, respectively. All panels, mean±s.e.m.

To locate the hESC-CM grafts, I used a human-specific cardiac marker, beta-myosin heavy chain (β -MHC/MYH7), whereas adult rat CMs express α -MHC/MYH6. As for the NRVM grafts, I stained for Xist (X-inactive specific transcript), which was specific for the female NRVM cells engrafted in our male recipients. Due to gender differences in cardiac resilience (Regitz-Zagrosek et al. 2010; Huang et al. 2016; Maric-Bilkan et al. 2016) and cardiac cellular composition (Lim 2020; Litviňuková et al. 2020; Squiers et al. 2020), I decided to maintain male rats in all treatment arms with female-derived CMs. Prior to cardiac graft identification, baseline Xist staining in female rat hearts was conducted as a positive control to confirm our Xist staining for engrafted female rat heart cells in male rats, **Figure 27**.

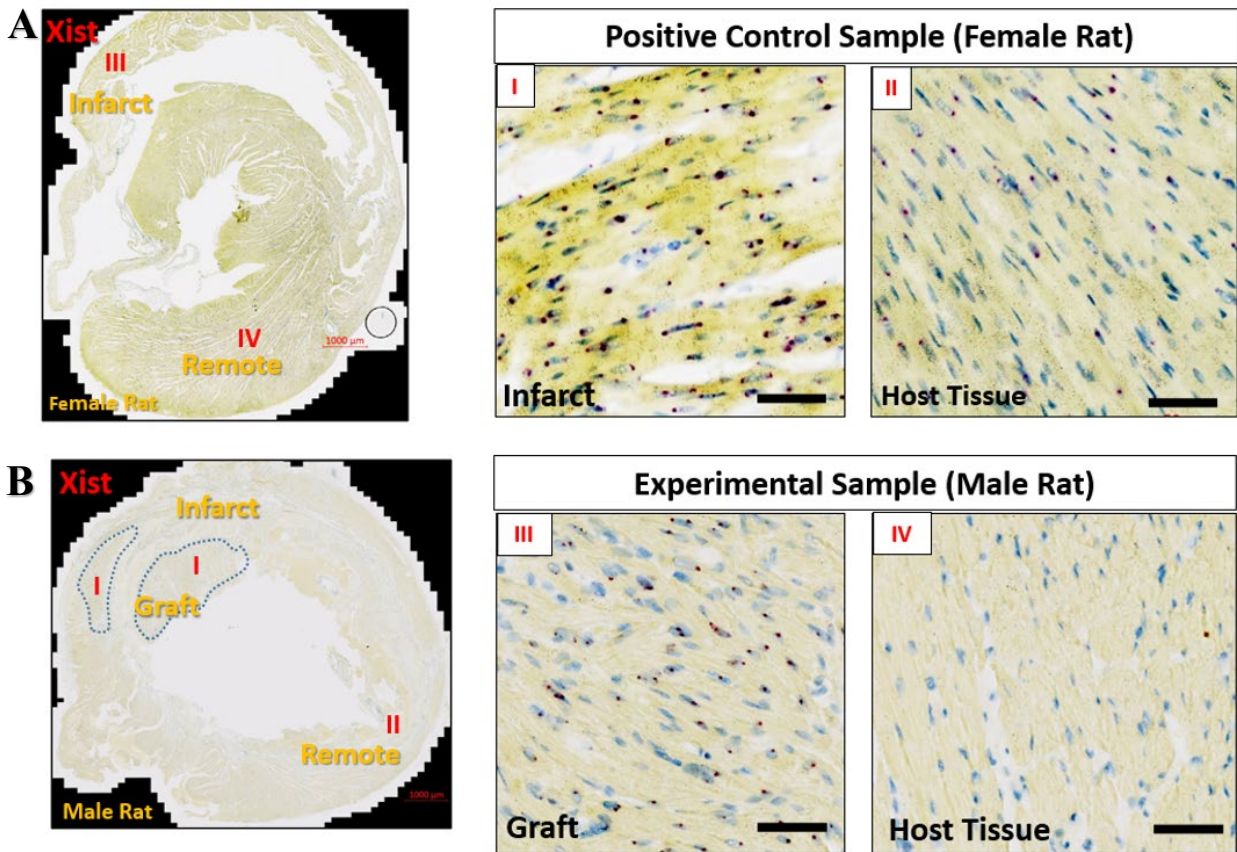


Figure 27: Baseline Xist (X-inactive specific transcript) in female rats, compared to infarcted male rats with cardiac grafts.

A Representative transverse sections of infarcted female rat heart stained for Xist (X-inactive specific transcript, RNAScope, red) throughout infarct and remote zones (*I, II*) acting as positive control and baseline for NRVM graft size calculation. **A** Scale bar 1 mm. *I, II*) Scale bar, 50 μ m. **B** infarcted male rat heart transverse sections stained for Xist (X-inactive specific transcript, RNAScope, red) to locate engrafted female rat heart cells found within infarcted regions (*III*). *IV*) No Xist was visualised in remote regions, thus enabling graft size calculation in the NRVM group. **B** Scale bar 1 mm. *III, IV*) Scale bar 50 μ m.

Despite the hostility of a chronic infarct environment, both NRVM and EPI+CM cells engrafted within the scar and border zone with host myocardium at three months post-cellular therapy, **Figure 28**. Species-matched (NRVM) cardiac graft demonstrated large myofibrils with sarcomeric alignment and aligned Cx-43 gap junctions at cell-cell intercalated discs, indistinguishable from host myocardium, **Figure 28A & B**. Combination therapy (Epi+CM) formed sizeable cardiac grafts within the infarct zone, demonstrating ongoing sarcomeric (β MHC, specific for grafted human CMs) and Cx-43 gap junction alignment, **Figure 28C & D**. Further elucidation of graft-host electrical connectivity is given in *Section 3:1:2:5*. As for the animals who died at 1-month post cellular therapy, they already displayed cardiac grafts by one month, implying early cell survival and engraftment, **Figure 36**. Both species-matched NRVM and epicardial-augmented hESC-CMs were able to survive and form long-term engraftments up till three months post-cellular therapy, within the chronic infarct environment.

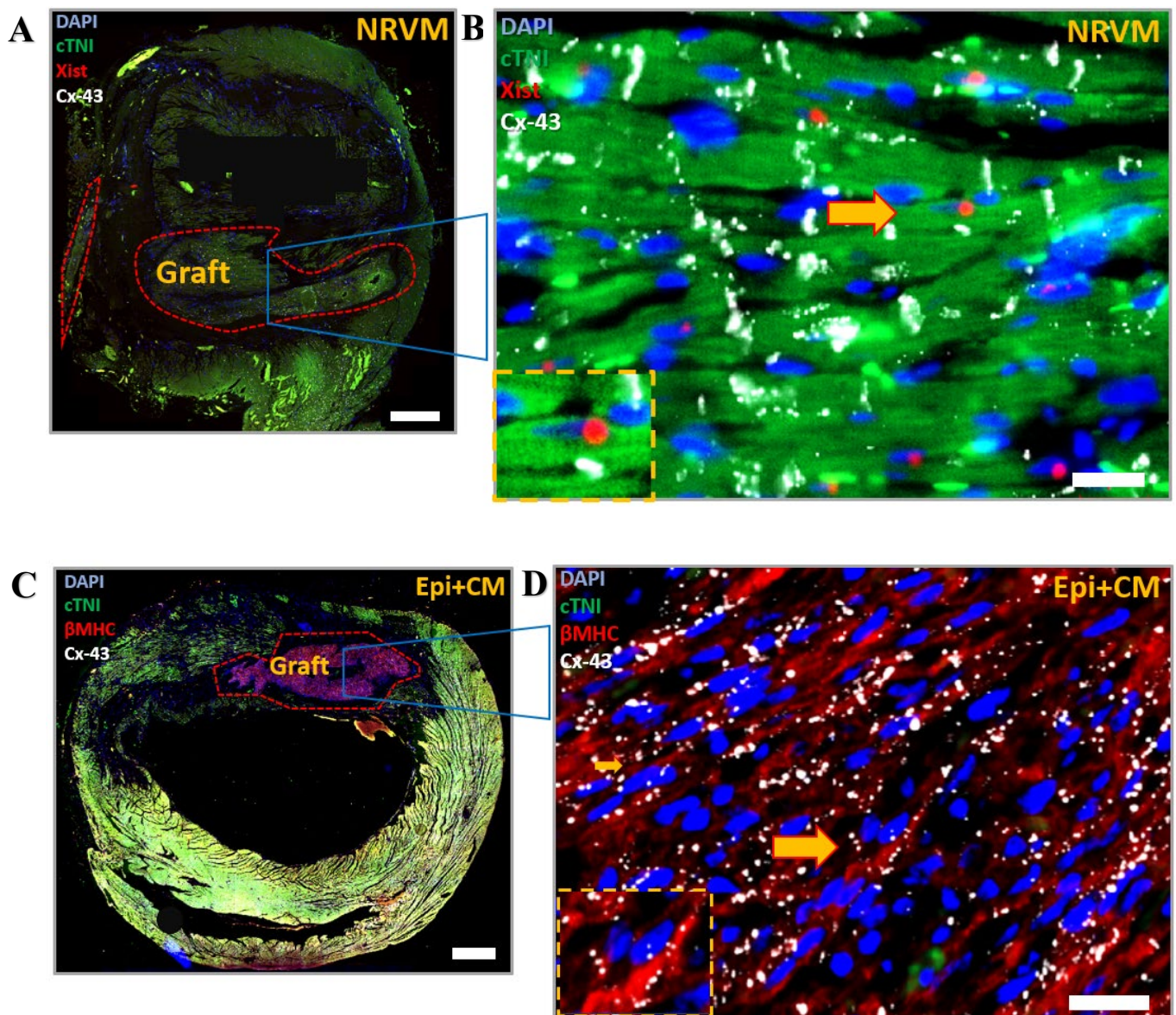


Figure 28: Both species-matched and combination cellular therapy engrafted and displayed sizeable grafts in chronically infarcted rat hearts

In all study groups (Sham, NRVM, Epi+CM), the chronically infarcted rats received intramyocardial injections at one month after MI. **A** Transverse section of infarcted rat heart with NRVM cardiac grafts in situ. Xist (red) stains for transplanted female NRVM. Scale bar 1 mm. **B** NRVM graft showed alignment of sarcomeres (cTNI, green) and Cx-43 (white) gap junctions. Scale bar 20 μ m. **C** Epi+CM cardiac grafts in situ with ongoing sarcomeric (β MHC, red specific for grafted human CMs) and Cx-43 (white) gap junction alignment. Scale bar 1 mm. **D** Epi+CM graft showed aligned sarcomeres with Cx43⁺ gap junctions. Scale bar 20 μ m.

The Epi+CM group recorded an average graft size of $1.2\pm 1.3\%$ of LV whilst NRVM's average graft size was $2.7\pm 1.9\%$ of LV, at 3 months post-injection; albeit not statistically different, **Figure 29**. Compared with reported graft sizes in the literature, combination therapy (Epi+CM) in the chronic MI setting resulted in graft size ~1.4-fold larger than hESC-CMs alone, whilst species-matched therapy resulted in graft size ~3.2-fold larger than hESC-CMs alone (Fernandes et al. 2010). Notably, hESC-CMs monotherapy displayed no cardiac functional benefits (Fernandes et al. 2010). Our cardiac functional changes post-cellular therapy suggested a trend towards correlation with cardiac graft sizes for both NRVM and Epi+CM, **Figure 29**. However, there was insufficient animals to draw any conclusions on the effect of graft size on cardiac function.

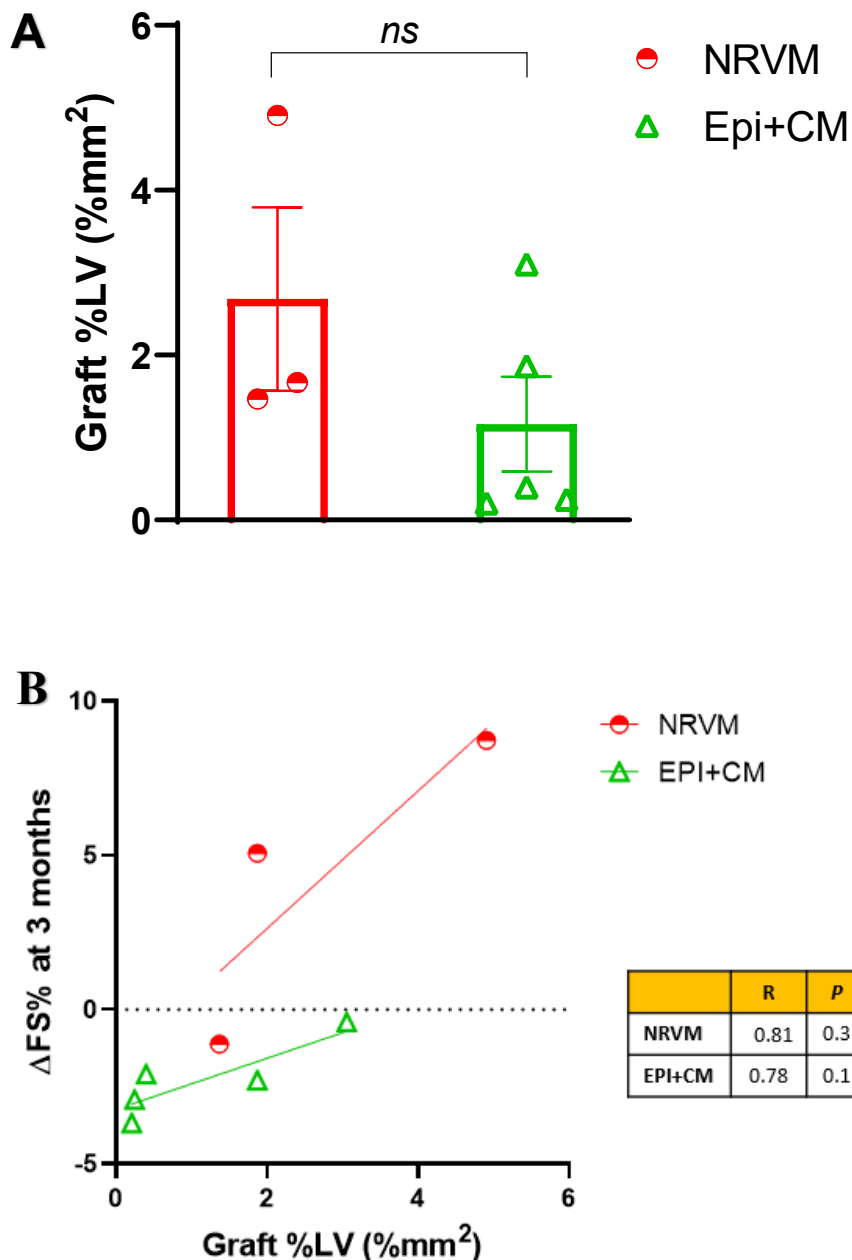


Figure 29: Engrafted CMs had sizeable grafts despite the chronically scarred myocardium

A Respective histological cardiac graft sizes; quantified as % left ventricle (LV) **B** Pearson's correlation of cardiac graft size with Δ FS% (change in fractional shortening) at 3 months. In Epi+CM, one animal did not have grafts at 3 months due to intra-operative technical challenges and was excluded from histological analyses. N=8 in total for histologic analysis of cardiac grafts after 3 months; NRVM and Epi+CM, N=3 and 5 animals, respectively. Mean values; error bars represent s.e.m. Two-sided P values were calculated using unpaired t-test unless otherwise stated.

3:1:2:4 Cardiac grafts proliferated in vivo

To understand the biological process underlying graft formation *in vivo*, I examined whether the engrafted CMs could proliferate *in vivo*. All the rats were pulsed with the thymidine analogue BrdU on days 1, 4, 7 and 14 after cellular injection. BrdU is incorporated during the S-phase of the cell cycle, thereby granting an overview of cellular proliferation over time, *in vivo*. This method was preferred over other mitotic markers, e.g. ki-67 phosphorylated Histone 3 or Aurora-B kinase, that would only offer a single snapshot of cellular proliferation *in vivo*. Proliferating CMs were identified via co-localised staining of BrdU and cTNI for NRVM, whilst hESC-CMs were identified by co-localization of BrdU and β MHC.

Graft CMs in both species matched (NRVM) and combination therapy (Epi+CM) groups showed BrdU^{+ve} CMs at 3 months post-cellular therapy, **Figure 30**. Thus, our respective cardiac grafts demonstrated proliferation *in vivo* over 3 months, despite the chronically infarcted environment.

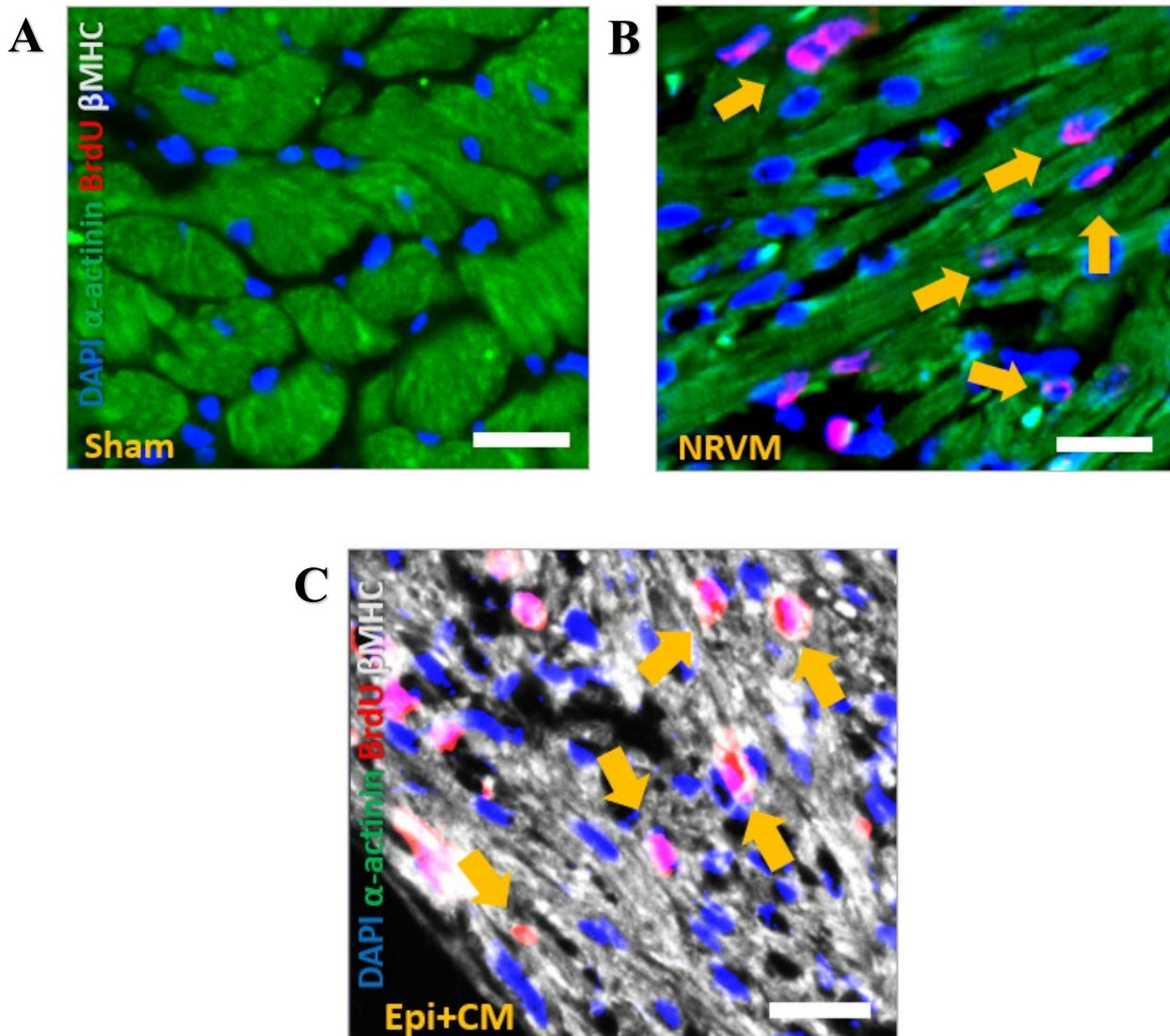


Figure 30: Both species-matched and combination cellular therapy's engrafted CMs proliferated *in vivo*

A Sham did not have any proliferating CMs. **B** Proliferating BrdU⁺ve CMs in NRVM cardiac grafts, as shown by co-localization of BrdU (nuclear, red) and α -actinin (green). **C** Proliferating BrdU⁺ve CMs in Epi+CM cardiac grafts, as shown by co-localization of BrdU (nuclear, red) and human-specific β MHC (white). Yellow arrows point to proliferating BrdU⁺ve CMs with nuclear co-localisation of BrdU (red). Scale bar, 20 μ m.

Interestingly, EPI+CM showed greater cumulative proliferation index at 3 months, compared to NRVM; Epi+CM = $15.9 \pm 0.78\%$ vs NRVM = $12.7 \pm 1.04\%$, ($p=0.044$),

Figure 31. A similar observation of proliferating BrdU⁺ve hESC-CMs within the rat chronic infarcts was made (Fernandes et al. 2010). However, our result is the first

reported quantification of CM's proliferation rate within the chronic MI setting, and comparable to hESC-CM's proliferation rate within subacute MI settings (Liu et al. 2018; Bargehr et al. 2019). Reassuringly, the chronic, fibrotic environment did not deter grafted CM's proliferative capacity in either the species matched (NRVM) or combination therapy (Epi+CM) groups.

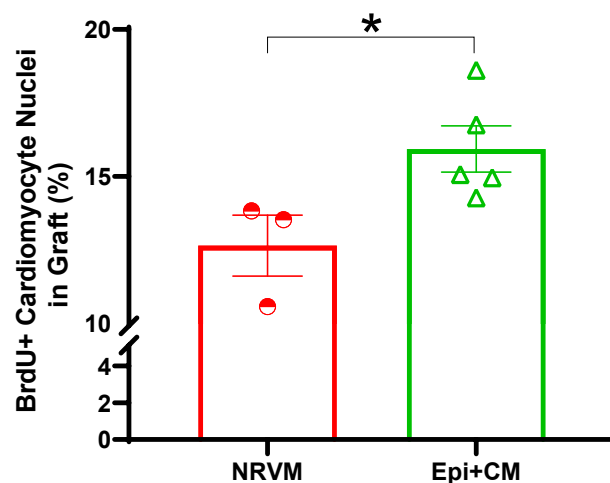


Figure 31: Combination therapy (Epi+CM) had a higher proliferative rate *in vivo*

To investigate whether cellular therapy could invoke cardiac repair in the chronic MI setting, all chronically infarcted rodents received cellular injections. At 3 months after cellular injections, all animals were harvested and investigated for the presence of engrafted CM proliferation *in vivo*. 3 groups: Sham (Vehicle-control), NRVM (species-matched cellular therapy) and Epi+CM (combination cellular therapy). Proliferation rate (%) of BrdU⁺ve CMs in NRVM and Epi+CM cardiac grafts, respectively. In Epi+CM, one animal did not have a graft at 3 months, traced back to intra-operative technical challenges. This animal was excluded from histological analyses. N=8 in total for histologic analyses of cardiac grafts after 3 months; NRVM and Epi+CM, N=3 and 5 animals, respectively. All panels: mean values; error bars represent s.e.m. *P<0.05.

A greater proliferative index in Epi+CM did not lead to greater cardiac graft size, compared to NRVM. Possible reasons included differences in the extent of cell survival post-injection or cellular density within grafts. Due to the relative immaturity of both the NRVM and the hESC-CMs, cellular isotropy and mononucleated CMs were assumed and hence, nuclear density=cellular density (Liu et al. 2018). Each transverse section of the LV was cut at 1 mm thickness in a serial manner, from apex to base for total graft size (mm²) calculations. Thus, the graft CM density and the total graft CMs per animal were calculated, as detailed in *Section 2:3:4*.

On average, Epi+CM had 1.5-fold greater CM density in grafts compared to NRVM (Epi+CM=5.1±1.2 X10⁵ vs NRVM= 3.5±2.5 X10⁵ CMs per mm³); *p*-0.374, **Figure 32A**. Total graft CMs per animal were Epi+CM=1.9±1.0 X10⁶ and NRVM= 2.3±1.2 X10⁶, *p*-0.795, **Figure 32B**. Overall, hESC-CMs in the combination therapy group (Epi+CM) were more proliferative with higher cellular density and lower total graft CMs. These observations implied that hESC-CMs suffered more death during the cellular injections and were likely less mature at point of injection compared to NRVM. However, the epicardial-augmented hESC-CMs were able to overcome this challenge with a greater proliferative index than species-matched NRVM, whilst in a chronic infarct environment.

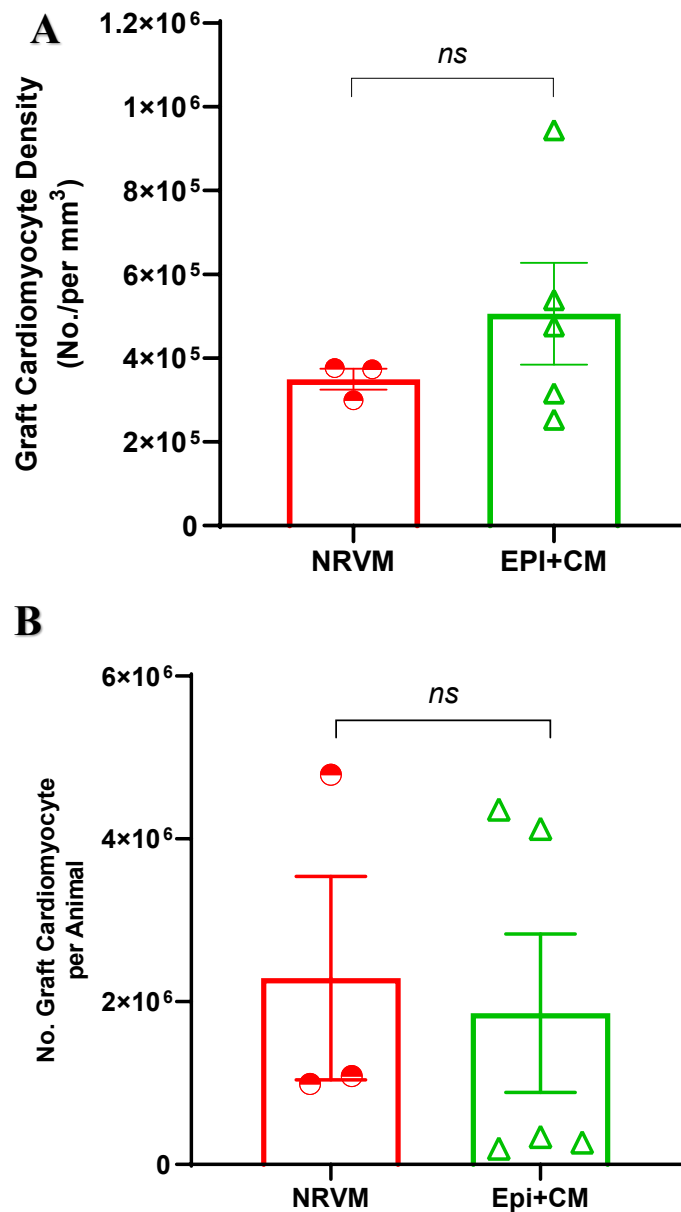


Figure 32: Both types of cellular therapy had similar CM densities in their respective cardiac grafts

A Epi+CM cardiac grafts showed greater graft CM density, compared to NRVM. **B** The average number of graft CMs per animal was similar for both NRVM and Epi+CM. In Epi+CM, one animal did not have graft at 3 months due to intra-operative technical challenges and was excluded from histological analyses. N=8 in total for histologic analysis of cardiac grafts after 3 months; NRVM and Epi+CM, n=3 and 5 animals, respectively. All panels: mean values; error bars represent s.e.m. *P<0.05. Two-sided P values were calculated using unpaired t-test unless otherwise stated.

3:1:2:5 Cardiac grafts displayed sarcomeric maturation and Cx-43 gap junction connectivity in vivo

The literature reports that CM proliferation and maturation are intrinsically linked with trade-offs in both directions, as proliferation requires sarcomeric disassembly (Karbassi et al. 2019; Guo and Pu 2020). However, the goal of 'primary remuscularization' in cellular therapy is eventual graft maturation which delivers sufficient cardiac contractility to salvage 'pump' failure associated with chronic MI. Numerous studies in the subacute MI setting reported graft maturation *in vivo* (Gerbin et al. 2015; Kadota et al. 2018; Liu et al. 2018; Bargehr et al. 2019). Having observed CM proliferation in our chronic MI model, it was necessary to investigate the maturity of the engrafted CMs.

At three months after cellular injection, implanted CMs in the species-matched group (NRVM) expressed cTnI with demonstrably larger and more organised myofibrils despite the chronically scarred environment, **Figure 33A**. Notably, the combination therapy group (Epi+CM) displayed ongoing sarcomeric maturation at 3 months, as shown by partial sarcomere isoform switching from immature ssTnI (slow skeletal Troponin I) to mature cTnI (cardiac Troponin I), **Figure 33B**; a switch typically observed during maturation (Ruan et al. 2015). Corresponding to observed maturation of the engrafted NRVM, NRVM had greater sarcomeric length ($2.92\pm 0.08\mu\text{m}$ vs $1.71\pm 0.05\mu\text{m}$, $p<0.0001$), cell diameter ($10.4\pm 0.82\mu\text{m}$ vs $7.83\pm 0.32\mu\text{m}$, $p=0.0472$) and cell size ($665.6\pm 14.6\mu\text{m}^2$ vs $322.1\pm 42.7\mu\text{m}^2$, $p<0.0001$), compared with engrafted hESC-CMs (Epi+CM)s at 3 months after cellular therapy, **Figure 33C, D & E**.

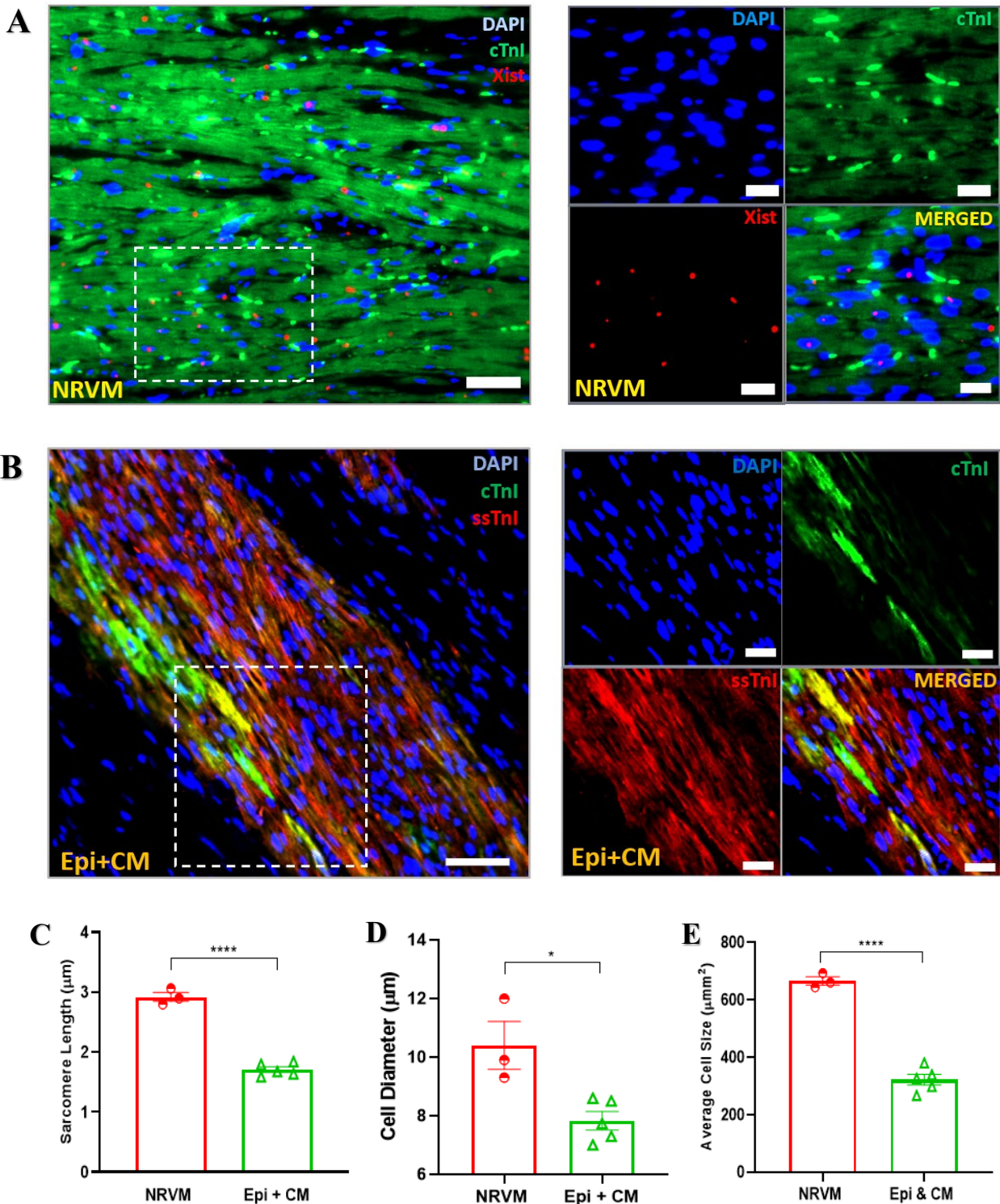


Figure 33: Engrafted CMs displayed sarcomeric maturation *in vivo*

A At 3 months, NRVM grafts showed complete cTnI (mature troponin isoform, green) with large, compact myofibrils whilst **B** Epi+CM showed ongoing switching from ssTnI (slow skeletal isoform, red) to cTnI (green). Scale bar, 50 μm & 20 μm . Within-graft quantification of **C**) sarcomere length, **D**) CM cell diameter, **E**) CM cell size. N=8 in total for histologic analysis of cardiac grafts after 3 months; NRVM and Epi+CM, N=3 and 5 animals, respectively. All

panels: mean values; error bars represent s.e.m. * $P < 0.05$ **** $P < 0.0001$. Two-sided P values were calculated using unpaired t-test unless otherwise stated.

To confirm the maturation of engrafted CMs *in vivo*, the CMs' sarcomeric alignment were quantified. Calculation of sarcomeric alignment for individual NRVM and hESC-CMs *in vitro*, **Figure 34A**. Mature CMs display well-aligned sarcomeres, denoting an efficient contractile apparatus, **Table 2**. Sarcomeric alignment was inversely proportional to the angle of sarcomeres (θ) from the long axis of a CM (Young and Engler 2011). NRVM consistently displayed a smaller θ angle **Figure 34B**, compared to Epi+CM, **Figure 34C**, at 3 months post-cellular therapy. Similarly, NRVM had significantly greater sarcomeric alignment than Epi+CM at 3 months post-cellular therapy, (0.203 ± 0.032 vs 0.045 ± 0.0075 , $p = 0.0008$), **Figure 34D&E**. These sarcomeric parameters implied that NRVM displayed greater CM maturation *in vivo*. Both species-matched and epicardial-augmented hESC-CMs grafts could mature *in vivo*, albeit to a greater extent in species-matched therapy.

Several reasons could potentially explain the hESC-CM's maturation lag *in vivo*. Prior to cellular therapy, NRVM already displayed aligned sarcomeres *in vitro*, compared to hESC-CMs, **Figure 34A**. There were clear differences in cellular maturity levels prior to cellular injections. At 1 month after cellular therapy, comparative observations of NRVM and Epi+CM cellular maturity showed similar trends, **Figure 35**. Unfortunately, previous reports of hESC-CMs monotherapy in the chronic infarct environment did not report any sarcomeric measurements or ssTNI-cTNI switching (Fernandes et al. 2010; Shiba et al. 2014). Both species-matched NRVM and epicardial-augmented hESC-CMs displayed quantifiable maturation within the chronically scarred environment, albeit to different extents.

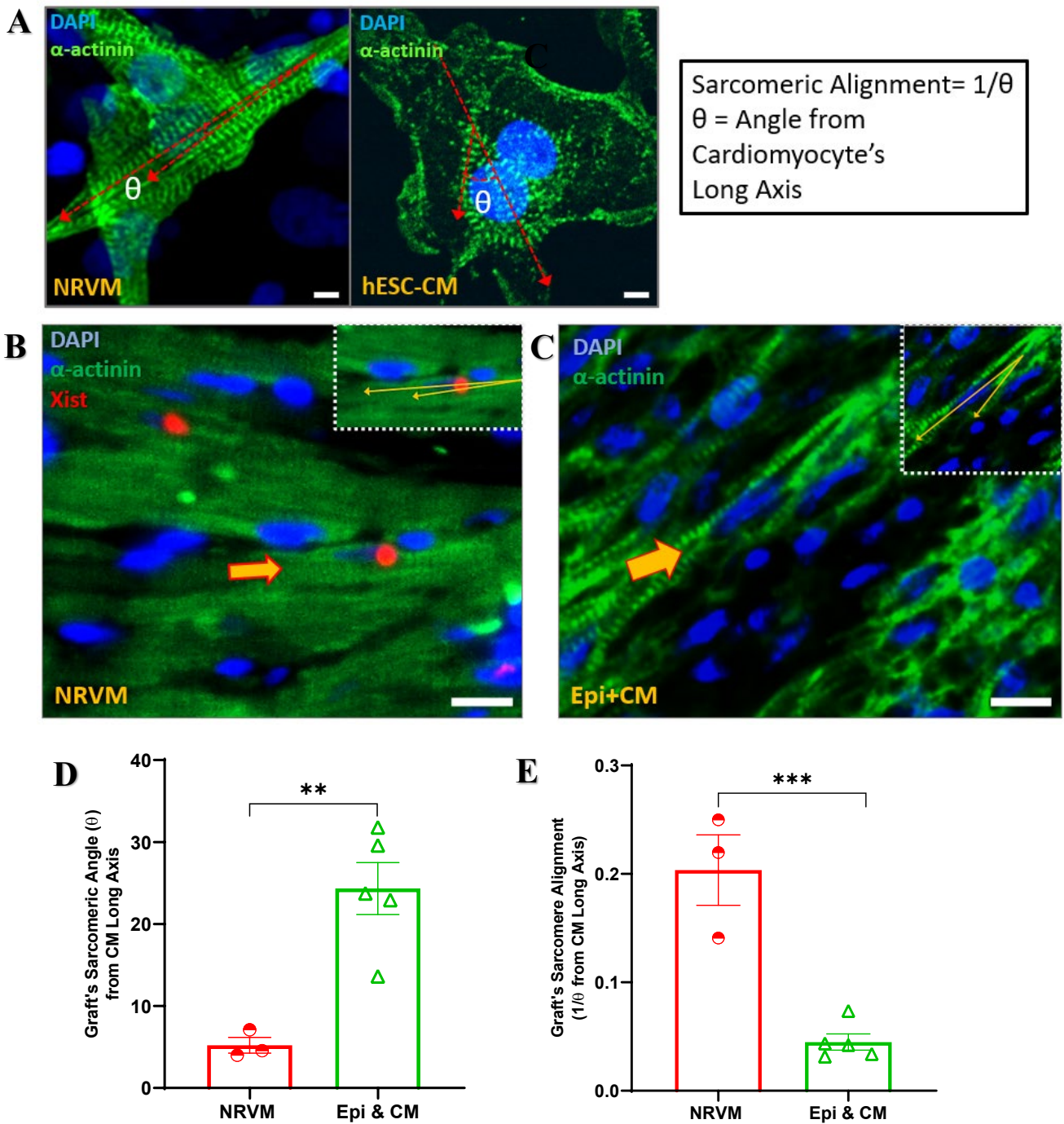


Figure 34: Within-graft sarcomeres matured and aligned *in vivo*

A Calculation of sarcomeric alignment of individual NRVM or hESC-CM, *in vitro*. Scale bar 2 μ m. **B** NRVM and **C** Epi+CM's within-graft sarcomere alignment (α -actinin, green) *in vivo*, at 3 months post-cellular therapy. Arrows point to a single CM within grafts. Scale bar 10 μ m. **D** Within-graft sarcomere angle (θ) from the CM long axis and **E** sarcomeric alignment ($1/\theta$) for NRVM and Epi+CM. At 3 months, N=8 in total for histologic analyses; NRVM and Epi+CM, N=3 and 5 animals, respectively. Mean values; error bars represent s.e.m.; **P<0.005, ***P<0.001. Two-sided P values were calculated using unpaired t-test unless otherwise stated.

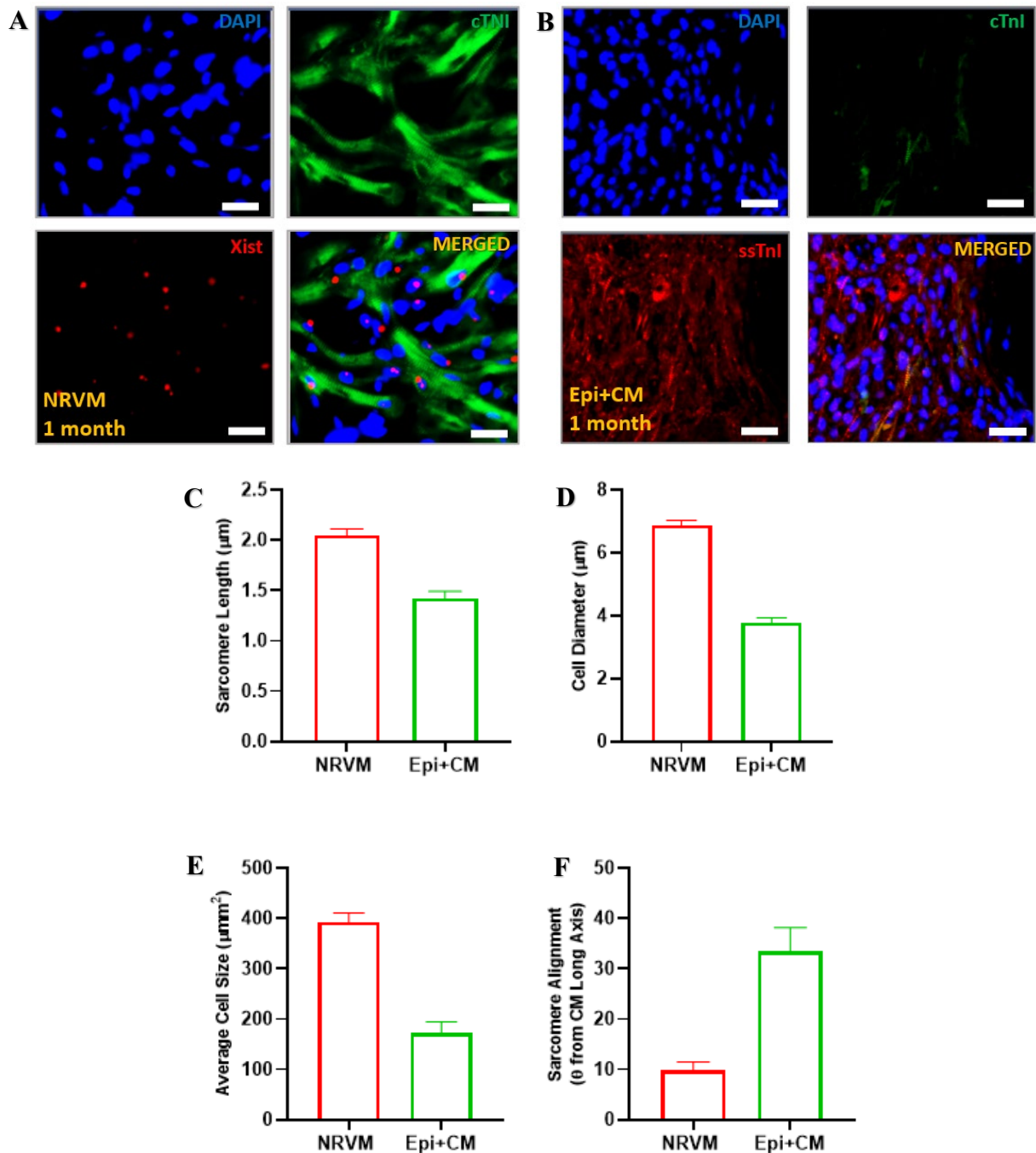


Figure 35: Respective cardiac graft maturity at one month after cellular therapy

A At one month, NRVM grafts showed complete cTnI (mature troponin isoform, green) with disorganised myofibrils whilst **B** Epi+CM started switching from ssTnI (slow skeletal isoform, red) to cTnI (green). Scale bar 20 μm . At 1 month after cellular therapy, within-grafts' quantification of **C**) sarcomere length, **D**) CM cell diameter, **E**) CM cell size and **F**) sarcomere alignment was different between NRVM and Epi+CM. At one month, N=1 for each of the NRVM and Epi+CM study arms was available for histologic analysis. Mean values; error bars represent s.e.m.

Aside from within-graft sarcomeric maturation, intercellular and graft-host electrical connectivity is required for functional, contractile myocardium. The lack of connexin-43 (Cx-43) gap junctions in implanted skeletal myoblasts, contributing to a lack of integration with host tissue and subsequent life-threatening arrhythmias, had been emphasized as one of the key failures of the MAGIC Trial (Roell et al. 2007; Menasché et al. 2008). Thus, our species-matched (NRVM) and combination therapy (Epi+CM) grafts were interrogated for the presence of Cx-43 gap junctions, the alignment and graft-host gap junction connectivity; all of which constituted as histological evidence for electrical connectivity.

With respect to cell-cell electrical connectivity at 3 months, NRVM grafts displayed greater alignment of Cx-43 gap junctions, with EPI+CM showing partial alignment of Cx-43, **Figure 36**. These observations hinted at maturing cardiac grafts within the chronically scarred environment. As above, these observations supported the concept of a 'maturation lag' for EPI+CM compared to NRVM (*Section 3:1:2:5*). Cx-43 gap junction connectivity between the graft and host myocardium was observed in the infarct border zones in both groups, which were highly suggestive of electrical connectivity with host myocardium, **Figure 36**. Curiously, there were no observable differences in graft-host Cx-43 connectivity between species-match (NRVM) and combination therapy (Epi+CM) groups, thereby hinting that CM maturity might not be a factor here. Our collective histological evidence of Cx-43 gap junction alignment and electrical connectivity was consistent with a contractile *contribution* from the matured NRVM and maturing Epi+CM grafts, respectively.

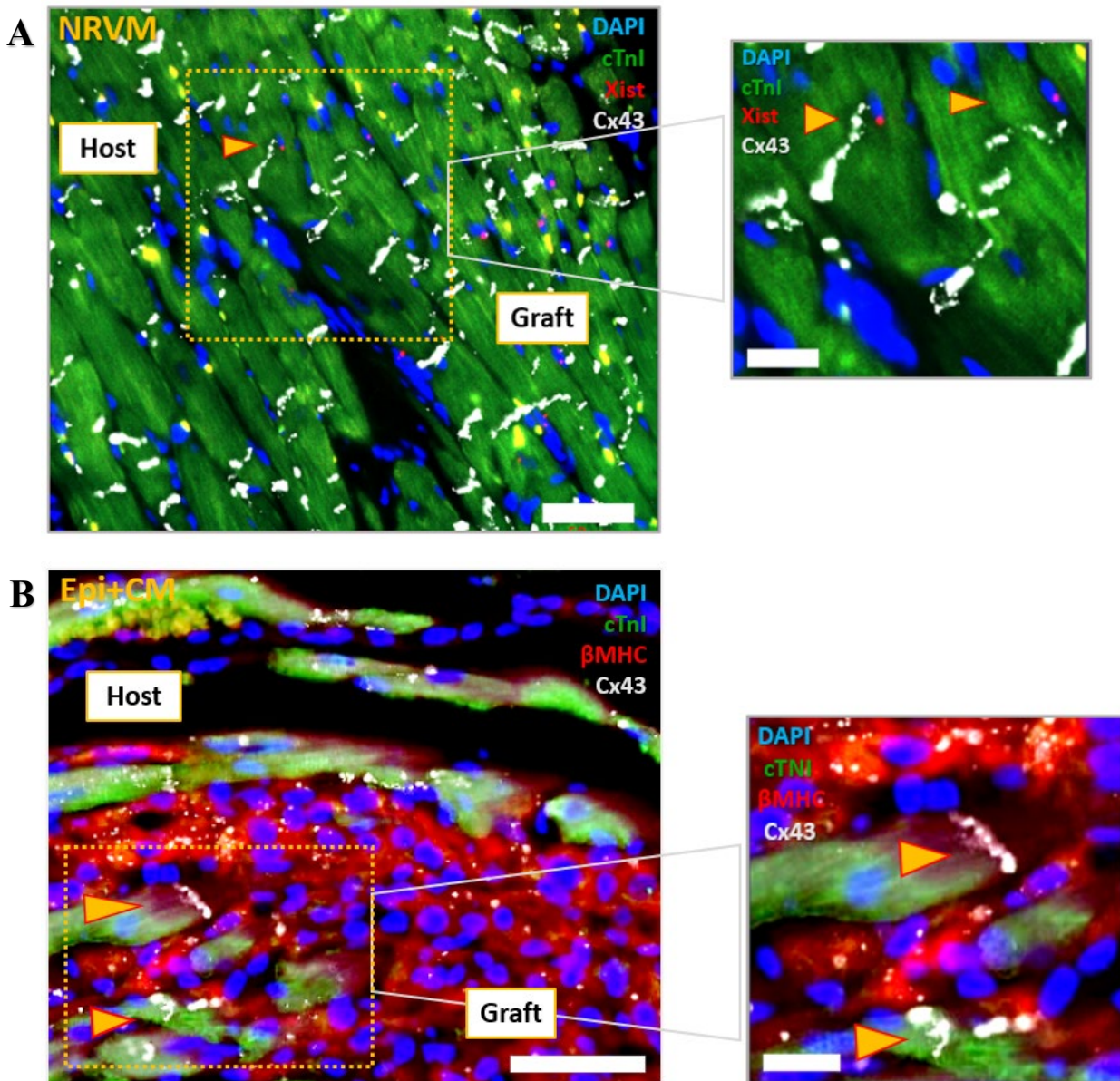


Figure 36: Both cellular treatment groups displayed graft-host Connexin-43 gap junction connectivity

To investigate whether cellular therapy could invoke cardiac repair in the chronic MI setting, all chronically infarcted rodents received cellular injections. At 3 months after cellular injections, all animals were harvested and investigated for the presence of graft-host connexin-43 gap junction connectivity. Three groups: Sham (Vehicle-control), NRVM (species-matched cellular therapy) and Epi+CM (combination cellular therapy). **A** At 3 months, NRVM grafts displayed histological evidence of connexin-43 gap junctions (white, arrows) interface between graft (Xist, red) and host tissue, respectively. Scale bar 50 μ m, 20 μ m. **B** Epi+CM grafts demonstrated similar observations between hESC-CMs (β MHC, red) and rat cardiac tissue (cTNI, green). Scale bars 50 μ m, 20 μ m.

3:1:2:6 Cardiac grafts displayed vascularization in vivo

To support cardiac engraftment, proliferation, maturation, and electrical connectivity *in vivo*, a robust blood supply in connection with the host is required. One of the key challenges of cellular therapy is sufficient graft vascularization (Bertero and Murry 2018), which might prove particularly challenging in a chronic infarct environment with maturing scar (Fernandes et al. 2010; Shiba et al. 2014). Both species-match (NRVM) and combination therapy (Epi+CM) cardiac grafts were investigated for histological evidence of within-graft vascularization and graft-host vascular connectivity.

Firstly, I stained for the presence of CD31, which is a specific endothelial cell marker, all neovessels and venules (Bargehr et al. 2019). At three months, within-graft vascularization had notably more CD31+ve neovessels in EPI+CMs grafts (803.9 ± 112.7 vessels/mm²) than NRVM (411.7 ± 88.8 vessels/mm²), with a trend towards significance, $p=0.0535$, **Figure 37B, C & D**. Similarly, Epi+CM had significantly more CD31+ve vessels (819.7 vessels/mm²) in the remote myocardium, compared to NRVM (241.1 ± 30 vessels/mm², $p=0.0062$) and Sham (201 ± 101 vessels/mm², $p=0.0023$) respectively, **Figure 37F**. Although hESC-epicardial cells can differentiate into cardiac fibroblasts and SMCs *in vitro* (Iyer et al. 2015) and GFP+ve cells were present in our Epi+CM grafts at 3 months, **Figure 38A**, the CD31+ve-coated vessels were GFP-negative and human mitochondria (HuMito)-negative, indicating a host origin, **Figure 38B**. Similarly, CD31+ve vessels in NRVM grafts were Xist-negative, **Figure 38C**. Overall, our observations suggested pro-angiogenic signalling by both species matched (NRVM) and combination therapy (Epi+CM) grafts *in vivo*, despite the chronic infarct environment.

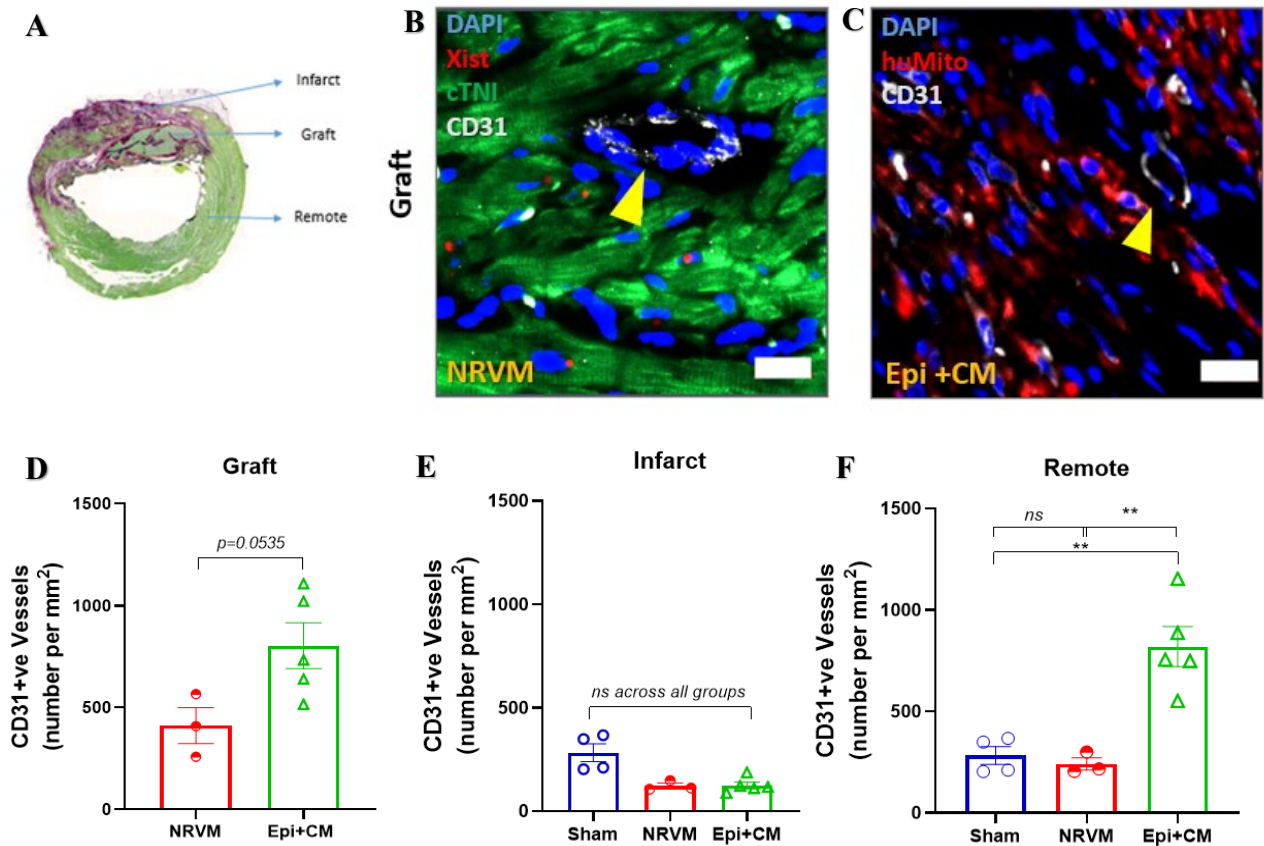


Figure 37: Combination therapy (CM+Epi) promoted CD31⁺ve neovascularization

To investigate whether cellular therapy could invoke cardiac repair in the chronic MI setting, all chronically infarcted rodents received cellular injections. At 3 months after cellular injections, all animals were harvested and investigated for the presence of neovascularization in **A** Graft, infarcted and remote areas of the infarcted rat heart. Three groups: Sham (Vehicle-control), NRVM (species-matched cellular therapy) and Epi+CM (combination cellular therapy). CD31+ve neovessels (yellow arrow) within **B**) NRVM (Xist-red, cTNI-green) and **C**) Epi+CM (huMito, red) cardiac grafts. Scale Bar 20 μ m. The density of CD31+ve neovessels within **D**) grafts, **E**) infarct and **F**) remote areas. N=12 in total for histologic analyses after 3 months; Sham, NRVM and Epi+CM, N=4, 3 and 5 animals, respectively. Mean values; error bars represent s.e.m. *P<0.05.

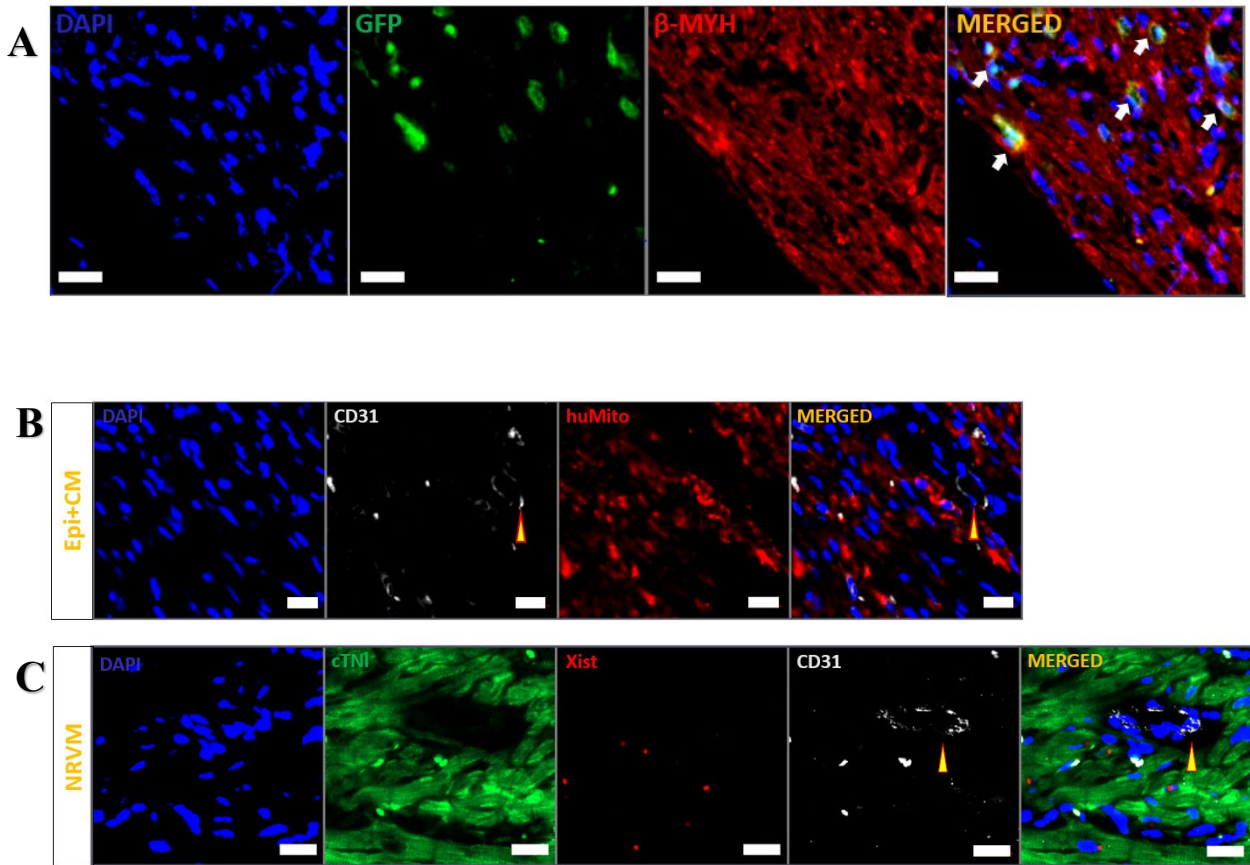


Figure 38: $CD31^{+ve}$ neovascularization in both NRVM and Epi+CM cardiac grafts were derived from their chronically infarcted rat hosts

A GFP-positive epicardial cells (green, arrow) present within cardiac grafts at 3 months endpoint. Scale Bar, 20 μ m. $CD31^{+ve}$ neovascularization (white, arrow) within both **B** Epi+CM (huMito, red) and **C** NRVM (Xist-red, cTnI-green) grafts were huMito-negative and Xist-negative, respectively. This denoted host-origin for $CD31^{+ve}$ neovascularization. Scale Bar, 20 μ m. N=12 in total for analyses after 3 months; Sham, NRVM and Epi+CM, N=4, 3 and 5 animals, respectively.

The presence of hESC-epicardium within my Epi+CM grafts likely promoted greater pro-angiogenic signalling, as previously observed in the subacute MI setting (Bargehr et al. 2019). Our hESC-epicardium augmentation of CD31^{+ve} vascularization could have enabled greater hESC-CM proliferation, maturation, and engraftment *in vivo*, leading to cardiac functional benefits; thereby potentially explaining the lack of cardiac functional gains observed with hESC-CMs monotherapy (Fernandes et al. 2010).

Next, I stained for the presence of smooth-muscle actin (SMA+ve) cells as a marker of smooth muscle cells (SMC) encoachment of vessels - an observation indicative of vessel maturity. I observed similar within-graft SMA+ve vessel density in both NRVM (89.1 ± 18.8 vessels/mm²) and Epi+CM (78.9 ± 22.2 vessels/mm²), $p=0.76$, **Figure 39 A, B & C**. Notably, remote host myocardium displayed similar CD31+ve and SMA+ve vessel density as their respective grafts for both Epi+CM and NRVM, **Figure 39E**. Crucially, this observation implied homogenous vascular blood supply between the cardiac graft and host myocardium. Identical to the CD31+ve neovascularization, SMA-coated vessels were GFP-negative, human mitochondria (HuMito)-negative and Xist-negative, thereby denoting a host origin, **Figure 40A & B**. Both NRVM and Epi+CM grafts demonstrated similar host-derived vascular networks and blood supply as the host's coronary circulation, thereby reaffirming the functionality of our cardiac grafts.

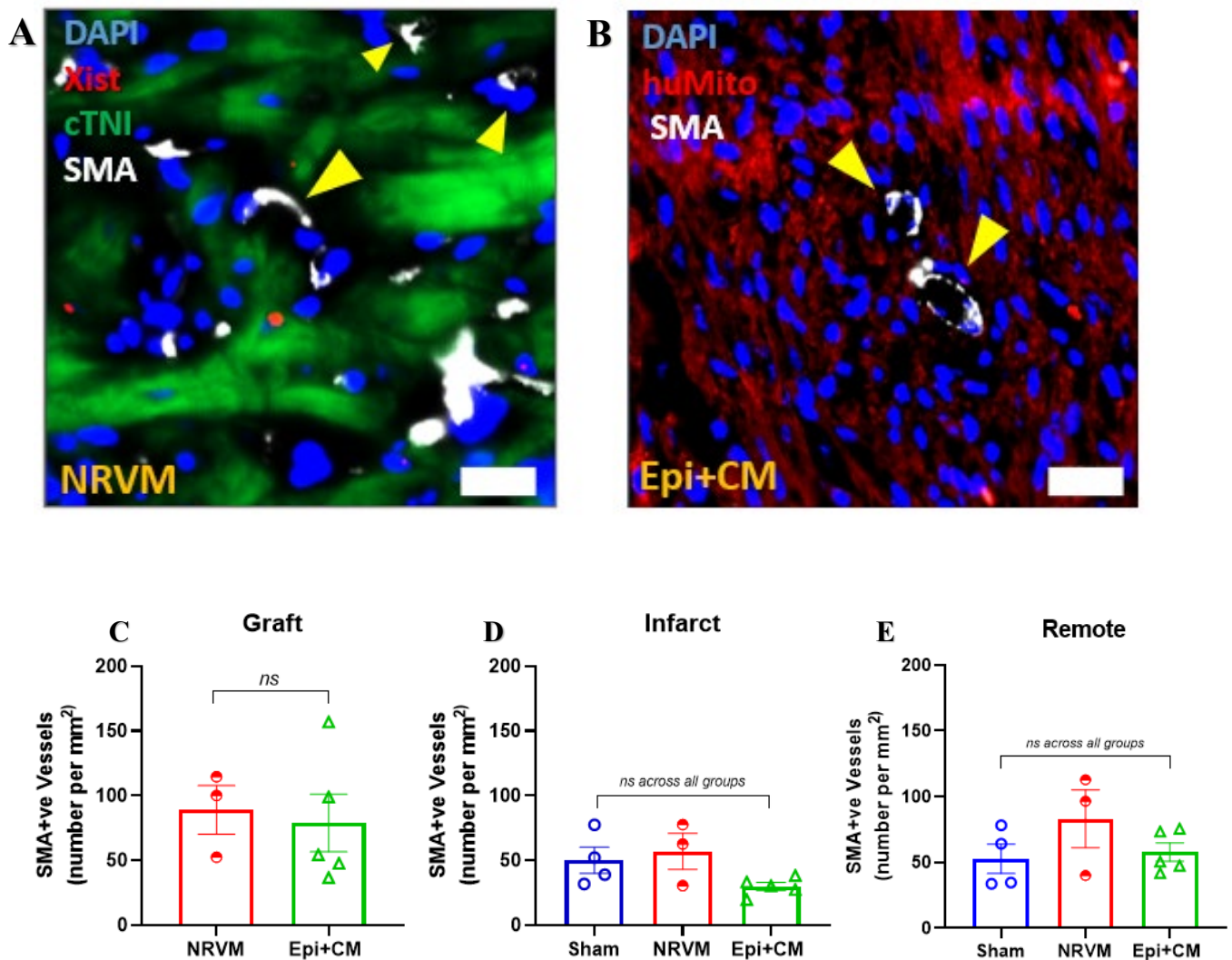


Figure 39: NRVM and Epi+CM displayed similar SMA^{+ve}-coated vessel density within the cardiac grafts, infarcted and remote regions of their hosts' myocardium

At 3 months after cellular injections, all animals were harvested and investigated for the presence of SMA^{+ve}-coated vascularization in cardiac graft, infarcted and remote areas of the infarcted rat heart. **A** NRVM (Xist-red, cTNI-green) grafts displayed mature SMA+ve vascularization (white, arrow). **B**) Similarly, Epi+CM grafts (huMito, red) showed similar SMA+ve vessels (white, arrow). Scale Bar 20 μm. Comparison of mature SMA+ve vessel density within **C**) grafts, **D**) infarcts, **E**) remote regions between NRVM, Epi+CM and Sham group, respectively. N=12 in total for analyses after 3 months; Sham, NRVM and Epi+CM, N = 4, 3 and 5 animals, respectively. Mean values; error bars represent s.e.m.

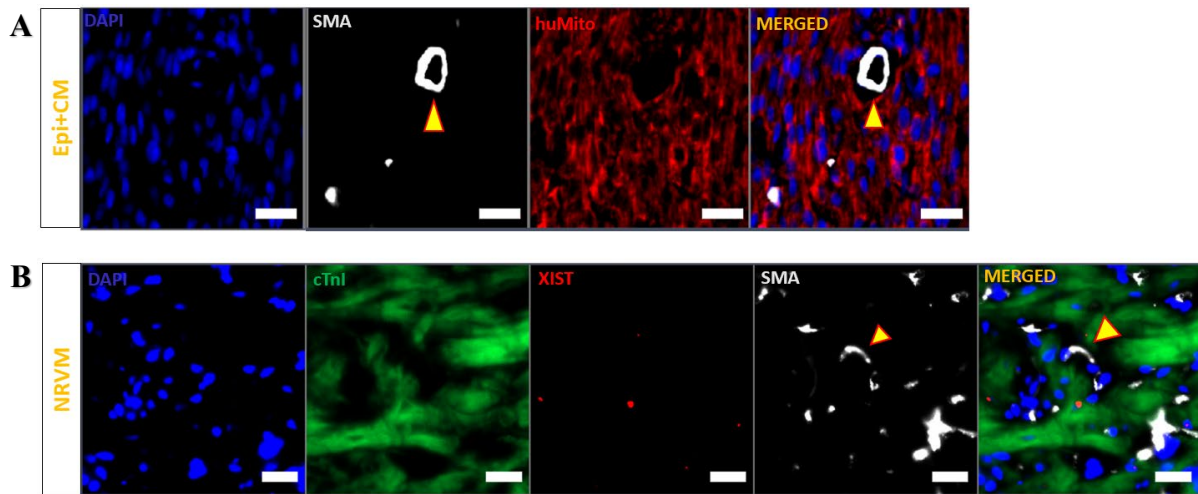


Figure 40: Cardiac grafts showed host-derived SMA^{+ve} mature vascularization

A Mature SMA^{+ve} vessels (white, yellow arrow) within Epi+CM (huMito, red) and **B** NRVM (Xist-red, cTnI-green) grafts were both huMito-negative and Xist-negative. Scale Bar 20 μ m. N=12 in total for analyses after 3 months; Sham, NRVM and Epi+CM, N=4, 3 and 5 animals, respectively.

Collectively, my results showed that both species matched (NRVM) and combination (Epi+CM) therapy developed sizeable, long-term cardiac engraftment within the chronically infarcted myocardium, underpinned by graft CM proliferation, maturation, and Cx-43 connectivity, together with a host-derived vascular supply. Altogether, these cardiac grafts demonstrated potential to attenuate cardiac dysfunction in the chronic heart failure setting. However, there were insufficient number of animals to draw definitive conclusions. To conduct the chronic MI rat experiment with a larger number of animals, I proceeded to establish the cardiac regenerative rodent model in Cambridge.

3:2 Establishing the Cardiac Regenerative Animal

Model in Cambridge

The importance of animal models in translational studies cannot be overstated, especially with stem cells and cardiac regeneration (Patten and Hall-Porter 2009; Riehle and Bauersachs 2019). Due to the relevance of the cardiac regenerative MI rodent model for our future studies, I set up this surgical animal model at the University of Cambridge. This model encompassed MI and ischaemic heart failure diseased states, together with cardiac regeneration intervention in a rat model. This technology transfer was deemed feasible based on the operative log of 50 successful rodent surgeries with no operative and/or under 30-day mortality in the Murry Lab, University of Washington. These surgeries formed the study described above and assistance on other projects. The animal model set-up in University of Cambridge is detailed in ***Appendix 9.3.***

The animal model set-up was initially envisioned to propel further animal studies forward locally. Despite the willingness of the Sinha lab and swift problem-solving, further animal studies could not be completed before the animal facility had to move location by March 2020. Given the long follow-up time in these animal studies, they could not be re-established and completed within my PhD timeframe. This situation was exacerbated by the national lockdown enforced due to the Covid19 pandemic. Consequently, the focus switched to the third aim of this doctoral thesis, namely 'Is epicardial-FN the key mediator of epicardial-myocardial crosstalk?' This question is crucial to our understanding of cellular therapy and cardiac regeneration.

4.RESULTS CHAPTER II

4:1 Epicardial-FN as a key mediator of Epicardial-Myocardial Crosstalk

Thus far, I demonstrated that co-delivery of hESC-epicardium enhanced hESC-CM survival, maturation, and proliferation in the chronic MI setting. The advantage conferred by hESC-epicardium led to the attenuation of cardiac dysfunction in the chronic MI setting. The benefits of co-delivering a key stromal cell, i.e., epicardial cells, follows our recent report of favourable cardiac repair in the subacute MI setting (Bargehr et al. 2019). The epicardium plays a pivotal role in cardiac development and disease, widely postulated to be implemented by the extensive epicardial-myocardial crosstalk (Smart and Riley 2012; Cao and Poss 2018). From a mechanistic viewpoint, I hypothesized that our observed cardiac functional benefits may be underpinned by the epicardial-myocardial crosstalk.

Growing evidence points towards epicardial-FN as a putative key mediator of epicardial-myocardial crosstalk (Wang et al. 2013, Cao and Cao 2018). In the zebrafish, epicardial-FN was instrumental in directing cardiac regeneration (Wang et al. 2013). Our bulk RNA-sequencing data showed upregulated *FN1* expression in hESC-epicardium compared to hESC-neural crest cells (Bargehr et al. 2019). We also noted increased FN deposition in 3D-EHTs and in subacute MI rat hearts, in the presence of hESC-epicardium and hESC-CMs (Bargehr et al. 2019). In the subacute MI setting, epicardial-FN showed potential for modulating cardiac regeneration, within the context of epicardial-myocardial crosstalk (Bargehr et al. 2019).

Given this evidence, I first ascertained whether epicardial-FN was also differentially deposited within the chronic MI setting. Then, I proceeded to interrogate the effects of loss of FN function with the 3D-engineered heart tissues (3D-EHTs). With the 3D-EHTs, I investigated whether the loss of epicardial-FN function attenuated hESC-CMs' maturation. The overarching hypothesis was that epicardial-FN is the putative key mediator for epicardial-myocardial crosstalk; a process crucial in enabling the epicardial-augmentation of hESC-CMs' engraftment and cardiac functional recovery in infarcted rat hearts. The results of these loss-of-function experiments are detailed below.

4:1:1 Increased FN deposition with Epi+CM cardiac grafts

Notably, I observed a unique pattern of FN deposition in the chronically injured hearts which received the hESC-cellular (Epi+CM) therapy, compared to NRVM or sham, **Figure 41B**. Both Sham and NRVM showed similar patterns of FN deposition; most visibly at the sub-endocardium, **Figure 41A & C**. In the Epi+CM group, there was significantly more FN deposition within cardiac graft regions compared to NRVM, **Figure 42B & E**. However, there were no differences in FN deposition between the infarcted or remote regions for all groups, **Figure 42 C-D, F-G**. Altogether, the evidence indicated that hESC-epicardium had a specific effect on FN secretion and deposition.

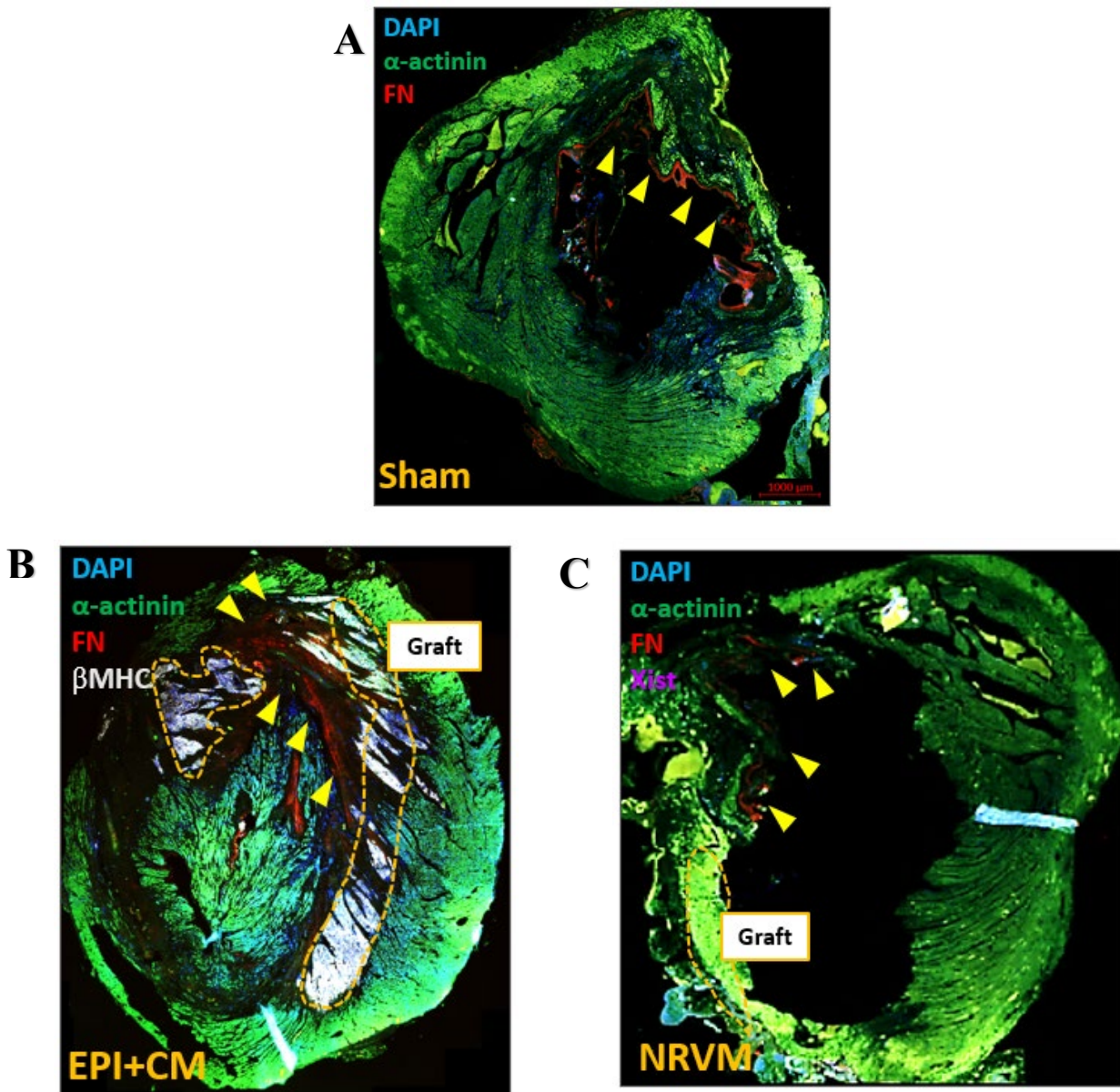


Figure 41: The different patterns of FN deposition in chronically infarcted rat hearts

At 3 months after cellular injections, all animals were harvested and investigated for the presence of FN deposition within the infarcted rat hearts. Three groups: Vehicle control (Sham), species-matched cellular therapy (NRVM), combination therapy (Epi+CM). The overall distribution of FN (red) in **A**) Sham-Vehicle, **B**) Epi+CM and **C**) NRVM sections in infarcted rodent hearts with cardiac grafts in situ. Yellow arrows point to FN deposition (red). β MHC (white) is specific for grafted human CMs while Xist (purple) stains for transplanted female NRVM. Scale bar 1 mm.

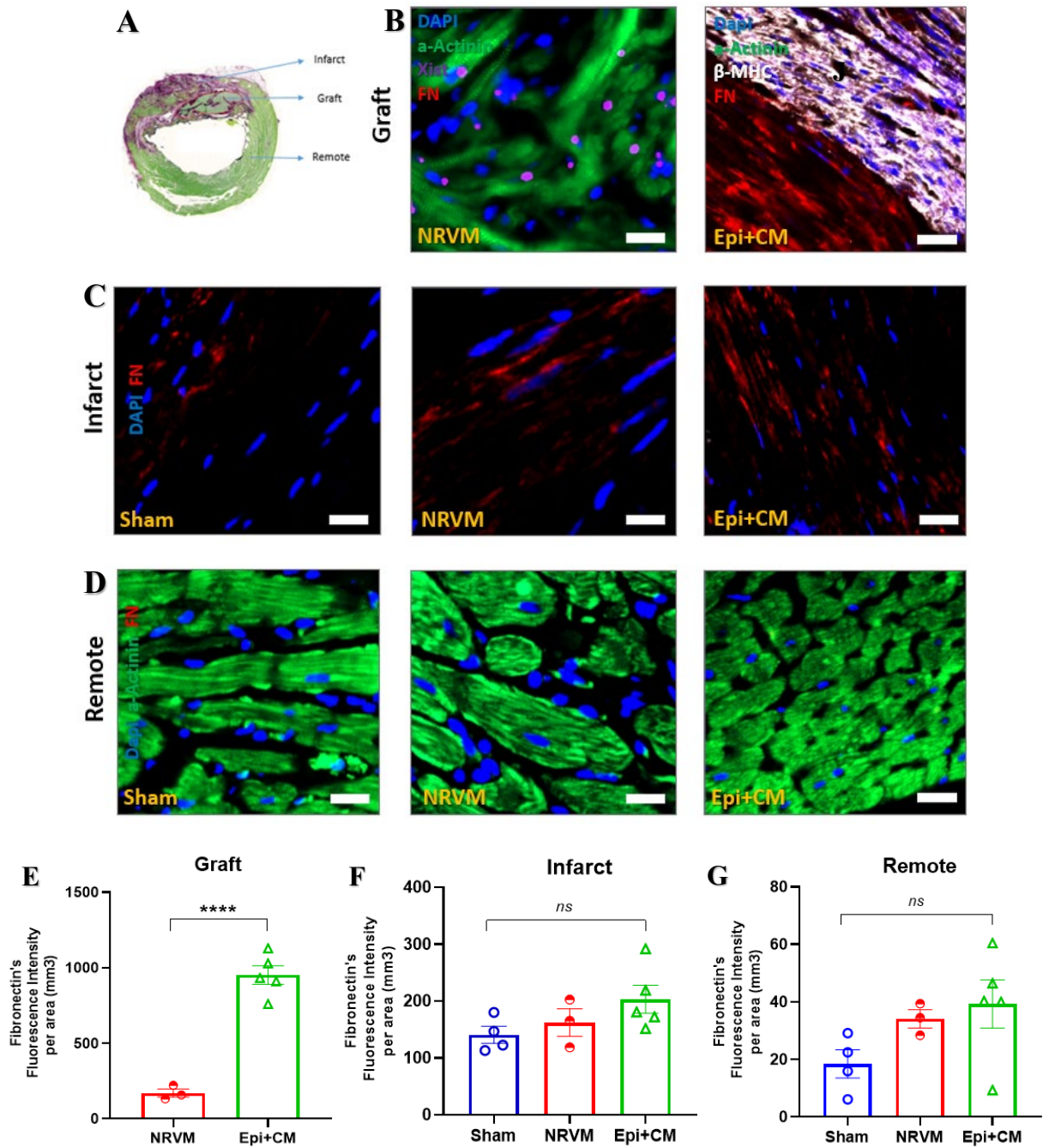


Figure 42: EPI+CM engraftment altered the fibronectin deposition in chronically infarcted rat hearts

A Schematic of heart areas assessed for FN deposition. FN deposition (red) respectively for NRVM and Epi+CM around **B**) graft areas, **C**) infarct and **D**) remote regions. Quantification of FN deposition (red) respectively for Sham vs NRVM vs Epi+CM at **E**) graft areas, **F**) infarct and **G**) remote regions. Scale bar 20 μ m. N=12 in total for histologic analysis of cardiac grafts after 3 months; Sham, NRVM and Epi+CM, N=4, 3 and 5 animals, respectively. Mean values; error bars represent s.e.m. ****P<0.0001.

4:1:2 Functional assessments of 3D-EHTs

Collectively, there was increased FN deposition in 3D-engineered heart tissues (3D-EHTs), in both subacute MI and chronic MI settings. Increased FN deposition was only observed in the combined presence of hESC-epicardium and hESC-CMs. With this growing evidence, I postulated that epicardial-FN underpinned the epicardial-myocardial crosstalk, which enabled superior CM survival, maturation, and proliferation *in vivo*. To test this hypothesis, I interrogated the loss-of-FN function utilising 3D-EHTs, **Figure 43**.

3D-EHTs are widely used as a high-throughput platform for drug screening, disease modelling and mechanistic studies (Vunjak Novakovic et al. 2014; Hansen et al. 2010; Ronaldson-Bouchard et al. 2018). 3D-EHTs enable the quantification of Frank-Starling active force generation, **Figure 43** and Ca^{2+} -handling, **Figure 44**, by hESC-CMs. Both Frank-Starling active force generation and Ca^{2+} -handling reflect the maturity of hESC-CMs' (Guo and Pu 2020, Ronaldson-Bouchard et al. 2018). The degree of hESC-CM active force generation is dependent on excitation-contraction coupling (Kane et al. 2015). The benefits of hESC-epicardium on CM maturation were most clearly shown using 3D-EHTs (Bargehr et al. 2019). Thus, the 3D-EHTs represent a practical and relevant assay for studying the effects of FN loss-of-function.

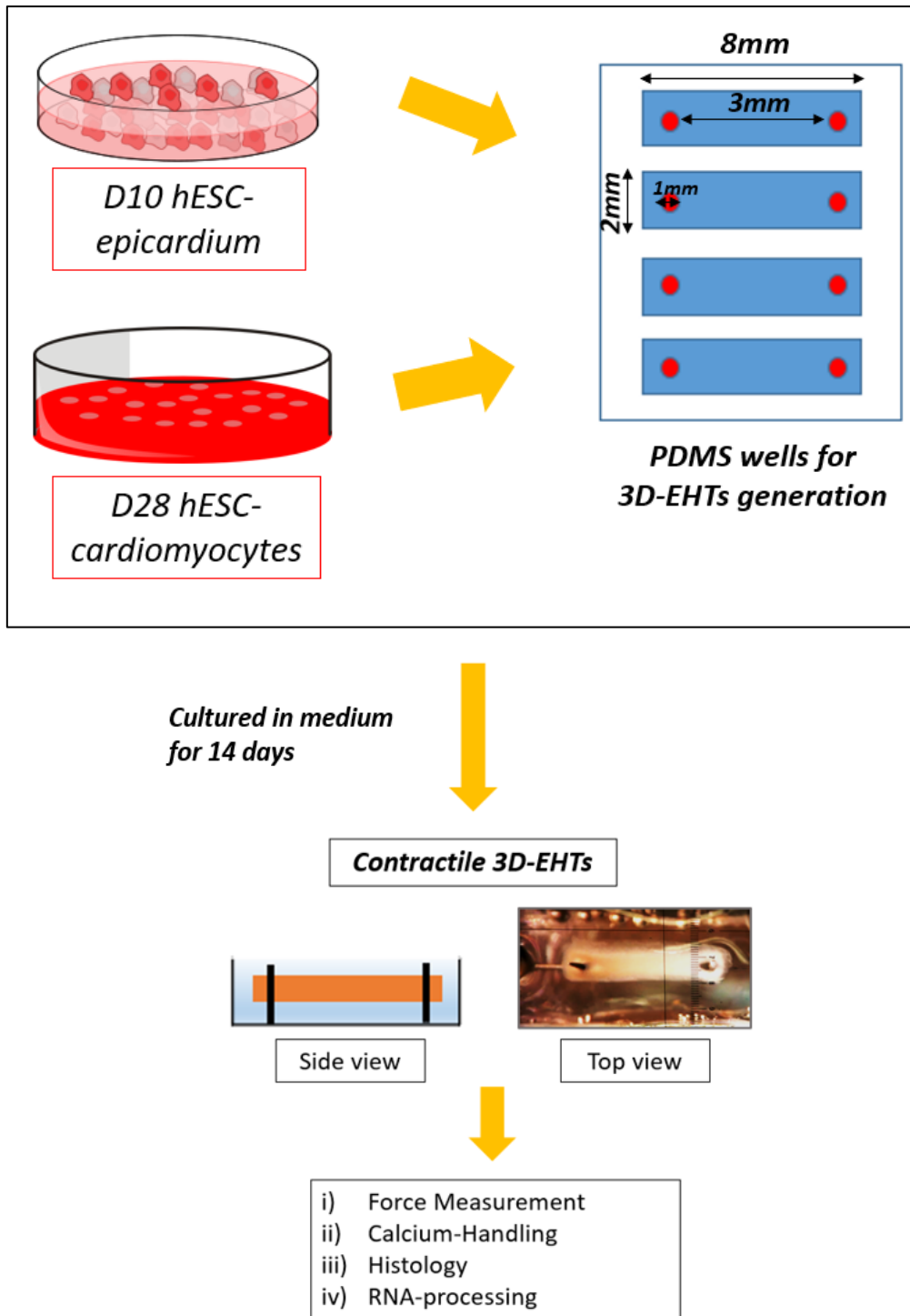


Figure 43: 3D-EHT workflow with hESC-epicardium & hESC-CMs

Epicardial cells and CMs are resuspended in a collagen gel and casted in fabricated PDMS troughs with two posts positioned at each end. 3D-EHTS were incubated for two weeks prior to functional studies, e.g. force or Ca^{2+} -handling measurements. Tissue constructs can subsequently be cryo-embedded and sectioned for histologic analysis or used for functional studies, investigating Ca^{2+} -handling and force production.

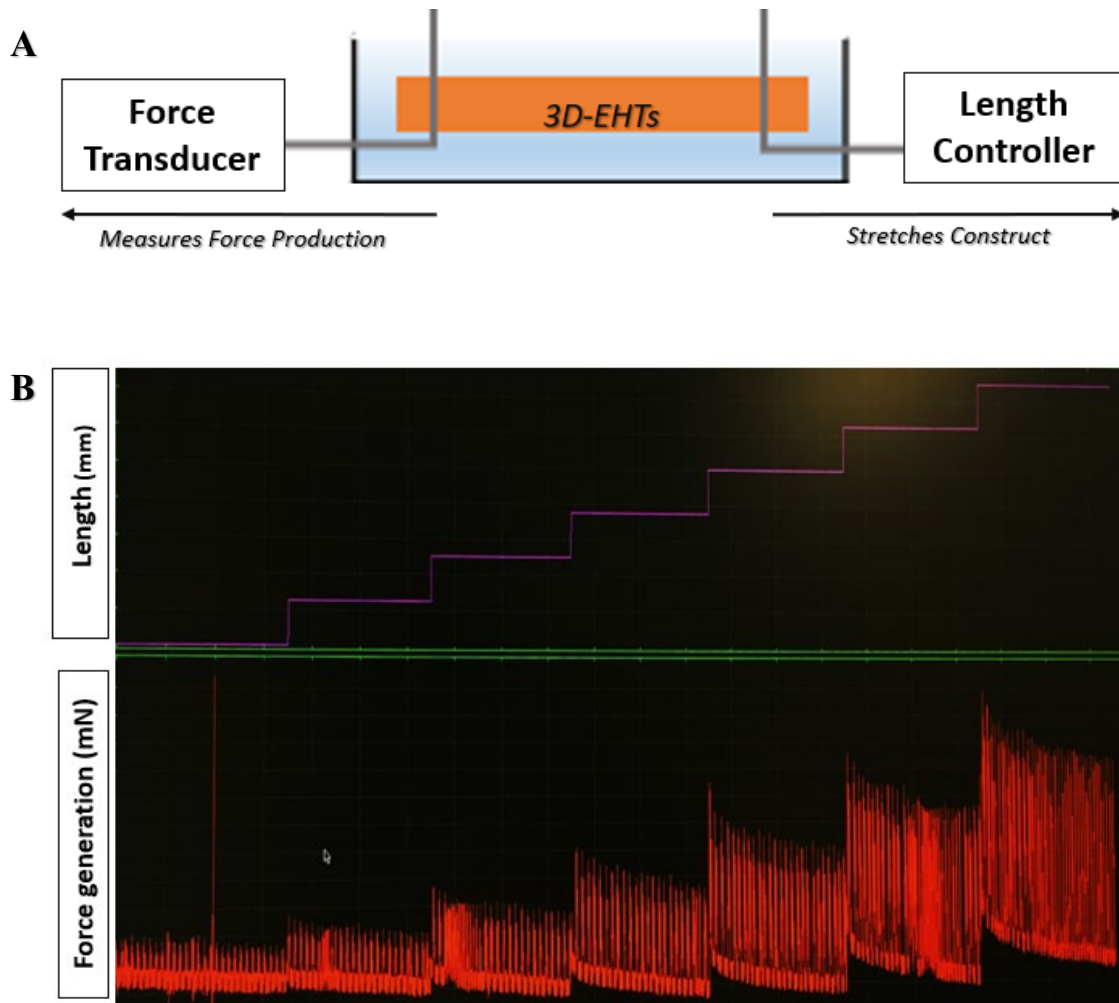


Figure 44: Frank-Starling force measurement of 3D-EHTs

A For measurement of force production, the 3D-EHTs were taken out of their PDMS troughs and transferred to a myograph with two arms, one is representing a high-speed length controller, the other a force transducer. Whilst bathed in Tyrode's solution, the 3D-EHTs were stretched with the length controller (over six increments) to assess the response to increased tension, in accordance with the Frank-Starling law. **B** Length and force production were recorded, which demonstrated that increasing tissue strain resulted in increasing force production. Myograph traces were used to quantify active and passive force production between experimental groups.

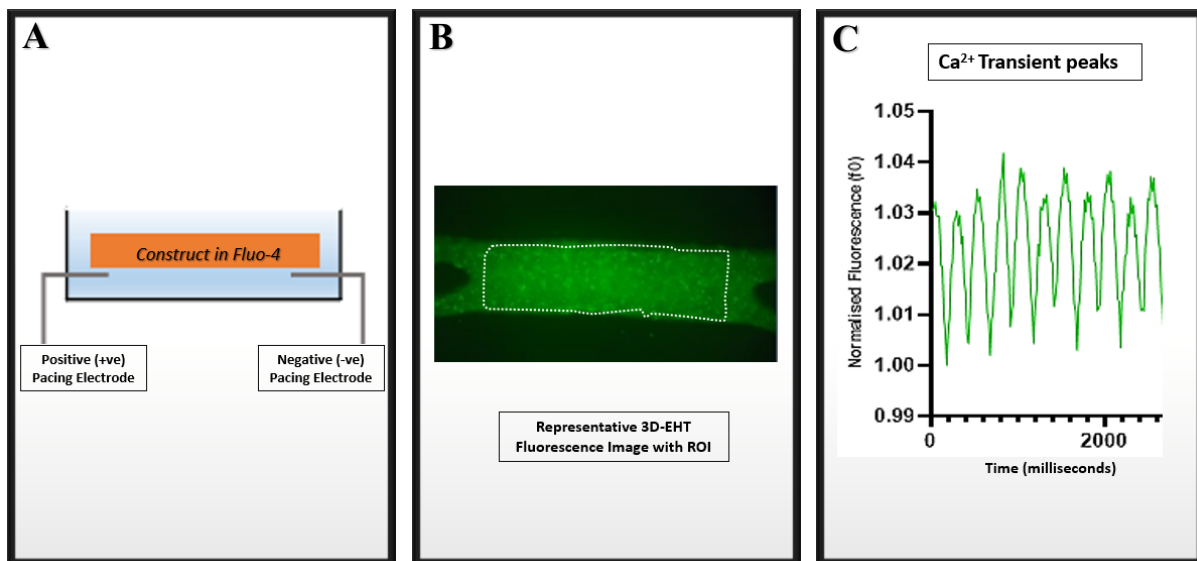


Figure 45: Measurements of Ca²⁺-handling by paced 3D-EHTs

A For measurement of Ca²⁺-handling, the 3D-EHTs were taken out of their PDMS troughs and transferred to the C-PACE with two electrode arms to create a field stimulus for pacing at 1Hz, 1.5Hz and 2 Hz. After incubation in Fluo-4 and whilst bathed in Tyrode's solution, the Ca²⁺-handling by 3D-EHTs were measured. **B** Representative image analysis of a single 3D-EHT with the central part of 3D-EHT (region of interest, ROI) used to for measurements. **C** Representative data readout of Ca²⁺ transients were used to quantify calcium kinetics of individual 3D-EHTs.

4:1:3 Optimal ratio of Epi:CM within 3D-EHTs

The Ca²⁺-handling apparatus and excitation-contraction coupling in 3D-EHTs composed of hESC-CMs alone are underdeveloped, with slower calcium dynamics than mature, adult CMs (Ruan et al. 2015). We previously showed that co-culture with a key stromal cell type, hESC-epicardium, resulted in greater force generation and electrical connectivity (Bargehr et al. 2019). However, the optimal ratio of Epi:CM within 3D-EHTs remained unclear. Prior to studying loss-of-FN function in 3D-EHTs (also referred to here as constructs), it was necessary to determine the optimal ratio of hESC-epicardium to hESC-CMs in 3D-EHTs. Thus, I conducted a dose-response

study. This study used a constant total cell number whilst varying the % of stromal cells in each group of 3D-EHTs. There were four groups i) CM Only ii) CM+10%Epi iii) CM+30%Epi iv) CM+50%Epi.

The dose-response study confirmed that the optimal ratio of hESC-epicardium to hESC-CMs was 1:9, that is 10% hESC-epicardium in each 3D-EHT. CM+10%Epi consistently generated the highest Frank-Starling active force, **Figure 46**. Only CM+10%Epi recorded a slope of active force significantly different from zero, $p=0.0127$ **Figure 46**. However, there was no difference between groups, although there was a trend towards statistical difference between CM+10%Epi and CM+50%Epi, $p=0.0912$, **Figure 46**. As for passive force production, only the slope of CM+10%Epi was significantly higher than zero; $p=0.0224$, **Figure 47**. To calculate the slope of the force against stepwise strain, I used linear regression to generate the slope of each condition. Immature CMs are unable to generate a Frank-Starling active force (Karbassi et al. 2020; Ronaldson-Bouchard et al. 2018), therefore the slope is 0. Then, the slope of each condition was compared to 0 to investigate whether any Frank-Starling response was present. All force generation dataset were analysed in this similar fashion.

Accordingly, CM+10%Epi demonstrated significantly higher calcium upstroke velocity and Ca^{2+} -handling, likely due to improved excitation-contraction coupling secondary to CM maturation, **Figure 48**. Altogether, these results suggested that CM+10%Epi had the optimal stromal cell composition in 3D-EHTs. All loss-of-FN function studies with 3D-EHTs proceeded with an Epi:CM ratio at 1:9.

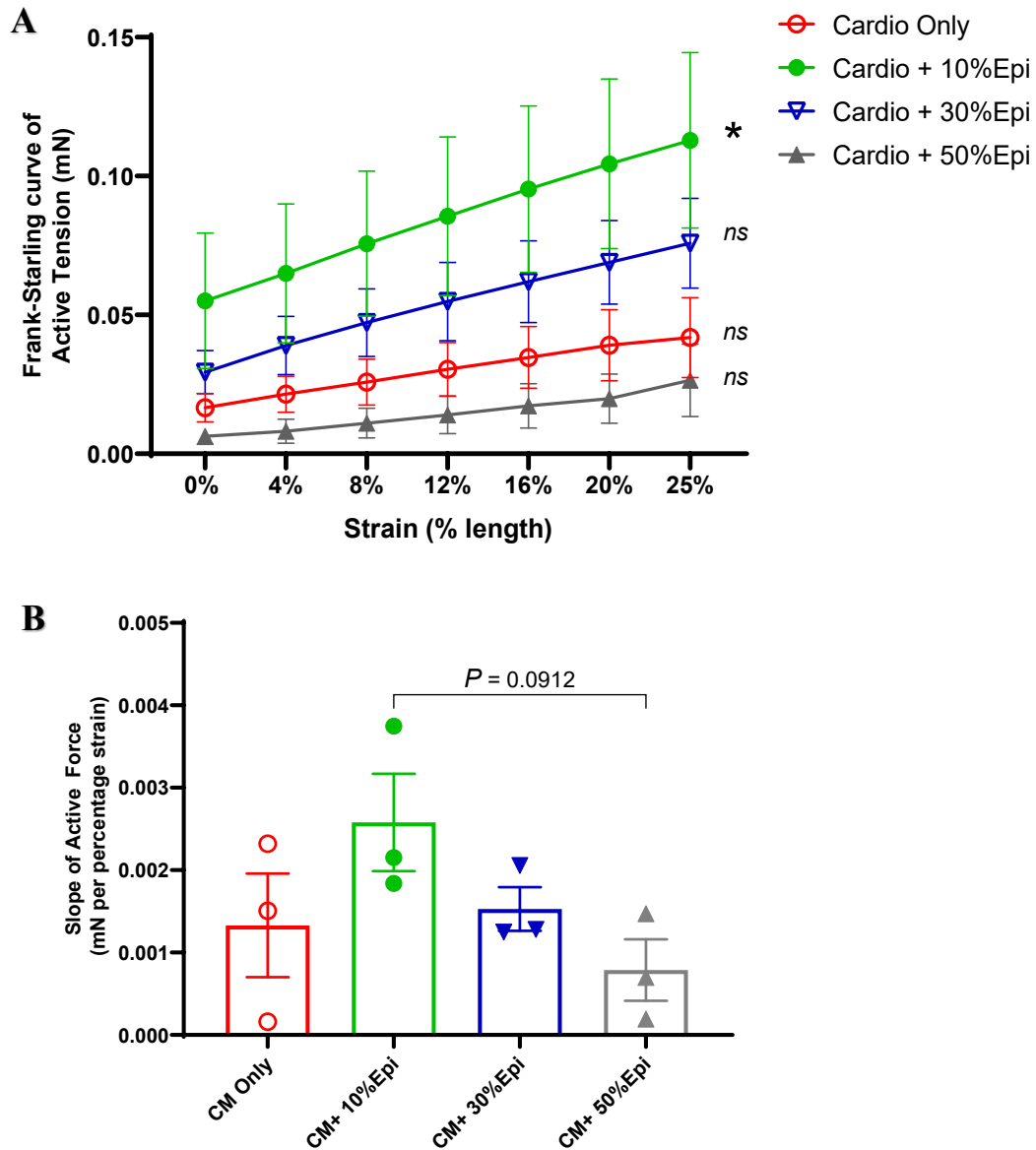


Figure 46: 3D-EHTs with 10% hESC-epicardium displayed the greatest active force production

A Frank-Starling curves of active force production by 3D-EHTs with CM only, CM+10% hESC-epicardium, CM+30% hESC-epicardium and CM+50% hESC-epicardium. Only the slope of CM+10% hESC-epicardium was significantly higher than zero; $p=0.0127$. **B** 3D-EHTs with 10% hESC-EPI had the highest slope of active force compared to other groups, albeit with no statistical difference between groups. There was a trend towards statistical significance between 10%hESC-Epi vs 50%hESC-Epi. Each experimental group included N=3 biological replicates, all generated and measured separately. Each biological replicate consisted of three technical triplicates. Mean values; error bars represent s.e.m. $*P<0.05$. Two-sided P values were calculated using a one-way ANOVA with post-hoc correction for multiple comparisons.

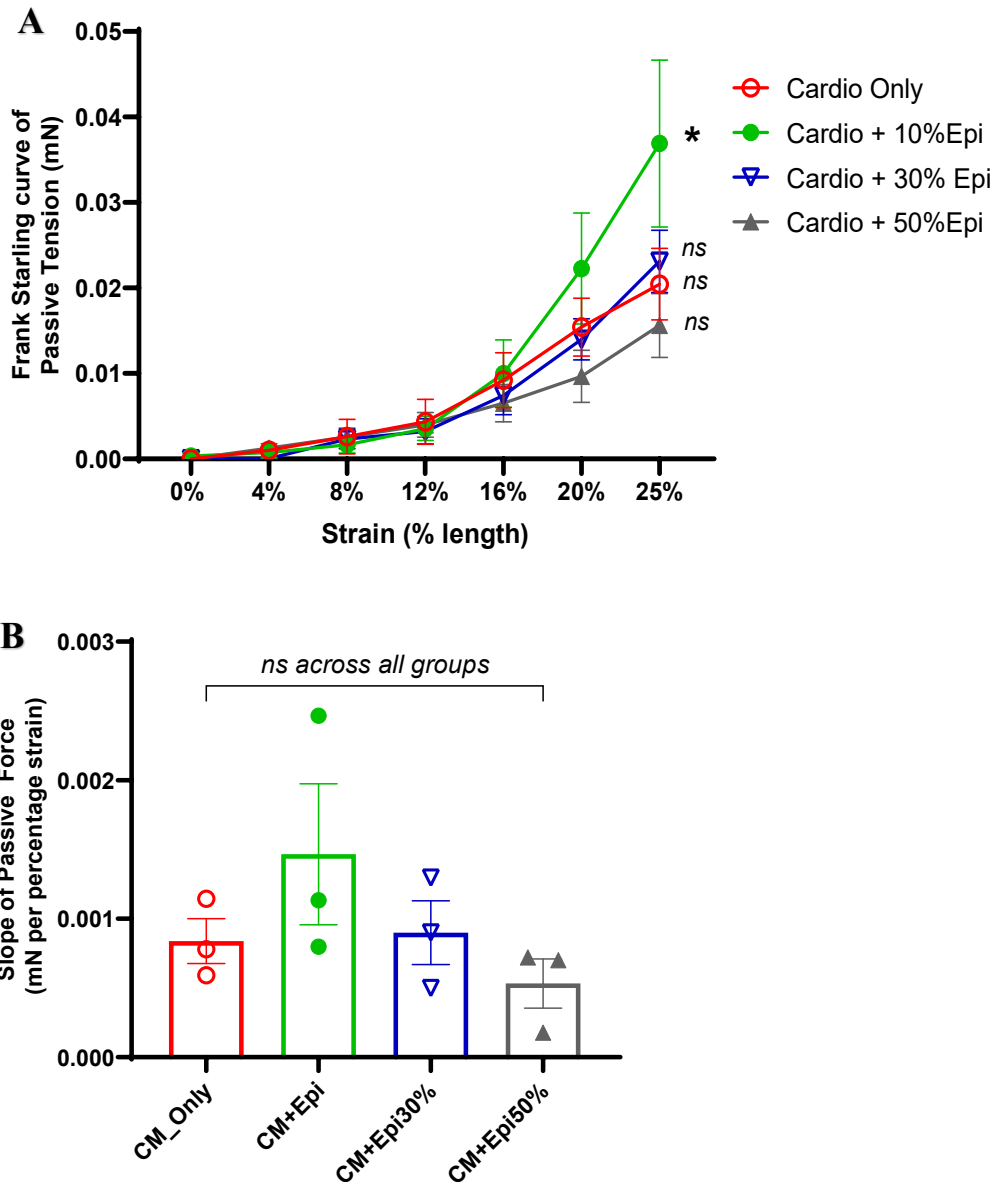


Figure 47: 3D-EHTs with 10% hESC-epicardium had greatest passive force production

A Frank-Starling curves of passive force production of 3D-EHTs containing CM only, CM+10% hESC-epicardium, CM+30% hESC-epicardium and CM+50% hESC-epicardium. Only the slope of CM+10% hESC-epicardium was significantly higher than 0; $p=0.0224$. **B** 3D-EHTs with 10% hESC-EPI had the highest slope of passive force compared to other groups, albeit with no statistical difference between groups. Mean values; error bars represent s.e.m. * $P<0.05$. Two-sided P values were calculated using a one-way ANOVA with post-hoc correction for multiple comparisons. Each experimental group included N=3 biological replicates, all generated and measured separately. Each biological replicate consisted of three technical triplicates.

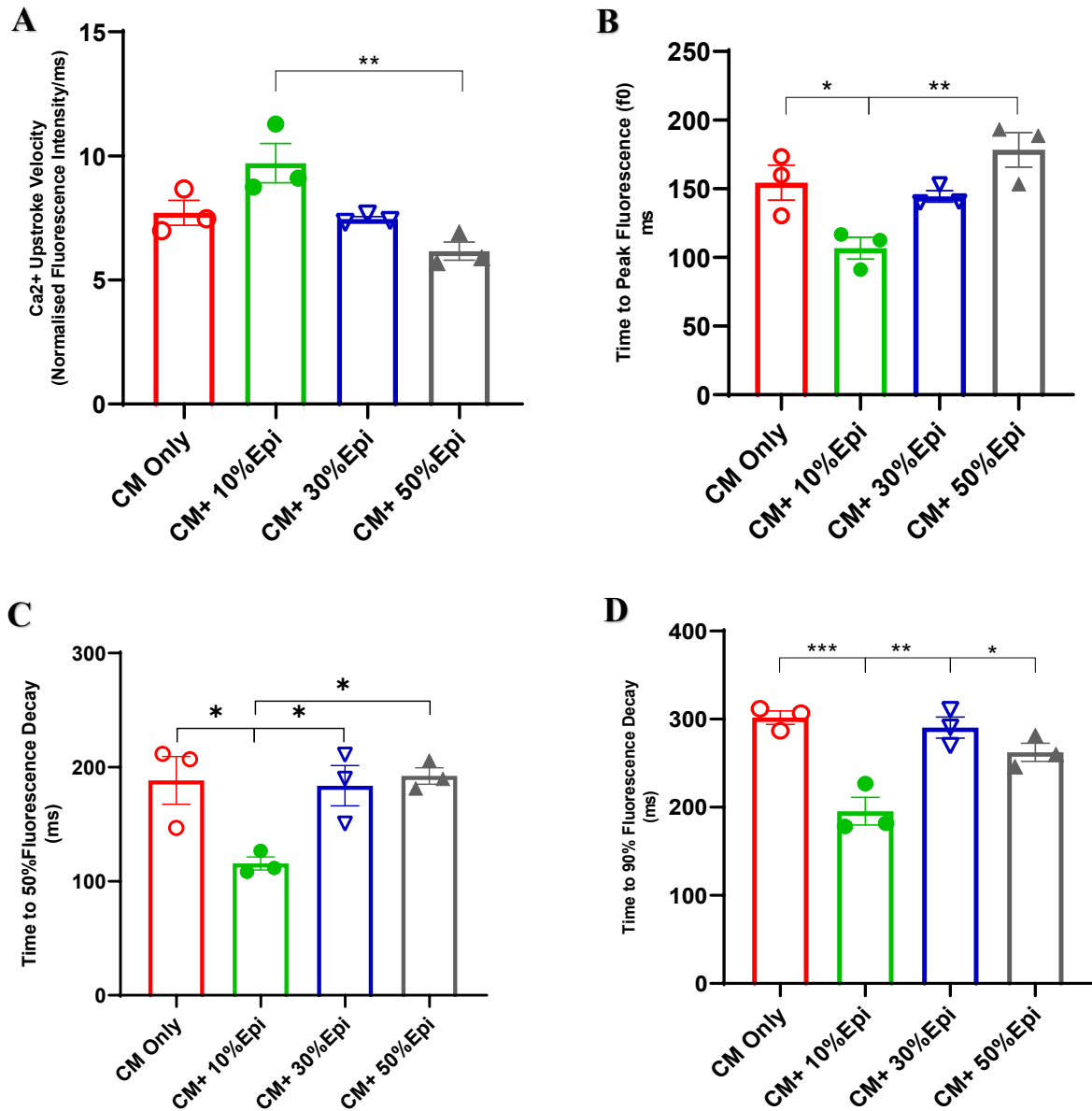


Figure 48: 3D-EHTs with 10% hESC-Epicardium displayed the most optimal calcium kinetics

Quantification of the calcium kinetics of 3D-EHTs with CM only, CM+10% hESC-epicardium, CM+30% hESC-epicardium and CM+50% hESC-epicardium. **A** Time from baseline to peak Ca²⁺ amplitude was significantly shorter for CM+10% hESC-epicardium. **B** Ca²⁺ upstroke velocity was significantly faster for CM+10% hESC-epicardium. Correspondingly, **C** time from peak to 50% and **D** time from peak to 90% amplitude decay were also significantly shorter for CM+10% hESC-epicardium. Mean values; error bars represent s.e.m. * $P < 0.05$. ** $P < 0.005$ *** $P < 0.0001$. Two-sided P values were calculated using a one-way ANOVA with post-hoc correction for multiple comparisons. Each experimental group included N=3 biological replicates, with 3 technical triplicates each.

4:2 Fibronectin (FN) Loss-of-function studies

The promiscuity of FN-integrin binding and the reported embryonic lethality of FN deletion (George et al. 1993; Pulina et al. 2011), led to the design of multimodal FN loss-of-function studies. The studies utilized downstream small peptide inhibitor and genetically induced loss of epicardial-FN, with both constitutive and temporally modulated loss of *FN1* expression. Each modality conferred a different level of control over epicardial-*FN1* expression and FN function, at the different developmental stages of hESC-epicardium. My composite findings enabled a comprehensive investigation of the effects of loss of epicardial-FN function and offer novel insights into the dynamic nature of epicardial-FN, in the presence of hESC-CMs.

4:2:1 Small Peptide (pUR4) inhibition of FN

Fibronectin is a ubiquitous protein with varied functions, with multiple alternative splicing sites (Pankov and Yamada 2002; Schwarzbauer and DeSimone 2011). To account for the fibronectin's numerous alternatively spliced isoforms, I initially used a small peptide, pUR4, to inhibit fibronectin polymerization. pUR4 is a 49-residue recombinant peptide derived from the F1 adhesin of *Streptococcus pyogenes*, which mimics the cell surface binding site of 5 N-terminal type I modules in FN (Tomasini-Johansson et al. 2001; Valiente-Alandi et al. 2018), thereby preventing FN binding to cell-surface receptors (integrins) and subsequent fibrillogenesis, as shown in **Figure 48A**. This strategy allowed a broad, downstream inhibition of FN action.

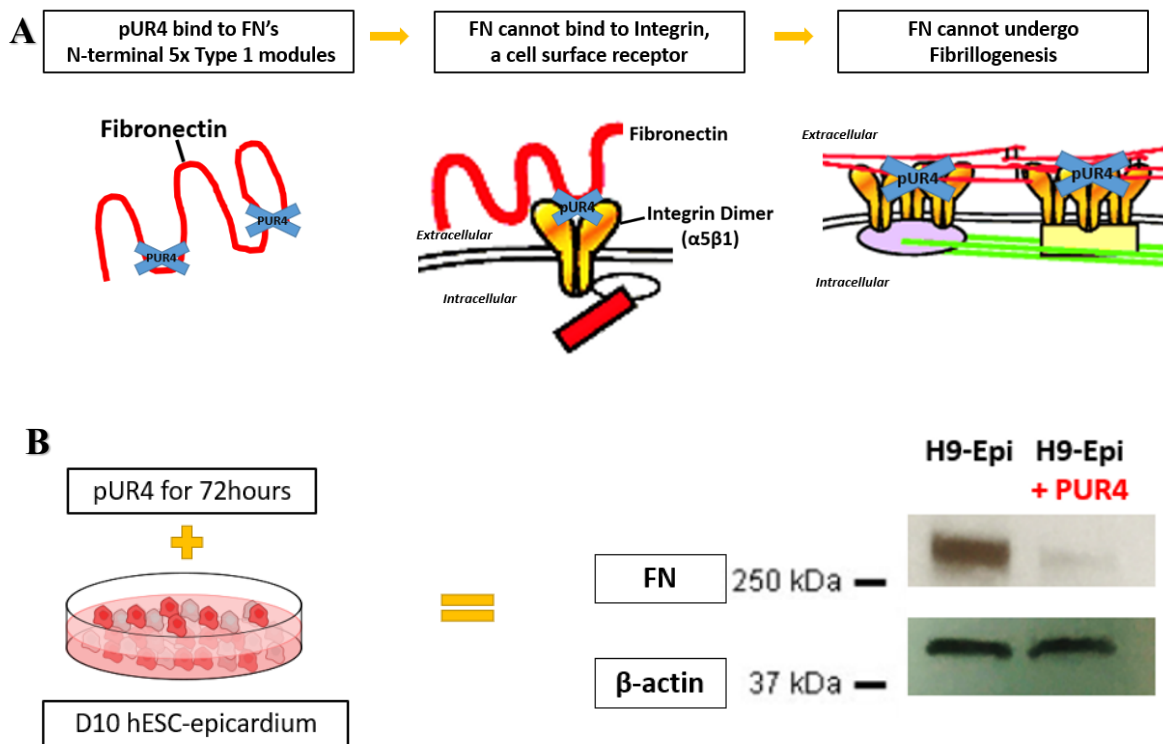


Figure 49: Inhibition of fibronectin activity by pUR4

A Schematic of pUR4 action on fibronectin. pUR4 is a 49-residue recombinant peptide derived from the F1 adhesin of *Streptococcus pyogenes*, which mimics the cell surface binding site of 5 N-terminal type I modules of FN, therefore preventing FN binding to cell surface receptors (integrins). Due to this blockade, fibronectin is unable to form fibrils and transduce intracellular or extracellular signals **B** Addition of recombinant pUR4 to hESC-epicardium in a monolayer over 72 hours led to the loss of polymerized fibronectin, as shown by the lack of 250 kDa fibronectin on a western blot.

4:2:1:1 Effect of pUR4 inhibition of FN on 3D-EHTs force generation

First, I hypothesized that loss-of-FN function would lead to decreased contractile force generation by hESC-CMs. 3D-EHTs have been established as the closest physiological model for assessing hESC-CM force production and Ca²⁺-handling (Ronaldson-Bouchard et al. 2018). Prior to force measurements in 3D-EHTs, the addition of pUR4 to an hESC-epicardium monolayer for 72 hours resulted in the loss of polymerized fibronectin (250kDA), **Figure 49B**. The effects of pUR4 inhibition in 3D-EHTs was studied using four groups i) CM Only, ii) CM+Epi, iii) CM+Epi+pUR4, and iv) CM+pUR4. The CM Only group was chosen as a negative control. We previously showed that 3D-EHTs with CM Only did not increase FN deposition, compared to Epi+CM 3D-EHTs (Bargehr et al. 2019). Meanwhile, the CM+pUR4 group was added as a control for any non-specific effects of pUR4. All groups were tested for their active and passive force generation, alongside their Ca²⁺-handling profiles.

The active force-length relationship demonstrated by mature 3D-EHTs was attenuated by pUR4 within the Epi+CM+pUR4 group. An active force-length relationship denotes the Frank-Starling mechanism and is a hallmark of CM maturity (Guo and Pu, 2020). pUR4 in the CM+Epi+pUR4 constructs significantly reduced active force generation compared to the CM+EPI constructs, **Figure 50**. The slope of active force by CM+Epi+pUR4 was 0.00056 ± 0.00028 mN/%strain, compared to 0.0021 ± 0.00047 mN/%strain recorded for CM+Epi, $p=0.0349$ **Figure 50**. However, passive force generation was conserved across all groups, **Figure 51**. The collective data implied that the inhibitory action of pUR4 on epicardial-FN specifically affected hESC-CM contractile force and maturation.

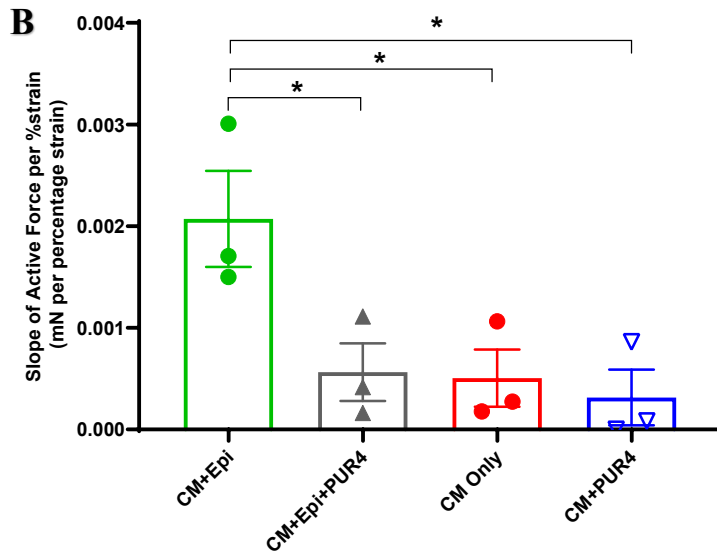
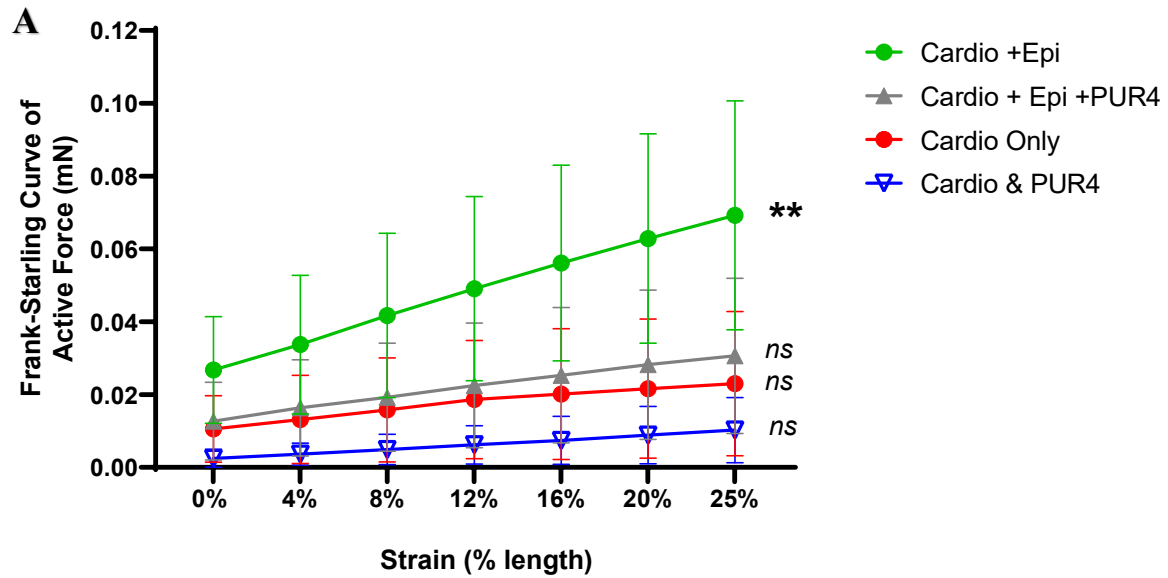


Figure 50: pUR4 inhibition of FN decreased active force production

A Frank-Starling curves of active force production of 3D-EHTs with CM only, CM+pUR4, CM+hESC-epicardium and CM+hESC-epicardium+pUR4. Only the slope for CM+10% hESC-epicardium was significantly higher than zero; $p=0.0048$. **B** 3D-EHTs containing CM+hESC-EPI had the highest slope of active force compared to other groups. pUR4 inhibition of CM+hESC-EPI led to significantly decreased active force; $p=0.0349$. Each experimental group included N=3 biological replicates, all generated and measured separately. Each biological replicate consisted of three technical triplicates. Mean values; error bars represent s.e.m. * $P<0.05$, ** $P<0.005$. Two-sided P values were calculated using a one-way ANOVA with post-hoc correction for multiple comparisons.

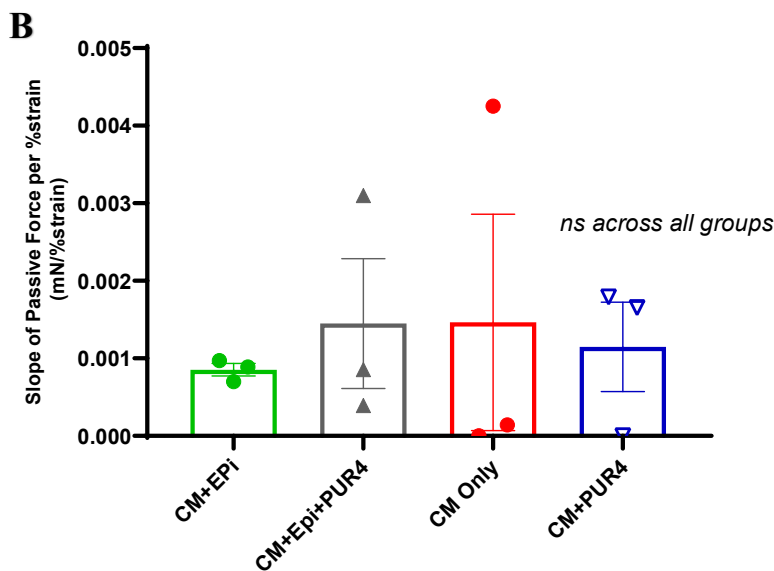
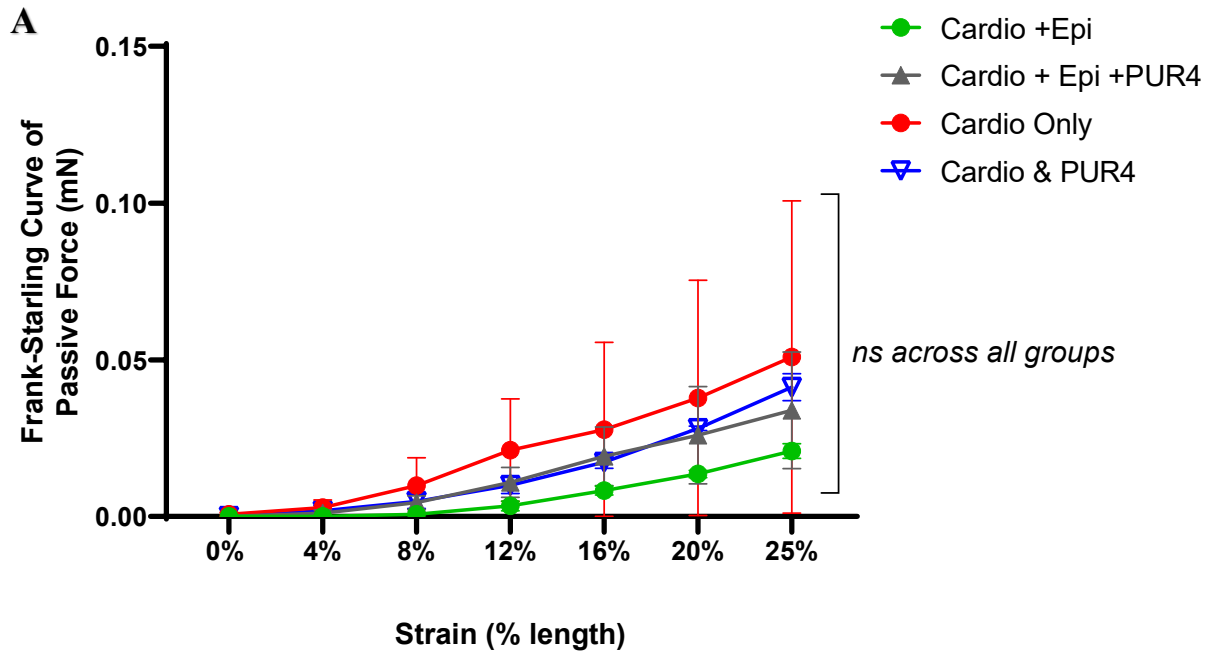


Figure 51: pUR4 inhibition of FN conserved passive force production

A Frank-Starling curves of passive force production of 3D-EHTs containing CM only, CM+pUR4, CM+hESC-epicardium and CM+hESC-epicardium+pUR4. No slope was significantly higher than zero. **B** 3D-EHTs across all groups recorded similar slopes of passive force production. Each experimental group included N=3 biological replicates, all generated and measured separately. Each biological replicate consisted of three technical triplicates. Mean values; error bars represent s.e.m. * $P < 0.05$. Two-sided P values were calculated using a one-way ANOVA with post-hoc correction for multiple comparisons.

Active force generation by 3D-EHTs is regulated by the efficiency of the excitation-contraction coupling apparatus (Bers 2002; Kane et al. 2015). hESC-CM maturity directly affects the efficiency of excitation-contraction coupling, as increased maturity brings better organisation of sarcomeres and t-tubules, together with increased calcium channel density in the sarcoplasmic reticulum (SR) (Guo and Pu 2020), **Table 2**. To initiate excitation-contraction coupling, cellular membrane potential changes lead to Ca^{2+} efflux from the sarcoplasmic reticulum (SR), which induces further Ca^{2+} release from the SR (Bers 2002). Ca^{2+} -induced Ca^{2+} release triggers actin-myosin contraction and leads to active force generation (Bers 2002). Then, cytoplasmic Ca^{2+} is sequestered back into the sarcoplasmic reticulum to be ready for the next contraction (Bers 2002). Hence, the 3D-EHT Ca^{2+} upstroke velocity and time to peak fluorescence (TTP) are surrogate markers for the efficiency of Ca^{2+} -induced Ca^{2+} release. Ca^{2+} upstroke velocity is calculated as peak Ca^{2+} fluorescence intensity/(time to peak fluorescence; TTP). Meanwhile, time to 90% (T90) and time to 50% (T50) fluorescence decay is affected by the rate of Ca^{2+} sequestration into SR. Thus, the kinetics of Ca^{2+} transients in the 3D-EHTs indicate the efficiency of the excitation-contraction coupling machinery, together with CM's maturation status.

pUR4 inhibition of FN function hampered the efficiency of Ca^{2+} -handling in 3D-EHTs, **Figure 52**. EPI+CM inhibited by pUR4 had a lower Ca^{2+} upstroke velocity compared to Epi+CM; Epi+CM+pUR4=7.538±0.29 f0/ms vs. Epi+CM=9.612±0.21 f0/ms, $p=0.012$, **Figure 53A**. Accordingly, EPI+CM+pUR4 took one-third longer to reach peak fluorescence intensity (TTP) compared to Epi+CM. The TTP for Epi+CM+pUR4 was 149.3±2.2ms, whilst the Epi+CM group TTP was 107.6±2.2ms, $p=0.014$, **Figure 53B**. As for Ca^{2+} sequestration into SR, there was no difference for time for 50% or 90% fluorescence decay across all groups, **Figure 53C & D**. Although not statistically

significant, there was a noticeable increase in time to 90% fluorescence decay (T90), which was one-third longer with FN inhibition, **Figure 53D**. Overall, the loss of epicardial-secreted FN function in the 3D-EHTs decreased the efficiency of Ca^{2+} handling and, consequently, the excitation-contraction coupling machinery and active force generation.

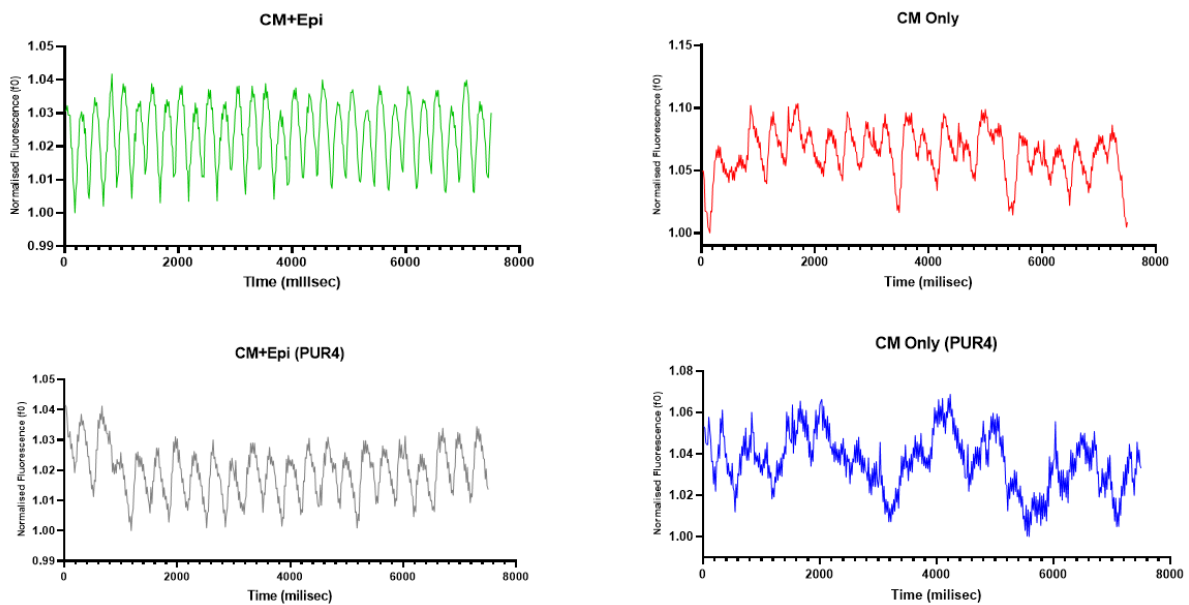


Figure 52: pUR4 inhibition of FN attenuated Ca^{2+} -handling in 3D-EHTs

To investigate whether the loss of epicardial-FN function via pUR4 inhibition attenuated the maturation of hESC-CMs in 3D-EHTs, the kinetics of Ca^{2+} transients displayed by all four experimental groups were determined. The 3D-EHT groups were i) Epi+CM, ii) Epi+CM+puR4, iii) CM only and iv) CM Only+pUR4. Representative Ca^{2+} transients illustrated clear, regular Ca^{2+} peaks in Epi+CM, which were attenuated in Epi+CM+pUR4. Both CM only and CM+pUR4 groups exhibited weak and irregular signals.

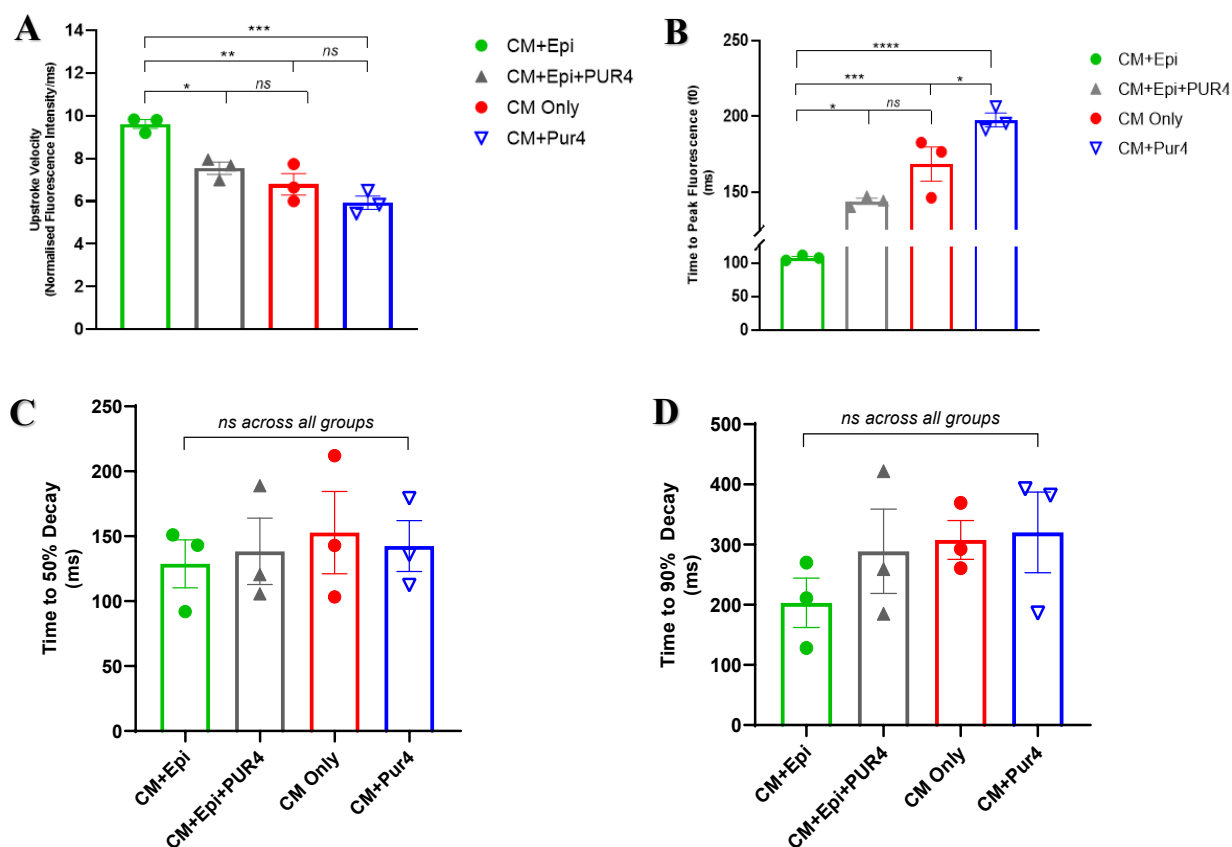


Figure 53: pUR4 inhibition of FN attenuated Ca^{2+} -handling by 3D-EHTs containing epicardial cells

A Quantification of calcium kinetics revealed significantly lower Ca^{2+} upstroke velocity with CM+EPI+pUR4 compared to other EHTs, $p=0.0122$. **B** Correspondingly, there was a significantly longer time to peak fluorescence (TTP) for Epi+CM+pUR4, $p=0.0144$. **C** Time to 50% fluorescence decay (T50) and **D** time to 90% fluorescence decay (T90) of Ca^{2+} -signals were each conserved across all groups. Each experimental group included N=3 biological replicates, all generated and measured separately. Each biological replicate consisted of three technical replicates. Mean values; error bars represent s.e.m. * $P<0.05$, ** $P<0.005$, *** $P<0.001$, **** $P<0.0001$. Two-sided P values were calculated using a one-way ANOVA with post-hoc correction for multiple comparisons.

As for pUR4 inhibition in 3D-EHTs with CM only, there were reduced active force production and attenuated Ca^{2+} -handling compared to CM Only, **Figures 50, 52 & 53**. Directed differentiations of hESC-CMs often record around ~10-20% stromal contaminants (Mummery et al. 2012). Prior to 3D-EHT generation, hESC-CMs underwent lactate selection to yield a >80% cTNT⁺ population. Notably, the attenuation of 3D-EHT performance due to pUR4 inhibition with hESC-CMs alone, was less compared to pUR4 inhibition of hESC-epicardium in the Epi+CM 3D-EHTs, **Figures 50, 52 & 53**. It seemed likely that pUR4 also inhibited the FN secreted by the stromal contaminants within hESC-CM differentiations.

In summary, the loss of FN function in the Epi+CM+pUR4 group significantly reduced epicardial augmentation of hESC-CM contractile function. With 3D-EHTs, hESC-cardiomyocyte contractile function directly correlated with maturity level (Karbassi et al. 2020, Guo and Pu 2020). Thus, these findings suggest that the loss of FN activity hampered hESC-CM maturation in 3D-EHTs, underpinned by dysregulated epicardial-myocardial crosstalk.

4:2:1:2 Effects of pUR4 inhibition of FN on hESC-cardiomyocytes' maturation

To investigate how pUR4-inhibited FN attenuated 3D-EHT contractile performance, the degree of hESC-CM maturation between the four groups was assessed: i) CM Only ii) CM+Epi iii) CM+Epi+pUR4 iv) CM+pUR4. The degree of CM maturation was determined by myofibril analyses at the sarcomeric organisation, protein, and RNA level.

In the 3D-EHTs, pUR4 inhibition of epicardial-secreted FN resulted in immature sarcomere assembly, **Figure 54A**. Compared with Epi+CM, pUR4 inhibition in the Epi+CM+pUR4 group led to significantly shorter sarcomeric length ($1.52\pm 0.05\mu\text{m}$ vs $1.75\pm 0.06\mu\text{m}$, $p=0.0382$), **Figure 54B**. Accordingly, Epi+CM+pUR4 also exhibited less well aligned sarcomeres (0.079 ± 0.003 a.u. vs 0.127 ± 0.015 a.u., $p=0.0479$), when compared to Epi+CM, **Figure 54C**. Notably, the decreased CM maturity displayed by Epi+CM+pUR4 corresponded to decreased fibronectin deposition, **Figure 54D**. Upon observation and quantification, the sarcomeric parameters of Epi+CM+pUR4 were comparable to CM Only, akin to immature hESC-CMs alone. Thus, pUR4 inhibition of epicardial-secreted FN in Epi+CM also attenuated hESC-CM maturation, as judged by the level of sarcomere assembly.

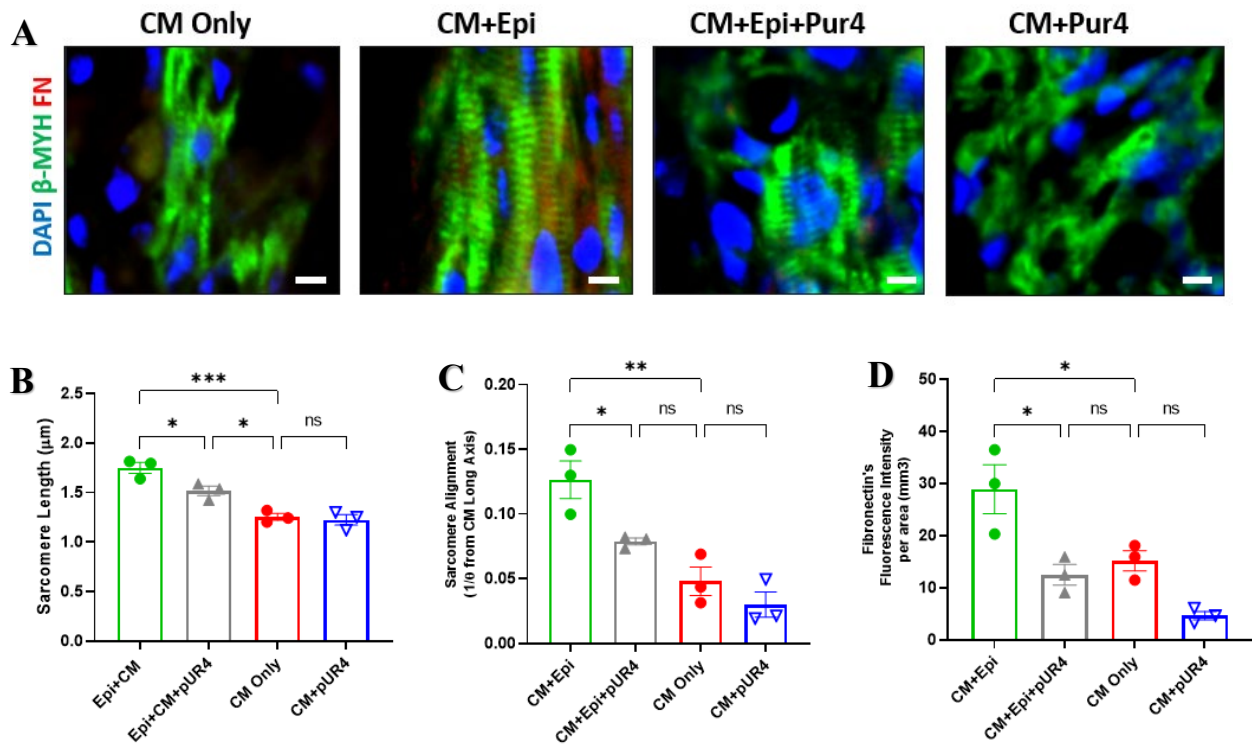


Figure 54: Loss of epicardial-FN decreased hESC-CMs maturation

A Representative section of 3D-EHTs demonstrating the differences in hESC-CMs' sarcomeric alignment (β MHC, green) and FN (red) deposition within each experimental group. Scale bar 5 μm . CM+Epi had the greatest sarcomeric maturation. With the pUR4 inhibition of epicardial-secreted FN, the hESC-cardiomyocyte **B** sarcomere length and **C** sarcomeric alignment were significantly reduced. **D** Correspondingly, there was significantly reduced FN deposition. Each experimental group included N=3 biological replicates with three technical triplicates each. Mean values; error bars represent s.e.m. * $P < 0.05$ ** $P < 0.005$, *** $P < 0.001$.

Next, I interrogated whether pUR4-inhibition of epicardial-FN in 3D-EHTs, would affect the RNA expression of cardiac maturity markers, e.g. *MYH 7/6* ratio, *RYR* and *SERCA2*. In human ventricular muscle, the β -myosin heavy chain subunit (β MHC, encoded by *MYH7*) is predominant compared with the α -heavy chain subunit (α MHC, encoded by *MYH6*), and increases in the ratio of *MYH7* to *MYH6* are associated with hESC-CM maturation, **Table 2**. Although not significant, likely due to the size of experimental error, the Epi+CM+pUR4 group had a decreased *MYH7/6* ratio, when compared to Epi+CM, **Figure 55A**.

RYR encodes for the sarcoplasmic reticulum (SR) Ca^{2+} -ATPase channel which enables SR Ca^{2+} efflux that initiates excitation-contraction coupling (Kane et al. 2015). *SERCA2* encodes for the SR Ca^{2+} -ATPase channel for Ca^{2+} influx into the SR, which instigates exit from excitation-contraction coupling (Kane et al. 2015). Thus, increased *RYR* and *SERCA2* expressions are associated with efficient Ca^{2+} -handling; a defining feature of mature CMs, (Guo and Pu 2020), **Table 2**. Although not significant, likely due to the size of experimental error, the Epi+CM+pUR4 group had decreased *RYR* expression, when compared to Epi+CM, **Figure 55B**. However, there were no clear trends across all groups for *SERCA2*, **Figure 55C**. The technical difficulties in procuring good-quality RNA from the 3D-EHTs likely contributed to the equivocal results. Thus, the *MYH7/MYH6* RNA expression ratio and *RYR* expression only hinted at a possible decrease in CM maturity with pUR4 inhibition of epicardial-FN.

The histological evidence and genetic expression of cardiac structural proteins showed reduced maturation of hESC-CMs with pUR4-inhibition of FN function. Within the 3D-EHTs, loss of epicardial-FN function appeared to undermine the epicardial-augmentation of hESC-CM maturation.

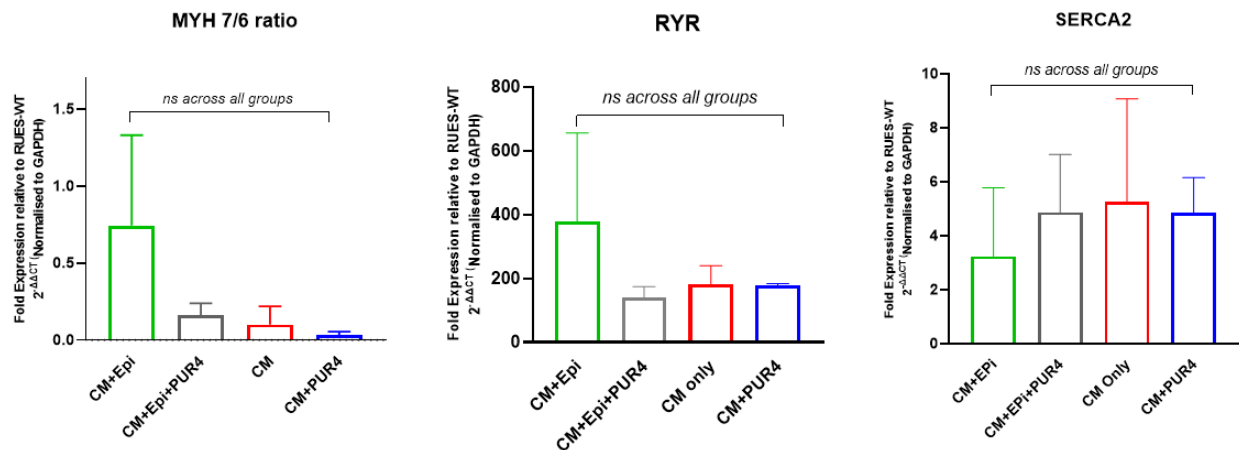


Figure 55: Effects of pUR4 inhibition on the key markers of hESC-CM's maturity

Panel of key genetic markers of hESC-cardiomyocyte maturity. **A** Despite the lack of statistical significance, Epi+CM had an increased *MYH7/6* expression ratio compared to the other groups. **B** There was a noticeable trend of upregulated *RYR* for the Epi+CM group, albeit not significant. Both the *MYH7/6* ratio and *RYR* expression were reduced with pUR4 inhibition. **C** *SERCA2* was not affected by the loss of FN. N=3 biological replicates, all generated and measured separately. Each biological replicate consisted of three technical triplicates. Mean values; error bars represent s.e.m. Two-sided P values were calculated using a one-way ANOVA with post-hoc correction for multiple comparisons.

4:2:1:4 pUR4 inhibition of FN altered downstream integrin $\alpha5\beta1$ signalling in 3D-EHTs

The inhibition of epicardial-FN in 3D-EHT co-cultures of Epi+CM manifested broadly as an hESC-CM functional loss. One possible hypothesis is the attenuation of maturation of CM by the loss of epicardial-FN, thereby placing epicardial-FN at the centre stage of epicardial-myocardial crosstalk. If so, how does epicardial-FN communicate with hESC-CMs? By staining for the main cellular signal transducer of FN activity, integrin $\alpha5\beta1$, it was found that the activated form of integrin $\alpha5\beta1$ was correspondingly reduced alongside the loss of FN, **Figure 56A**. Thus, it is highly probable that epicardial-FN communicates with hESC-CMs via integrin $\alpha5\beta1$. Epicardial-FN clearly plays a role in epicardium-myocardial crosstalk, but the extent and significance of that role remains to be determined.

Interestingly, our cells did not upregulate their *FN1* expression in response to FN inhibition by pUR4, **Figure 56B**. Thus, we screened for the expression of another key cardiac ECM e.g. *POSTN*, known to be associated with EPDCs (Weeke-Klump et al. 2010), dynamic ECM turnover in zebrafish cardiac regeneration (Garcia-Puig et al. 2019) and more commonly, activated cardiac fibroblasts (Hermans et al. 2016; Tallquist and Molkentin 2017). Although not statistically significant, *POSTN* expression appeared to be upregulated in the presence of FN inhibition, **Figure 56C**. As with many other cellular components when they are depleted, certain functions of FN may be compensated for by other molecules, in this case most likely an extracellular matrix protein (or proteins). Given that my current *POSTN* data was inconclusive, further work would be required to determine the role of *POSTN* and screen for the upregulation of other ECM components during pUR4 inhibition of FN.

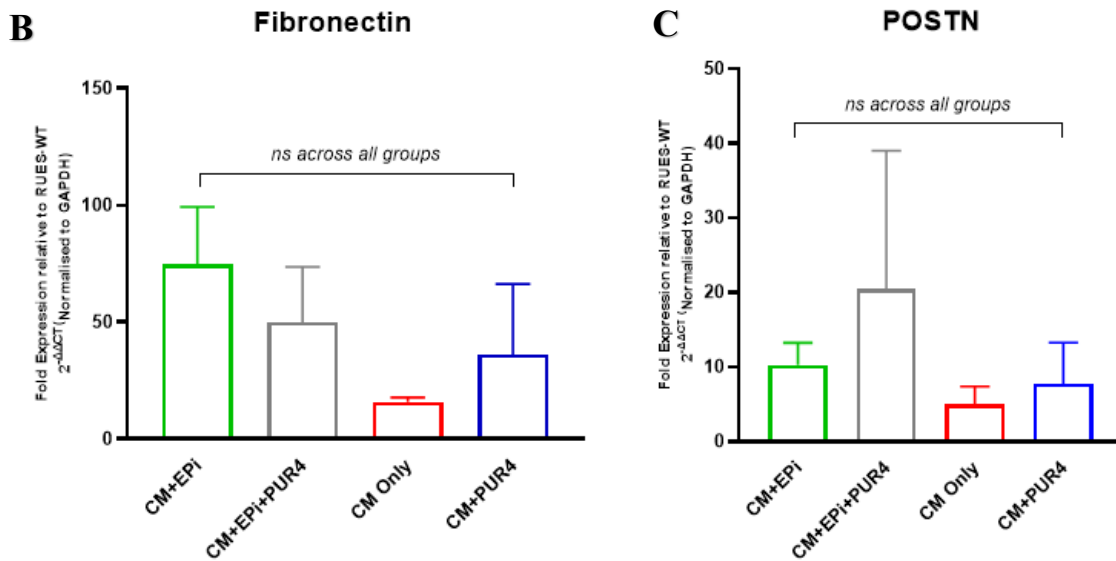
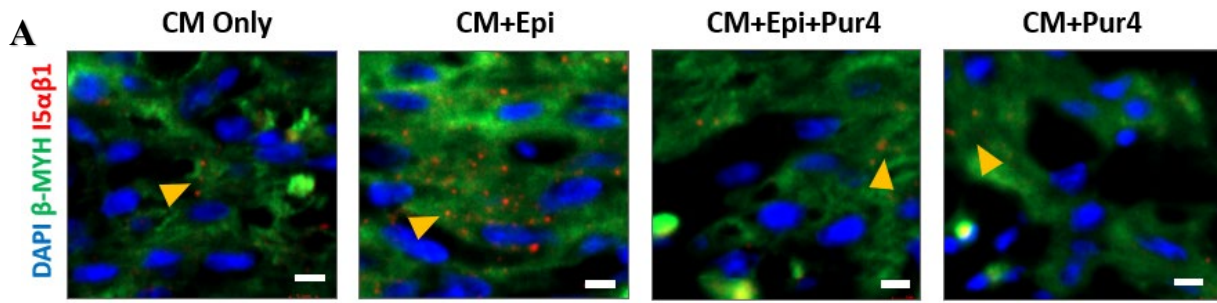


Figure 56: pUR4 inhibition reduced integrin-signalling and altered ECM composition

A 3D-EHT sections showed hESC-CMs (β MHC, green) in the CM+EPI group with correspondingly more integrin 5 α β 1 (red; yellow arrow) clustering. Scale bar 5 μ m. FN binds to the cell membrane receptor integrin 5 α β 1 as its main intracellular signal transducer. **B** RT-qPCR results of *FN1* and *POSTN* expression in 3D-EHTs. There was a trend towards increased *FN1* expression in the presence of hESC-epicardium in 3D-EHTs. Conversely, there was a trend towards reduced *FN1* expression with pUR4 inhibition in Epi+CM. **C** With the loss of *FN1* expression, another key extracellular matrix protein, *POSTN*, showed a trend towards upregulation with the addition of pUR4. N=3 biological replicates. Each biological replicate consisted of three technical triplicates. Mean values; error bars represent s.e.m.

Collectively, pUR4-inhibition of epicardial-FN function in 3D-EHTs, resulted in the attenuation of hESC-CM maturation, which broadly manifested as decreased active force-length generation, inefficient Ca²⁺-handling and lack of sarcomeric assembly. The loss of epicardial-FN function in 3D-EHTs also decreased FN-integrin signalling with hESC-CMs. Thus, epicardial-FN may be a key mediator of epicardial-myocardial crosstalk.

4:3 Genetically Induced Loss-of-FN function

Despite some insights gained, the downstream inhibition of FN by pUR4 carried some limitations. Namely, pUR4 broadly inhibited all FN secreted by hESC-epicardium and any stromal contaminants associated with hESC-CMs. A more precise loss of epicardial-FN function was required. The loss of epicardial-FN function by genetic deletion of *FN1* expression was studied further in 2 ways: i) Crispr-Cas9-mediated knockout of FN (KOFN) in an hESC cell line and ii) tetracycline-induced knockdown of FN in mature hESC-derived epicardium.

4:3:1 Loss-of-FN function negatively affects 3D-EHTs' contractile function

4:3:1:1 Derivation of Crispr-Cas9-mediated KOFN epicardium

Although the role of FN in embryonic development has been well-discussed (Schwarzbauer and DeSimone, 2011), *FN1* expression had not been causally linked in the specification of epicardium or subsequent EMT (Cheng et al. 2013). The hESC-derived knockout FN (KOFN) cell line was generated, and the expression of pluripotency markers confirmed, **Figure 57**. The hESC-KOFN hESC cell line was successfully differentiated into epicardium with the addition of recombinant human (FN) at the stage of lateral plate mesoderm and at days 1-3 after directed differentiation to epicardium. This was confirmed by expression of the key epicardial markers *WT1*, *TCF21* and *BNC1* as detected by qPCR, **Figure 58A**, alongside observation of a classical cobblestone morphology, **Figure 58B**. KOFN-epicardium showed reduced *FN1* expression at the RNA level and no protein expression detectable by immunostaining, **Figure 59**.

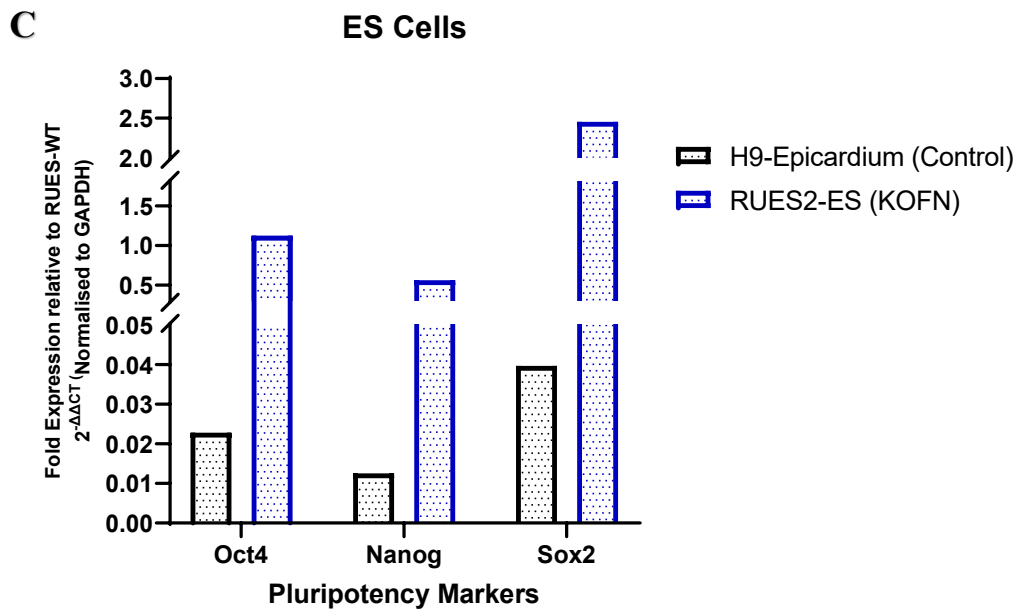
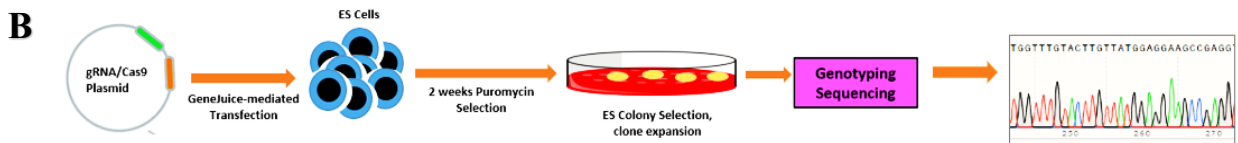
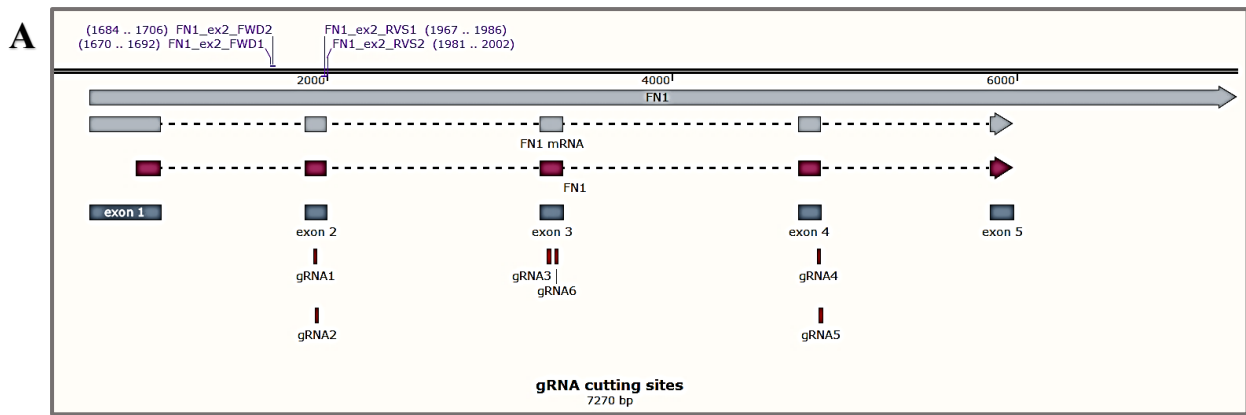


Figure 57: Generation of Crispr-Cas9 knockout FN hESC cell line (KOFN)

A Overview of the design of gRNA incisions sites along with *FN1* exons. **B** Schematic of workflow for GeneJuice-mediated transfection of hESC cells with Crispr-Cas9 gRNAs to generate knockout-FN cell lines. **C** Knock-out FN in RUES2 hESC cells had markedly higher pluripotency marker expression than hESC-epicardium differentiated from H9, the hESC parental line.

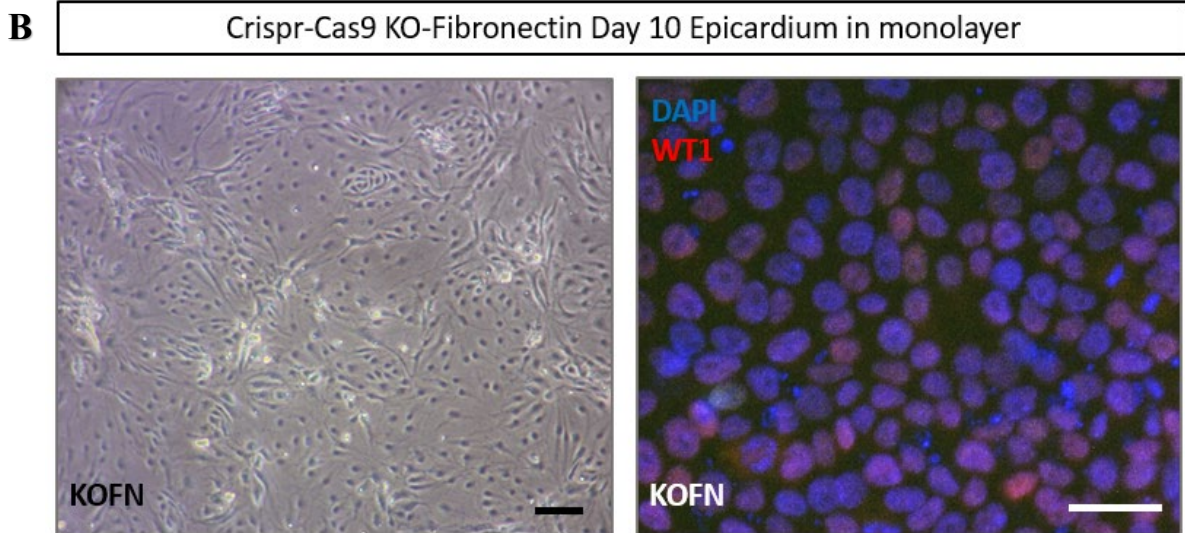
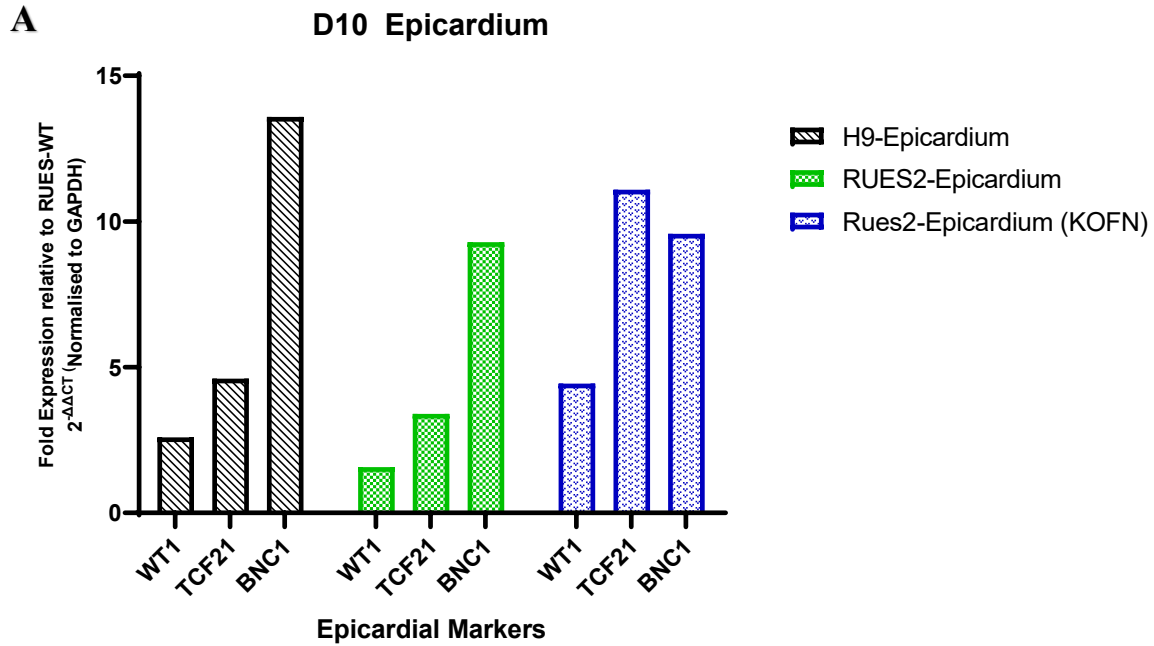


Figure 58: Differentiation of Crispr-Cas9-mediated KOFN to the epicardium

A Crispr-Cas9-mediated KOFN epicardium expressed classical epicardium markers such as *WT1*, *TCF21* and *BNC1* at day 10 after directed differentiation from lateral plate mesoderm. This panel of epicardial markers are expressed at similar levels to wild-type H9-derived epicardium and wild-type RUES2-derived epicardium. **B** Representative brightfield image showing that Crispr-Cas9 KOFN epicardium exhibit 'cobblestone' morphology, a hallmark of human foetal epicardium; whilst immunofluorescence showed scattered *WT1* (transcription factor, red) expression. Scale bar, 20 μm .

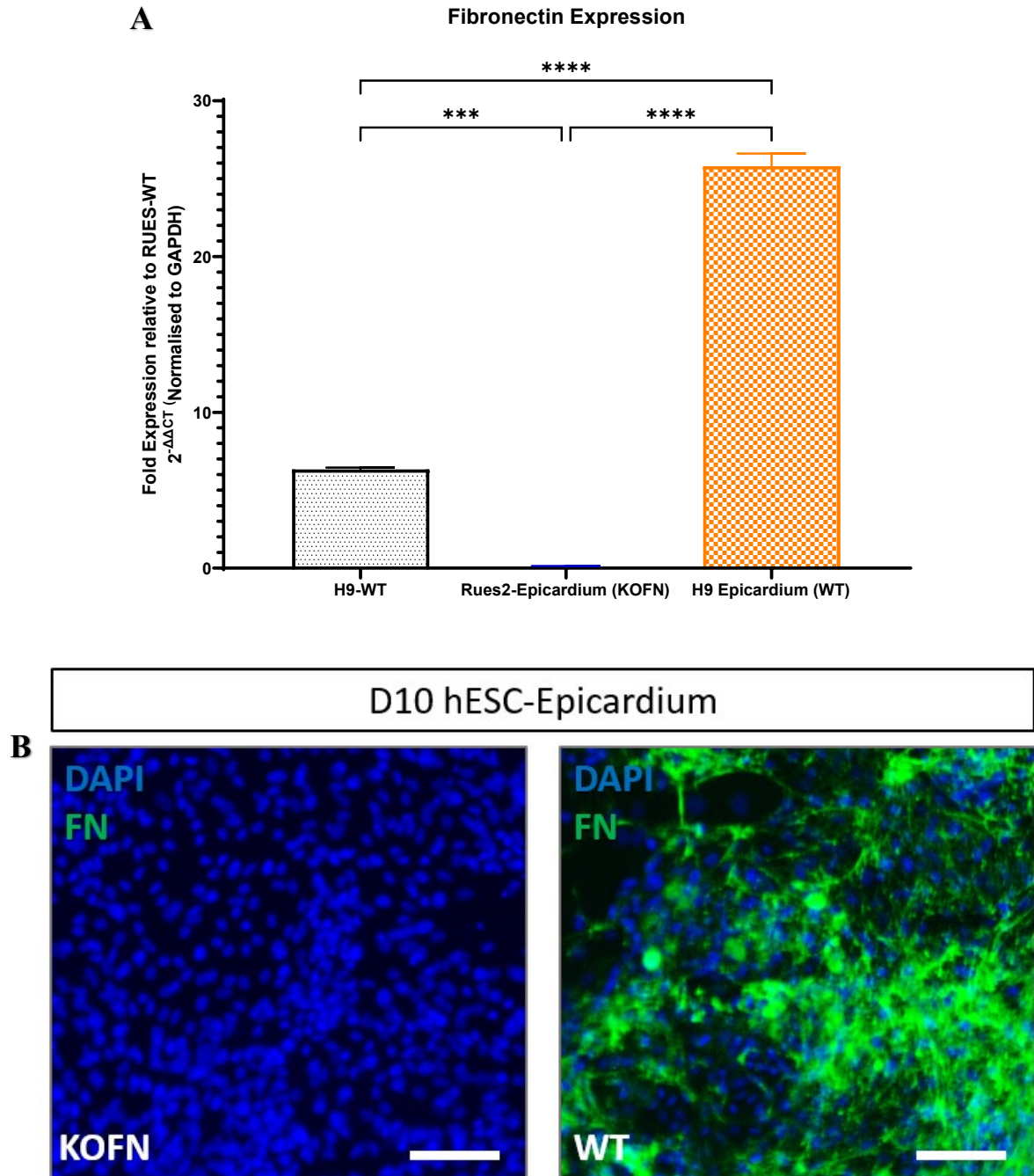


Figure 59: CRISPR-Cas9 KOFN epicardium demonstrates loss of *FN1* expression

A Crispr-Cas9-mediated KOFN epicardium had significantly reduced *FN1* expression at the RNA level compared to both wild-type H9 hESC cells and H9-derived epicardium. ****

$p < 0.0001$, *** $p < 0.0005$. Mean values; error bars represent s.e.m. N=3 biological replicates.

B Representative immunofluorescence image showing that Crispr-Cas9 KOFN epicardium, grown as a monolayer, did not express FN (green) compared to its wild-type counterpart.

Scale bar 50 μm .

4:3:1:2 Crispr-Cas9-mediated KOFN epicardium decreased 3D-EHTs' contractile function

The effects of complete loss of epicardial-FN, with *FN1* deleted from the hESC stage, was investigated. There were three groups of 3D-EHTs i) CM Only ii) CM+Epi, and iii) CM+KOFN Epi. All cells were derived from hESC, as discussed earlier. Both wild-type (WT) epicardium and KOFN-epicardium were derived from hESC, and directly differentiated to the same maturity level: D10 after Wnt, Bmp4 and Retinoic Acid induction (Iyer et al. 2015) All cells were then harvested to generate 3D-EHTs for subsequent functional analyses, i.e., force production and Ca²⁺-handling, alongside analyses of key CM maturation markers at the sarcomeric protein and RNA level.

Similar to pUR4 inhibition of epicardial-FN, the loss of epicardial-FN by genetic deletion, also reduced the active force production and active force-length relationship in 3D-EHTs. Two weeks after 3D-EHT culture, the loss-of-FN function with KOFN-Epi significantly decreased active force production, $p=0.0322$, akin to 3D-EHTs with hESC-CMs alone. Only the CM+Epi active force slope was significantly higher than zero; $p=0.0044$, **Figure 60A**, thereby demonstrating the classical Frank-Starling mechanism and indicating CM maturation. CM+EPI had the highest slope of active force compared to other groups, **Figure 60B**, thereby reliably reproducing earlier reported results by the Sinha Lab (Bargehr et al. 2019). Loss of epicardial-FN abrogated the benefits conferred by hESC-epicardium onto hESC-CMs within the 3D-EHTs. However, 3D-EHT passive force production was not affected by the loss of epicardial-FN, **Figure 61**. Collectively, these results further confirmed a key role of epicardial-FN in mediating the epicardial-augmentation of hESC-CM contractile function and maturation.

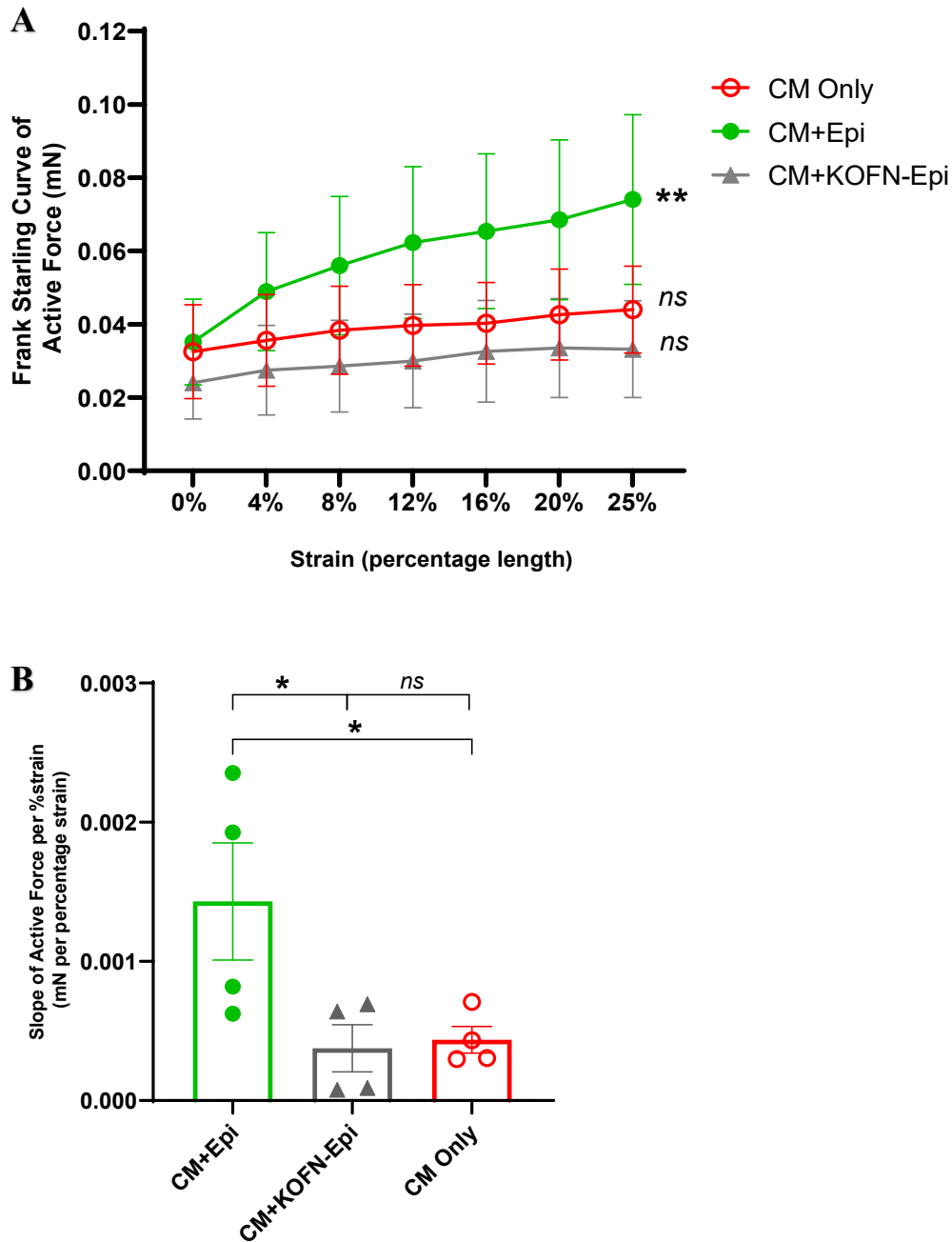


Figure 60: CRISPR-Cas9- mediated KOFN hESC-epicardium decreased active force production by 3D-EHTs

A Frank-Starling curves of active force production by 3D-EHTs containing CM only, CM+EPI and CM+KOFN-EPI. Only the slope for CM+Epi is significantly higher than zero; $p=0.0044$. **B** CM+EPI had the highest slope of active force compared to other groups. Loss-of-FN function with KOFN-Epi significantly decreased active force production; $p=0.0322$. Similarly, CM Only had significantly less active force, $p=0.044$. $N=4$ biological replicates, all generated and measured separately. Each biological replicate consisted of 3 technical triplicates. Mean values; error bars represent s.e.m. $*P<0.05$, $**P<0.005$. Two-sided P values were calculated using a one-way ANOVA with post-hoc correction for multiple comparisons.

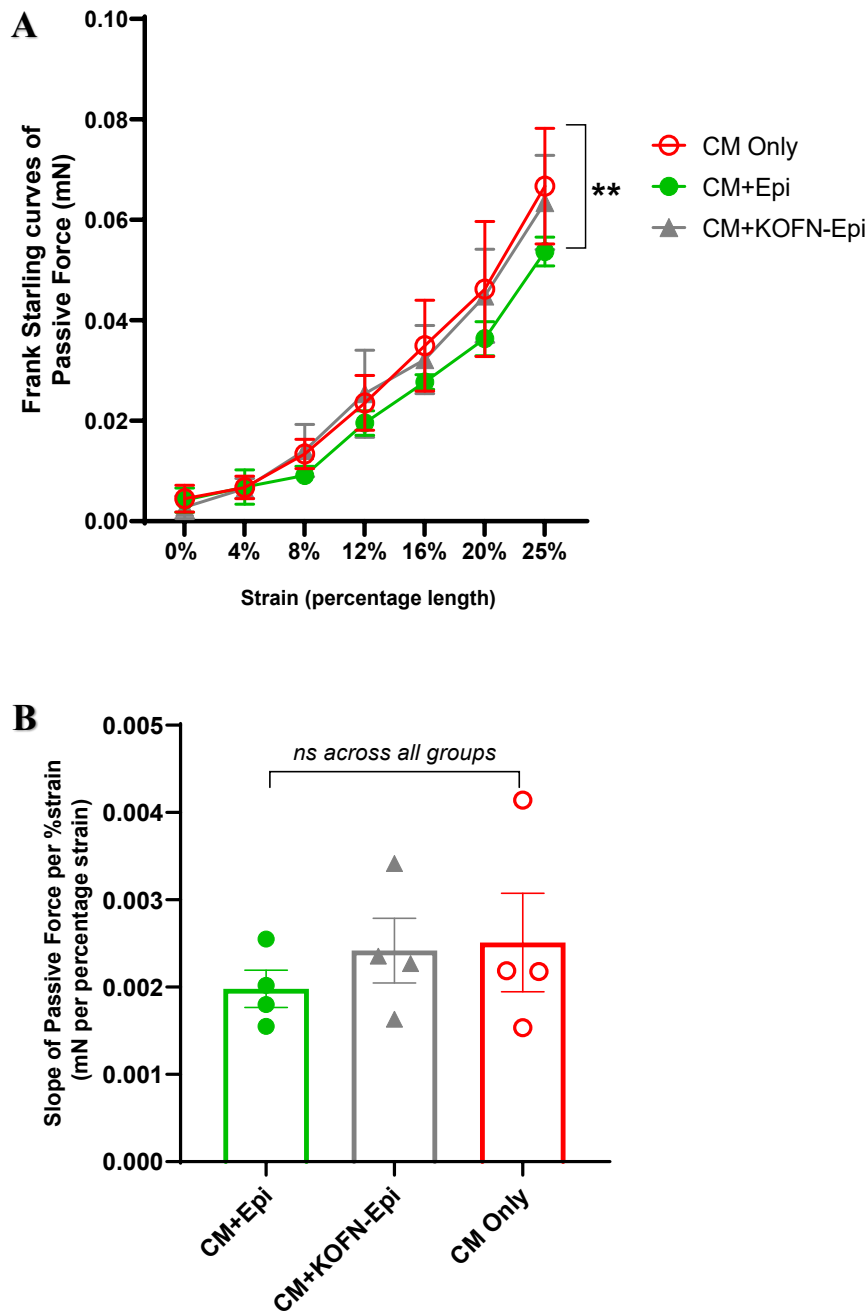


Figure 61: CRISPR-Cas9-mediated KOFN in hESC-epicardium conserved passive force production by 3D-EHTs

A Frank-Starling curves of passive force production of 3D-EHTs containing CM only, CM+EPI and CM+KOFN-EPI. All the slopes are significantly higher than zero; CM only ($p=0.0015$), CM+Epi ($p=0.0089$), CM+KOFN-EPI ($p=0.002$). **B** All groups had similar slopes of passive force production. Each experimental group included N=4 biological replicates, all generated and measured separately. Each biological replicate consisted of three technical triplicates. Mean values; error bars represent s.e.m. $**P<0.005$. Two-sided P values were calculated using a one-way ANOVA with post-hoc correction for multiple comparisons.

Similarly, the loss of FN expression in KOFN-epicardium led to inefficient Ca^{2+} -handling by the 3D-EHTs. Inefficient Ca^{2+} -handling is a defining feature of immature CMs (Guo and Pu 2020). Loss of epicardial-FN in CM+KOFN-EPI significantly reduced Ca^{2+} upstroke velocity, compared to CM+Epi, $p=0.0486$, **Figure 62A**, together with a significantly longer time to peak fluorescence (TTP), $p=0.0201$, **Figure 62B**. CM+EPI had significantly shorter times to 50% fluorescence decay (T50), $p=0.0473$ and to 90% fluorescence decay (T90), $p=0.0152$ when compared to CM only; reliably reproducing earlier published results (Bargehr et al. 2019), **Figure 62 C & D**. 3D-EHTs with Epi+CM and CM Only, respectively, denoted negative and positive controls within our experiments. Again, Ca^{2+} sequestration and SR influx appeared spared from the effects of loss of epicardial-FN expression, as there were no significant differences in T50 or T90 with CM+KOFN-EPI, **Figure 62 C & D**. Loss of epicardial-FN expression reduced the efficiency of Ca^{2+} -handling and, therefore, the excitation-contraction coupling machinery with direct consequences for hESC-CM contractile function.

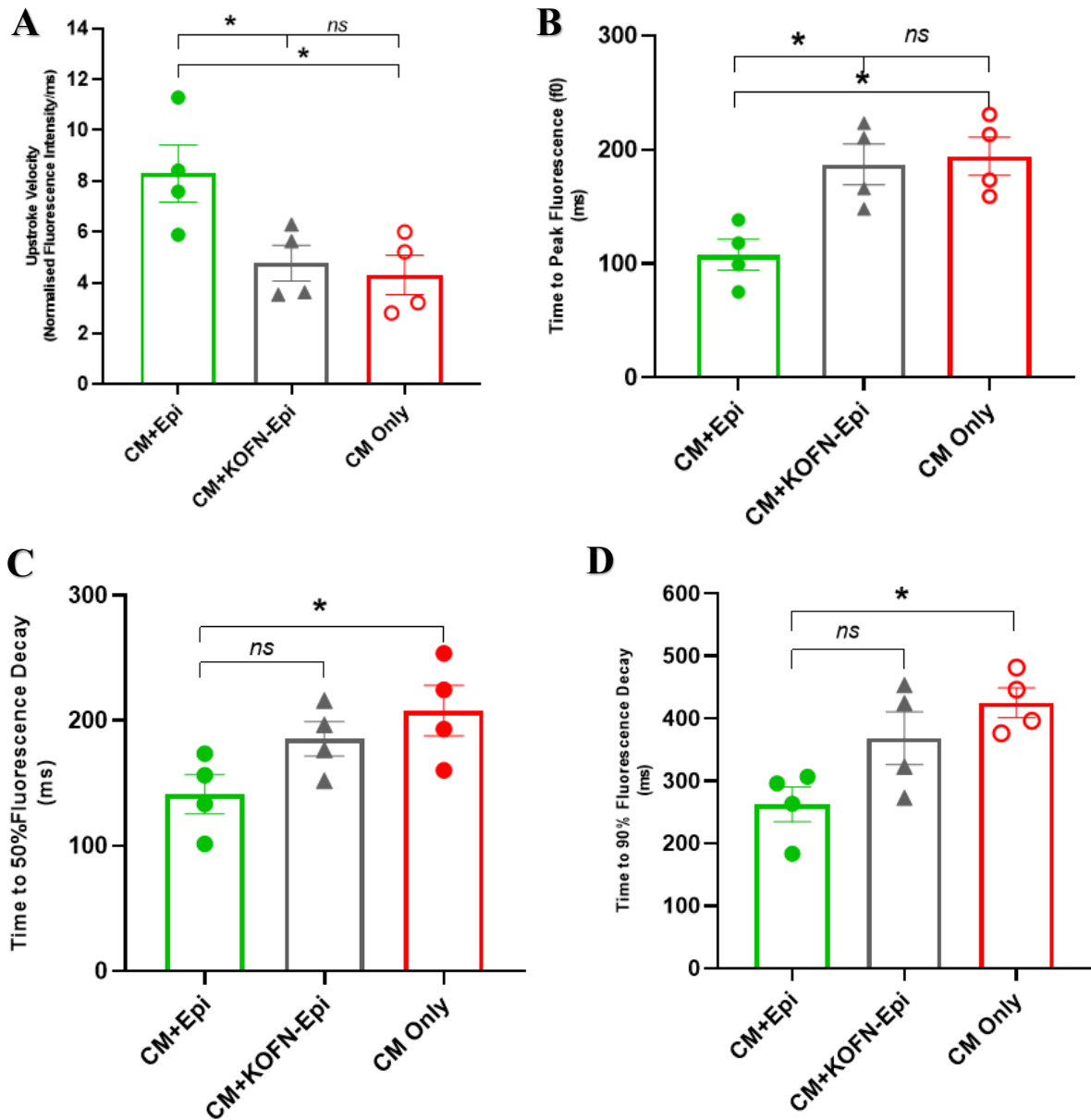


Figure 62: CRISPR-Cas9-mediated KOFN in hESC-epicardium attenuated Ca^{2+} Handling

Calcium kinetics by 3D-EHTs containing CM only, CM+EPI and CM+KOFN-EPI. **A** CM+KOFN-EPI reduced Ca^{2+} upstroke velocity with **B** longer time to peak fluorescence (TTP). CM+EPI had shorter time to **C** 50% fluorescence decay (T50) and **D** to 90% fluorescence decay (T90). N=4 biological replicates with 3 technical triplicates each. Mean values; error bars represent s.e.m. *P<0.05.

The loss of FN expression in KOFN-Epi also resulted in immature sarcomere assembly, thereby explaining the attenuated active force production and Ca²⁺ handling. From the histology, 3D-EHTs with KOFN-Epi showed reduced sarcomeric alignment, **Figure 63A** and decreased clusters of integrin $\alpha 5\beta 1$, **Figure 63B**. Notably, KOFN-Epi had significantly shorter sarcomeric length when compared with Epi+CM, ($1.21\pm 0.07\mu\text{m}$ vs $1.62\pm 0.09\mu\text{m}$, $p=0.0386$), **Figure 63C**. Similarly, KOFN-Epi had significantly less well aligned sarcomeres and decreased FN deposition, **Figure 63D & E**. In 3D-EHTs with KOFN-Epi, the sarcomeric parameters were similar to immature hESC-CMs alone, **Figure 63**. Thus, the loss of FN expression in KOFN-Epi obviated hESC-epicardium augmentation of hESC-CM maturation in 3D-EHTs.

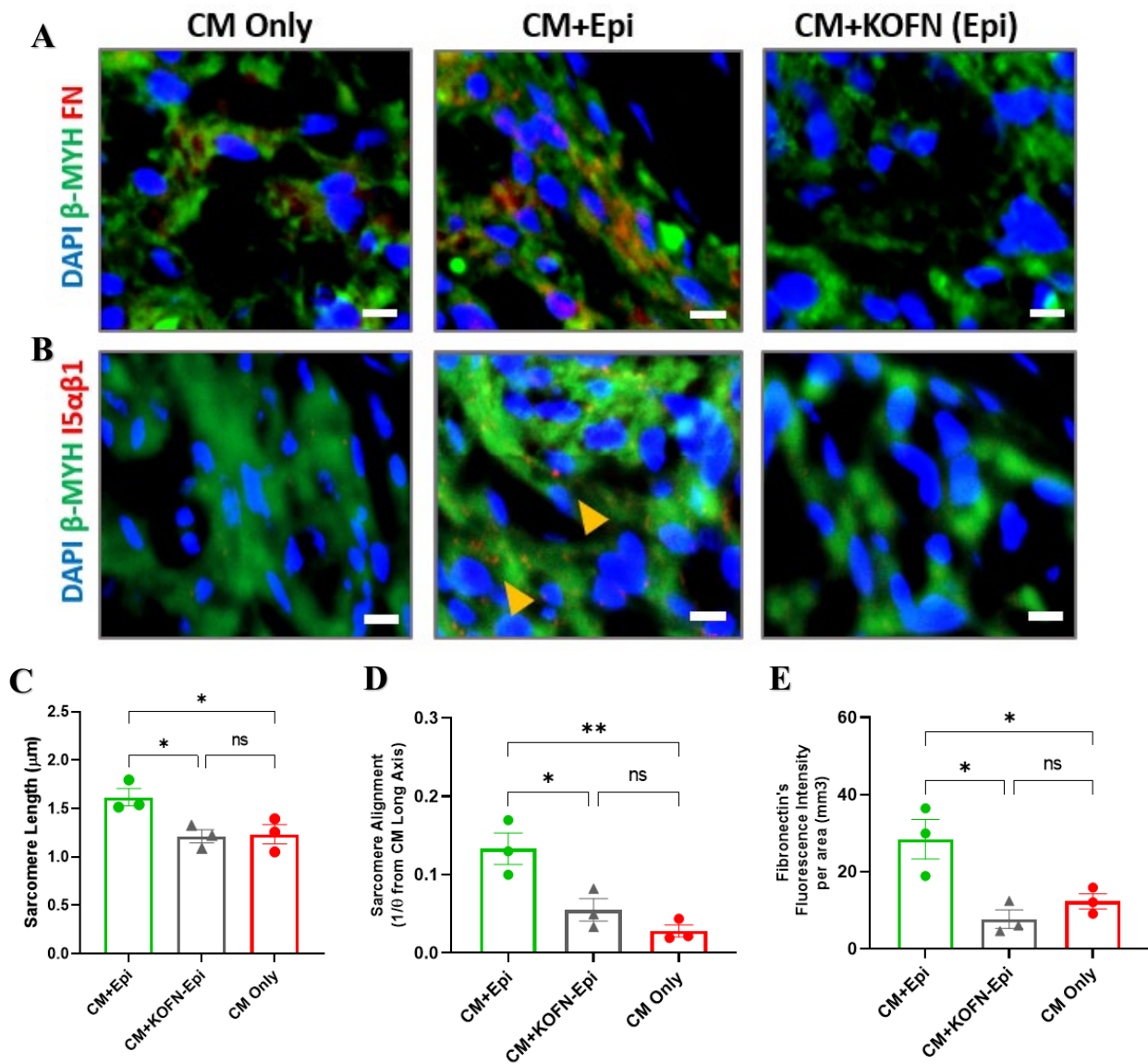


Figure 63: CRISPR-Cas9 mediated KOFN-Epi attenuated CM maturation due to decreased FN deposition and reduced integrin 5αβ1 clustering

A 3D-EHT sections from hESC-CMs (βMHC, green) in CM+EPI, with higher FN (red) deposition and **B** integrin 5αβ1 clustering (red; yellow arrows). Scale bar 5 μm. Epi+CM had the greatest sarcomeric maturation. With the loss of FN in KOFN-Epi, the hESC-CM **C** sarcomere length and **D** sarcomeric alignment were significantly reduced. **E** Correspondingly, there was significantly reduced FN deposition. Each experimental group had N=3 biological replicates, with 3 technical triplicates each. Mean values; error bars represent s.e.m. *P<0.05 **P<0.005, ***P<0.001.

The effect of loss of FN expression by KOFN-Epi in 3D-EHTs on the mRNA expression of cardiac maturity markers, e.g. *MYH 7/6* ratio, *RYR* and *SERCA2*, was examined next. Firstly, the loss of FN expression in KOFN-Epi as visualised at the mRNA level was determined, and found to be not statistically significant, **Figure 64A**. This finding for 3D-EHTs contrasted with the RT-qPCR analyses of FN expression in hESC-epicardium grown as a monolayer, **Figure 59**. As alluded to earlier (*Section 4:2:1:4*), there were inherent technical difficulties in obtaining good quality mRNA from 3D-EHTs. This technical challenge might have contributed towards the magnitude of experimental error and concomitant lack of statistical significance. Corresponding with reduced *FN1* mRNA expression, the 3D-EHTs with KOFN-Epi had decreased *MYH7/6* ratios, denoting less mature hESC-CMs, although again not statistically significant, **Figure 64A & B**. There appeared to be a slight reduction in *RYR* and a minimal rise in *SERCA2*, albeit not statistically significant, **Figure 64C & D**. Thus far, this panel of data, even though inconclusive, suggested that loss of *FN1* expression in hESC-epicardium reduced CM maturation as measured by mRNA levels. Due to technical difficulties with obtaining mRNA samples from 3D-EHTs, this mRNA dataset warranted cautious interpretation.

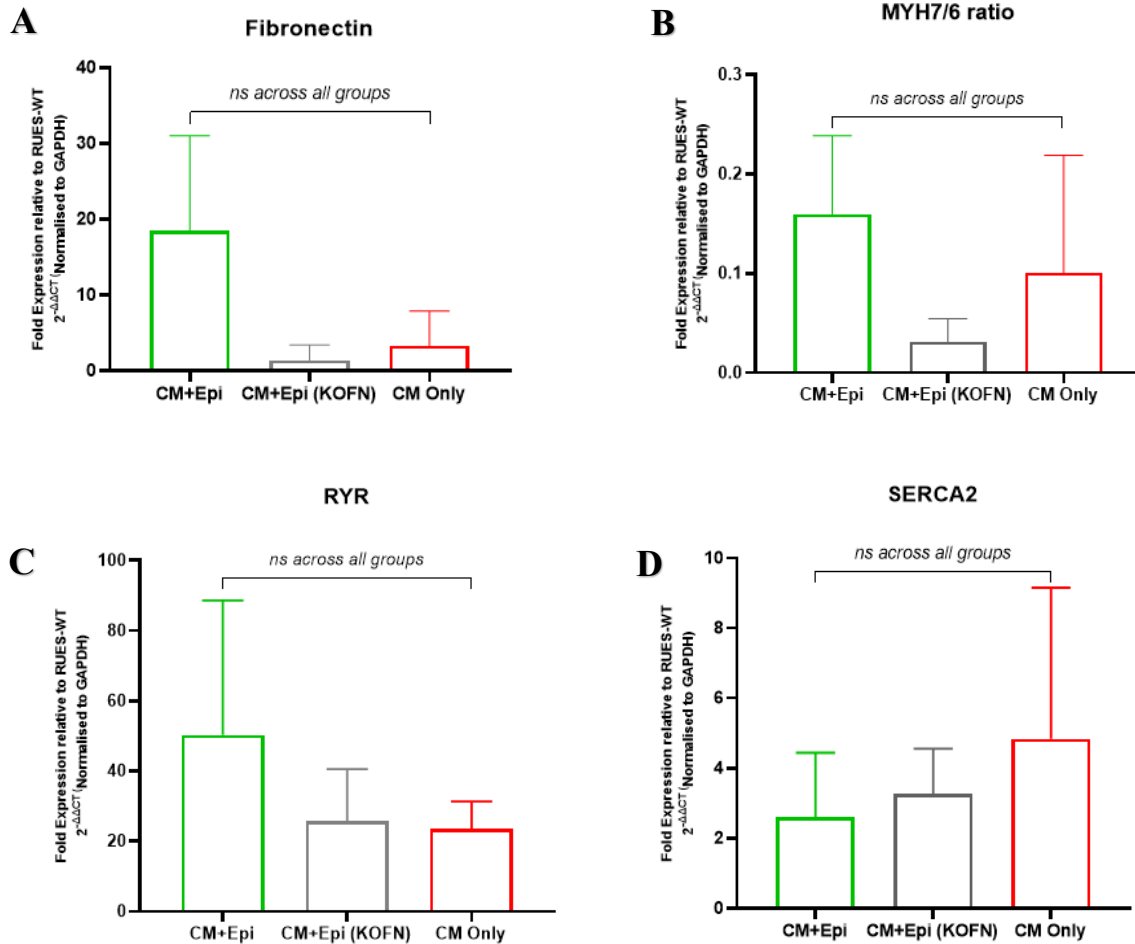


Figure 64: CRISPR-Cas9-mediated KOFN-Epicardium and key markers of cardiac maturity in 3D-EHTs

A There was a trend towards increased *FN1* expression in Epi+CM. Conversely, there was a trend towards decreased *FN1* expression in KOFN-epicardium. With the loss-of-FN function, there were trends towards decreased **B** *MYH7/6* ratio and **C** *RYR* expression, whilst **D** *SERCA2* was slightly increased, albeit not statistically significant. N=3 biological replicates with 3 technical triplicates. Mean values; error bars represent s.e.m.

Overall, KOFN-epicardium demonstrated a pattern of diminished CM function and maturation in 3D-EHTs, similar to observations with pUR4 inhibition of FN in Epi+CM 3D-EHTs. Loss of FN function in KOFN-epicardium visibly attenuated the active force-length relationship and Ca^{2+} -handling in 3D-EHTs, together with decreased CM maturation at the sarcomere assembly level. Growing evidence suggest that epicardial-FN is a key mediator for epicardial-myocardial crosstalk, leading to augmented hESC-CM maturation and function.

4:3:2 Temporal modulation of loss-of-FN function decreased 3D-EHTs' contractile function

Loss of FN function had consistently decreased 3D-EHT contractile function, as shown by both peptide inhibition of FN and genetic deletion of *FN1* expression. KOFN-epicardium required the addition of human recombinant FN at the lateral plate mesoderm stage to ensure progression to epicardial identity. This observation hinted at a specific FN role during epicardial specification and contrasted with the sparse literature pertaining to epicardial-FN interaction. Our observations of this KOFN-epicardium behaviour hinted that it exhibited an aberrant hESC-epicardial identity, despite the representative epicardial markers, **Figure 58**. To negate the potential confounding factors, I constructed a genetically modified cell line which enabled temporal modulation of genetically induced loss of *FN1* expression.

4:3:2:1 Generation of tetracycline-induced FN knockdown in hESC-derived epicardium

Cognizant that fibronectin has a wide-ranging role during embryonic development (Schwarzbauer and DeSimone, 2011) and our own experiences (*Section 4:3:1:1*), I interrogated the loss of FN function after hESC-epicardium achieved maturity at D10 post-directed differentiation (Iyer et al. 2015; Bargehr et al. 2019). For this, a stably integrated, tetracycline-inducible short-hairpin guided knockdown of the expression of a gene of interest (sOPTiKD) was used, (Bertero et al. 2015), **Figure 65**. Crucially, this elegant system enabled temporal control of *FN1* expression, **Figure 66A**. The hESC-sOPTiKDFN cell line was confirmed to be pluripotent as judged by expression of *Oct4*, *Sox2* and *Nanog* at the RNA level, **Figure 66B**. The hESC-sOPTiKDFN cell line was successfully differentiated into epicardium, which was confirmed via RNA expression of the key epicardial markers *WT1*, *TCF21* and *BNC1* **Figure 66C**. sOPTiKDFN-epicardium also displayed the classical ‘cobblestone’ morphology in brightfield microscopy and expression of the WT1 transcription factor at protein level as detected by immunocytochemistry, **Figure 67**.

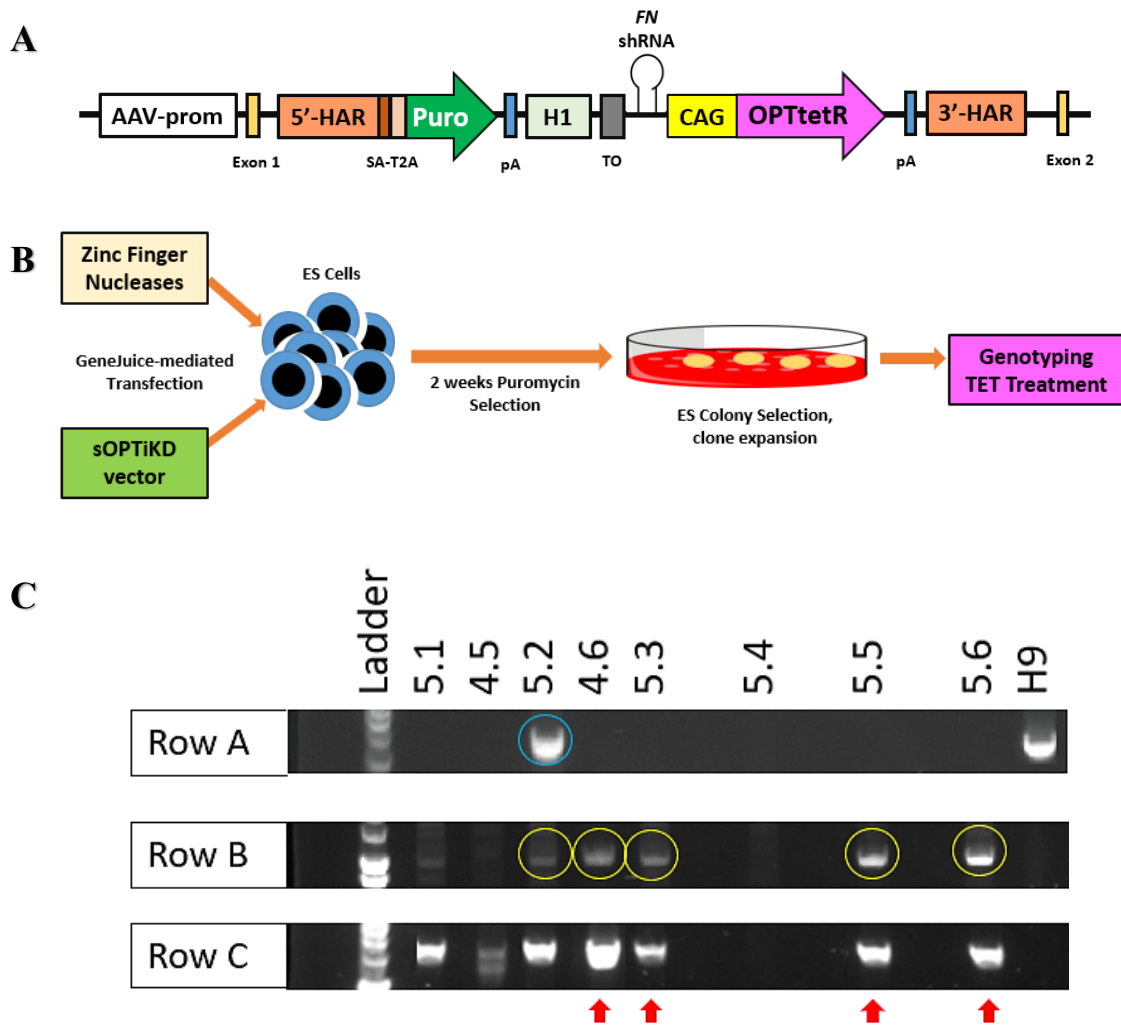


Figure 65: sOPTiKDFN clones derived from transfection with the sOPTiKD vector

A Schematic showing the transgenic allele that was generated via sOPTiKD transfection of hESCs. AAV-prom, AAVS1 locus promoter; 5'-HAR/3'-HAR, 5' upstream and 3' downstream homology arms, respectively; SA, splice acceptor; T2A, self-cleaving T2A peptide; Puro, puromycin resistance; H1, H1 human RNA polymerase III promoters; TO, tet operon; pA, polyadenylation signal; CAG, CAG promoter; OPTtetR, optimised TET repressor. **B** GeneJuice-mediated transfection strategy for sOPTiKD vector insertion within AAVS1 locus of ES cells, with subsequent colony selection and expansion for genotyping. **C** Genotyping gels of sOPTiKD clones. Row A is a representative gel for detection of homozygous targeted clones; WT H9 gave a band at 1692 bp, whereas no band indicated homozygous transgene integration. All clones except '5.2' (labelled 'het', blue circle) appeared to be homozygous-targeted. Row B was a representative gel for 5' vector integration, indicated by a gel band at 1103bp (yellow circle). Row C was a representative gel for 3' vector integration, as indicated by gel band at 1447bp. In this example, clones 4.6, 5.3, 5.5, and 5.6 were homozygous-targeted with vector integration at 5' and 3' (red arrow).

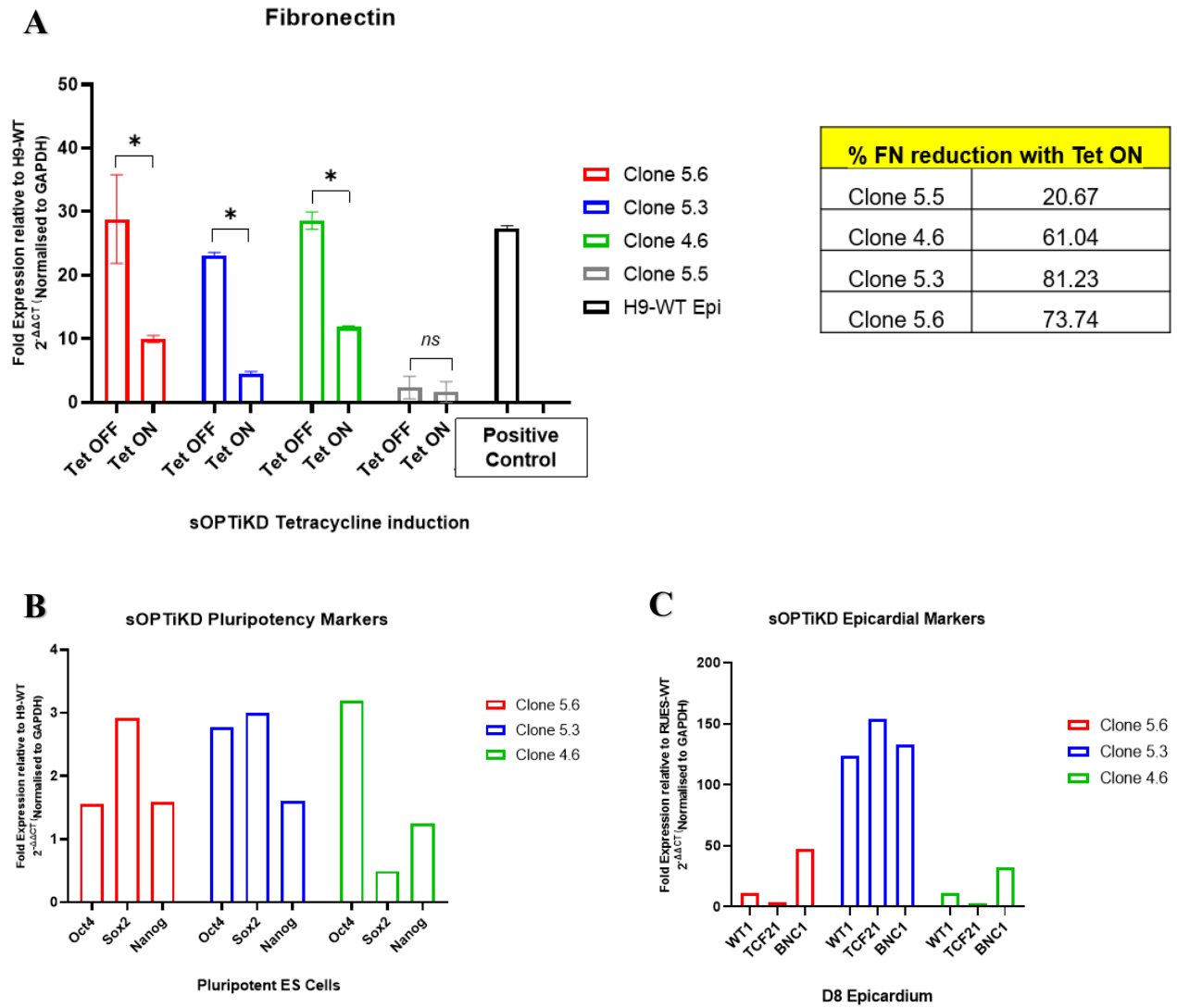


Figure 66: sOPTiKD Clone 5.3 selected for Epicardial Differentiations

A sOPTiKD-FN clones had different *FN1* expression upon tetracycline-knockdown. Clone 5.3 has the greatest *FN1* reduction. Clone 5.5 had no *FN1* reduction. N=2 biological replicates. * p<0.05. **B** All clones showed similar levels of pluripotency markers **C** Clone 5.3 expressed higher levels of the epicardial markers *WT1*, *TCF21* and *BNC1*. N=1 biological replicate. **D** Clone 5.3 differentiated to D8 hPSC-epicardium with 24 hours of tetracycline. Scale bar 20 μ m.

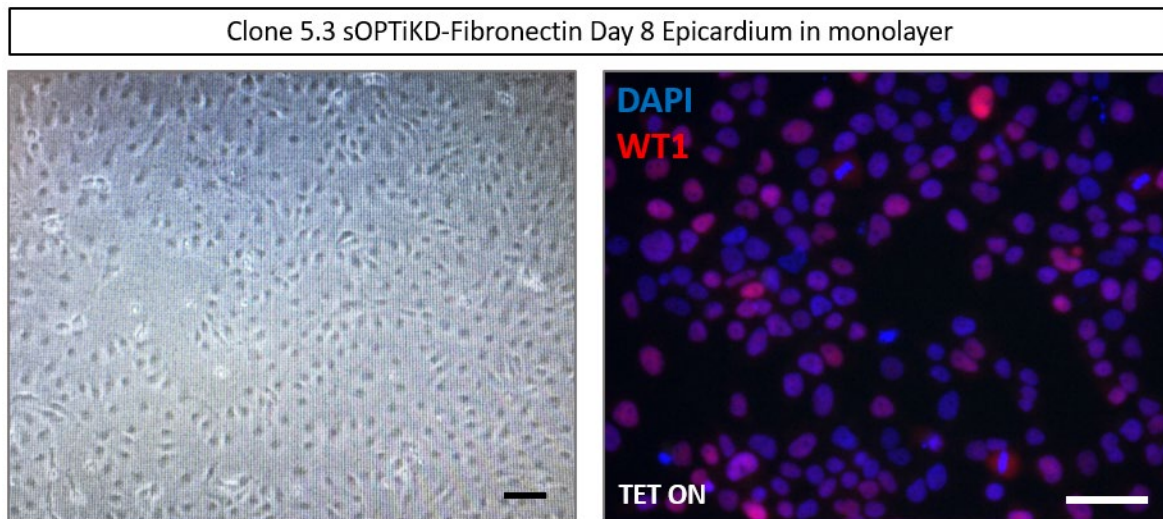


Figure 67: sOPTiKD Clone 5.3 differentiated to epicardium

Clone 5.3 differentiated to D8 hPSC-epicardium with 24 hours of tetracycline, showing cobblestone morphology and expression of WT1 (red). Scale bar 20 μ m.

4:3:2:2 Tetracycline-induced knockdown of FN in hESC-derived epicardium attenuated 3D-EHTs' contractile function

Following the successful generation of the sOPTiKD-FN cell line, I examined whether the loss of epicardial-FN at D10 epicardium affected the 3D-EHT contractile function. There were three groups of 3D-EHTs with i) CM only, ii) CM+sOPTiKD-FN Epi (Tet OFF) and iii) CM+sOPTiKD-FN Epi (Tet ON). For CM+sOPTiKD-FN Epi (Tet ON), tetracycline induction was started at D8 post-directed differentiation of sOPTiKDFN epicardium, prior to incorporation into 3D-EHTs three days later. As 3D-EHTs, CM+sOPTiKD-FN Epi (Tet ON) received tetracycline daily during the two weeks of culture. Addition of tetracycline induced the knockdown of *FN1* expression, **Figure 66A**. All experimental groups underwent functional analyses of Frank-Starling active force generation and Ca^{2+} -handling, together with analyses of the key CM maturation marker, sarcomeric assembly.

Tetracycline-induced loss of epicardial-FN in 3D-EHTs significantly decreased active force production compared to without tetracycline; $p=0.0382$, **Figure 68A**. Only the CM+sOPTiKD-FN Epi (Tet OFF) active force slope was significantly higher than zero ($p=0.0048$), **Figure 68A**, thereby exhibiting the Frank-Starling mechanism and CM maturation. CM+sOPTiKD-FN Epi (Tet OFF) also had the highest slope of active force compared to other groups, **Figure 68B**. Reassuringly, our genetically modified hESC-epicardium conveyed similar benefits within 3D-EHTs; both proving the robustness of our protocol (Iyer et al. 2015) and enabling its designation as the negative experimental control for our loss-of-FN function studies. Reiterating earlier observations, loss of FN did not affect passive force generation, **Figure 69**. These results confirmed that loss of epicardial-FN abrogated the benefits conferred by hESC-epicardium onto hESC-CM maturation and contractile function.

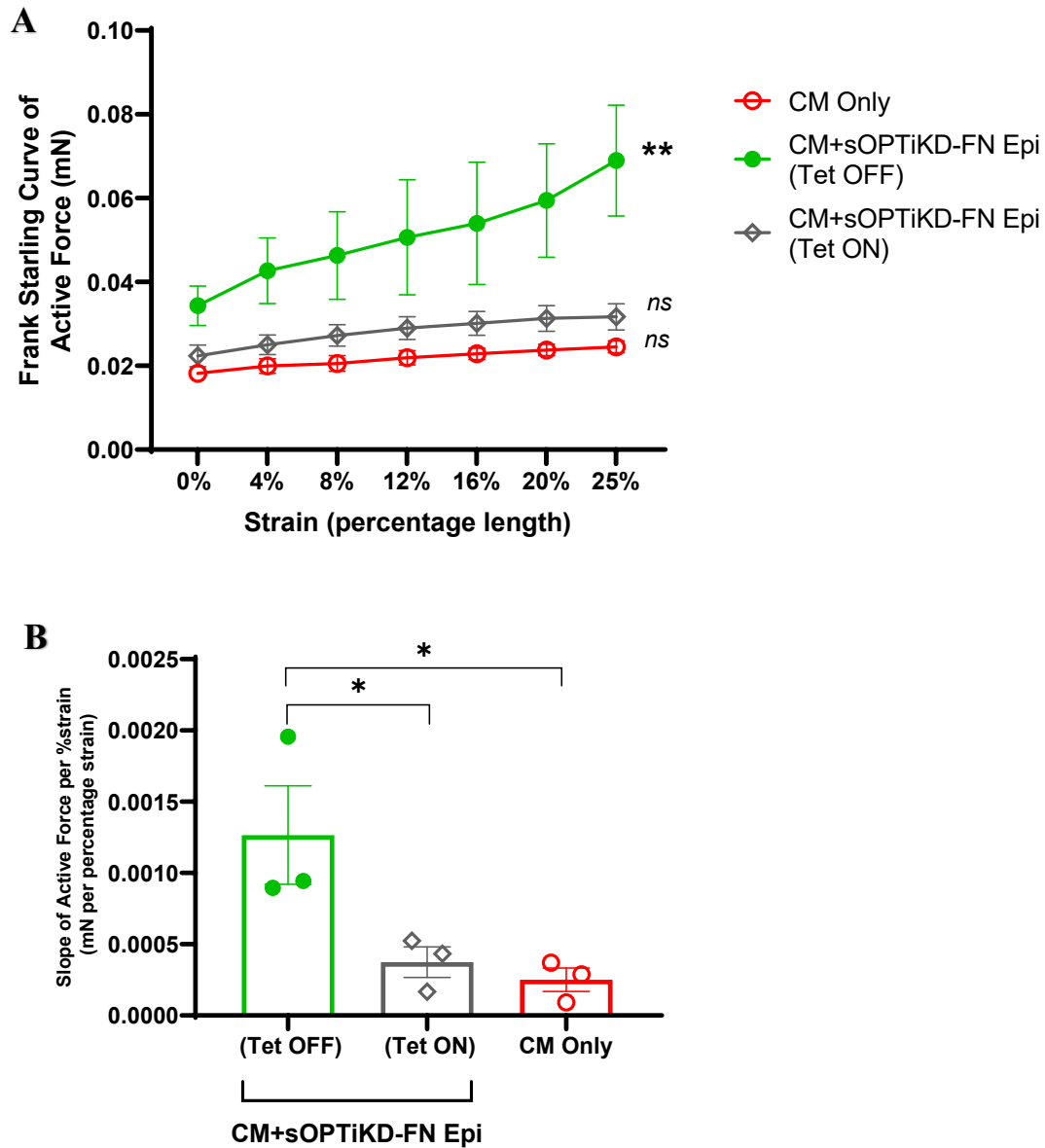


Figure 68: Tetracycline-induced loss-of-FN function decreased active force in 3D-EHTs

Epicardium in all groups was differentiated from the sOPTiKD-FN cell line. D10 sOPTiKD-FN epicardium received tetracycline to induce loss of FN. **A** Frank-Starling curves of active force by 3D-EHTs with CM only, CM+sOPTiKD-FN Epi (Tet OFF) and CM+sOPTiKD-FN Epi (Tet ON). Only the slope of (Tet OFF) was significantly higher than zero. **B** (Tet OFF) had the highest slope of active force compared to other groups. (Tet ON) had significantly decreased active force production compared to (Tet OFF). N=3 biological replicates with three technical triplicates each. Mean values; error bars represent s.e.m. * $P < 0.05$, ** $P < 0.005$.

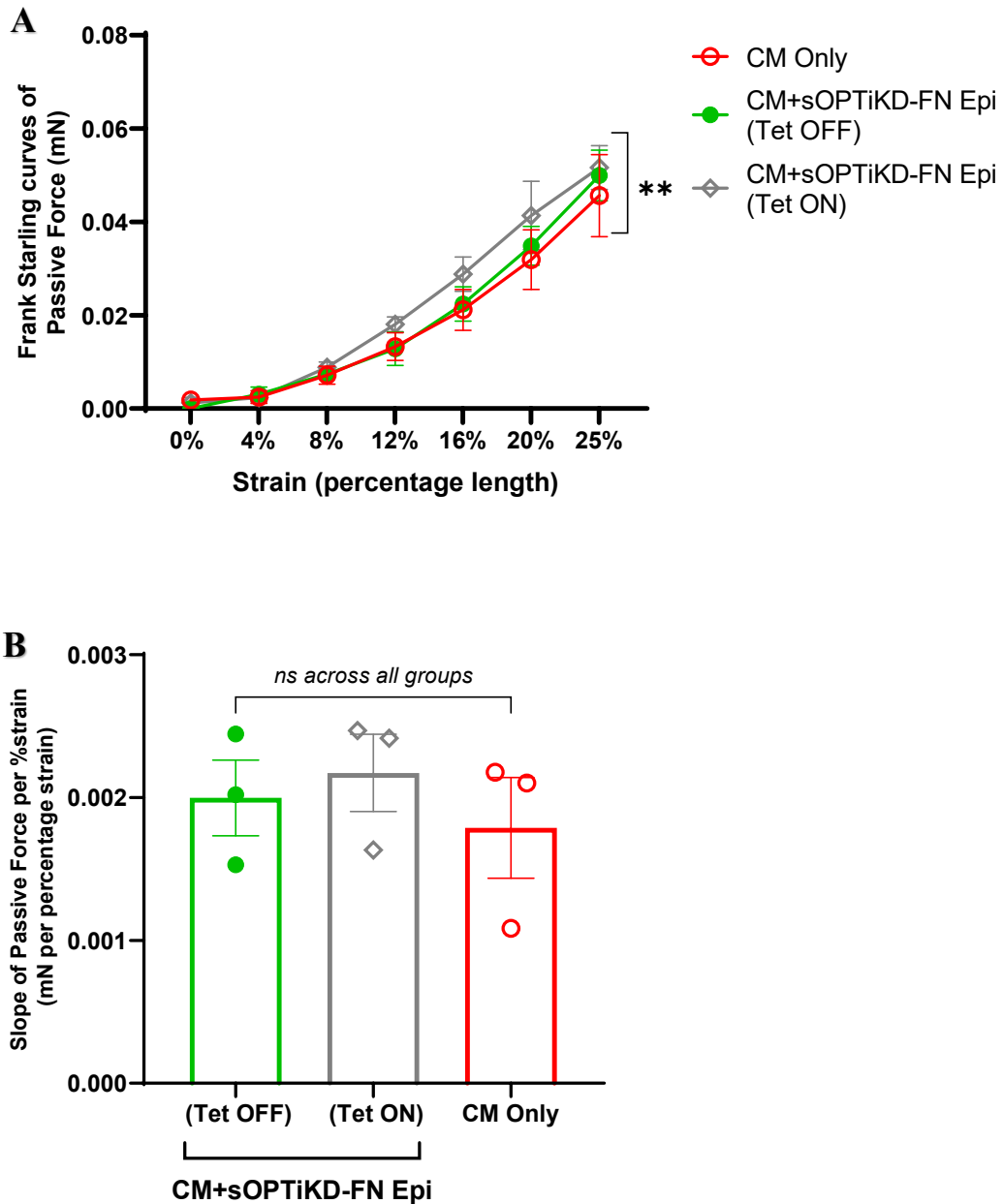


Figure 69: Tetracycline-induced loss-of-FN function in sOPTiKD- Epi conserved passive force in 3D-EHTs

A Frank-Starling curves of passive force production of 3D-EHTs containing CM only, CM+sOPTiKD-FN Epi (Tet OFF) and CM+sOPTiKD-FN Epi (Tet ON). All slopes were significantly higher than zero. **B** There was no difference in the slope of passive force across all groups. N=3 biological replicates with three technical triplicates each. Mean values; error bars represent s.e.m. * $P < 0.05$, ** $P < 0.005$.

Similarly, tetracycline-induced loss of epicardial-FN decreased the efficiency of Ca^{2+} -handling, causing reversion to the immature Ca^{2+} -handling profile of hESC-CMs alone. CM+sOPTiKD-FN Epi (Tet OFF) had significantly higher Ca^{2+} upstroke velocity than CM Only; $p=0.0253$, whilst tetracycline-induced loss of FN reduced Ca^{2+} upstroke velocity with a trend towards statistical significance, $p=0.0820$, **Figure 70A**. Loss of FN with (Tet ON) and CM only 3D-EHTs nearly doubled the time to peak fluorescence (TTP) for CM+sOPTiKD-FN Epi (Tet OFF) $p=0.0227$ & $p=0.0408$ respectively, **Figure 70B**. Compared to CM+sOPTiKD-FN Epi (Tet OFF), time to 50% Fluorescence decay (T50) was significantly shortened for CM only, $p=0.0377$; whilst loss of FN with (Tet ON) showed a trend towards significance, $p=0.0613$, **Figure 70C**. Time to 90% fluorescence decay (T90) was not significantly different between groups, **Figure 70D**. For the 3D-EHTs, the attenuation of Ca^{2+} handling was less pronounced with siKDFN-derived epicardium, compared to the KOFN-derived epicardium. Nonetheless, any reduction in epicardial-FN appeared to eliminate hESC-epicardium augmentation of hESC-CM maturation in 3D-EHTs.

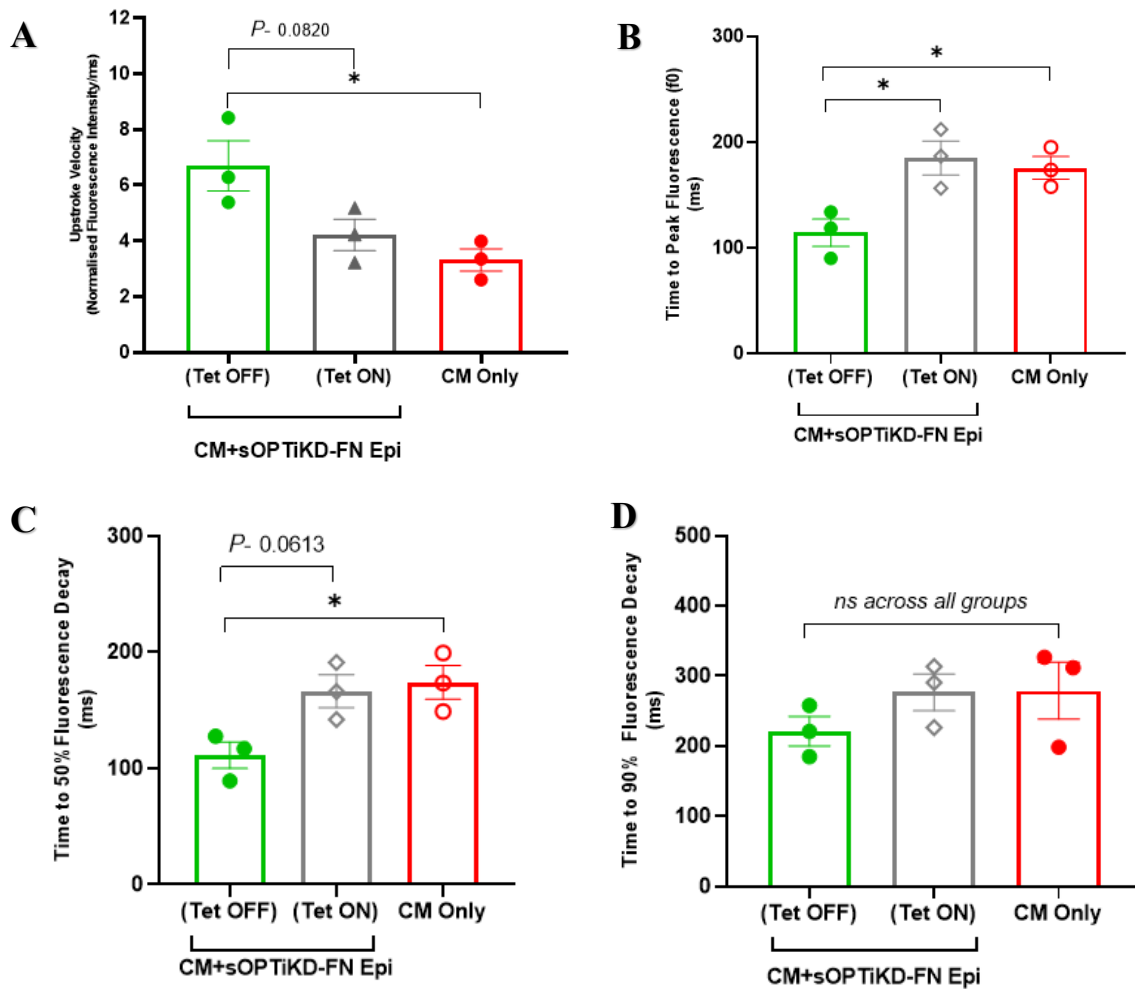


Figure 70: Tetracycline-induced loss-of-FN function decreased the efficiency of Ca^{2+} handling by 3D-EHTs

A Quantification of calcium kinetics in the 3 experimental groups, composed of i) CM only, ii) CM+Epi (Tet OFF) and iii) CM+Epi (Tet ON). CM+Epi (Tet OFF) had significantly higher Ca^{2+} upstroke velocity than CM Only; $p=0.0253$, whilst loss of FN (Tet ON) showed a trend towards significant reduction. **B** Loss of FN (Tet ON) and CM Only had a significantly longer time to peak fluorescence (TTP), $p=0.0227$ & $p=0.0408$ respectively. **C** Time to 50% Fluorescence decay (T50) was significantly shortened for CM only, $p=0.0377$; whilst loss of FN (Tet ON) showed a trend towards a significant increase. **E** Time to 90% fluorescence decay (T90) was not significantly different between groups. Mean values; error bars represent s.e.m. * $P<0.05$. $N=3$ biological replicates with 3 technical replicates each.

Giving credence to earlier observations of reduced CM maturity with epicardial-FN loss, CM+sOPTiKD-FN Epi (Tet ON) exhibited decreased sarcomeric assembly parameters. 3D-EHTs with CM+sOPTiKD-FN Epi (Tet ON) showed reduced sarcomeric alignment, **Figure 71A**. CM+sOPTiKD-FN Epi (Tet ON) had significantly shorter sarcomeric length ($1.19\pm 0.12\mu\text{m}$ vs $1.74\pm 0.17\mu\text{m}$, $p=0.048$), when compared with Epi+CM, **Figure 71B**. CM+sOPTiKD-FN Epi (Tet ON) and CM Only had similar sarcomeric parameters, corresponding to a similar reduction in fibronectin deposition, **Figure 71B-D**. From the observations and quantifications of sarcomeric parameters, loss of epicardial-FN appears to remove hESC-epicardium augmentation of hESC-cardiomyocyte maturation in 3D-EHTs.

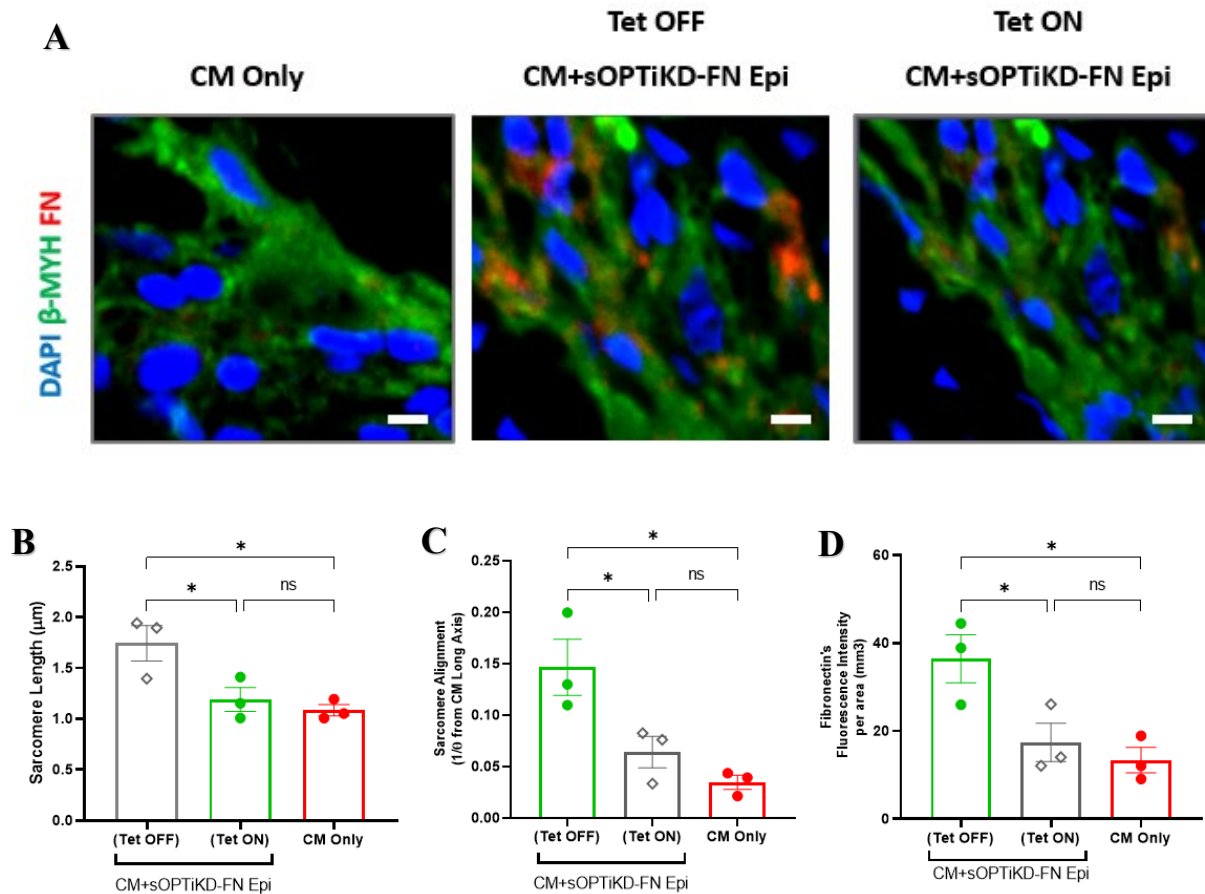


Figure 71: Tetracycline-induced loss-of-FN function in sOPTiKD-Epi decreased sarcomeric maturation in 3D-EHTs

A 3D-EHTs sections of i) CM only, ii) CM+Epi (Tet OFF) and iii) CM+Epi (Tet ON). CM+EPI (Tet ON) had less organised hESC-CMs (β MHC, green) with decreased FN (red) deposition. With the loss of FN in CM+Epi (Tet OFF), the hESC-CM **B** sarcomere length and **C** sarcomeric alignment were significantly reduced. **D** Correspondingly, there was significantly reduced FN deposition. Each experimental group had N=3 biological replicates, with 3 technical triplicates each. Mean values; error bars represent s.e.m. *P<0.05.

Due to the technical challenges in obtaining mRNA from 3D-EHTs and the unconvincing results obtained using this RNA, RT-qPCR was not used further for analysing 3D-EHTs. The effects of loss of epicardial-FN function on CM maturity were demonstrated clearly at the sarcomeric protein level with immunostaining. If further interrogation of upstream genetic regulation of epicardial-FN, becomes desirable,

RNA-sequencing of the 3D-EHTs may represent a more reliable, and higher-throughput technique.

Overall, the decline of 3D-EHT contractile function was consistent across two different models of genetically induced loss of epicardial-FN function. This unique pattern of cardiomyocyte functional loss included decreased active force-length relationship, inefficient Ca^{2+} -handling and immature sarcomeric assembly. Furthermore, this decline in CM maturation and contractile force resembled the functional loss with pUR4 inhibition of FN in 3D-EHTs, thereby showing consistent results across all the different FN functional loss or blockade methods used. Thus far, the evidence suggests that epicardial-FN underpins epicardial-myocardial crosstalk, leading to epicardial augmentation of hESC-cardiomyocyte maturation.

4:4 Recombinant Human FN does not completely rescue the loss-of-FN function in 3D-EHTs

Given the compelling results from our loss-of-FN function studies, the possibility that recombinant human fibronectin (huFN) could recover or replace the genetically induced loss of epicardial-FN in 3D-EHTs was investigated. As alluded to above, cellular FN is highly heterogenous, with up to 20 splice variants in humans (Wickstrom et al. 2011). The wide variety of FN isoforms might pose a challenge, particularly if there is a specific epicardial-FN isoform for communicating with hESC-CMs. However, KOFN hESC cells were successfully differentiated into KOFN-epicardium when supplemented with commercially sourced recombinant human FN. This observation suggested that it might be feasible to perform a rescue of FN function with the 3D-EHTs studies. Thus, I proceeded into a set of rescue-of-FN function studies with recombinant human FN.

4:4:1 Recombinant human FN partially salvaged the 3D-EHTs' contractile function

For the rescue-of-FN function experiments, there were four groups of 3D-EHTs containing i) CM only, ii) CM+sOPTiKD-FN Epi (Tet OFF), iii) CM+sOPTiKD-FN Epi (Tet ON), and iv) CM+sOPTiKD-FN Epi (Tet ON) + Rescue. hESC-epicardium in each group was differentiated from the sOPTiKD-FN cell line. As above, D10 sOPTiKD-FN epicardium received tetracycline to induce loss of epicardial-FN. Rescue-of-FN 3D-EHTs received both tetracycline induction of epicardial-FN loss and recombinant human FN, daily. Recombinant human fibronectin was added daily to the medium during the two-week culture of 3D-EHTs. To ascertain whether the loss of epicardial-FN function in 3D-EHTs could be rescued by recombinant human FN, all 3D-EHTs underwent analyses of Frank-Starling active force generation, Ca²⁺-handling and of the key CM maturation markers at the sarcomeric assembly level.

Recombinant human FN appeared to partially rescue the loss of epicardial-FN function in 3D-EHTs, in terms of active force generation. For the Frank-Starling active force generation, the slopes for all groups were significantly higher than zero, **Figure 72**. 3D-EHTs containing CM+sOPTiKD-FN Epi (Tet OFF) had the highest active force slope, **Figure 72A**, forming a reliable positive control for this experiment. Epicardial-FN loss in 3D-EHTs (Tet ON) had significantly less active force compared to (Tet OFF), $p < 0.0001$, **Figure 72B**. The rescue of epicardial-FN loss group had a higher active force slope compared to (Tet ON), trending towards statistical significance, $p = 0.0527$, **Figure 72B**. Passive force generation was equivocal across all groups, **Figure 73**. The active force generation profiles suggested that loss of epicardial-FN function in 3D-EHTs could be partially salvaged by recombinant human FN.

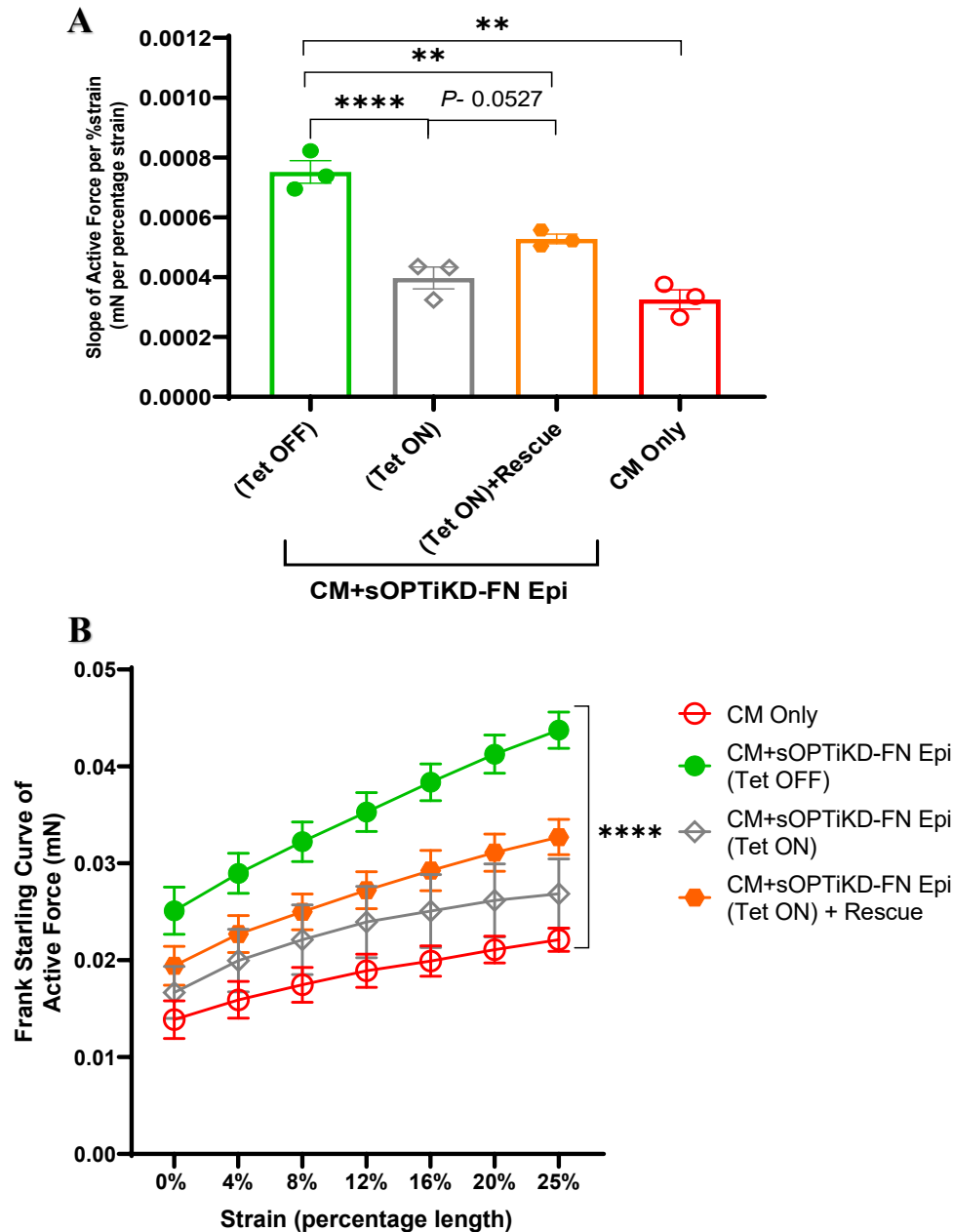


Figure 72: Rescue-of-FN with human recombinant FN partially salvaged active force production by 3D-EHTs

D10 sOPTiKD-FN epicardium received tetracycline to induce FN loss. Rescue-of-FN received both tetracycline induction and recombinant human FN. **A** Active force production by CM only, CM+sOPTiKD-FN Epi (Tet OFF), CM+sOPTiKD-FN Epi (Tet ON) and CM+sOPTiKD-FN Epi (Tet ON) + Rescue-of-FN. All slopes were significantly higher than zero **B** (Tet ON) produced significantly less active force compared to (Tet OFF). Rescue-of-FN had a higher slope of active force than (Tet ON), with a trend towards statistical significance. N=3 biological replicates with 3 technical triplicates each. Mean values; error bars represent s.e.m. * $P < 0.05$, ** $P < 0.005$, *** $P < 0.001$, **** $P < 0.0001$.

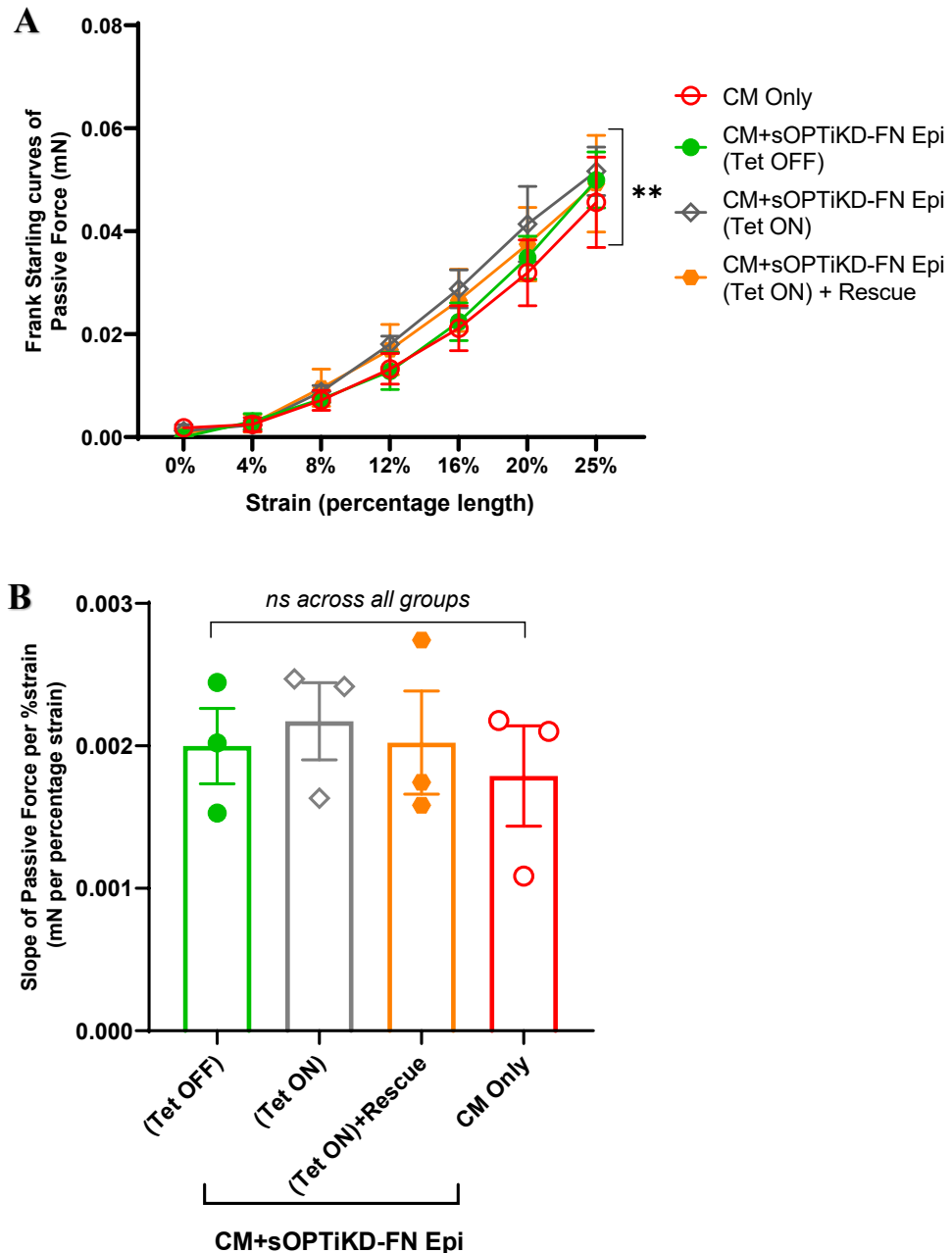


Figure 73: Rescue-of-FN function with human recombinant FN did not affect the passive force generated by 3D-EHTs

A Frank-Starling curves of passive force production of 3D-EHTs containing CM only, CM+sOPTiKD-FN Epi (Tet OFF), CM+sOPTiKD-FN Epi (Tet ON) and CM+sOPTiKD-FN Epi (Tet ON) + Rescue-of-FN. All slopes were significantly higher than zero. **B** There was no difference in the slope of passive force across all groups. N=3 biological replicates, all generated and measured separately. Each biological replicate consisted of three technical triplicates. Mean values; error bars represent s.e.m. * $P < 0.05$, ** $P < 0.005$. Two-sided P values were calculated using a one-way ANOVA with post-hoc correction for multiple comparisons.

Unfortunately, the addition of human recombinant FN did not recover the inefficient Ca^{2+} handling due to the loss of epicardial-FN. 3D-EHT calcium kinetics were assessed as a surrogate marker for hESC-CM's excitation-contraction coupling efficiency and maturity. As a positive control, CM+sOPTiKD-FN Epi (Tet OFF) had significantly higher Ca^{2+} upstroke velocity and the shortest time to peak fluorescence (TTP), compared to all groups, **Figure 74A & B**. Notably, rescue of epicardial-FN had a significantly lower Ca^{2+} upstroke velocity compared to (Tet OFF), $p=0.0448$, **Figure 74A**. Rescue of epicardial-FN had a higher TTP compared to (Tet OFF), with a trend towards statistical significance, $p=0.0884$, **Figure 74B**. Moreover, the calcium kinetics demonstrated by the rescue of epicardial-FN group were comparable to (Tet ON). As above, time to 50% fluorescence decay (T50) and time to 90% fluorescence decay (T90) were not significantly different between groups, **Figure 74C & D**. In contrast to the active force data, the analyses of calcium kinetics implied that recombinant human FN failed to completely rescue the loss of epicardial-FN function in 3D-EHTs.

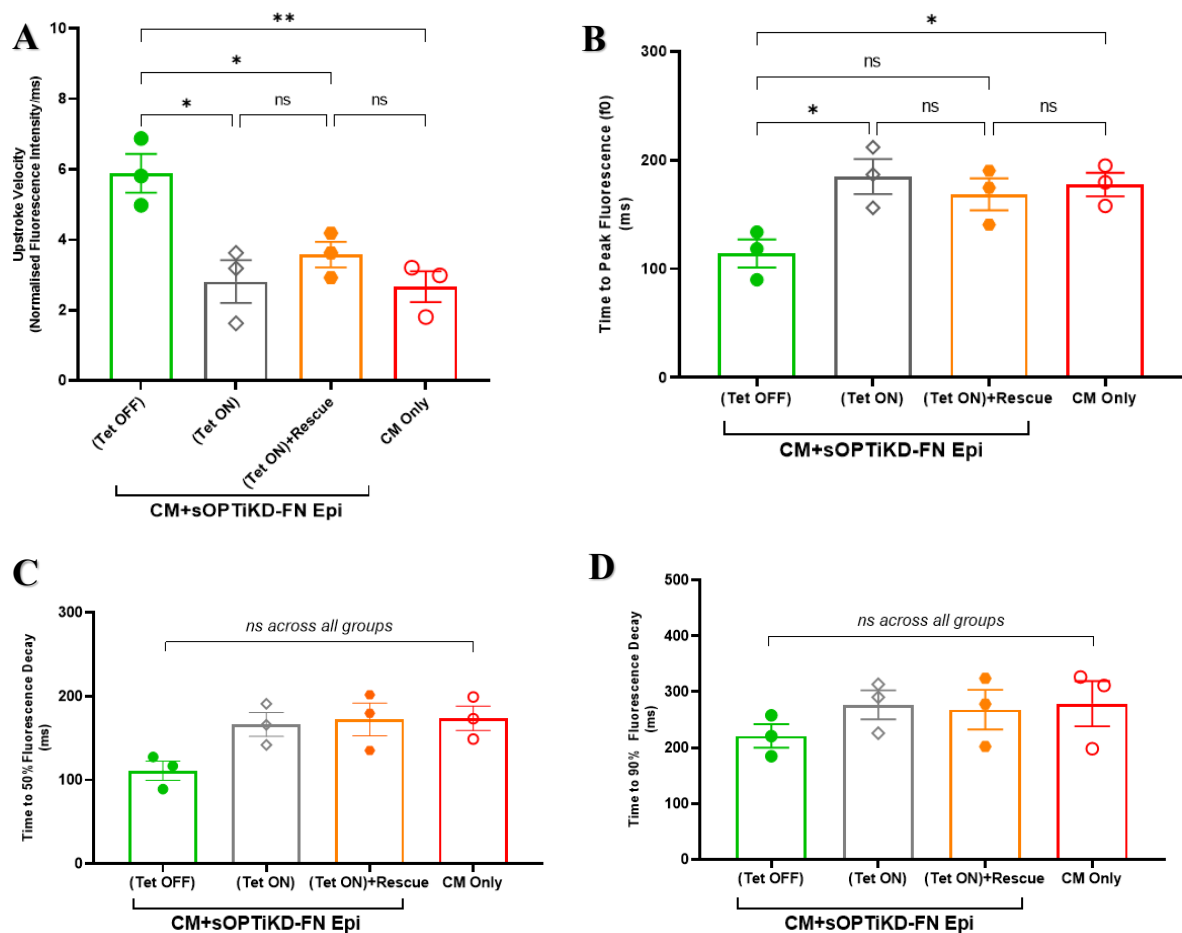


Figure 74: Rescue of epicardial-FN with human recombinant FN did not recover the inefficient Ca^{2+} handling by 3D-EHTs

Calcium kinetics in 3D-EHTs containing CM only, CM+Epi (Tet OFF), CM+Epi (Tet ON) and CM+Epi (Tet ON) +Rescue. **A**, **B** CM+Epi (Tet OFF) had significantly higher Ca^{2+} upstroke velocity than all groups, with the shortest time to peak Fluorescence (TTP). **C** Time to 50% Fluorescence decay and **D** Time to 90% Fluorescence decay were not significantly different between groups. N=3 biological replicates with 3 technical replicates each. Mean values; error bars represent s.e.m. * $P < 0.05$, ** $P < 0.005$. Two-sided P values were calculated using a one-way ANOVA with post-hoc correction for multiple comparisons.

Given the contrasting observations from the active force production and analyses of Ca^{2+} kinetics, the effects of rescue of epicardial-FN on sarcomeric assembly, a marker of CM maturity, were also examined. 3D-EHTs with CM+sOPTiKD-FN Epi (Tet OFF) showed the greatest sarcomeric parameters with highest FN deposition, **Figure 75**; thereby denoting a positive control. Meanwhile, CM+sOPTiKD-FN Epi (Tet ON) exhibited decreased sarcomeric parameters, identical to CM Only, **Figure 75**. The rescue of epicardial-FN function recorded sarcomeric parameters lower than (Tet OFF) but marginally higher than (Tet ON), with no clear statistical significance in either direction, **Figure 75B & C**. There was significantly less FN deposition in the rescue of epicardial-FN group, compared to (Tet OFF), $p=0.0221$, **Figure 75D**. This observation suggested that delivery of recombinant human FN might affect the rescue of epicardial-FN function in 3D-EHTs. Unfortunately, the rescue of epicardial-FN function with recombinant human FN, did not completely translate into improved sarcomere assembly.

Overall, the evidence implied that recombinant human FN could partially rescue the loss of epicardial-FN function, but further fine-tuning would be required. The rescue of epicardial-FN was clearest from the active force generation profile but was not corroborated by the analyses of calcium kinetics and sarcomeric assembly. Based on these results, I postulated that epicardial FN secretion might be dynamic and guided by epicardial-myocardial crosstalk. Rescue of epicardial-FN function appeared to require more than a daily, single standard dose of human recombinant FN. Thus, recombinant human FN is likely necessary, but insufficient, for the rescue of epicardial-FN function in 3D-EHTs.

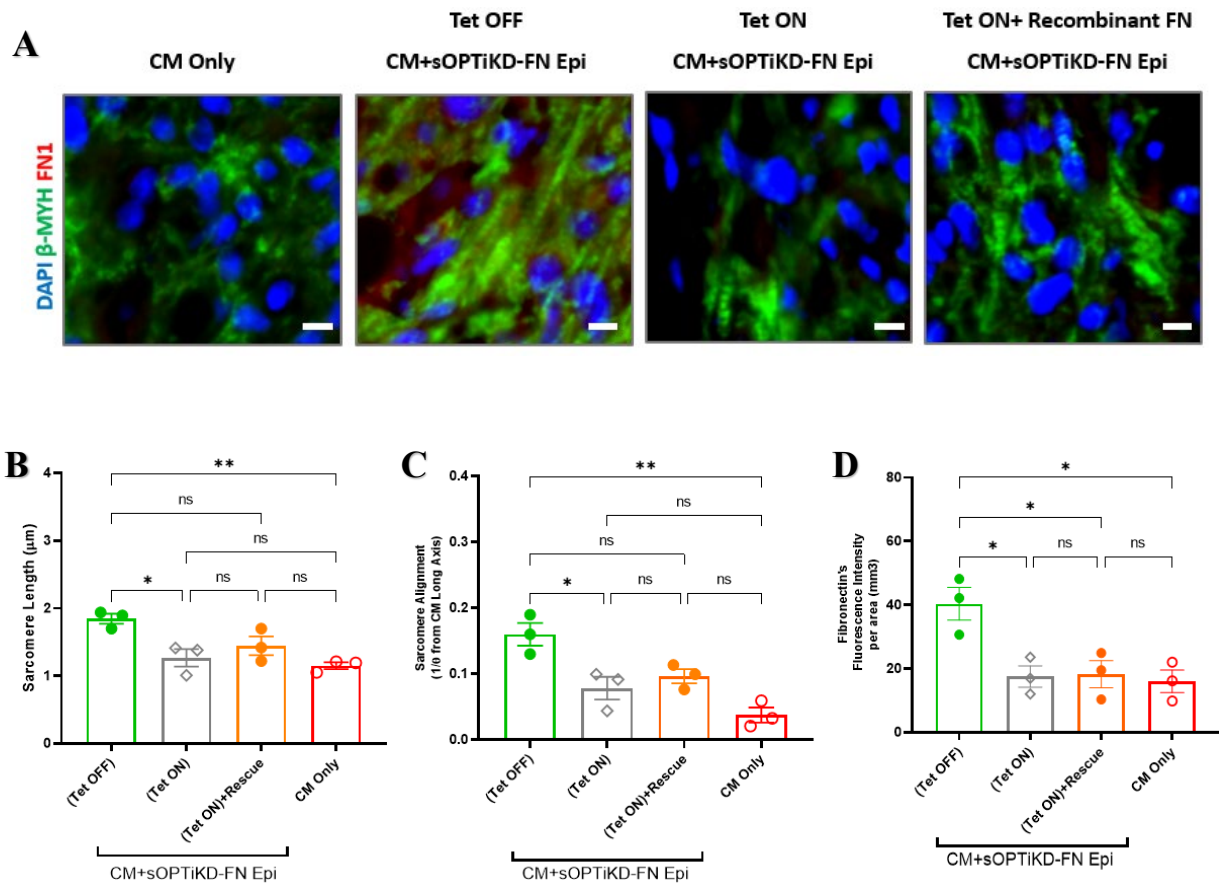


Figure 75: Rescue-of-FN function with human recombinant FN did not improve the maturation of hESC-CMs in 3D-EHTs

A 3D-EHTs sections of CM only, CM+Epi (Tet OFF), CM+Epi (Tet ON) and CM+Epi (Tet ON) +Rescue. CM+Epi (Tet ON) +Rescue showed organisation of hESC-CMs (β MHC, green) and FN (red) deposition, comparable to (Tet ON). Scale bar 5 μ m. With the rescue of epicardial-FN, the hESC-CM's **B** sarcomere length and **C** sarcomeric alignment were higher than (Tet ON) but lower than (Tet OFF), albeit not statistically significant in either direction. **D** Notably, the rescue of the epicardial-FN group had significantly lower FN deposition compared to (Tet OFF). Each experimental group had N=3 biological replicates, with 3 technical triplicates each. Mean values; error bars represent s.e.m. * P <0.05, ** P <0.005.

Collectively, all three different modalities of FN loss consistently demonstrated that epicardial FN was important for hESC-CM's contractile function and maturity in 3D-EHTS. These results were specially strengthened, given that each experimental group had its own internal positive (Epi+CM) and negative control (CM Only) with reproducible trends throughout these studies. The slight difference in response within each modality of epicardial-FN loss hinted that the epicardial secretion of FN was tightly regulated, specific, and guided by epicardial-myocardial crosstalk. Unfortunately, we could only draw a conclusion based upon hESC-CM's maturation from the 3D-EHTs. Other putative functions of epicardial-FN within the epicardial-myocardial cross talk such as proliferation, angiogenesis, and ECM turnover, cannot be deduced from this work. Next, I shall discuss my findings and future experiments to further delineate epicardial-FN's key role in mediating the epicardial-myocardial crosstalk.

5. DISCUSSION

A diagnosis of chronic heart failure carries a 50% 5-year mortality, only slightly less virulent than lung cancer. Yet, there are no sustainable therapies for this clinical condition. Ischaemic heart failure is the direct result of irreversible cardiomyocyte loss secondary to myocardial infarction. Exogenous cardiac regeneration uses cellular therapy to replenish the cardiomyocyte loss; a process for which the term 'primary remuscularisation' has been coined (Laflamme and Murry 2011). Replacing the lost cardiomyocyte contractile units in the chronically infarcted hearts could salvage the declining cardiac pump function. Thus, cellular therapy carries great potential for chronic heart failure patients.

Cellular therapy is conceptually akin to a heart transplant, except at a less invasive scale and could be fashioned as an 'off-the-shelf' therapy. However, the majority of successful cardiac regenerations with hESC/IPSC-derived CMs was performed in subacute timepoints post-MI (Laflamme et al. 2007; Caspi et al. 2007; Fernandes et al. 2015; Gerbin et al. 2015; Shiba et al. 2016; Liu et al. 2018; Bargehr et al. 2019). Intervention at this timepoint may reduce the incidence of chronic heart failure in the future but does not directly address the chronic heart failure state.

Thus far, mixed results were obtained with the delivery of NRVM into a chronic MI rat model (Li et al. 1996; Sakakibara et al. 2002; Huwer et al. 2003), whilst the delivery of hESC-CMs alone in a chronically infarcted rat heart showed no benefits (Fernandes et al. 2010). Combination cellular therapy with hESC-epicardium had not yet been trialled in the chronic MI state. Combination therapy with hESC-epicardium was based upon the synergistic epicardial-myocardial crosstalk observed during cardiac

development, which led to the augmentation of hESC-CMs function and cardiac regeneration in the subacute MI setting (Bargehr et al. 2019). However, the exact mechanisms underpinning epicardial-myocardial crosstalk remain unclear.

In my doctoral thesis, I addressed the current knowledge gap in hESC/IPSC-derived CMs' potential to salvage the chronically infarcted myocardium by exploring an optimal cellular therapy with i) species-matched cell type and ii) co-delivery of hESC-epicardium. Both therapeutic groups showed potential to attenuate cardiac dysfunction in the chronic MI state. However, definitive conclusions could not be drawn due to small sample size. Future adequately powered studies would be required to validate this preliminary finding. Alongside this, I explored the mechanism underpinning epicardial-myocardial crosstalk leading to an augmented cardiac regenerative response. I showed that epicardial-FN is a necessary mediator for epicardial-myocardial crosstalk. Discussion of the findings from this work, within the context of the wider literature, experimental limitations and the future directions that may advance cellular therapy towards clinical translation, now follow.

5:1 Can Cellular Therapy regenerate the Chronically Infarcted Rat Heart?

Our preliminary findings suggested that both species-matched (NRVM) and combination (Epi+CM) cellular therapy could potentially attenuate cardiac dysfunction in the chronic MI setting, as there were long-term cardiomyocyte engraftment, proliferation, maturation and vascularisation *in vivo*. The small study size precluded any definitive conclusions. Future work includes an adequately powered chronic MI rat study to validate my preliminary findings.

The chronic MI state is more formidable than its subacute counterpart, given its large areas of scarring, spherical LV dilatation and pathophysiological remodelling (Jessup and Brozena 2003; Houser 2012). To address the challenges of the chronic infarct environment, I first clarified the optimal animal model, cellular preconditioning, then trialled the optimal cell types with and without, combinatorial approaches.

5:1:1 Optimisation of cardiac regenerative rodent MI models

Delivery of hESC-epicardium with PSC and heat-shock improved cell survival in the athymic nude rat model. To examine the effects of PSC and heat-shock, hESC-epicardium was delivered at four days post-MI – an experimental timepoint shown to be favourable for cellular therapy (Zhang et al. 2001; Laflamme et al. 2007; Fernandes et al. 2015). PSC is a method of cellular preconditioning to mitigate the three interlinked pathways of ischaemia, *anoikis* and inflammation which lead to high rates of post-injection cell death (Müller-Ehmsen et al. 2002; Laflamme et al. 2007). Previously, the benefits of PSC were only demonstrated with hESC-CMs in the subacute MI setting (Laflamme et al. 2007; Chong et al. 2014; Gerbin et al. 2015; Liu et al. 2018). My results confirmed that PSC could also be useful adjuncts for other cell types such as hESC-epicardium.

Minimal hESC-epicardium survived in the acute MI mouse model, despite cellular preconditioning with PSC and heat-shock. During acute MI, the local micro-environment is exceptionally hostile to the newly injected cells (Zhang et al. 2001; Laflamme et al. 2007). Currently, there are proven clinical treatments for acute MI, such as primary percutaneous coronary interventions (Yancy et al. 2017). To extrapolate into the clinical setting, cellular injections during acute MI would involve the patient undergoing open-heart surgery during the acute MI state, which is an

unsafe clinical setting with physiological instability and highly friable, bleeding tissues. Given the experimental findings and clinical considerations, I chose to address cellular therapeutics options for the chronic heart failure state using the chronic MI animal model.

For the chronic heart failure setting, the delivery of cellular therapy to the patient could be planned, with opportunities for physiological optimisation. At this clinical stage, the cardiac tissues are stable, despite the scarring. Furthermore, cellular therapy could be delivered alongside concomitant cardiac interventions e.g. coronary artery bypass grafts. These are clinical and procedural considerations which make the chronic MI setting safer and receptive to cellular therapy.

The challenges of using hESC-CMs in the mouse model led to selection of the rat model for further studies. Mice exhibit heart rates in the range 450-600bpm, compared to rats with a range of 250-400bpm, whilst hESC-CMs could be paced up to ~150-200bpm *in vitro* (Shiba et al. 2013; Gerbin et al. 2015; Riehle and Bauersachs 2019). Cellular injections without leakage at ~500-600bpm are technically challenging. Furthermore, any human cellular integration with the mouse host have to overcome the difference of ~400bpm in CM contraction rates, compared to just ~200bpm difference with rats (Riehle and Bauersachs 2019). Overcoming a difference of 500bpm is unfeasible, as CM contraction rates are guided by the efficiency of excitation-contraction coupling, based upon ATP availability, intra-/extra-cellular calcium homeostasis and structural limitations of actin-myosin binding. Hence, the rat MI model offers a pragmatic middle ground to assess the feasibility of cellular therapy in regenerating chronically infarcted hearts.

In summary, the pilot animal studies clarified the importance of PSC for cellular preconditioning, the technical advantages in using the rat model and highlighted the clinical applicability of chronic rather than acute MI for cardiac regenerative studies.

5:1:2 Cellular therapy regenerated the chronically infarcted rat hearts

Our preliminary study showed that both species-matched and combination therapy could potentially attenuate cardiac dysfunction in the chronic MI setting. In the next sections, I shall discuss the findings specific to each type of cellular therapy and how they inform upon the next steps toward clinical translation.

5:1:2:1 *Species-matched cellular therapy*

Species-matched cellular therapy potentially demonstrated improved cardiac contractility compared to the control group. However, given the small sample size, we cannot draw any definitive conclusions with regards to cardiac function. Our histological evidence showed concomitant long-term cardiac engraftments, cardiomyocyte proliferation, maturation, and connexin-43 gap junction connectivity. The species-matched cardiac grafts were vascularised by the host, to the same extent as the host myocardium. Despite the hostile and chronically scarred environment, species-matched cellular therapy resulted in 'primary remuscularization'. To examine whether the improved contractility of the engrafted CMs promoted cardiac functional recovery, an adequately powered study would be warranted.

Species-matched cellular therapy could feasibly improve cardiac function in the rat chronic MI model as our preliminary findings correlated with previous findings in the subacute MI setting (Chong et al. 2014; Liu et al. 2018). A closer evolutionary distance

between the species of graft cells and host (i.e., human cells in non-human primate) had been shown to significantly improve cardiac function in the subacute MI setting (Chong et al. 2014; Liu et al. 2018). A similar degree of cardiac recovery was observed when non-human primate iPSC-derived CMs were transplanted into the infarcted hearts of non-human primates (Shiba et al. 2016). In contrast, when human-derived CMs were placed into a rat host after subacute MI, there was only attenuation of cardiac dysfunction (Laflamme et al. 2007), perhaps highlighting a species-dependent cardiac repair gap.

How does species-matched cellular therapy enhance cardiac regeneration? Our species-matched cellular therapy likely enhanced the injected CMs' survival due to matched beating rate, calcium contractile kinetics, and decreased immunogenicity (Milani-Nejad and Janssen 2013; Shiba et al. 2016; Kadota et al. 2017). Rat CMs predominantly expressed the α -MHC (>94-100%), with faster contraction kinetics, rather than the slower β -MHC expressed by human-derived CMs (Milani-Nejad and Janssen 2013). In the rat heart, the overly paced human-derived CMs would be in tetany with a rapid depletion of their ATP energy stores - likely to signal cellular distress. By matching our NRVM to the host rat heart rate, it led to cell survival and integration, as evidenced by our NRVM myofibrils closely resembling the host rat myocardium in sarcomeric and Cx-43 alignment, **Figure 36**. A species-matched cellular therapy also reduces immunogenicity and attacks by the host immune response to a xenograft. Furthermore, signalling pathways governing cellular maturation, proliferation and integration with the host would be matched at the protein, genetic and biochemical level (Halstead et al. 2020; Matsuda et al. 2020; Rayon et al. 2020). These species-matched factors led to cell survival and durable engraftment; thereby potentially augmenting cardiac repair in our chronically infarcted rats.

Our species-matched cellular therapy displayed long-term cardiac engraftment, visible up till 3 months after cellular therapy. In contrast to earlier chronic MI rat studies (Li et al. 1996; Sakakibara et al. 2002; Huwer et al. 2003), my study utilised PSC and doubled the number of injected NRVMs; both well-described factors to enhance cell survival and cardiac engraftments in the subacute MI setting (Laflamme et al. 2005, 2007; Robey et al. 2009). Unfortunately, there were no recorded cardiac graft sizes in the earlier NRVM studies for comparison, (Li et al. 1996; Sakakibara et al. 2002; Huwer et al. 2003). Our optimised species-matched cellular therapy potentially enhanced cell survival which resulted in long-term cardiac engraftment, thereby plausibly leading to improved cardiac contractility in the chronically infarcted rat heart.

Apart from species-matching, NRVMs also represented the optimal cell type to first assess the salvageability of the hostile, chronic MI environment. Firstly, P1-7 neonatal rats can regenerate after cardiac injury, thereby harbouring a robust regenerative response (Porrello et al. 2011; Lam and Sadek 2018). Secondly, adult rat CMs did not survive transplantation into rat hearts (Reinecke et al. 1999). Thirdly, NRVMs are still mononucleated and highly proliferative, thereby most analogous to hESC-derived CMs in cellular maturity (Yang et al. 2014; Kadota et al. 2017). Furthermore, NRVMs had greater cTNT+ve purity than rat ESC-derived CMs (Merkl et al. 2013; Dahlmann et al. 2018). Generation of rat ESC-derived CMs only records ~20% cTNT+ve cells (Dahlmann et al. 2018), compared to >80% cTNT+ve cells for NRVM and hESC-derived CMs, respectively (Kadota et al. 2017). Finally, the robust 'workhorse' NRVMs were used in a multitude of proof-of-concept cardiac regenerative studies (Zimmermann et al. 2002, 2006; Müller-Ehmsen et al. 2002). Altogether, NRVMs exhibited sufficient species compatibility, cellular plasticity, resilience, and proliferative potential to salvage a hostile, chronic MI environment.

Nonetheless, my findings could also reflect the contributions of species-matched non-myocyte stromal cells within our species-matched cellular therapy. Recently, Wang and colleagues described the unique transcriptomic landscape of P1 non-myocytes during neonatal heart regeneration and their putative roles in orchestrating cardiac regeneration (Wang et al. 2020). Notably, the pro-regenerative (P1) vs. non-regenerative (P8) epicardial and cardiac fibroblast populations were markedly different (Wang et al. 2020). Thus, the species-matched and pro-regenerative (P1) stromal contaminants in our NRVM cellular therapy could have enhanced cardiac repair in our chronically infarcted rat hearts. Future experiments using spatial transcriptomics to elucidate the spatial interactions of injected NRVMs and stromal cells *in vivo* would be interesting.

Our species-matched cardiac grafts portrayed greater CM maturity *in vivo* **Figure 33**. This observation might explain why species-matched cellular therapy could potentially salvage the hostile, chronically failing rat heart. Then, what are the key factors that enhance cardiac graft maturity?

Our NRVMs were more mature than hESC-CMs, prior to intramyocardial injections, **Figure 34A**. NRVM exhibited aligned sarcomeres whilst hESC-CMs still maintained sarcomeric disorganisation, **Figure 34A, Table 2**. Moreover, our NRVMs' pre-injection maturity level and survival appeared intertwined. PSC was initially designed as cellular preconditioning to improve hESC-CMs' survival as the foetal-like hESC-CMs lacked resilience (Laflamme et al. 2007). Conversely, adult rat CMs are quite fragile upon ventricular dissociation, as they need to maintain a cardiac syncytium and their binucleated nature (Reinecke et al. 1999). Thus, P1/P2 NRVMs strike the right balance of 'adolescence-like' maturity (Yang et al. 2014) and resilience for intramyocardial injections, leading to greater cell survival, cardiac graft size and maturation.

Matching the species of transplanted CMs to the *in vivo* environment enhanced cardiac graft maturation. Our NRVM cardiac grafts showed complete connexin-43 gap junction alignment and large myofibrils, closely resembling the chronically infarcted host myocardium, **Figure 36**. In the subacute MI setting, NRVM matured faster than hESC-CMs in the adult rat heart (Kadota et al. 2017). There is consensus that the *in vivo* environment directly affects the maturation of any transplanted CMs, due to the environmental biophysical and biochemical cues, together with cellular crosstalk with non-myocyte stromal cells (Kadota et al. 2017; Cho et al. 2017; Karbassi et al. 2020; Guo and Pu 2020). Supraphysiological electrical pacing promoted hESC-CMs maturation in 3D-EHTs (Ronaldson-Bouchard et al. 2018), thus highlighting the instrumental role of electrophysiological cues. Our species-matched cellular therapy likely led to more efficient cellular crosstalk and matched contractile kinetics, which augmented cardiac graft maturation in the chronically infarcted rat hearts.

Our species-matched cellular therapy showed that the chronically infarcted rat heart was potentially amenable to cardiac regeneration. My findings highlighted the need for durable and mature cardiac grafts for effective cardiac regeneration of the chronically infarcted heart. For clinical purposes, we envision using hESC-CMs instead. To recapitulate the above findings with the less mature hESC-CMs, we would need an adjunctive cellular therapy such as hESC-epicardium, previously shown to augment hESC-CMs survival, proliferation, and maturation in the subacute MI setting (Bargehr et al. 2019).

5:1:2:2 Combination cellular therapy

Our preliminary findings implied that the combination therapy [EPI+CM] group was able to prevent further decline in cardiac dysfunction by the 3rd month of follow-up, despite of the chronically scarred myocardium. An adequately powered study is required to validate these early findings. Nonetheless, our findings reiterated the potential of epicardial cells as a key stromal cell in creating a supportive microenvironment for hESC-CMs in the chronic MI model. Thus, an adjunctive cellular therapy may be indicated to salvage the chronic heart failure state.

In this study, hESC-epicardium was not impaired by the chronic infarct environment and was able to augment the hESC-CMs' survival, proliferation, maturation, and vascularisation *in vivo*, which likely led to long-term cardiac grafts in the chronically infarcted rat hearts. Due to the small sample size, definitive conclusions with regards to graft size cannot be drawn.

Our epicardial-augmented hESC-CMs were highly proliferative, despite the chronic MI setting. The proliferative rates were comparable to other cardiac regenerative studies in the subacute MI setting (Gerbin 2015, Liu 2018). The pro-mitogenic effects of epicardium on CMs during cardiac development had been well-documented (Cao and Poss, 2018). Other pre-clinical studies utilising human-derived or hESC-epicardium have also demonstrated the epicardial-augmentation of CM proliferation (Weeke-Klimp et al. 2010; Winter et al. 2007, 2009; Bargehr et al. 2019). Our co-delivery of hESC-epicardium may have recapitulated the synergistic epicardial-myocardial crosstalk during cardiac embryogenesis and thereby, augmented the hESC-CMs' proliferative capacity *in vivo*.

Apart from epicardial-augmentation, hESC-CM's proliferative capacity also reflected its relative immaturity compared to NRVM (Kadota et al. 2017). Prior to cellular injection, our hESC-derived CMs are observably less mature than NRVMs, **Figure 34A**. Cardiomyocyte maturation and proliferation are inextricably linked. The cost of maturation is the cellular proliferative capacity as sarcomeric disassembly is required for cell proliferation (Karbassi et al. 2020; Guo and Pu 2020). Nonetheless, the epicardial-augmented hESC-CMs retained their proliferative capacity in the chronic MI environment, with subsequent formation of sizeable cardiac grafts and favourable cardiac repair.

Together with proliferation, co-delivery of hESC-epicardium potentially augmented hESC-CMs maturation in our chronically infarcted rat hearts. The hESC-CMs underwent maturation *in vivo*, likely explaining our observed delay in cardiac recovery. The *in vivo* environment is instrumental for the maturation of hESC-CMs (Kadota et al. 2017; Cho et al. 2017; Guo and Pu 2020); a critical biological process hastened by the addition of hESC-epicardium, as observed in the subacute MI and 3D-EHT setting (Bargehr et al. 2019). Although Fernandes *et al.* reported maturing CMs with hESC-CMs alone, that chronic MI study reported negative results (Fernandes et al. 2010). In the subacute MI setting, hESC-epicardium accelerated hESC-CMs maturation *in vivo*, compared to hESC-CMs alone (Bargehr et al. 2019). For the chronically infarcted hearts, the co-delivery of hESC-epicardium could similarly speed up hESC-CMs maturity *in vivo* to form mature cardiac grafts with the potential to attenuate cardiac dysfunction. The speed of cellular maturation *in vivo* may be *more* pertinent in the chronic MI setting.

An abundance of host-derived vascularisation within both species-matched and combination hESC-derived cardiac grafts were also observed. The graft vascular

supply connected with the host vascular supply in both species-matched and hESC-derived cardiac grafts. This histological observation correlated with other studies of cardiac engraftments in the subacute MI setting (Gerbin et al. 2015; Liu et al. 2018; Bargehr et al. 2019). Apart from maintaining a vessel network within our cardiac grafts, these observations hinted at pro-angiogenic signalling secreted by the engrafted cells.

Despite the chronic MI setting, the epicardial-augmented cardiac grafts demonstrated increased CD31+ve neovascularization, compared to species-matched cardiac grafts. Our rat host myocardium also showed augmented CD31+ve neovascularization, which hinted at an organ-wide, heightened vascularisation response, promoted by hESC-epicardium. As the vascular supply within our cardiac grafts was host-derived, the hESC-epicardium might have secreted pro-angiogenic factors (Winter et al. 2007, 2009; Riley and Smart 2011). Lack of vascularisation had been highlighted as a key reason for the failed hESC-CM monotherapy in the chronic MI setting (Fernandes et al. 2010; Shiba et al. 2014). The unique promotion of neovascularization by hESC-epicardium might have contributed towards greater hESC-CMs survival, proliferation, engraftment, and cardiac recovery in our chronically infarcted rat hearts.

This preliminary work demonstrated that both species-matched and combination cellular therapy could plausibly salvage the chronically infarcted myocardium, albeit to different extents. In both types of CM-based cellular therapy, there were mature and durable cardiac grafts, underpinned by CM engraftment, proliferation, maturation, and vascularisation *in vivo*. Despite the hostile chronic MI environment, optimizing the cell types had yield durable and mature cardiac grafts, with the potential to reverse the course of the failing heart. Thus, combination cell therapy with hESC-epicardium and hESC-CMs may hold translational potential, as a heart failure treatment for our patients.

5:1:3 Clinical challenges posed by cellular therapy

Demonstrating that CM-based cellular therapy could potentially rescue the chronically failing heart had addressed a notable gap in the cardiac regeneration field. More importantly, these results have taken us closer towards clinical translation. However, our findings raised several key clinical challenges that need to be addressed prior to clinical translation.

5:1:3:1 Cellular therapy is associated with arrhythmias

Pre-clinical studies have reported arrhythmic events associated with the delivery of hESC-CMs to regenerate the infarcted hearts (Shiba et al. 2013; Liu et al. 2018; Romagnuolo et al. 2019). These arrhythmic events had been associated with the immaturity of engrafted hESC-CMs (Liu et al. 2018; Romagnuolo et al. 2019). Liu *et al.* demonstrated with exhaustive electrophysiological studies that the nidus of arrhythmic events is the immature hESC-cardiac graft, events which reduce in frequency as the graft matured *in vivo* (Liu et al. 2018). Although these arrhythmic events are self-terminating, they carry significant clinical risks. To reduce the arrhythmic events, it is reasoned that more mature hESC-CMs at the point of intramyocardial injections may be required.

However, would a more mature hESC-CM proliferate or integrate well *in vivo*? Given that our more mature species-matched therapy resulted in superior cardiac grafts and well-aligned connexin-43 gap junctions, a closer look at P1/P2 NRVM behaviour *in vivo*, in real-time, may guide us. Adolescence-like maturity is likely the aim (Yang et al. 2014), as injected adult rat CMs did not integrate and died *in vivo* (Reinecke et al. 1999). Furthermore, the need for the proliferation-maturation balancing act has been

noted (Karbassi et al. 2020; Guo and Pu 2020). Thus, further work is warranted to determine the optimal maturity level of CMs, to reduce the pro-arrhythmic risks.

5:1:3:2 Cellular therapy-related arrhythmias: contractile benefits or paracrine solutions?

Given the pro-arrhythmic risks of CM-based cellular therapy, should the focus be on paracrine mechanisms over contractile cell therapy? A proportion of chronic heart failure patients already suffer from arrhythmic events, thereby risking further aggravation with ‘pro-arrhythmic’ cellular therapy (Menasché et al. 2018). Different groups had explored the alternative approach of delivering only paracrine signals to the infarcted heart via cardiac progenitor cells, patches or exosomes (Gnecchi et al. 2008; Zhu et al. 2018; Menasché et al. 2018; Gao et al. 2020). However, these studies only reported modest results. Furthermore, the cardiac regenerative paracrine signals remained undefined.

In all likelihood, our exogenously delivered contractile cell types conferred both contractile and paracrine benefits amongst themselves and/or with the host tissue and system. Despite durable and mature cardiac grafts in the chronic MI environment, our graft sizes and those reported in literature account (Fernandes et al. 2010) for graft sizes ~ 1-3% of LV, thereby improved cardiac function would likely need both improved contractility via ‘primary remuscularization’ at the infarct *and* paracrine effects on the host myocardium. As evidenced by host-derived vascularization within the cardiac grafts (*Section 3:1:2:6*), the contractile cell types likely acted as a continuous source of paracrine signalling to the host tissue and organ system. A comparative study of hESC-CMs and adult stem cells showed superior cardiac repair by hESC-CMs in the subacute MI setting, likely due to increased contractile force afforded by primary

'remuscularization' (Fernandes et al. 2015). Thus, both paracrine signalling and contractile force are required for successful cardiac regeneration.

Potentially, we could creatively circumvent the arrhythmic events by outlining the optimal cellular maturity pre-injection and modulate cellular maturation *in vivo* via genetically-edited and temporally-modulated 'designer cells'. Before personalised 'designer cells' for chronic heart failure can be created, clarity on the paracrine signalling involved is needed.

5:1:3:3 Cellular therapy is associated with immunogenicity

For our proof-of-concept studies in the chronically infarcted rat hearts, we tackled the immunogenicity concerns by utilising athymic nude rats and a week of cyclosporine injections. The attack on donor stem cells is predominantly driven by the adaptive immune system. Thus, our athymic nude rats lack the adaptive immune system. Furthermore, cyclosporine inhibits Il-2 transcription with subsequent inactivation of T-cells. Downregulation of the adaptive immune system appeared sufficient for robust graft survival in our study, as corroborated by other rat studies in the subacute MI setting (Laflamme et al. 2007; Gerbin et al. 2015; Bargehr et al. 2019). Of note, ageing athymic nude rats were reported to develop oligoclonal T cells (Vaessen et al. 1986; Rolstad 2001). Future longer-term rodent studies may consider regular cyclosporine instead.

As for clinical translation, the immunogenicity of cellular therapy poses a significant challenge. To circumvent this, several strategies have been explored, such as allogeneic cell transplantation derived from banked iPSC lines or MHC-matching (Kawamura et al. 2016; Shiba et al. 2016). Allogeneic MHC-matched and species-matched iPSC-derived CMs could regenerate the infarcted non-human primate heart,

with the reduction to a single immunosuppressive agent (Kawamura et al. 2016; Shiba et al. 2016). However, a significant immune response remained (Kawamura et al. 2016).

Requiring a lifetime on a triple immunosuppressive regimen is both clinically and cost prohibitive. Although patient-specific iPSCs could be generated, *de novo* mitochondrial DNA mutations could still evoke an immunogenic response (Deuse et al. 2019). thereby requiring genetically edited hypoimmunogenic iPSCs (Mattapally et al. 2018; Murata et al. 2020; Han et al. 2019). Thus, a better solution may be utilized such as genetically edited hypoimmunogenic cells with the knockout of two key components of MHC complexes I and II, namely β 2 microglobulin and class II MHC class transactivator (Mattapally et al. 2018), together with the expression of immunomodulatory factors such as PD-L1, HLA-G and CD47 from the AAVS locus (Han et al. 2019). These 'designer cells' have shown promise in early pre-clinical studies (Deuse et al. 2019).

In view of translating Epi+CM cellular therapy into patients, dual-cellular therapy would pose a greater immunogenicity concern than monotherapy. A more pragmatic approach may be to delineate the paracrine signalling underpinning the epicardial-myocardial crosstalk, thereby granting novel, acellular approaches in modulating hESC-CMs *in vivo*.

5:2 Epicardial-FN is Necessary for Epicardial-Myocardial Crosstalk

The synergism between epicardium and CMs witnessed in cardiac development and injury (Gittenberger-De Groot et al. 2000; Lie-Venema et al. 2007; Lepilina et al. 2006), 3D-EHTs and exogenous cellular therapy (Winter et al. 2007, 2009; Bargehr et al. 2019), makes the co-injection of hESC-epicardium and hESC-CMs (Epi+CM) an attractive candidate for heart regeneration in patients. The exact mechanisms underlying the beneficial effects of Epi+CM remain to be elucidated, but are likely due to a mixture of paracrine signalling and 'primary remuscularization'. To translate safely into clinics, we need to delineate the epicardial-myocardial crosstalk.

Based on our bulk RNA-sequencing data and observations made by the Sinha Lab (Bargehr et al. 2019), we focused upon the role of epicardial-FN. From the chronic MI rodent studies, a different pattern of FN distribution was also observed in the presence of Epi+CM grafts, compared to NRVM and Sham. FN deposition concentrated predominantly around the Epi+CM cardiac grafts, whilst remained subendocardial in the other graft types tested. These observations were compelling. Thus, I hypothesized that epicardial-FN was a putative key mediator in epicardial-myocardial crosstalk, leading to enhanced cardiac regeneration in rodent MI studies. This hypothesis was tested using a set of loss of epicardial-FN function and rescue of epicardial-FN function studies *in vitro*.

5:2:1 Ratio of Epi:CM in 3D-EHTs

To study the mechanism of epicardial-myocardial crosstalk, I need to mimic the developmental ratios to determine the optimal ratios of Epi: CM. A balance must be sought between the amount of contractile cell type and the synthetic, supportive stromal cell type (Giacomelli et al. 2017; 2020). My study determined that the optimal ratio of epicardium to the CMs was 1:9, as this ratio produced the highest active force generation and Ca^{2+} -handling. This ratio of CM to stromal cell has been similarly used by other bioengineering groups in their respective 3D-EHTs (Giacomelli et al. 2017; 2020; Ronaldson-Bouchard et al. 2018). After the determination of the optimal CM:Epi ratio for 3D-EHTs, a series of loss of epicardial-FN function studies in 3D-EHTs was performed.

5:2:2 Loss-of-FN function decreased hESC-CM maturation and attenuated 3D-EHTs' contractile function

Loss of epicardial-FN function abrogated the epicardial-augmentation of hESC-CM maturation in 3D-EHTs. Loss of epicardial-FN function resulted in the lack of an active force-length relationship, inefficient Ca^{2+} handling and immature sarcomeric organisation, which were defining features of immature CMs (Karbassi et al. 2020; Guo and Pu 2020), **Table 2**. The effects of the loss of epicardial-FN were consistent across three different methods of blocking or minimizing epicardial-FN expression, which encompassed i) peptide inhibition of FN polymerisation, ii) Crispr-cas9-mediated knockout of epicardial-FN and iii) tetracycline-induced shRNA-mediated reduction in epicardial-FN expression in 3D-EHTs. Our loss of epicardial-FN function directly attenuated CM maturation in 3D-EHTs. Notably, the 3D-EHTs with loss of

epicardial-FN function displayed similar functional readouts as hESC-CM alone, thereby lending further weight to the hypothesis that epicardial-FN is a key mediator in epicardial-myocardial crosstalk.

Given the multifaceted role of FN, do these findings reflect the loss of FN or epicardial-FN? Initially, this was tested with downstream inhibition of fibronectin polymerisation by a small peptide (pUR4) (Tomasini-Johansson et al. 2001; Valiente-Alandi et al. 2018). Polymerised fibronectin carries wide-ranging influence over crucial cellular processes, inclusive of adhesion, growth, proliferation, migration, survival, and differentiation (Schwarzbauer and DeSimone 2011). A broad pUR4-mediated inhibition of FN function led to vastly different results in the combined presence of Epi+CM, compared to CM alone, in 3D-EHTs. There was a greater loss of CM maturation in the combined presence of Epi+CM. Furthermore, the results from the genetically induced loss of epicardial-FN function were similar to the pUR4 inhibition studies. Infarcted rodents receiving hESC-epicardium alone did not exhibit increased FN deposition (Bargehr et al. 2019), suggesting that epicardial-FN was only upregulated in response to hESC-CMs. Thus far, evidence suggested that epicardial-FN was plausibly a key mediator of epicardial-myocardial crosstalk and therefore, uniquely indispensable to hESC-CMs.

If so, how does epicardial-FN communicate with hESC-CMs within 3D-EHTs? Our loss of epicardial-FN function also decreased FN-integrin signalling with hESC-CMs. Polymerised FN signals through a cell surface receptor, integrin- $\alpha 5\beta 1$, as its key signal transducer (Hynes 1987; Wickström et al. 2011), thereby enabling extracellular and intracellular communication. Integrins usually act as mechano-transducers by converting mechanical cues into biochemical signals (Israeli-Rosenberg et al. 2014).

The activated integrin- $\alpha 5\beta 1$ signals through multiple pathways that govern various crucial cellular processes such as cell migration, survival, cell cycle progression, and differentiation (Wickström et al. 2011; Schwarzbauer and DeSimone 2011). Our results suggested that epicardial-FN communicated with hESC-CMs via integrin- $\alpha 5\beta 1$. A comparative experiment of loss of integrin- $\alpha 5\beta 1$ function with loss of epicardial-FN function would be required to confirm our observations. Thus far, and with some caution, I postulate that epicardial FN-integrin signalling represents a major communication channel within epicardial-myocardial crosstalk, that regulates hESC-CM maturation.

Epicardial-FN is instrumental in mediating the epicardial-myocardial crosstalk during cardiac regeneration in the zebrafish (Wang et al. 2013). In the zebrafish, injury-activated epicardial cells secrete the fibronectin isoform (*fn1*) which binds to integrin $\beta 3$ receptors to integrate CMs within the site of injury (Wang et al. 2013). *Fn1* loss-of-function mutations disrupted zebrafish heart regeneration, leading to fibrosis instead of a contiguous wall of new muscle (Wang et al. 2013). The findings from my loss of FN-function 3D-EHTs studies shared similarities with the zebrafish model, thus further strengthening the evidence that epicardial-FN could be a key mediator of epicardial-myocardial crosstalk.

5:2:3 Rescue of loss-of-FN function with human recombinant

FN

Our studies to rescue the loss-of-FN function with recombinant, human FN (huFN) proved partially successful for active force-length production. However, both Ca^{2+} -handling profiles and sarcomere assembly remained inefficient and immature. So, why

did the rescue of epicardial-FN function did not completely work? The findings can be dissected from both technical and biological perspectives.

From the technical perspective, adding huFN into the media daily might not lead to efficient uptake by the CMs encased within the 3D-EHTs. huFN might need to be embedded within the 3D-EHTs to be efficacious. Future studies could incorporate huFN within the 3D-EHTs during construction. However, the 3D-EHTs were constructed from geltrex and collagen. Both components of the extracellular matrix which were optimised for a specific Young's modulus to support force measurements. Thus, 3D-EHTs might not be the optimal assay to study the rescue of epicardial-FN function studies.

From the biological perspective, epicardial-FN might be a specific spliced isoform of fibronectin and different from the commercially sourced huFN used in this work. FN has many alternative splicing sites, giving rise to 20 isoforms in the human, with many roles in regulating crucial biological processes during development and disease (Schwarzbauer and DeSimone 2011; Astrof et al. 2007; Valiente-Alandi et al. 2018). Further studies using a combination of mass spectrometry and proteomics to isolate and characterize our epicardial-FN would be useful. These studies should grant specific insights into epicardial-FN isoforms and potential binding sites. Nonetheless, the rescue of epicardial-FN function studies highlighted the specificity of epicardial-FN for augmentation of hESC-CMs.

Another explanation could be that huFN failed to rescue due to the dynamic nature of epicardial-FN secretion, as guided by the evolving needs of the maturing hESC-CMs in 3D-EHTs. In the zebrafish, the ECM, inclusive of epicardial-FN, displays a dynamic spatiotemporal nature to enable successful cardiac regeneration (Mercer et al. 2013).

The FN-integrin signalling pathway transmits biophysical and biochemical cues from the environment to invoke specific cellular processes, such as cellular survival, migration, proliferation, or maturation (Hynes 1987; Wickström et al. 2011). As the hESC-CMs mature over time, a consistent daily dose of huFN might fail to match fluctuations in levels possibly required by CMs at different stages of maturation. If so, recapitulating this by the addition of recombinant human FN alone may be exceedingly difficult.

Nonetheless, a clear and reproducible loss-of-FN function across three modalities was demonstrated. Our findings also supported another hypothesis that epicardium communicated with CMs via an epicardial-FN-integrin signalling pathway. Refining the exact role of epicardial-FN proved elusive, potentially due to the multifaceted role of FN. Moreover, the epicardial-myocardial crosstalk governs many different processes during cardiac development and disease (Wang et al. 2011; 2015; González-Rosa et al. 2012; Von Gise et al. 2012; Cao and Poss 2018). To examine the broader implications of loss of epicardial-FN function, an *in vivo* study utilising rat MI model would be highly warranted. Quite plausibly, epicardial-FN could have more downstream effects than just the augmentation of CM maturation.

To gain a bird's eye view of the role of epicardial-FN within epicardial-myocardial crosstalk, our group recently mapped an epicardium-myocardium interactome, utilizing single-cell sequencing data. Focusing solely on epicardial-FN, the interactome demonstrated that epicardial-FN putatively signalled via different receptors and soluble factors; with downstream effects ranging from ECM turnover, cell survival, proliferation, and angiogenesis (Ong, Bargehr, Knight-Schrijver et al. manuscript in preparation). The epicardial-FN and CM interactome is shown in **Figure 80, Appendix 9.4**.

As for the combination therapy of hESC-epicardium and hESC-CMs as potential cellular therapy for heart failure, the epicardial-FN function studies strongly implied that hESC-epicardium is irreplaceable. hESC-epicardium needs to be constantly present to adapt to the changing needs of hESC-CMs. The dynamic nature of epicardial-myocardial crosstalk appeared to be crucial for the augmentation of hESC-CM contractile function, both *in vitro* and *in vivo*.

5:3 Study Limitations

5:3:1 Chronic MI rat model

The *in vivo* study used had several limitations. Most importantly, there were a limited number of animals in each group due to the complexity of the procedure and a long follow-up period. This limited the statistical power of several analyses. Each of the study arms was conducted in a serial manner, due to the necessity of training and collaborative efforts. Given this, all the intra-myocardial injections were performed by the same person (A.M.), and she was blinded to the pre-injection cardiac function of each animal. In addition, all the echocardiographic analyses were performed by an independent, blinded assessor. Despite the serial non-randomised nature of the study, we gained important insights into the specific trends of cardiac function post-cellular therapy. The detailed histological analyses aligned with the preliminary findings for the species-matched and combination therapy groups. However, the small sample size precluded any definitive conclusions.

To validate our preliminary findings, we plan to conduct a randomised, double-blinded chronic MI rodent study in spring 2022 in collaboration with Professor Charles E Murry, University of Washington, USA. This study would be adequately powered as outlined

in Section 2:2:1. Given the challenges with our initial study, this definitive study would be conducted as a single-phase study at the University of Washington, USA. We will utilise the same surgical and echocardiographic operator throughout to reduce operator error.

Next, we were limited by the type of cardiac imaging modality used in this preliminary study. We used 2D-echocardiography in the short axis view (SAX) to evaluate cardiac contractility (FS%), similar to previously reported studies (Laflamme et al. 2007; Fernandes et al. 2010; 2015; Bargehr et al. 2019). With 2D-ECHO, we cannot evaluate the cardiac output, contraction of the graft area or synchronicity of graft contractions. At the time of study, we were limited by lack of access to improved versions of rodent cardiac imaging e.g. MRI or high-frequency speckle tracing echocardiography, which will be further discussed in *Section 6:1:1*.

Another limitation is how well chronic infarcts in young athymic nude rats mimic the sequelae of a middle-aged patient with a chronically failing heart after myocardial infarction. A middle-aged patient could also have other cardiac risk factors such as diabetes, atherosclerosis, and obesity. The chronic MI rat model is a proof-of-concept study to assess the feasibility of cellular therapy in a chronically scarred heart. In a stepwise progression of questioning, proceeding into the usage of diabetic rats, atherosclerotic rat models, rats on high-fat diets or ageing rats may be helpful. This bridge between pristine animal studies and complex human patients is a well-trodden but obstacle-laden path to clinical translation.

5:3:2 The 3D-Engineered Heart Tissues

As for the mechanistic study of FN in 3D-EHTs, there were several limitations. Firstly, there was considerable variability amongst the biological and technical replicates across all groups for the force generation profile, Ca^{2+} -handling and RNA expression experiments. The reasons were due to different cellular differentiation and variable construct generation. As EHTs are hydrogel-based and CMs are sensitive to local tension, the exact cell:gel ratio is critical for cellular maturation. However, 3D-EHTs are the most physiologically relevant model to assess cardiac maturation via Frank-Starling force generation and Ca^{2+} -handling (Stoehr et al. 2014; Ronaldson-Bouchard et al. 2018). Thus, we addressed the limitations above by ensuring CM purity (>80% cTNT+ve) and increased cell viability during casting with heat-shock at 42°C.

As for imaging of Ca^{2+} transients, the background fluorescence is a confounding variable as the H9 cell line used is GFP⁺. We circumvented this confounder by pacing our 3D-EHTs during the measurements. Furthermore, I had only analysed the kinetics of Ca^{2+} transients, rather than absolute values. A more elegant approach would be to utilize a hESC-CM with a genetically encoded calcium sensor (Broyles et al. 2018).

Another limitation is that the mechanistic insights gained from the 3D-EHTs studies could only clarify the effects of epicardial-FN on hESC-CM's maturation, within a developmental context. Apart from CM maturation, hESC-epicardium also augmented CM proliferation, tissue angiogenesis and ECM turnover *in vivo*. Thus, our current 3D-EHTs studies could not fully clarify the role of epicardial-FN in our cardiac regenerative rodent studies. Whether epicardial-FN played a role in any of these epicardial-specific benefits would need to be elucidated in assays, other than 3D-EHTs. Nonetheless, epicardial-FN is proving to be a key mediator for epicardial-augmented cellular

therapies, based upon the observations of epicardial-FN's role in our 3D-EHTs, animal MI models and bulk RNA-sequencing data.

6. FUTURE WORK AND DIRECTION

Despite the encouraging results from our proof-of-concept studies, significant roadblocks to translating our findings into patients remain. In terms of clinical priority, these are arrhythmic events due to cellular immaturity, immunogenicity, and cellular adaptation to the chronic, fibrotic environment. As for scientific prioritisation, elucidation of the mechanistic underpinnings of paracrine signalling leading to cardiomyocyte survival, proliferation and maturation is a must. This elucidation would greatly aid in addressing all the key challenges discussed throughout.

6:1 Cellular therapy to salvage chronic heart failure

6:1:1 Cardiovascular imaging

For future work, characterization of cardiac function in the rodent MI models would benefit from a gold standard imaging modality, i.e., magnetic resonance imaging (MRI); widely used across small and large animal models for accurate assessment of cardiac function (Fernandes et al. 2010; Chong et al. 2014; Liu et al. 2018; Romagnuolo et al. 2019). MRI enables the measurement of cardiac volume changes in real-time, thereby giving cardiac output and ejection fraction (EF%) as a more encompassing measure of cardiac function. Crucially, MRI enables assessment of

scar evolution overtime via T1/T2 weighted images (Romagnuolo et al. 2019). Cardiac functional recovery, in the context of fibrosis attenuation to regenerate the infarcted heart, remains a major roadblock for this field. Thus, MRI is particularly important for the study of chronic heart failure models.

High-frequency speckle tracking echocardiography (STE) also measures cardiac function including global and regional contractility (Bhan et al. 2014; Earl et al. 2021). STE utilises high-frequency probes (30–50 MHz) with higher spatial resolution (30 μm) to track regional deformity, longitudinal and radial strain. Given this refined resolution, STE's accuracy is comparable to cardiac MRI (Bhan et al. 2014). Apart from cardiac function, STE could identify the infarct region to quantify engrafted CMs' contractility in relation to host myocardium. Compared to MRI, echo is more accessible with shorter anaesthetic duration, but the accuracy is operator dependent. Thus, STE is a promising imaging modality to evaluate the efficacy of cellular therapy.

Both MRI and high-frequency speckle tracking echocardiography would offer a better resolution of both cardiac function and scar evolution over time, thereby enabling more accurate studies as we advance towards clinical translation.

6:1:2 Cardiac electrophysiological studies

Further delineation of graft-host electrical integration with *ex vivo* cardiac calcium-mapping studies (Shiba et al. 2013; 2014; Gerbin et al. 2015) or *in vivo* electrophysiological studies (Kehat et al. 2004; Chong et al. 2014; Liu et al. 2018; Romagnuolo et al. 2019) are warranted. In our chronic heart failure rat model, there was histological evidence of connexin-43 gap junction connectivity within graft and graft-host, hinting at electrical integration with the host. However, there were also large

areas of scarring, potentially impeding electrical connectivity. The only way to prove functional graft-host electrical integration is via *ex vivo* calcium-mapping in the rodent model. This might be quite challenging and limited by the size of the cardiac grafts. A better approach would be electrophysiological (EP) studies *in vivo*. EP studies would give real-time analyses of electrical connectivity, together with insights into any ‘pro-arrhythmic’ cellular events. However, EP studies are only feasible in large animal models of cardiac regeneration. As graft-host electrical connectivity is a pressing question and arrhythmic events carry significant clinical risks, conducting EP studies in large animal models of cardiac regeneration, would represent the next step towards clinical translation.

6:1:3 Species-specific ESC/IPSC-derived CMs for pre-clinical studies in cardiac regeneration

Given the augmented cardiac repair with species-matched therapy, the question ‘Are species-mismatched cellular therapies impeding the full potential of hESC/IPSC-derived CMs to regenerate the infarcted rat heart?’ should be asked.

To address this question, the usage of rat-ESCs/IPSCs to derive CMs and epicardium would be commended (Merkl et al. 2013; Dahlmann et al. 2018). Studies utilising species-matched IPSC-CMs derived from non-human primates had yielded sizeable cardiac grafts, albeit in the subacute MI setting (Kawamura et al. 2016; Shiba et al. 2016). Drawing upon all the subacute MI studies (Kawamura et al. 2016; Shiba et al. 2016) and this work, species-matched cellular therapy appears to be beneficial for the infarcted heart.

Collectively, these observations are reassuring for the translation of human-derived cells for heart failure patients. Therefore, the only benefit that rat-ESC/IPSC CMs could offer is a higher-throughput study. If we are limited by imaging and EP studies in the rat model, perhaps going directly into a large animal model may be more fruitful instead.

6:1:4 Pre-clinical development of cellular therapy to regenerate the chronically infarcted heart

As for the next steps in translation and pre-clinical development of cellular therapy for clinics, we firstly need to interrogate the efficacy of Epi+CM cellular therapy in a pre-clinical large animal model, i.e., a pig or non-human primate heart failure model. The scientific insights to be gained from a large animal model are numerous; encompassing *in vivo* electromechanical integration studies (Chong et al. 2014; Liu et al. 2018; Romagnuolo et al. 2019), real-time region-specific cardiac functional studies, live-tracking of grafted cells (Ostrominski et al. 2020), detailing clinically relevant cellular dosages (Chong et al. 2014; Liu et al. 2018) and immunosuppressive regimen (Kawamura et al. 2016; Shiba et al. 2016), whilst trialling different strategies for cellular implantation, such as surgical open-heart approaches for direct intramyocardial injections or percutaneous angioplasty-guided cellular delivery via the femoral artery. On the practical clinical side, these insights would guide the planning and adaptation of current hospital infrastructure for cellular-treated patient pathways.

In the UK, only the TBRC (Translational Biomedical Research Centre, University of Bristol) could offer an all-encompassing service with large-scale cellular production with a bioreactor, large animal MRI, and a trained team of animal technicians to care

for the animals and assist in the cellular interventions. As discussed throughout this thesis, the chronic heart failure model is especially challenging, given the long timeframe required to observe any reversal of its pathophysiological remodelling. Nevertheless, a carefully planned, long-term large animal study with adequate funding is required, as the clinical need clearly outweighs the cost.

6:1:5 Anti-fibrotic therapies as an adjunct to cellular therapy for chronic heart failure

A potential challenge yet to be addressed is the amount of fibrosis in the heart failure setting. A fibrotic response following a myocardial infarction is necessary to prevent immediate cardiac rupture. However, the mammalian fibrotic response outlasts the acute phase of the myocardial infarction and is not cleared away (Frangogiannis and Kovacic 2020), unlike the zebrafish cardiac regenerative model (Wang et al. 2011, 2013; Kikuchi et al. 2011; Cao et al. 2017; Cao and Poss 2018). Persistent local and generalised myocardial fibrosis exacerbates cardiac dysfunction post-MI (Frangogiannis and Kovacic 2020) and likely to provide a physical impedance to our transplanted cells for graft-host integration.

Various anti-fibrotic therapies, ranging from cell-based to small molecules, are being trialled by different groups (Aghajanian et al. 2019; Chothani et al. 2019). Chothani *et al.* demonstrated the feasibility of central post-transcriptional regulation of cardiac fibrosis by RNA-binding proteins (Chothani et al. 2019). Aghajanian and colleagues utilized genetically engineered T-cells to recognize and 'eat-up' pathological cardiac fibrosis (Aghajanian et al. 2019). Invoking endogenous cardiomyocyte proliferation with microRNA cocktail appeared to attenuate the size of post-MI scar (Gabisonia et

al. 2019). A potential approach to tackle fibrosis is to employ both exogenous cellular therapies with ‘designer’ cells and endogenous cardiomyocyte proliferation to ‘bridge the fibrotic gap’. Despite the promises of cellular therapy and advances in cellular genetic modulation, a considerable distance is yet to be covered.

6:2 Elucidation of epicardial-FN’s role in epicardial-myocardial crosstalk

6:2:1 ‘Cardiac injury’ 3D-EHT models

My current 3D-EHTs model only confer a cardiac developmental context. To address this limitation, we could utilise a ‘cardiac injury’ model within 3D-EHTs. A ‘cardiac injury’ 3D-EHTs model could be established in two ways: i) ‘acute injury’ model could be induced by the addition of a cocktail of pro-inflammatory cytokines (e.g. IL-6, TNF-alpha) or ii) ‘chronic heart failure’ 3D-EHTs model driven by chronic catecholamine toxicity (Tiburcy et al. 2017). Both ‘cardiac injury’ 3D-EHT models would better simulate our heart failure animal model.

More importantly, the ‘cardiac injury’ 3D-EHTs model would enable a specific epicardial FN question to be answered, ‘Would epicardial FN still be beneficial in the injury setting?’ The FN has a contradictory role in cardiac development and disease (Schwarzbauer and DeSimone 2011; Wickström et al. 2011; Valiente-Alandi et al. 2018). Thus, one postulated that the injury-activated and developmental-activated pathways for epicardial-FN secretion and downstream action may be *distinct*.

Unlike the animal model, the ‘cardiac injury’ 3D-EHTs would be unencumbered by host immune cells infiltration. Any interrogation of the role of epicardial-FN would only be

contextualised within epicardial-myocardial crosstalk during injury. Thus, the 'cardiac injury' 3D-EHTs model represents a stepwise and high throughput manner of elucidating the role played by epicardial-FN within our cardiac grafts.

6:2:2 Does epicardial-FN promote angiogenesis?

3D-EHTs lack a vascular supply. To interrogate the role of epicardial-FN on angiogenesis, I would propose using the chick embryo chorioallantoic membrane model (Iyer et al. 2015; Bargehr et al. 2019). In our Epi+CM cardiac grafts, there were anecdotal observations of increased CD31+ve angiogenesis and FN deposition within similar coordinates on our rat heart sections. Furthermore, FN's role in angiogenesis is well-described (Astrof and Hynes 2009). Thus, one postulated that epicardial-FN was pro-angiogenic and led to the enhanced neovascularization observed in our epicardial-augmented cardiac grafts.

Examining this hypothesis *in ovo* by using our inducible KD-FN cell line co-cultured with hESC-CMs, with subsequent quantification of angiogenesis would grant further insights. If epicardial-FN is indeed pro-angiogenic, this would imply that epicardial-FN's benefits are not limited to hESC-cardiomyocyte maturation, i.e., epicardial-FN is multipotent.

6:2:3 Is the epicardial-FN secretion affected by epicardial heterogeneity?

Gambardella and colleagues have demonstrated that our hESC-epicardium is heterogeneous (Gambardella et al. 2019). hESC-epicardium is composed of two subpopulations with different cellular preponderances to differentiate into SMC or cardiac fibroblasts (Gambardella et al. 2019). The two subpopulations also

demonstrated major differences in GO (gene ontology) terms encompassing key processes, such as myogenesis, fibrosis and angiogenesis (Gambardella et al. 2019). The final cell fate adopted by our implanted epicardial cells could directly affect CM proliferation, tissue tension or vascularisation within our cardiac grafts, and thereby the degree of myocardial recovery in our infarcted rat hearts.

Thus, we would need to isolate the two subpopulations and determine the relative benefits of each subpopulation on hESC-CM maturation with the 3D-EHTs studies. Next, determining if epicardial-FN secretion is favoured by a particular subpopulation and whether epicardial-FN contributes to subpopulation crosstalk would be needed. Then, we would utilise a dual-reporter cell line to investigate the two subpopulations within our cardiac regenerative rodent studies. Collectively, these comprehensive experiments would offer greater clarity on the role of epicardial-FN, in the context of epicardium heterogeneity and cardiac regeneration.

6:2:4 Positioning epicardial-FN within the epicardial-myocardial crosstalk's genetic blueprint

FN is a ubiquitous protein secreted by many different cell types and interacts with various pathways (Schwarzbauer and DeSimone 2011). Whilst some insights were gained from using 3D-EHTs to study the loss of epicardial-FN in mediating epicardial-myocardial crosstalk, this was quite low-throughput from the mechanistic viewpoint.

A high-throughput CRISPR-cas9-mediated library screen of epicardial-myocardial co-cultures, focused on the role of epicardial-FN, could allow us to identify entire pathways regulated by epicardial-FN, together with specific interactions with CMs and downstream cellular functions. The CRISPR-cas9-mediated library screen could grant the resolution required to outline each step of the identified vital pathways. This

approach could be complemented by using RNAscope technology and spatial transcriptomics to study the epicardial-FN modulated key pathways *in vivo*. Altogether, this could yield a blueprint of epicardial-myocardial crosstalk, with emphasis on the role of epicardial-FN in epicardial-myocardial crosstalk.

As cardiac regeneration advances towards clinical translation, delineating the mechanistic underpinnings of epicardial-myocardial crosstalk is increasingly crucial. The need for mechanistic insights to be gained, in parallel with cardiac regeneration successes in pre-clinical animal models, cannot be overemphasised.

7. CONCLUSIONS

This doctoral work demonstrated that regenerating the chronically failing heart with CMs of the optimal maturity and similar species, delivered with an appropriate supportive stroma, was possible. Furthermore, I showed that epicardial-secreted fibronectin played a pivotal role in epicardial-myocardial crosstalk. Merging our understanding of the pathophysiological progression of the chronically infarcted heart and the role of hESC-epicardium is crucial, to cure chronic heart failure. Exogenous cardiac regeneration with cardiomyocyte-based cellular therapy still represents our best hope for the ideal heart failure treatment.

Moving forward, our collaborative efforts must focus on delineating the mechanistic underpinnings of epicardial-myocardial crosstalk, whilst translating these benefits into regenerating the chronically infarcted myocardium. Then, perhaps we are inching closer to clinical translation, safely and with care.

8. APPENDIX

8:1 Causes and timing of animal deaths within the chronic MI rodent study

	Animal Groups	Timing of Death (calculated as days from pre-injection ECHO Exclusion, which is D21 post-MI)	Cause of Death
1	Sham	D8	Intraoperative Death
2	NRVM	D81	Found dead in cage
3	NRVM	D35	Died during echocardiography
4	Epi+CM	D35	Euthanized due to drastic weight loss

Table 15: Causes of animal deaths

8:2 Histological and echocardiographic parameters in the chronic MI rodent study

Parameter	Sham	NRVM	Epi+CM
Histologic			
Infarct Area (%LV)	18.22±3.61	19.50±1.9	19.66±1.1
Echocardiography			
Fractional Shortening (%), D21 post-MI	28.12±3.6	18.15±1.2	21.66±1.1
Fractional Shortening (%), 1st month post-injection	27.01±3.1	22.89±4.2	14.85±1.6
Fractional Shortening (%), 2nd month post-injection	21.59±4.6	22.76±3.9	22.19±2.5
Fractional Shortening (%), 3rd month post-injection	18.18±2.3	22.38±3.6	19.0±1.2

Table 16: Histological and echocardiographic parameters

8:3 Practical details of the Cambridge set-up of cardiac regenerative rodent model

The Cambridge set-up was performed over 2 Phases with a modest improvement of animal survival over time, **Figure 76**. There were specific challenges in each phase, which I would discuss in turn, together with tried and tested solutions that worked locally. Finally, I would also discuss and address future solutions for ongoing challenges with this complex surgical animal model.

Broadly, the key procedural steps were divided into i) anaesthetic induction, intubation, and ventilation, ii) Operative Part 1- myocardial infarction and recovery, iii) Operative Part 2- intramyocardial cellular injections and recovery. These steps were discussed in detail in **Methods** and further illustrated below.

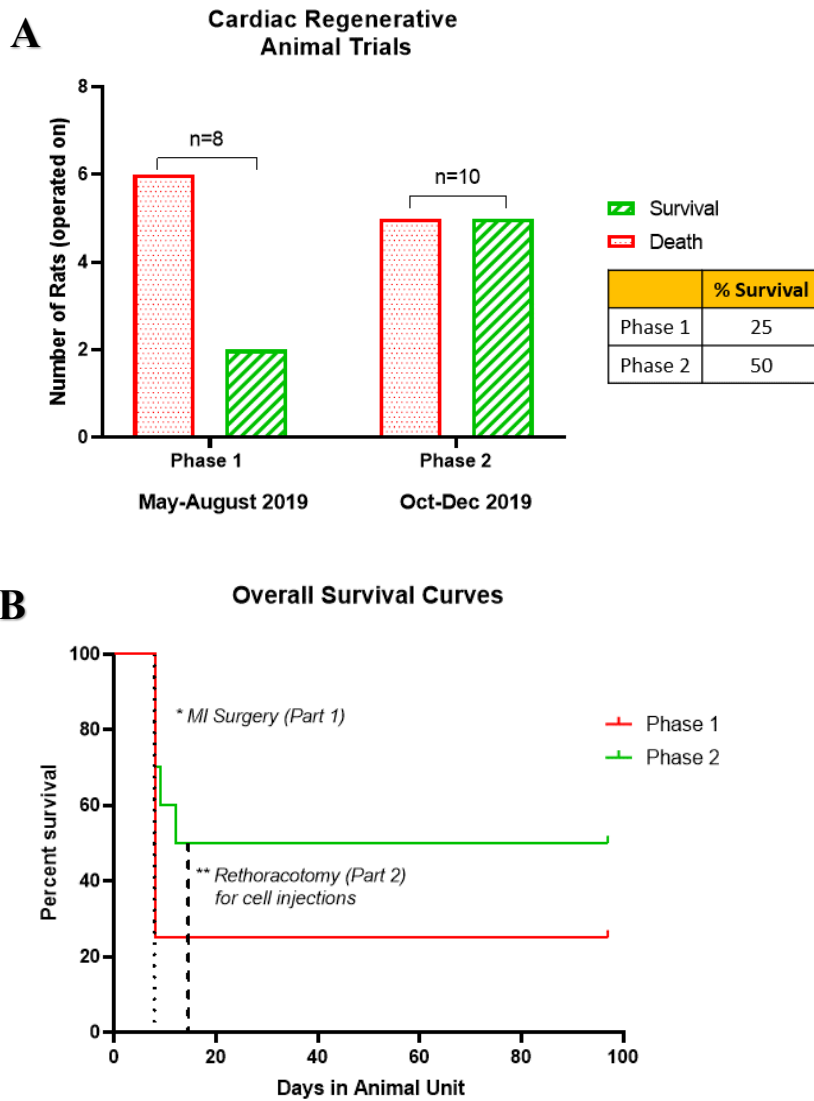


Figure 76: Overall survival with Cambridge set-up of the cardiac regenerative model

A Local set-up of the cardiac regenerative rat MI model was conducted over two periods, termed Phase 1 (May-August 2019) and Phase 2 (October-December 2019). **B** Procedural survival rate improved to 50% in Phase 2.

8:3:1 Phase 1 Rodent Studies

During the Phase 1 studies, our animal survival was dismal at 25%, and all deaths occurred peri-operatively **Figure 76**. The cause of death was predominantly due to anaesthetic and intubation concerns as listed below in **Table 17**.

Phase 1- Cause of Death	No. of animals
Failed Intubations due to lack of anaesthetic depth	2
Incorrect ET Tube positioning during thoracotomy	2
ET Tube dislodgement during chest closure	1
Intraoperative Arrhythmia	1

Table 17: Cause of death for individual rats in Phase 1

Of note, there were key differences between the local and our collaborator's anaesthetic regimen, intubation set-up and ventilator. **Figure 77** illustrated the key steps during anaesthetic induction and intubation. Firstly, the lack of pre-specified rodent intubation stands for optimal positioning made the vocal cords visualization more challenging, **Figure 77B**. Secondly, for the anaesthetic regimen, the local ketamine concentration was delivered in a pre-mix with xylazine. The ketamine and xylazine concentration were higher than our collaborator's lab. However, there was difficulty attaining the depth of anaesthesia required to visualise and stop vocal cords movements for direct endotracheal intubation, **Figure 77C&D**. Instead, there were repeated oropharyngeal intubations, leading to increasing hypoxia and subsequent animal death. Our local experience could be due to different UK/USA-specific commercial preparations of anaesthetic agents or delivery in pre-mix has affected its potency.

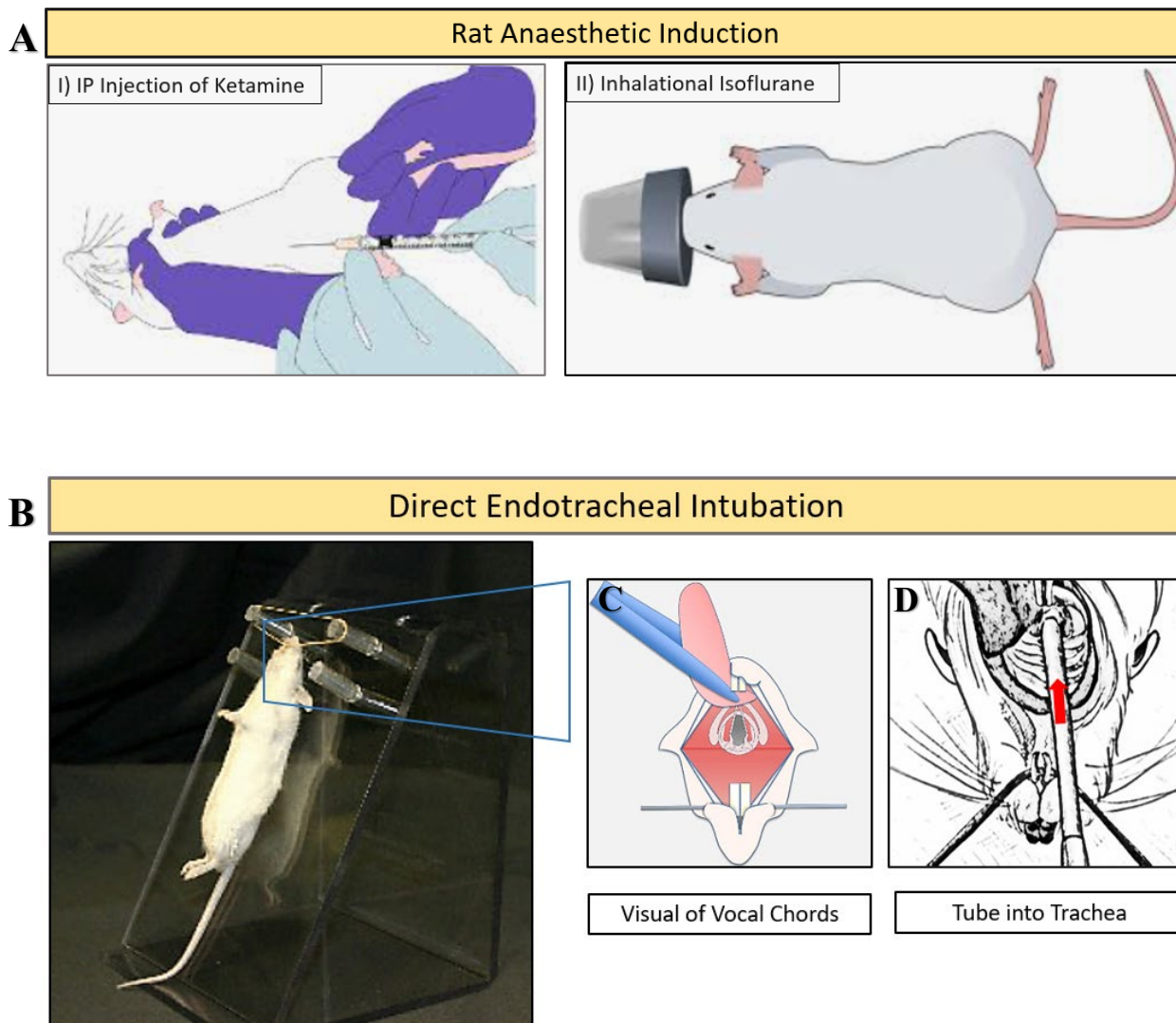


Figure 77: Optimization of anaesthetic induction and direct endotracheal intubation in rats

A The rat is initially induced with injectable anaesthetic agents, delivered via intraperitoneal injections. This is followed by short-burst of isoflurane-rich oxygenation via nose cone. **B** For the optimized intubation method, the anaesthetized rat is suspended from its front teeth, via a pre-specified intubation stand. This suspension enabled lengthening and straightening of the rat for **C** its vocal cords and trachea visualization. **D** Upon vocal cords visualisation, the endotracheal tube is introduced via a hollow metal tube (red arrow).

To balance the optimal anaesthetic depth for intubation and throughout the 90 mins surgical procedure, we reduced the local ketamine/xylazine dose whilst adding Buprenorphine pre-operatively to ensure sufficient analgesia throughout the procedure. Furthermore, we added Xylocaine spray orally after anaesthetic induction to stop vocal cords movements during intubation. Upon consulting with our London colleagues in Imperial College, we included a metal tube introducer within the endotracheal (ET) tube to enable better physical guidance and purchased a rodent-specific intubation stand. All these efforts led to consistently successful intubations, and we were able to proceed into surgery.

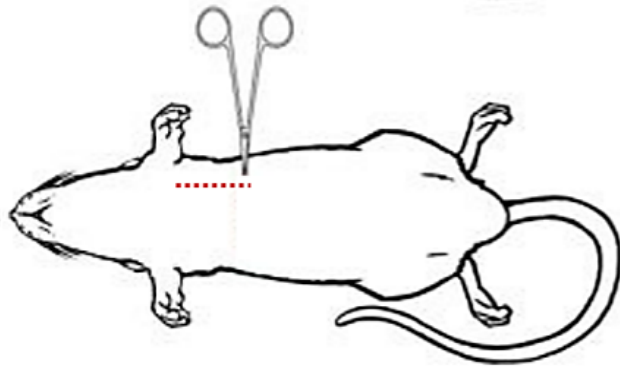
The next challenge after intubation was the malpositioning of the ET tube during surgery, leading to one-lung ventilation or complete dislodgement with subsequent hypoxic deaths. This is due to a lack of cuff around the ET tube to secure its position in the trachea, as expected in the clinical setting. To circumvent this, we purchased an oxygen monitoring device to enable rapid diagnosis of intraoperative hypoxia and correction of ET tube position. With all the new devices and adapted anaesthetic regime, we were able to proceed and complete the entire MI surgery.

The steps of MI surgery are as detailed in **Figure 78**. We opted for a left-lateral thoracotomy approach for better exposure of the left ventricle and clearing the tissue field for the second surgery, i.e., intramyocardial injections. The proximal LAD is often ligated during this procedure to enable a large anterolateral MI, but this could trigger a life-threatening arrhythmic event; similar to clinical observations. Thus, we had one sudden cardiac death at the completion of the surgery, attributable to MI-related arrhythmia. Arrhythmias was partly attenuated by the delivery of our local anaesthetic block, a mixture of lidocaine/bupivacaine. By the end of Phase 1, we had solved the anaesthetic, intubation, and intra-operative monitoring challenges.

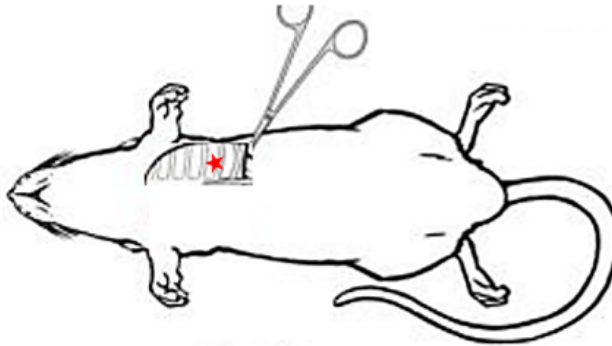
A

Intraoperative Part 1: LAD Ligation for MI

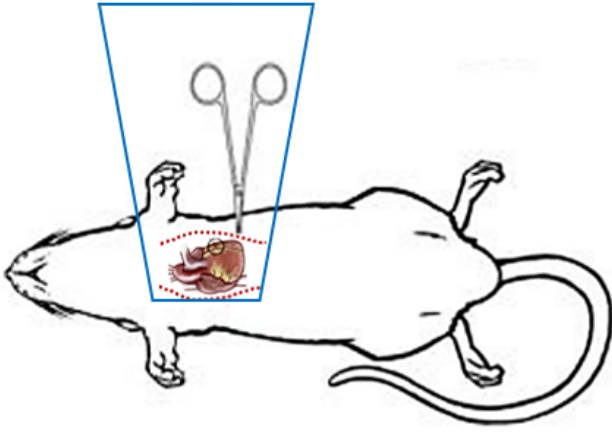
i) Left Lateral
Thoracotomy



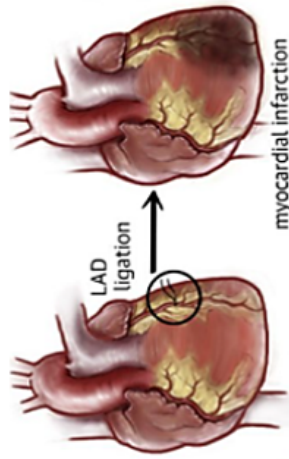
ii) Rib Incision at 4th
intercostal space



iii) Visualization
of the heart



iv) Left anterior descending artery
(LAD) ligation for 60 mins ischaemic-
reperfusion (I/R) injury



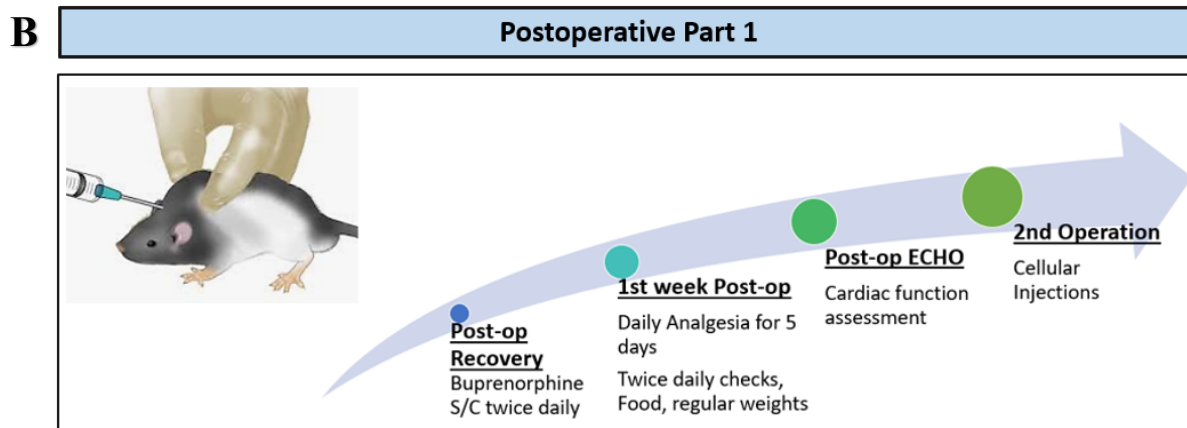


Figure 78: Step-by-step procedure for invoking myocardial infarction in rats

A The anaesthetized and intubated rat is positioned on its back for subsequent surgeries. There is a total of 4 steps for invoking MI; i) left lateral skin incision to visualise the ribcage ii) 3rd or 4th rib incision to gain access into the thoracic cavity, iii) pericardium is then clear to enable visualization of the left ventricle and the LAD and iv) proximal LAD is ligated to simulate MI. LV blanching is observed throughout the 60 min I/R injury. The chest is closed. **B** The rat is subsequently recovered with the listed post-operative observations, analgesia regimen and study protocol.

8:3:2 Phase 2 Rodent Studies

In Phase 2, we observed a doubling in our rodent survival to 50%, as shown above in **Figure 76**. Given the key technical tweaks that were discussed above, we were able to proceed into surgeries with all our animals. However, the new cause-of-deaths were now predominantly due to post-operative recovery and further arrhythmias as listed below in **Table 18**.

Phase 2 Cause of Death	No. of animals
Surgical emphysema due to Direct lung injury	1
Early Post-operative acute respiratory distress (Scheduled Euthanasia)	2
Immediate Post-operative arrhythmia	2

Table 18: Individual rat's cause of death during Phase 2

I will further discuss each cause of death in detail and outline solutions. One animal had direct lung injury during thoracotomy with widespread surgical emphysema. Subsequently, he was euthanised. This incidence was likely due to anatomical differences, and to circumvent this; we temporarily halted ventilation during thoracotomy for future surgeries. With this technical change, we continued successfully into full surgeries with animal survival.

Subsequently, we had two animals demonstrating acute respiratory distress in the early days post-operatively. They were cyanotic and gasping for breath. Upon closer visualisation, the wound was clean, and all respiratory movements were equal. As stated in our animal study plan, we proceeded into euthanasia for animal distress. For one animal which developed acute respiratory distress four days after the surgery, there were no signs of tamponade, but bilateral atelectasis was observed during post-mortem. Tamponade is bleeding within the pericardial cavity, causing heart compression and pump failure. Atelectasis describes the collapse of lung alveoli due to the lack of local inspiration. Thus, acute respiratory distress is likely due to atelectasis secondary to post-operative pain.

For subsequent surgeries, we doubled the post-operative buprenorphine dose and increased the duration of administration to 5 days, after consultation with our local veterinarian. Following the changes in postoperative analgesic regimen, we

proceeded into successful MI surgeries with an uneventful postoperative period with other animals.

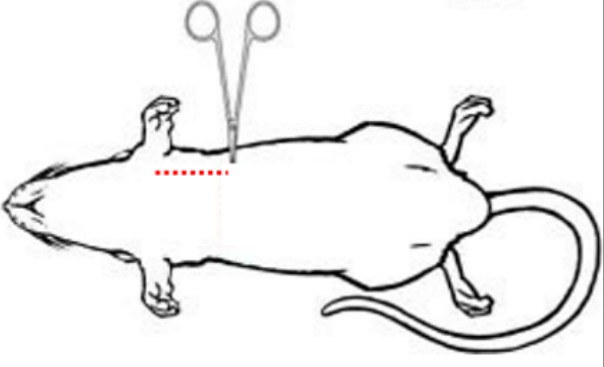
In another animal with acute respiratory distress on postoperative day 1, there was clear haemothorax with lung collapse upon post-mortem. The haemothorax was likely due to bleeding from neurovascular bundle underlining the rib, which was incised during thoracotomy. Due to the need to have a large field of entry for intramyocardial cellular injections, we need to adhere to the rib incisions. To reduce postoperative bleeding, we ensured better rib approximation during thoracotomy closure with double sutures within the intercostal space. This will prevent any dislodgement from the rodent's active movements. Stable rib approximation will lead to faster healing and prevent any aberrant rib vessel from bleeding with the resulting haemothorax.

With subsequent surgeries, we completed both MI and intramyocardial cellular injections (Sham-Matrigel) for five animals who survived till their study endpoint. Step-by-step of Operative Part 2: intramyocardial cellular injections are as listed in **Figure 79**. Overall, our Phase 2 studies had shown considerable progress in establishing the cardiac regenerative MI rodent model in Cambridge.

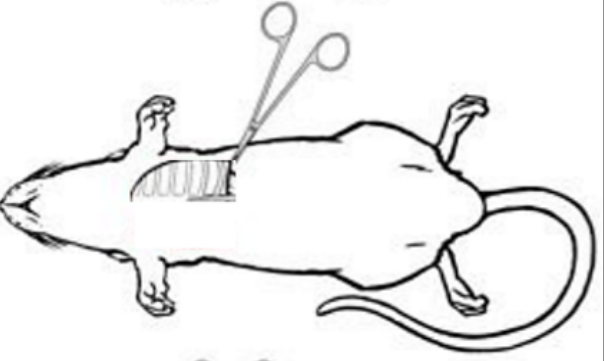
A

Intraoperative Part 2: Intramyocardial Cellular Injections

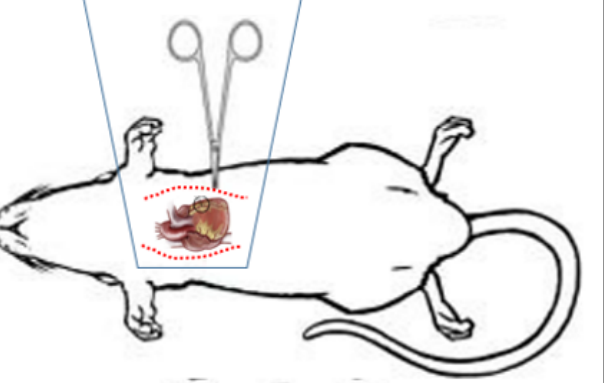
i) Left Lateral Thoracotomy



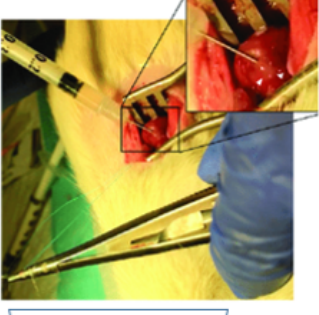
ii) Rib Incision at 4th intercostal space



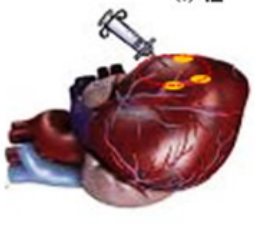
iii) Visualization of the heart



iv) Stabilization of LV Apex for injections



v) Intramyocardial injections in LV infarct & border zones



3 x 33ul injections

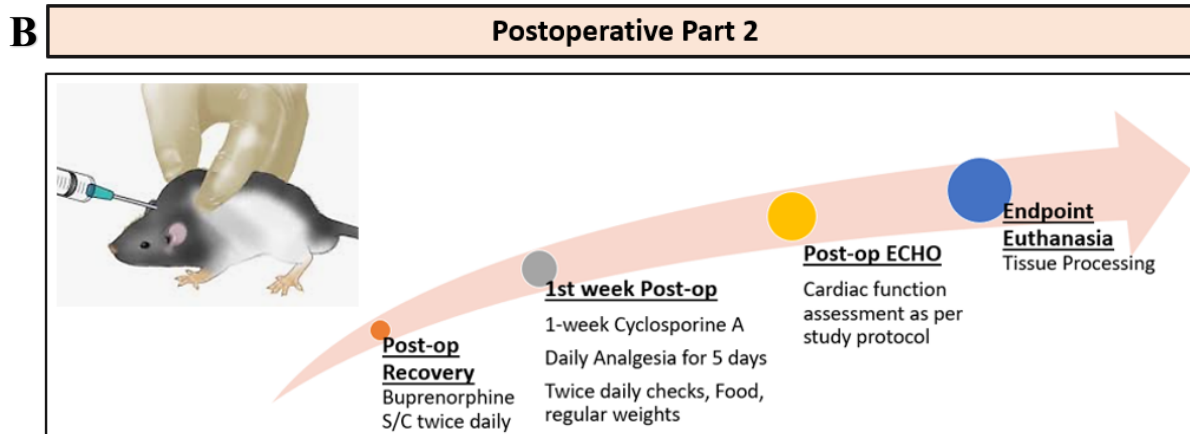


Figure 79: Step-by-step protocol for intramyocardial cellular injections in rats

A For the second surgery, the anaesthetized and intubated rat is positioned on its back for subsequent surgeries. There is a total of 5 steps for cellular delivery via intramyocardial cellular injections; i) left lateral skin incision to visualise the ribcage ii) 3rd or 4th rib incision to gain access into the thoracic cavity. iii) The pericardium and adhesions are then cleared to enable visualization of the infarcted left ventricle and apex. iv) The LV apex is stabilised for subsequent v) intramyocardial cellular injections in 3 areas- infarct and border zones. Haemostasis and the chest is closed. **B** The rat is subsequently recovered with the listed post-operative observations, analgesia regimen and study protocol.

8:3:3 Considerations for future cardiac regenerative rat studies

Following all the local adaptations with the anaesthetic regimen, intubation, ventilation, intra-operative measures, and postoperative analgesia, we still observed occasional sudden cardiac deaths. This is likely due to arrhythmias, a life-threatening event. Unfortunately, due to the nature of our disease model, this is an unavoidable consequence. One future option would be to insert 12-lead ECG into our rodent models. This would enable us to pinpoint and quantify the arrhythmic events with greater accuracy. Although we were unlikely to successfully treat or prevent it within the rodent setting, it is a worthwhile biological observation, given that hESC/IPSC-derived cell therapy is associated with tachyarrhythmias (Chong et al. 2014; Liu et al. 2018). An animal model would not only enable us to test the efficacy of stem cell therapy but also offer new biological insights into cell behaviour *in vivo*, over time. Thus, all procedural steps need to be streamlined and optimised during an animal model to ensure that our future experimentations are robust. Despite the sizeable challenges in local technical transfer, it was undoubtedly a worthwhile pursuit.

8:4 Interactome map of epicardial-FN with CM

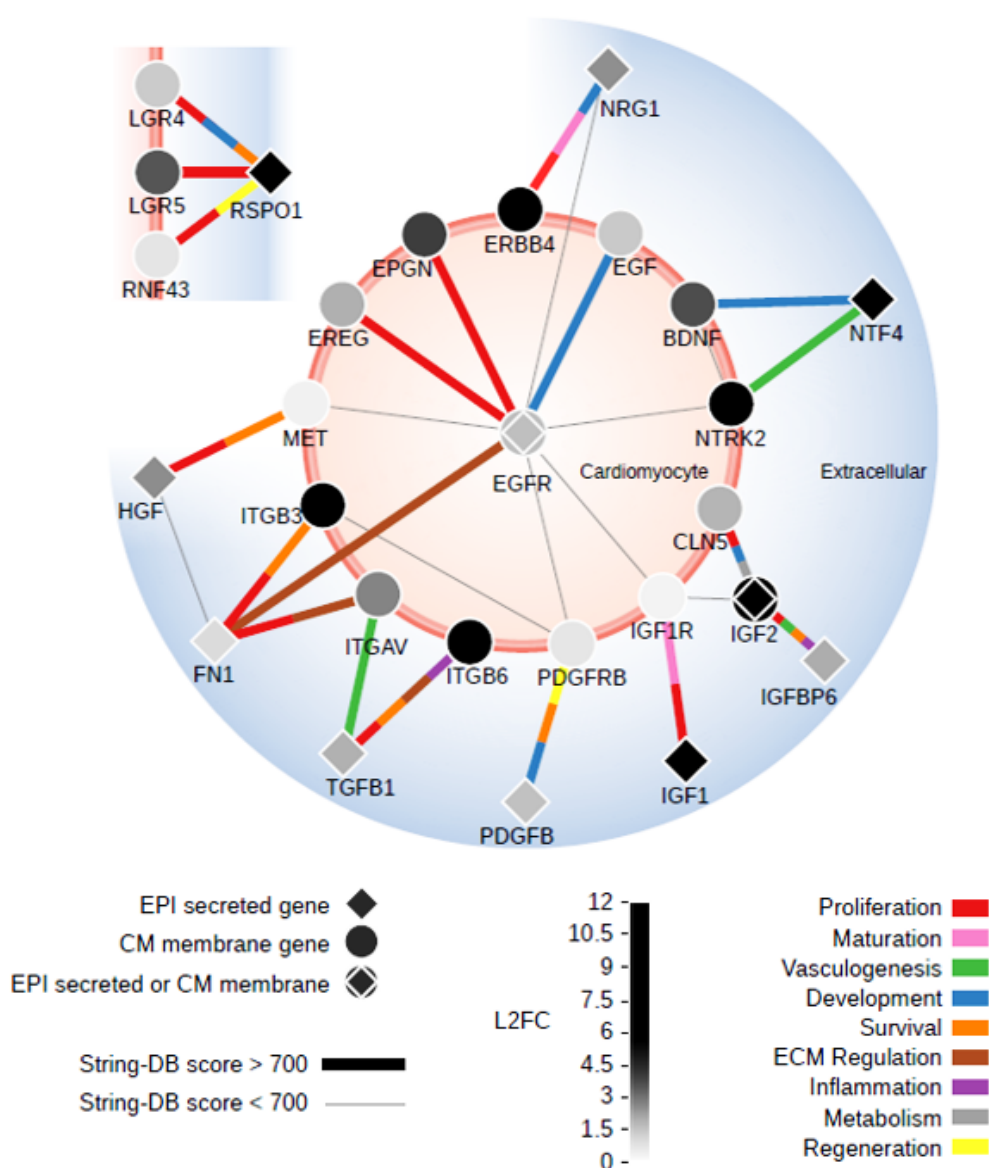


Figure 80: Map of the interactome between epicardial-FN and hESC-CMs

Based on single-cell sequencing data, the Sinha lab produced a map of the interactome between hESC-epicardium and hESC-CMs to elucidate the epicardial-myocardial crosstalk. *FN1* expressed by the epicardium interacted with several CM membrane genes (*ITGB3*, *ITGAV*), a soluble factor (*HGF*) and a receptor tyrosine kinase of the ErbB family (*EGFR*). These interactions appeared to directly affect numerous cellular biological processes such as survival, proliferation, and ECM regulation. (With thanks to Dr. Bargehr & Dr. Knight-Schrijver, manuscript in preparation).

9. REFERENCES

- Abu-Issa, Radwan, and Margaret L. Kirby. 2007. "Heart Field: From Mesoderm to Heart Tube." *Annual Review of Cell and Developmental Biology* 23: 45–68.
<https://doi.org/10.1146/annurev.cellbio.23.090506.123331>.
- Acharya, Asha, Seung Tae Baek, Guo Huang, Banu Eskiocak, Sean Goetsch, Caroline Y. Sung, Serena Banfi, et al. 2012. "The BHLH Transcription Factor Tcf21 Is Required for Lineagespecific EMT of Cardiac Fibroblast Progenitors." *Development (Cambridge)* 139 (12): 2139–49. <https://doi.org/10.1242/dev.079970>.
- Aghajanian, Haig, Toru Kimura, Joel G. Rurik, Aidan S. Hancock, Michael S. Leibowitz, Li Li, John Scholler, et al. 2019. "Targeting Cardiac Fibrosis with Engineered T Cells." *Nature* 573 (7774): 430–33. <https://doi.org/10.1038/s41586-019-1546-z>.
- Ali, Shah R., Sara Ranjbarvaziri, Mahmood Talkhabi, Peng Zhao, Ali Subat, Armin Hojjat, Paniz Kamran, et al. 2014. "Developmental Heterogeneity of Cardiac Fibroblasts Does Not Predict Pathological Proliferation and Activation." *Circulation Research* 115 (7): 625–35. <https://doi.org/10.1161/CIRCRESAHA.115.303794>.
- Ardehali, Hossein, and Brian O'Rourke. 2005. "Mitochondrial KATP Channels in Cell Survival and Death." *Journal of Molecular and Cellular Cardiology* 39 (1): 7–16.
<https://doi.org/10.1016/j.yjmcc.2004.12.003>.
- Arnold, Sebastian J., and Elizabeth J. Robertson. 2009. "Making a Commitment: Cell Lineage Allocation and Axis Patterning in the Early Mouse Embryo." *Nature Reviews Molecular Cell Biology* 10 (2): 91–103. <https://doi.org/10.1038/nrm2618>.
- Arslan, Fatih, Mirjam B. Smeets, Paul W. Riem Vis, Jacco C. Karper, Paul H. Quax, Lennart G. Bongartz, John H. Peters, et al. 2011. "Lack of Fibronectin-EDA Promotes Survival and Prevents Adverse Remodeling and Heart Function Deterioration after Myocardial Infarction." *Circulation Research* 108 (5): 582–92.
<https://doi.org/10.1161/CIRCRESAHA.110.224428>.
- Askoxylakis, Vasileios, Christian Thieke, Sven T Pleger, Patrick Most, Judith Tanner, Katja Lindel, Hugo A Katus, Jürgen Debus, and Marc Bischof. 2010. "Long-Term Survival of Cancer Patients Compared to Heart Failure and Stroke: A Systematic Review."
<http://www.biomedcentral.com/1471-2407/10/105>.

- Astrof, Sophie, Denise Crowley, and Richard O. Hynes. 2007. "Multiple Cardiovascular Defects Caused by the Absence of Alternatively Spliced Segments of Fibronectin." *Developmental Biology* 311 (1): 11–24. <https://doi.org/10.1016/j.ydbio.2007.07.005>.
- Astrof, Sophie, and Richard O Hynes. 2009. "Fibronectins in Vascular Morphogenesis." *Angiogenesis*. <https://doi.org/10.1007/s10456-009-9136-6>.
- Baehr, Andrea, Kfir Baruch Umansky, Elad Bassat, Victoria Jurisch, Katharina Klett, Tarik Bozoglu, Nadja Hornaschewitz, et al. 2020. "Agrin Promotes Coordinated Therapeutic Processes Leading to Improved Cardiac Repair in Pigs." *Circulation* 142 (9): 868–81. <https://doi.org/10.1161/CIRCULATIONAHA.119.045116>.
- Baines, Christopher P., Robert A. Kaiser, Nicole H. Purcell, Scott N. Blair, Hanna Osinska, Michael A. Hambleton, Eric W. Brunshill, Jeffrey Robbins, and Jeffery D Molkentin. 2004. "Mitochondrial Permeability: Dual Role for the ADP/ATP Translocator?" *Nature* 430 (7003): 626–29. <https://doi.org/10.1038/nature02816>.
- Balsam, Leora B, Amy J Wagers, Julie L Christensen, Kofidis T, Weissman Irving L, and Robert C Robbins. 2004. "Haematopoietic Stem Cells Adopt Mature Haematopoietic Fates in Ischaemic Myocardium" 428 (April): 668–73. <https://doi.org/10.1038/nature02446>.Published.
- Banerjee, Monisha N., Roberto Bolli, and Joshua M. Hare. 2018. "Clinical Studies of Cell Therapy in Cardiovascular Medicine Recent Developments and Future Directions." *Circulation Research* 123 (2): 266–87. <https://doi.org/10.1161/CIRCRESAHA.118.311217>.
- Barbero, Cristina, Antonio Ravaglioli, Aravinda A. Page, Graham A. Betts, Stephen M. Fakelman, Evgeny Pavlushkov, Simon Messer, Barbora Parizkova, Marius Berman, and Steven Tsui. 2019. "Retrieval Team-Initiated Early Donor Management Increases the Donor Heart Utilization Rate for Transplantation." *European Journal of Cardio-Thoracic Surgery* 55 (3): 468–75. <https://doi.org/10.1093/ejcts/ezy293>.
- Bargehr, J., L.P. P Ong, M. Colzani, H. Davaapil, P. Hofsteen, S. Bhandari, L. Gambardella, et al. 2019. "Epicardial Cells Derived from Human Embryonic Stem Cells Augment Cardiomyocyte-Driven Heart Regeneration." *Nat Biotechnol* 37 (8): 895–906. <https://doi.org/10.1038/s41587-019-0197-9>.
- Bassat, Elad, Yara Eid Mutlak, Alex Genzelinakh, Ilya Y. Shadrin, Kfir Baruch Umansky, Oren Yifa, David Kain, et al. 2017. "The Extracellular Matrix Protein Agrin Promotes

- Heart Regeneration in Mice." *Nature* 547 (7662): 179–84.
<https://doi.org/10.1038/nature22978>.
- Bearzi, Claudia, Marcello Rota, Toru Hosoda, Jochen Tillmanns, Angelo Nascimbene, Antonella De Angelis, Saori Yasuzawa-Amano, et al. 2007. "Human Cardiac Stem Cells." *Proceedings of the National Academy of Sciences of the United States of America* 104 (35): 14068–73. <https://doi.org/10.1073/pnas.0706760104>.
- Beltrami, Antonio P., Laura Barlucchi, Daniele Torella, Mathue Baker, Federica Limana, Stefano Chimenti, Hideko Kasahara, et al. 2003. "Adult Cardiac Stem Cells Are Multipotent and Support Myocardial Regeneration." *Cell* 114 (6): 763–76.
[https://doi.org/10.1016/S0092-8674\(03\)00687-1](https://doi.org/10.1016/S0092-8674(03)00687-1).
- Benjamin, Emelia J., Paul Muntner, Alvaro Alonso, Marcio S. Bittencourt, Clifton W. Callaway, April P. Carson, Alanna M. Chamberlain, et al. 2019. *Heart Disease and Stroke Statistics-2019 Update: A Report From the American Heart Association. Circulation*. Vol. 139. <https://doi.org/10.1161/CIR.0000000000000659>.
- Bergmann, Olaf, Ratan D. Bhardwaj, Samuel Bernard, Sofia Zdunek, Fanie Barnabé-Heide, Stuart Walsh, Joel Zupicich, et al. 2009. "Evidence for Cardiomyocyte Renewal in Humans." *Science* 324 (5923): 98–102. <https://doi.org/10.1126/science.1164680>.
- Berlo, Jop H. Van, Onur Kanisicak, Marjorie Maillet, Ronald J. Vagnozzi, Jason Karch, Suh Chin J. Lin, Ryan C. Middleton, Eduardo Marbán, and Jeffery D. Molkentin. 2014. "C-Kit+ Cells Minimally Contribute Cardiomyocytes to the Heart." *Nature* 509 (7500): 337–41. <https://doi.org/10.1038/nature13309>.
- Bers, Donald M. 2002. "Cardiac Excitation–Contraction Coupling." *Nature* 415 (6868): 198–205. <https://doi.org/10.1038/415198a>.
- Bertero, Alessandro, and Charles E. Murry. 2018. "Hallmarks of Cardiac Regeneration." *Nature Reviews Cardiology* 15 (10): 579–80. <https://doi.org/10.1038/s41569-018-0079-8>.
- Bertero, Alessandro, Matthias Pawlowski, Daniel Ortmann, Kirsten Snijders, Loukia Yiangou, Miguel Cardoso De Brito, Stephanie Brown, et al. 2016. "Optimized Inducible ShRNA and CRISPR/Cas9 Platforms for in Vitro Studies of Human Development Using HPSCs." *Development (Cambridge)* 143 (23): 4405–18.
<https://doi.org/10.1242/dev.138081>.
- Bhan, Amit, Alexander Sirker, Juqian Zhang, Andrea Protti, Norman Catibog, William Driver,

- Rene Botnar, et al. 2014. "High-Frequency Speckle Tracking Echocardiography in the Assessment of Left Ventricular Function and Remodeling after Murine Myocardial Infarction." *Am J Physiol Heart Circ Physiol* 306: 1371–83.
<https://doi.org/10.1152/ajpheart.00553.2013>.-The.
- Bondue, Antoine, Gaëlle Lapouge, Catherine Paulissen, Claudio Semeraro, Michelina Iacovino, Michael Kyba, and Cédric Blanpain. 2008. "Mesp1 Acts as a Master Regulator of Multipotent Cardiovascular Progenitor Specification." *Cell Stem Cell* 3 (1): 69–84. <https://doi.org/10.1016/j.stem.2008.06.009>.
- Brennan, Jane, Cindy C. Lu, Dominic P. Norris, Tristan A. Rodriguez, Rosa S.P. Beddington, and Elizabeth J. Robertson. 2001. "Nodal Signalling in the Epiblast Patterns the Early Mouse Embryo." *Nature* 411 (6840): 965–69. <https://doi.org/10.1038/35082103>.
- Brignole, Michele, Angelo Auricchio, Gonzalo Baron-Esquivias, Pierre Bordachar, Giuseppe Boriani, Ole A. Breithardt, John Cleland, et al. 2013. "213 ESC Guidelines on Cardiac Pacing and Cardiac Resynchronization Therapy." *European Heart Journal* 34 (29): 2281–2329. <https://doi.org/10.1093/eurheartj/eh150>.
- Broyles, Connor, Paul Robinson, and Matthew Daniels. 2018. "Fluorescent, Bioluminescent, and Optogenetic Approaches to Study Excitable Physiology in the Single Cardiomyocyte." *Cells* 7 (6): 51. <https://doi.org/10.3390/cells7060051>.
- Bryant, Donald Marion, Caitlin Claire O'Meara, Nhi Ngoc Ho, Joseph Gannon, Lei Cai, and Richard Theodore Lee. 2015. "A Systematic Analysis of Neonatal Mouse Heart Regeneration after Apical Resection." *Journal of Molecular and Cellular Cardiology* 79: 315–18. <https://doi.org/10.1016/j.yjmcc.2014.12.011>.
- Bui, Anh, L, B Horwish, Tamara, and C Fonarow, Gregg. 2012. "Epidemiology and Risk Profile of Heart Failure." *Nature Publishing Group* 8 (1): 1–25.
<https://doi.org/10.1038/nrcardio.2010.165>.Epidemiology.
- Burrige, Paul W., Gordon Keller, Joseph D. Gold, and Joseph C. Wu. 2012. "Production of de Novo Cardiomyocytes: Human Pluripotent Stem Cell Differentiation and Direct Reprogramming." *Cell Stem Cell* 10 (1): 16–28.
<https://doi.org/10.1016/j.stem.2011.12.013>.
- Bywater, Megan J., Deborah L. Burkhart, Jasmin Straube, Arianna Sabò, Vera Pendino, James E. Hudson, Gregory A. Quaife-Ryan, et al. 2020. "Reactivation of Myc Transcription in the Mouse Heart Unlocks Its Proliferative Capacity." *Nature*

Communications 11 (1). <https://doi.org/10.1038/s41467-020-15552-x>.

Cai, Chen-Leng Leng, Jody C. Martin, Yunfu Sun, Li Cui, Lianchun Wang, Kunfu Ouyang, Lei Yang, et al. 2008. "A Myocardial Lineage Derives from Tbx18 Epicardial Cells." *Nature* 454 (7200): 104–8. <https://doi.org/10.1038/nature06969>.

Cao, Guodong, Wei Pei, Hailiang Ge, Qinhua Liang, Yumin Luo, Frank R. Sharp, Aigang Lu, Ruiqiong Ran, Steven H. Graham, and Jun Chen. 2002. "In Vivo Delivery of a Bcl-XL Fusion Protein Containing the TAT Protein Transduction Domain Protects against Ischemic Brain Injury and Neuronal Apoptosis." *Journal of Neuroscience* 22 (13): 5423–31. <https://doi.org/10.1523/jneurosci.22-13-05423.2002>.

Cao, Jingli, Adam Navis, Ben D. Cox, Amy L. Dickson, Matthew Gemberling, Ravi Karra, Michel Bagnat, and Kenneth D. Poss. 2016. "Single Epicardial Cell Transcriptome Sequencing Identifies Caveolin 1 as an Essential Factor in Zebrafish Heart Regeneration." *Development (Cambridge)* 143 (2): 232–43. <https://doi.org/10.1242/dev.130534>.

Cao, Jingli, and Kenneth D. Poss. 2018. *The Epicardium as a Hub for Heart Regeneration*. *Nature Reviews Cardiology*. Vol. 15. Springer US. <https://doi.org/10.1038/s41569-018-0046-4>.

Cao, Jingli, Jinhu Wang, Christopher P. Jackman, Amanda H. Cox, Michael A. Trembley, Joseph J. Balowski, Ben D. Cox, et al. 2017. "Tension Creates an Endoreplication Wavefront That Leads Regeneration of Epicardial Tissue." *Developmental Cell* 42 (6): 600-615.e4. <https://doi.org/10.1016/j.devcel.2017.08.024>.

Cao, Yingxi, and Jingli Cao. n.d. "Covering and Re-Covering the Heart: Development and Regeneration of the Epicardium." <https://doi.org/10.3390/jcdd6010003>.

Carmona, R., J. A. Guadix, E. Cano, A. Ruiz-Villalba, V. Portillo-Sánchez, J. M. Pérez-Pomares, and R. Muñoz-Chápuli. 2010. "The Embryonic Epicardium: An Essential Element of Cardiac Development." *Journal of Cellular and Molecular Medicine* 14 (8): 2066–72. <https://doi.org/10.1111/j.1582-4934.2010.01088.x>.

Carmona, Rita, Silvia Barrena, Antonio Jesús López Gambero, Anabel Rojas, and Ramón Muñoz-Chápuli. 2020. "Epicardial Cell Lineages and the Origin of the Coronary Endothelium." *FASEB Journal* 34 (4): 5223–39. <https://doi.org/10.1096/fj.201902249RR>.

Caspi, Oren, Irit Huber, Izhak Kehat, Manhal Habib, Gil Arbel, Amira Gepstein, Lior

- Yankelson, Doron Aronson, Rafael Beyar, and Lior Gepstein. 2007. "Transplantation of Human Embryonic Stem Cell-Derived Cardiomyocytes Improves Myocardial Performance in Infarcted Rat Hearts." *J Am Coll Cardiol* 50 (19): 1884–93. <https://doi.org/10.1016/j.jacc.2007.07.054>.
- Chablais, Fabian, and Anna Jaźwińska. 2012. "The Regenerative Capacity of the Zebrafish Heart Is Dependent on TGF β Signaling." *Development* 139 (11): 1921–30. <https://doi.org/10.1242/dev.078543>.
- Chen, Jenny X, Markus Krane, Marcus-Andre Deutsch, Li Wang, Moshe Rav-Acha, Serge Gregoire, Marc C Engels, et al. 2012. "Cellular Biology Inefficient Reprogramming of Fibroblasts into Cardiomyocytes Using Gata4, Mef2c, and Tbx5 Short Communication." <https://doi.org/10.1161/CIRCRESAHA.112>.
- Chen, Jiqui, Elie R. Chemaly, Li Fan Liang, Thomas J. la Rocca, Elisa Yaniz-Galende, and Roger J. Hajjar. 2011. "A New Model of Congestive Heart Failure in Rats." *American Journal of Physiology - Heart and Circulatory Physiology* 301 (3): 994–1003. <https://doi.org/10.1152/ajpheart.00245.2011>.
- Chen, Shao Liang, Wu Wang Fang, Fei Ye, Yu Hao Liu, Jun Qian, Shou Jie Shan, Jun Jie Zhang, et al. 2004. "Effect on Left Ventricular Function of Intracoronary Transplantation of Autologous Bone Marrow Mesenchymal Stem Cell in Patients with Acute Myocardial Infarction." *American Journal of Cardiology* 94 (1): 92–95. <https://doi.org/10.1016/j.amjcard.2004.03.034>.
- Chen, Tim H.P., Tsai Ching Chang, Ji One Kang, Bibha Choudhary, Takako Makita, Chanh M. Tran, John B.E. Burch, Hoda Eid, and Henry M. Sucov. 2002. "Epicardial Induction of Fetal Cardiomyocyte Proliferation via a Retinoic Acid-Inducible Trophic Factor." *Developmental Biology* 250 (1): 198–207. <https://doi.org/10.1006/dbio.2002.0796>.
- Chen, William C.W., Zhouguang Wang, Maria Azzurra Missinato, Dae Woo Park, Daniel Ward Long, Heng Jui Liu, Xuemei Zeng, Nathan A. Yates, Kang Kim, and Yadong Wang. 2016. "Decellularized Zebrafish Cardiac Extracellular Matrix Induces Mammalian Heart Regeneration." *Science Advances* 2 (11). <https://doi.org/10.1126/sciadv.1600844>.
- Cheng, Paul, Peter Andersen, David Hassel, Bogac L. Kaynak, Patraranee Limphong, Lonny Juergensen, Chulan Kwon, and Deepak Srivastava. 2013. "Fibronectin Mediates Mesendodermal Cell Fate Decisions." *Development (Cambridge)* 140 (12): 2587–96. <https://doi.org/10.1242/dev.089052>.

- Cheung, Christine, Andreia S Bernardo, Matthew W B Trotter, and Roger A Pedersen. 2012. "Generation of Human Vascular Smooth Muscle Subtypes Provides Insight into Embryological Origin-Dependent Disease Susceptibility" 30 (2): 165–73. <https://doi.org/10.1038/nbt.2107.Generation>.
- Chien, Kenneth R., Jonas Frisén, Regina Fritsche-Danielson, Douglas A. Melton, Charles E. Murry, and Irving L. Weissman. 2019. "Regenerating the Field of Cardiovascular Cell Therapy." *Nature Biotechnology* 37 (3): 232–37. <https://doi.org/10.1038/s41587-019-0042-1>.
- Cho, Gun Sik, Dong I. Lee, Emmanouil Tampakakis, Sean Murphy, Peter Andersen, Hideki Uosaki, Stephen Chelko, et al. 2017. "Neonatal Transplantation Confers Maturation of PSC-Derived Cardiomyocytes Conducive to Modeling Cardiomyopathy." *Cell Reports* 18 (2): 571–82. <https://doi.org/10.1016/j.celrep.2016.12.040>.
- Choi, Wen Yee, Matthew Gemberling, Jinhu Wang, Jennifer E. Holdway, Meng Chieh Shen, Rolf O. Karlstrom, and Kenneth D. Poss. 2013. "In Vivo Monitoring of Cardiomyocyte Proliferation to Identify Chemical Modifiers of Heart Regeneration." *Development (Cambridge)* 140 (3): 660–66. <https://doi.org/10.1242/dev.088526>.
- Chong, James JH, Xiulan Yang, Creighton W. Don, Elina Minami, Yen-Wen Liu, Jill J Weyers, William M. Mahoney, et al. 2014. "Human Embryonic Stem Cell-Derived Cardiomyocytes Regenerate Non-Human Primate Hearts." *Nature* 510 (7504): 273–77. <https://doi.org/10.1038/nature13233.Human>.
- Chothani, Sonia, Sebastian Schäfer, Eleonora Adami, Sivakumar Viswanathan, Anissa A. Widjaja, Sarah R. Langley, Jessie Tan, et al. 2019. "Widespread Translational Control of Fibrosis in the Human Heart by RNA-Binding Proteins." *Circulation* 140 (11): 937–51. <https://doi.org/10.1161/CIRCULATIONAHA.119.039596>.
- Christoffels, Vincent M., Thomas Grieskamp, Julia Norden, Mathilda T.M. Mommersteeg, Carsten Rudat, and Andreas Kispert. 2009. "Tbx18 and the Fate of Epicardial Progenitors." *Nature* 458 (7240): 2008–10. <https://doi.org/10.1038/nature07916>.
- Ciruna, Brian, and Janet Rossant. 2001. "FGF Signaling Regulates Mesoderm Cell Fate Specification and Morphogenetic Movement at the Primitive Streak." *Developmental Cell* 1 (1): 37–49. [https://doi.org/10.1016/S1534-5807\(01\)00017-X](https://doi.org/10.1016/S1534-5807(01)00017-X).
- Cleland, John G.F., Nick Freemantle, Erland Erdmann, Daniel Gras, Lukas Kappenberger, Luigi Tavazzi, and Jean Claude Daubert. 2012. "Long-Term Mortality with Cardiac

Resynchronization Therapy in the Cardiac Resynchronization-Heart Failure (CARE-HF) Trial.” *European Journal of Heart Failure* 14 (6): 628–34.
<https://doi.org/10.1093/eurjhf/hfs055>.

Conlon, Frank L., Karen M. Lyons, Norma Takaesu, Katrin S. Barth, Andreas Kispert, Bernhard Herrmann, and Elizabeth J. Robertson. 1994. “A Primary Requirement for Nodal in the Formation and Maintenance of the Primitive Streak in the Mouse.” *Development* 120 (7): 1919–28. [https://doi.org/10.1016/0168-9525\(94\)90026-4](https://doi.org/10.1016/0168-9525(94)90026-4).

Conrad, Nathalie, Andrew Judge, Jenny Tran, Hamid Mohseni, Deborah Hedgecote, Abel Perez Crespillo, Moira Allison, et al. 2018. “Temporal Trends and Patterns in Heart Failure Incidence: A Population-Based Study of 4 Million Individuals.” *The Lancet* 391 (10120): 572–80. [https://doi.org/10.1016/S0140-6736\(17\)32520-5](https://doi.org/10.1016/S0140-6736(17)32520-5).

Corbel, Stéphane Y., Adrienne Lee, Lin Yi, Jeffrey Duenas, Timothy R. Brazelton, Helen M. Blau, and Fabio M.V. Rossi. 2003. “Contribution of Hematopoietic Stem Cells to Skeletal Muscle.” *Nature Medicine* 9 (12): 1528–32. <https://doi.org/10.1038/nm959>.

Dahlmann, Julia, George Awad, Carsten Dolny, Sönke Weinert, Karin Richter, Klaus Dieter Fischer, Thomas Munsch, et al. 2018. “Generation of Functional Cardiomyocytes from Rat Embryonic and Induced Pluripotent Stem Cells Using Feeder-Free Expansion and Differentiation in Suspension Culture.” *PLoS ONE* 13 (3): 1–22.
<https://doi.org/10.1371/journal.pone.0192652>.

Darehzereshki, A, Nicole Rubin, Ying Huang, Joshua Billings, Robabeh Mohammadzadeh, and John Wood. 2015. “Differential Regenerative Capacity of Neonatal Mouse Hearts after Cryoinjury” 399 (1): 91–99. <https://doi.org/10.1016/j.ydbio.2014.12.018.Differential>.

Davidson, Lance A., Benjamin G. Hoffstrom, Raymond Keller, and Douglas W. DeSimone. 2002. “Mesendoderm Extension and Mantle Closure in *Xenopus Laevis* Gastrulation: Combined Roles for Integrin A5 β 1, Fibronectin, and Tissue Geometry.” *Developmental Biology* 242 (2): 109–29. <https://doi.org/10.1006/dbio.2002.0537>.

Davis, Michael E., Patrick C.H. Hsieh, Tomosaburo Takahashi, Qing Song, Shuguang Zhang, Roger D. Kamm, Alan J. Grodzinsky, Piero Anversa, and Richard T. Lee. 2006. “Local Myocardial Insulin-like Growth Factor 1 (IGF-1) Delivery with Biotinylated Peptide Nanofibers Improves Cell Therapy for Myocardial Infarction.” *Proceedings of the National Academy of Sciences of the United States of America* 103 (21): 8155–60.
<https://doi.org/10.1073/pnas.0602877103>.

- Dawn, Buddhadeb, Adam B Stein, Konrad Urbanek, Marcello Rota, Brian Whang, Raffaella Rastaldo, Daniele Torella, et al. 2005. "Cardiac Stem Cells Delivered Intravascularly Traverse the Vessel Barrier, Regenerate Infarcted Myocardium, and Improve Cardiac Function." www.pnas.org/cgi/doi/10.1073/pnas.0405957102.
- Dettman, Robert W., Wilfred Denetclaw, Charles P. Ordahl, and James Bristow. 1998. "Common Epicardial Origin of Coronary Vascular Smooth Muscle, Perivascular Fibroblasts, and Intermycardial Fibroblasts in the Avian Heart." *Developmental Biology* 193 (2): 169–81. <https://doi.org/10.1006/dbio.1997.8801>.
- Deuse, Tobias, Xiaomeng Hu, Sean Agbor-Enoh, Martina Koch, Matthew H. Spitzer, Alessia Gravina, Malik Alawi, et al. 2019. "De Novo Mutations in Mitochondrial DNA of iPSCs Produce Immunogenic Neopeptides in Mice and Humans." *Nature Biotechnology* 37 (10): 1137–44. <https://doi.org/10.1038/s41587-019-0227-7>.
- Dijk, A. Van, H. W.M. Niessen, W. Ursem, J. W.R. Twisk, F. C. Visser, and F. J. Van Milligen. 2008. "Accumulation of Fibronectin in the Heart after Myocardial Infarction: A Putative Stimulator of Adhesion and Proliferation of Adipose-Derived Stem Cells." *Cell and Tissue Research* 332 (2): 289–98. <https://doi.org/10.1007/s00441-008-0573-0>.
- Dobaczewski, M., M. Bujak, P. Zymek, G. Ren, M. L. Entman, and N. G. Frangogiannis. 2006. "Extracellular Matrix Remodeling in Canine and Mouse Myocardial Infarcts." *Cell and Tissue Research* 324 (3): 475–88. <https://doi.org/10.1007/s00441-005-0144-6>.
- Duan, Jinzhu, Costin Gherghe, Dianxin Liu, Eric Hamlett, Luxman Srikantha, Laurel Rodgers, Jenna N. Regan, et al. 2012. "Wnt1/Bcatenin Injury Response Activates the Epicardium and Cardiac Fibroblasts to Promote Cardiac Repair." *EMBO Journal* 31 (2): 429–42. <https://doi.org/10.1038/emboj.2011.418>.
- Dzamba, Bette J., Karoly R. Jakab, Mungo Marsden, Martin A. Schwartz, and Douglas W. DeSimone. 2009. "Cadherin Adhesion, Tissue Tension, and Noncanonical Wnt Signaling Regulate Fibronectin Matrix Organization." *Developmental Cell* 16 (3): 421–32. <https://doi.org/10.1016/j.devcel.2009.01.008>.
- Earl, Conner C., Frederick W. Damen, Melissa Yin, Kristiina L. Aasa, Sarah K. Burris, and Craig J. Goergen. 2021. "Strain Estimation of the Murine Right Ventricle Using High-Frequency Speckle-Tracking Ultrasound." *Ultrasound in Medicine and Biology* 47 (11): 3291–3300. <https://doi.org/10.1016/j.ultrasmedbio.2021.07.001>.
- Edsall, John T. 1978. "Some Early History of Cold-Insoluble Globulin." *Annals of the New*

York Academy of Sciences 312 (1): 1–10. <https://doi.org/10.1111/j.1749-6632.1978.tb16788.x>.

Eschenhagen, Thomas, Roberto Bolli, Thomas Braun, Loren J. Field, Bernd K. Fleischmann, Jonas Frisén, Mauro Giacca, et al. 2017. “Cardiomyocyte Regeneration: A Consensus Statement.” *Circulation* 136 (7): 680–86. <https://doi.org/10.1161/CIRCULATIONAHA.117.029343>.

Etzion, Sharon, Alexander Battler, Israel M. Barbash, Emanuela Cagnano, Parvin Zarin, Yosef Granot, Laurence H. Kedes, Robert A. Kloner, and Jonathan Leor. 2001. “Influence of Embryonic Cardiomyocyte Transplantation on the Progression of Heart Failure in a Rat Model of Extensive Myocardial Infarction.” *Journal of Molecular and Cellular Cardiology* 33 (7): 1321–30. <https://doi.org/10.1006/jmcc.2000.1391>.

Eulalio, Ana, Miguel Mano, Matteo Dal Ferro, Lorena Zentilin, Gianfranco Sinagra, Serena Zacchigna, and Mauro Giacca. 2012. “Functional Screening Identifies MiRNAs Inducing Cardiac Regeneration.” *Nature* 492 (7429): 376–81. <https://doi.org/10.1038/nature11739>.

Farooqi, Kanwal M., Nicole Sutton, Samuel Weinstein, Mark Menegus, Hugo Spindola-Franco, and Robert H. Pass. 2012. “Neonatal Myocardial Infarction: Case Report and Review of the Literature.” *Congenital Heart Disease* 7 (6). <https://doi.org/10.1111/j.1747-0803.2012.00660.x>.

Fernandes, S., A. V. Naumova, W. Z. Zhu, M. A. Laflamme, J. Gold, and C. E. Murry. 2010. “Human Embryonic Stem Cell-Derived Cardiomyocytes Engraft but Do Not Alter Cardiac Remodeling after Chronic Infarction in Rats.” *J Mol Cell Cardiol* 49 (6): 941–49. <https://doi.org/10.1016/j.jmcc.2010.09.008>.

Fernandes, Sarah, James J.H. Chong, Sharon L. Paige, Mineo Iwata, Beverly Torok-Storb, Gordon Keller, Hans Reinecke, and Charles E. Murry. 2015. “Comparison of Human Embryonic Stem Cell-Derived Cardiomyocytes, Cardiovascular Progenitors, and Bone Marrow Mononuclear Cells for Cardiac Repair.” *Stem Cell Reports* 5 (5): 753–62. <https://doi.org/10.1016/j.stemcr.2015.09.011>.

Fernández-Avilés, Francisco, Ricardo Sanz-Ruiz, Andreu M. Climent, Lina Badimon, Roberto Bolli, Dominique Charron, Valentin Fuster, et al. 2017. “Global Position Paper on Cardiovascular Regenerative Medicine.” *European Heart Journal* 38 (33): 2532–46. <https://doi.org/10.1093/eurheartj/ehx248>.

- Fisher, Sheila A., Carolyn Doree, Anthony Mathur, David P. Taggart, and Enca Martin-Rendon. 2016. "Stem Cell Therapy for Chronic Ischaemic Heart Disease and Congestive Heart Failure." *Cochrane Database of Systematic Reviews* 2016 (12). <https://doi.org/10.1002/14651858.CD007888.pub3>.
- Flather, Marcus D., Salim Yusuf, Lars Køber, Marc Pfeffer, Alistair Hall, Gordon Murray, Christian Torp-Pedersen, et al. 2000. "Long-Term ACE-Inhibitor Therapy in Patients with Heart Failure or Left-Ventricular Dysfunction: A Systematic Overview of Data from Individual Patients." *Lancet* 355 (9215): 1575–81. [https://doi.org/10.1016/S0140-6736\(00\)02212-1](https://doi.org/10.1016/S0140-6736(00)02212-1).
- Fogelgren, Ben, Noémi Polgár, Kornélia Molnárné Szauter, Zsuzsanna Újfaludi, Rozália Laczkó, Keith S.K. Fong, and Katalin Csiszar. 2005. "Cellular Fibronectin Binds to Lysyl Oxidase with High Affinity and Is Critical for Its Proteolytic Activation." *Journal of Biological Chemistry* 280 (26): 24690–97. <https://doi.org/10.1074/jbc.M412979200>.
- Forte, Elvira, Milena Bastos Furtado, and Nadia Rosenthal. 2018. "The Interstitium in Cardiac Repair: Role of the Immune–Stromal Cell Interplay." *Nature Reviews Cardiology* 15 (10): 601–16. <https://doi.org/10.1038/s41569-018-0077-x>.
- Frangogiannis, Nikolaos G., and Jason C. Kovacic. 2020. "Extracellular Matrix in Ischemic Heart Disease, Part 4/4: JACC Focus Seminar." *Journal of the American College of Cardiology* 75 (17): 2219–35. <https://doi.org/10.1016/j.jacc.2020.03.020>.
- Fransen, Margaret E., and Larry F. Lemanski. 1990. "Epicardial Development in the Axolotl, *Ambystoma Mexicanum*." *The Anatomical Record* 226 (2): 228–36. <https://doi.org/10.1002/ar.1092260212>.
- Frazier, O. H., Eric A. Rose, Patrick McCarthy, Nelson A. Burton, Alfred Tector, Howard Levin, Herbert L. Kayne, Victor L. Poirier, and Kurt A. Dasse. 1995. "Improved Mortality and Rehabilitation of Transplant Candidates Treated with a Long-Term Implantable Left Ventricular Assist System." *Annals of Surgery* 222 (3): 327–38. <https://doi.org/10.1097/00000658-199509000-00010>.
- Gabisonia, Khatia, Giulia Prosdocimo, Giovanni Donato Aquaro, Lucia Carlucci, Lorena Zentilin, Ilaria Secco, Hashim Ali, et al. 2019. "MicroRNA Therapy Stimulates Uncontrolled Cardiac Repair after Myocardial Infarction in Pigs." *Nature* 569 (7756): 418–22. <https://doi.org/10.1038/s41586-019-1191-6>.
- Galdos, Francisco X., Yuxuan Guo, Sharon L. Paige, Nathan J. Vandusen, Sean M. Wu, and

- William T. Pu. 2017. "Cardiac Regeneration: Lessons from Development." *Circulation Research* 120 (6): 941–59. <https://doi.org/10.1161/CIRCRESAHA.116.309040>.
- Gambardella, Laure, Sophie A. McManus, Victoria Moignard, Derya Sebukhan, Agathe Delaune, Simon Andrews, William G. Bernard, et al. 2019. "BNC1 Regulates Cell Heterogeneity in Human Pluripotent Stem Cell-Derived Epicardium." *Development (Cambridge)* 146 (24). <https://doi.org/10.1242/dev.174441>.
- Gao, Ling, Lu Wang, Yuhua Wei, Prasanna Krishnamurthy, Gregory P. Walcott, Philippe Menasché, and Jianyi Zhang. 2020. "Exosomes Secreted by hiPSC-Derived Cardiac Cells Improve Recovery from Myocardial Infarction in Swine." *Science Translational Medicine* 12 (561). <https://doi.org/10.1126/scitranslmed.aay1318>.
- Garcia-Puig, Anna, Jose Luis Mosquera, Senda Jiménez-Nez-Delgado, Cristina García-Pastor, Ignasi Jorba, Daniel Navajas, Francesc Canals, and Angel Raya. 2019. "Proteomics Analysis of Extracellular Matrix Remodeling During Zebrafish Heart Regeneration In Brief." *Molecular & Cellular Proteomics* 18: 1745–55. <https://doi.org/10.1074/mcp.RA118.001193>.
- George, E. L., E. N. Georges-Labouesse, R. S. Patel-King, H. Rayburn, and R. O. Hynes. 1993. "Defects in Mesoderm, Neural Tube and Vascular Development in Mouse Embryos Lacking Fibronectin." *Development* 119 (4): 1079–91.
- Georges-Labouesse, Elisabeth N., Elizabeth L. George, Helen Rayburn, and Richard O. Hynes. 1996. "Mesodermal Development in Mouse Embryos Mutant for Fibronectin." *Developmental Dynamics* 207 (2): 145–56. [https://doi.org/10.1002/\(SICI\)1097-0177\(199610\)207:2<145::AID-AJA3>3.0.CO;2-H](https://doi.org/10.1002/(SICI)1097-0177(199610)207:2<145::AID-AJA3>3.0.CO;2-H).
- Gerbin, Kaytlyn A., Xiulan Yang, Charles E. Murry, and Kareen L.K. K Coulombe. 2015. "Enhanced Electrical Integration of Engineered Human Myocardium via Intramyocardial versus Epicardial Delivery in Infarcted Rat Hearts." *PLoS ONE* 10 (7): 1–20. <https://doi.org/10.1371/journal.pone.0131446>.
- Giacomelli, Elisa, Milena Bellin, Luca Sala, Berend J. van Meer, Leon G. J. Tertoolen, Valeria V. Orlova, Christine L. Mummery, et al. 2017. "Three-Dimensional Cardiac Microtissues Composed of Cardiomyocytes and Endothelial Cells Co-Differentiated from Human Pluripotent Stem Cells." *Development*, dev.143438. <https://doi.org/10.1242/dev.143438>.
- Giacomelli, Elisa, Viviana Meraviglia, Giulia Campostrini, Amy Cochrane, Xu Cao, Ruben

- W.J. van Helden, Ana Krotenberg Garcia, et al. 2020. "Human-IPSC-Derived Cardiac Stromal Cells Enhance Maturation in 3D Cardiac Microtissues and Reveal Non-Cardiomyocyte Contributions to Heart Disease." *Cell Stem Cell* 26 (6): 862-879.e11. <https://doi.org/10.1016/j.stem.2020.05.004>.
- Gise, Alexander Von, and William T. Pu. 2012. "Endocardial and Epicardial Epithelial to Mesenchymal Transitions in Heart Development and Disease." *Circulation Research* 110 (12): 1628–45. <https://doi.org/10.1161/CIRCRESAHA.111.259960>.
- Gittenberger-de Groot, Adriana C., Mark Paul F.M. Vrancken Peeters, Monica M.T. Mentink, Robert G. Gourdie, and Robert E. Poelmann. 1998. "Epicardium-Derived Cells Contribute a Novel Population to the Myocardial Wall and the Atrioventricular Cushions." *Circulation Research* 82 (10): 1043–52. <https://doi.org/10.1161/01.RES.82.10.1043>.
- Gittenberger-De Groot, Adriana C, Mark-Paul F M Vrancken Peeters, Maarten Bergwerff, Monica M T Mentink, and Robert E Poelmann. 2000. "Epicardial Outgrowth Inhibition Leads to Compensatory Mesothelial Outflow Tract Collar and Abnormal Cardiac Septation and Coronary Formation." <http://www.circresaha.org>.
- Gnecchi, Massimiliano, Zhiping Zhang, Aiguo Ni, and Victor J. Dzau. 2008. "Paracrine Mechanisms in Adult Stem Cell Signaling and Therapy." *Circulation Research* 103 (11): 1204–19. <https://doi.org/10.1161/CIRCRESAHA.108.176826>.
- Gondokaryono, Srie Prihianti, Hiroko Ushio, François Niyonsaba, Mutsuko Hara, Hiroshi Takenaka, Sumanasiri T. M. Jayawardana, Shigaku Ikeda, Ko Okumura, and Hideoki Ogawa. 2007. "The Extra Domain A of Fibronectin Stimulates Murine Mast Cells via Toll-like Receptor 4." *Journal of Leukocyte Biology* 82 (3): 657–65. <https://doi.org/10.1189/jlb.1206730>.
- González-Rosa, Juan Manuel, Caroline E. Burns, and C. Geoffrey Burns. 2017. "Zebrafish Heart Regeneration: 15 Years of Discoveries." *Regeneration* 4 (3): 105–23. <https://doi.org/10.1002/reg2.83>.
- González-Rosa, Juan Manuel, Caroline E. Geoffrey E. Correspondence Geoffrey C Geoffrey Burns, Caroline E. Geoffrey E. Correspondence Geoffrey C Geoffrey Burns, Juan Manuel González-Rosa, Caroline E. Geoffrey E. Correspondence Geoffrey C Geoffrey Burns, Caroline E. Geoffrey E. Correspondence Geoffrey C Geoffrey Burns, and Caroline E. Geoffrey E. Correspondence Geoffrey C Geoffrey Burns. 2017. "Zebrafish Heart Regeneration: 15 Years of Discoveries." *Regeneration* 4 (3): 105–23.

<https://doi.org/10.1002/reg2.83>.

- González-Rosa, Juan Manuel, Marina Peralta, and Nadia Mercader. 2012. "Pan-Epicardial Lineage Tracing Reveals That Epicardium Derived Cells Give Rise to Myofibroblasts and Perivascular Cells during Zebrafish Heart Regeneration." *Developmental Biology* 370 (2): 173–86. <https://doi.org/10.1016/j.ydbio.2012.07.007>.
- González-Rosa, Juan Manuel, Michka Sharpe, Dorothy Field, Mark H. Soonpaa, Loren J. Field, Caroline E. Burns, and C. Geoffrey Burns. 2018. "Myocardial Polyploidization Creates a Barrier to Heart Regeneration in Zebrafish." *Developmental Cell* 44 (4): 433-446.e7. <https://doi.org/10.1016/j.devcel.2018.01.021>.
- Grieskamp, Thomas, Carsten Rudat, Timo H.W. Lüdtke, Julia Norden, and Andreas Kispert. 2011. "Notch Signaling Regulates Smooth Muscle Differentiation of Epicardium-Derived Cells." *Circulation Research* 108 (7): 813–23. <https://doi.org/10.1161/CIRCRESAHA.110.228809>.
- Groenewegen, Amy, Frans H. Rutten, Arend Mosterd, and Arno W. Hoes. 2020. "Epidemiology of Heart Failure." *European Journal of Heart Failure* 22 (8): 1342–56. <https://doi.org/10.1002/ejhf.1858>.
- Guo, Yuxuan, and William T. Pu. 2020. "Cardiomyocyte Maturation: New Phase in Development." *Circulation Research*, 1086–1106. <https://doi.org/10.1161/CIRCRESAHA.119.315862>.
- Halstead, Michelle M., Xin Ma, Chuan Zhou, Richard M. Schultz, and Pablo J. Ross. 2020. "Chromatin Remodeling in Bovine Embryos Indicates Species-Specific Regulation of Genome Activation." *Nature Communications* 11 (1). <https://doi.org/10.1038/s41467-020-18508-3>.
- Han, Xiao, Mengning Wang, Songwei Duan, Paul J. Franco, Jennifer Hyoje Ryu Kenty, Preston Hedrick, Yulei Xia, et al. 2019. "Generation of Hypoimmunogenic Human Pluripotent Stem Cells." *Proceedings of the National Academy of Sciences of the United States of America* 116 (21): 10441–46. <https://doi.org/10.1073/pnas.1902566116>.
- Hansen, Arne, Alexandra Eder, Marlene Bönstrup, Marianne Flato, Marco Mewe, Sebastian Schaaf, Bülent Aksehirlioglu, Alexander Schwörer, June Uebeler, and Thomas Eschenhagen. 2010. "Development of a Drug Screening Platform Based on Engineered Heart Tissue." *Circulation Research* 107 (1): 35–44.

<https://doi.org/10.1161/CIRCRESAHA.109.211458>.

Hartupee, Justin, and Douglas L Mann. 2016. "Neurohormonal Activation in Heart Failure with Reduced Ejection Fraction." <https://doi.org/10.1038/nrcardio.2016.163>.

Haubner, Bernhard J., Johanna Schneider, Ulrich Schweigmann, Thomas Schuetz, Wolfgang Dichtl, Corinna Velik-Salchner, Joerg I. Stein, and Josef M. Penninger. 2016. "Functional Recovery of a Human Neonatal Heart after Severe Myocardial Infarction." *Circulation Research* 118 (2): 216–21. <https://doi.org/10.1161/CIRCRESAHA.115.307017>.

Haubner, Bernhard Johannes, Martyna Adamowicz-Brice, Sanjay Khadayate, Viktoria Tiefenthaler, Bernhard Metzler, Tim Aitman, and Josef M. Penninger. 2012. "Complete Cardiac Regeneration in a Mouse Model of Myocardial Infarction." *Aging* 4 (12): 966–77. <https://doi.org/10.18632/aging.100526>.

Heling, Annette, Rene Zimmermann, Sawa Kostin, Yoshi Maeno, Stefan Hein, Bruno Devaux, Erwin Bauer, et al. 2000. "Extracellular Proteins in Failing Human Myocardium." *Circulation Research* 86 (8): 846–53.

Hermans, Kevin C M, Evangelos P. Daskalopoulos, and W. Matthijs Blankesteyn. 2016. "The Janus Face of Myofibroblasts in the Remodeling Heart." *Journal of Molecular and Cellular Cardiology* 91: 35–41. <https://doi.org/10.1016/j.yjmcc.2015.11.017>.

Hirai, Maretoshi, Ju Chen, and Sylvia M. Evans. 2016. "Tissue-Specific Cell Cycle Indicator Reveals Unexpected Findings for Cardiac Myocyte Proliferation." *Circulation Research* 118 (1): 20–28. <https://doi.org/10.1161/CIRCRESAHA.115.307697>.

Houser, Steven R. 2012. "Animal Models of Heart Failure." *Heart Failure, Second Edition*, 78–94. <https://doi.org/10.1161/res.0b013e3182582523>.

Huang, Chiung-Kuei, Soo Ok Lee, Eugene Chang, Haiyan Pang, and Chawnshang Chang. 2016. "Androgen Receptor (AR) in Cardiovascular Diseases." *Hypertension* 229: R1–16. <https://doi.org/10.1530/JOE-15-0518>.

Huang, Guo N, Jeffrey E Thatcher, John Mcanally, Yongli Kong, Xiaoxia Qi, Wei Tan, J Michael Dimaio, et al. 2012. "C/EBP Transcription Factors Mediate Epicardial Activation During Heart Development and Injury" 338 (6114): 1599–1603. <https://doi.org/10.1126/science.1229765.C/EBP>.

Huveneers, Stephan, Hoa Truong, Reinhard Fässler, Arnoud Sonnenberg, and Erik H.J.

- Danen. 2008. "Binding of Soluble Fibronectin to Integrin A5 β 1 - Link to Focal Adhesion Redistribution and Contractile Shape." *Journal of Cell Science* 121 (15): 2452–62. <https://doi.org/10.1242/jcs.033001>.
- Huwer, Hanno, Johannes Winning, Brigitte Vollmar, Cornelius Welter, Christoph Löhbach, Michael D. Menger, and Hans Joachim Schäfers. 2003. "Long-Term Cell Survival and Hemodynamic Improvements after Neonatal Cardiomyocyte and Satellite Cell Transplantation into Healed Myocardial Cryoinfarcted Lesions in Rats." *Cell Transplantation* 12 (7): 757–67. <https://doi.org/10.3727/000000003108747361>.
- HYNES, R. 1987. "Integrins: A Family of Cell Surface Receptors." *Cell* 48 (4): 549–54. [https://doi.org/10.1016/0092-8674\(87\)90233-9](https://doi.org/10.1016/0092-8674(87)90233-9).
- Hynes, Richard O. 2002. "Integrins: Bidirectional, Allosteric Signaling Machines." *Cell* 110 (6): 673–87. [https://doi.org/10.1016/S0092-8674\(02\)00971-6](https://doi.org/10.1016/S0092-8674(02)00971-6).
- . 2009. "The Extracellular Matrix: Not Just Pretty Fibrils." *Science* 326: 1216–19. <https://doi.org/10.1126/science.1176488>.
- Ieda, Masaki, Ji Dong Fu, Paul Delgado-Olguin, Vasanth Vedantham, Yohei Hayashi, Benoit G. Bruneau, and Deepak Srivastava. 2010. "Direct Reprogramming of Fibroblasts into Functional Cardiomyocytes by Defined Factors." *Cell* 142 (3): 375–86. <https://doi.org/10.1016/j.cell.2010.07.002>.
- Ieda, Masaki, Takatoshi Tsuchihashi, Kathryn N. Ivey, Robert S. Ross, Ting Ting Hong, Robin M. Shaw, and Deepak Srivastava. 2009. "Cardiac Fibroblasts Regulate Myocardial Proliferation through B1 Integrin Signaling." *Developmental Cell* 16 (2): 233–44. <https://doi.org/10.1016/j.devcel.2008.12.007>.
- Ingham, K. C., S. A. Brew, and B. S. Isaacs. 1988. "Interaction of Fibronectin and Its Gelatin-Binding Domains with Fluorescent-Labeled Chains of Type 1 Collagen." *Journal of Biological Chemistry* 263 (10): 4624–28. [https://doi.org/10.1016/s0021-9258\(18\)68828-3](https://doi.org/10.1016/s0021-9258(18)68828-3).
- Ingham, Kenneth C., Shelesa A. Brew, and Harold P. Erickson. 2004. "Localization of a Cryptic Binding Site for Tenascin on Fibronectin." *Journal of Biological Chemistry* 279 (27): 28132–35. <https://doi.org/10.1074/jbc.M312785200>.
- Israeli-Rosenberg, Sharon, Ana Maria Manso, Hideshi Okada, and Robert S. Ross. 2014. "Integrins and Integrin-Associated Proteins in the Cardiac Myocyte." *Circulation Research* 114 (3): 572–86. <https://doi.org/10.1161/CIRCRESAHA.114.301275>.

- Itou, Junji, Isao Oishi, Hiroko Kawakami, Tiffany J. Glass, Jenna Richter, Austin Johnson, Troy C. Lund, and Yasuhiko Kawakami. 2012. "Migration of Cardiomyocytes Is Essential for Heart Regeneration in Zebrafish." *Development (Cambridge)* 139 (22): 4133–42. <https://doi.org/10.1242/dev.079756>.
- Iyer, Dharini, Laure Gambardella, William G Bernard, Felipe Serrano, Victoria L Mascetti, Roger a Pedersen, Amarnath Talasila, and Sanjay Sinha. 2015. "Robust Derivation of Epicardium and Its Differentiated Smooth Muscle Cell Progeny from Human Pluripotent Stem Cells." *Development (Cambridge, England)* 142 (8): 1528–41. <https://doi.org/10.1242/dev.119271>.
- Jahr, Maike, Jan Schlueter, Thomas Brand, and Jörg Männer. 2008. "Development of the Proepicardium in *Xenopus Laevis*." *Developmental Dynamics* 237 (10): 3088–96. <https://doi.org/10.1002/dvdy.21713>.
- James, Spencer L., Degu Abate, Kalkidan Hassen Abate, Solomon M. Abay, Cristiana Abbafati, Nooshin Abbasi, Hedayat Abbastabar, et al. 2018. "Global, Regional, and National Incidence, Prevalence, and Years Lived with Disability for 354 Diseases and Injuries for 195 Countries and Territories, 1990-2017: A Systematic Analysis for the Global Burden of Disease Study 2017." *The Lancet* 392 (10159): 1789–1858. [https://doi.org/10.1016/S0140-6736\(18\)32279-7](https://doi.org/10.1016/S0140-6736(18)32279-7).
- Jessup, Mariell, and Susan Brozena. 2003. "Heart Failure." *The New England Journal of Medicine* Downloaded from *Nejm.Org* at CAMBRIDGE UNIVERSITY LIBRARY On. Vol. 348. www.nejm.org.
- Jing, Xiaodong, Yulin Gao, Songlin Xiao, Qin Qin, Xiaoming Wei, Yuling Yan, Ling Wu, et al. 2016. "Hypoxia Induced the Differentiation of Tbx18-Positive Epicardial Cells to CoSMCs." *Scientific Reports* 6 (January): 30468. <https://doi.org/10.1038/srep30468>.
- Jones, Nicholas R., Andrea K. Roalfe, Ibiye Adoki, F. D.Richard Hobbs, and Clare J. Taylor. 2019. "Survival of Patients with Chronic Heart Failure in the Community: A Systematic Review and Meta-Analysis." *European Journal of Heart Failure* 21 (11): 1306–25. <https://doi.org/10.1002/ejhf.1594>.
- Jopling, Chris, Eduard Sleep, Marina Raya, Mercè Martí, Angel Raya, and Carlos Izpisúa Belmonte. 2010. "NIH Public Access." *Sleep (Rochester)* 464 (7288): 606–9. <https://doi.org/10.1038/nature08899>.Zebrafish.
- Kadota, Shin, Lil Pabon, Hans Reinecke, and Charles E. Murry. 2017. "In Vivo Maturation of

- Human Induced Pluripotent Stem Cell-Derived Cardiomyocytes in Neonatal and Adult Rat Hearts.” *Stem Cell Reports* 8 (2): 278–89.
<https://doi.org/10.1016/j.stemcr.2016.10.009>.
- Kane, Christopher, Liam Couch, and Cesare M N Terracciano. 2015. “Excitation-Contraction Coupling of Human Induced Pluripotent Stem Cell-Derived Cardiomyocytes.” *Frontiers in Cell and Developmental Biology* | *Www.Frontiersin.Org* 3: 59.
<https://doi.org/10.3389/fcell.2015.00059>.
- Karbassi, Elaheh, Aidan Fenix, Silvia Marchiano, Naoto Muraoka, Kenta Nakamura, Xiulan Yang, and Charles E. Murry. 2020. “Cardiomyocyte Maturation: Advances in Knowledge and Implications for Regenerative Medicine.” *Nature Reviews Cardiology* 17 (6): 341–59. <https://doi.org/10.1038/s41569-019-0331-x>.
- Karra, Ravi, and Kenneth D. Poss. 2017. “Redirecting Cardiac Growth Mechanisms for Therapeutic Regeneration.” *Journal of Clinical Investigation* 127 (2): 427–36.
<https://doi.org/10.1172/JCI89786>.
- Katz, Tamar C., Manvendra K. Singh, Karl Degenhardt, José Rivera-Feliciano, Randy L. Johnson, Jonathan A. Epstein, and Clifford J. Tabin. 2012. “Distinct Compartments of the Proepicardial Organ Give Rise to Coronary Vascular Endothelial Cells.” *Developmental Cell* 22 (3): 639–50. <https://doi.org/10.1016/j.devcel.2012.01.012>.
- Kawamura, Takuji, Shigeru Miyagawa, Satsuki Fukushima, Akira Maeda, Noriyuki Kashiyama, Ai Kawamura, Kenji Miki, et al. 2016. “Cardiomyocytes Derived from MHC-Homozygous Induced Pluripotent Stem Cells Exhibit Reduced Allogeneic Immunogenicity in MHC-Matched Non-Human Primates.” *Stem Cell Reports* 6 (3): 312–20. <https://doi.org/10.1016/j.stemcr.2016.01.012>.
- Kehat, Izhak, Dorit Kenyagin-Karsenti, Mirit Snir, Hana Segev, Michal Amit, Amira Gepstein, Erella Livne, Ofer Binah, Joseph Itskovitz-Eldor, and Lior Gepstein. 2001. “Human Embryonic Stem Cells Can Differentiate into Myocytes with Structural and Functional Properties of Cardiomyocytes.” *Journal of Clinical Investigation* 108 (3): 407–14.
<https://doi.org/10.1172/JCI200112131>.
- Kehat, Izhak, Leonid Khimovich, Oren Caspi, Amira Gepstein, Rona Shofti, Gil Arbel, Irit Huber, Jonathan Satin, Joseph Itskovitz-Eldor, and Lior Gepstein. 2004. “Electromechanical Integration of Cardiomyocytes Derived from Human Embryonic Stem Cells.” *Nature Biotechnology* 22 (10): 1282–89. <https://doi.org/10.1038/nbt1014>.

- Khan, M., E. Nickoloff, T. Abramova, J. Johnson, S. K. Verma, P. Krishnamurthy, A. R. Mackie, et al. 2015. "Embryonic Stem Cell-Derived Exosomes Promote Endogenous Repair Mechanisms and Enhance Cardiac Function Following Myocardial Infarction." *Circulation Research* 117 (1): 52–64.
<https://doi.org/10.1161/CIRCRESAHA.117.305990>.
- Kikuchi, Kazu, Vikas Gupta, Jinhu Wang, Jennifer E. Holdway, Airon A. Wills, Yi Fang, and Kenneth D. Poss. 2011. "Tcf21+ Epicardial Cells Adopt Non-Myocardial Fates during Zebrafish Heart Development and Regeneration." *Development* 138 (14): 2895–2902.
<https://doi.org/10.1242/dev.067041>.
- Kikuchi, Kazu, Jennifer E. Holdway, Andreas A. Werdich, Ryan M. Anderson, Yi Fang, Gregory F. Egnaczyk, Todd Evans, et al. 2010. "Primary Contribution to Zebrafish Heart Regeneration by Gata4+ Cardiomyocytes." *Nature* 464 (7288): 601–5.
<https://doi.org/10.1038/nature08804>.
- Kim, Ho Dirk, Choon Sik Yoon, Hyun Kim, and Bong Jin Rah. 1999. "Expression of Extracellular Matrix Components Fibronectin and Laminin in the Human Fetal Heart." *Cell Structure and Function*. <https://doi.org/10.1247/csf.24.19>.
- Kim, Jieun, Qiong Wu, Yolanda Zhang, Katie M. Wiens, Ying Huang, Nicole Rubin, Hiroyuki Shimada, et al. 2010. "PDGF Signaling Is Required for Epicardial Function and Blood Vessel Formation in Regenerating Zebrafish Hearts." *Proceedings of the National Academy of Sciences of the United States of America* 107 (40): 17206–10.
<https://doi.org/10.1073/pnas.0915016107>.
- Kishi, Shuji, Junzo Uchiyama, Anne M. Baughman, Tadateru Goto, Mao C. Lin, and Stephanie B. Tsai. 2003. "The Zebrafish as a Vertebrate Model of Functional Aging and Very Gradual Senescence." *Experimental Gerontology* 38 (7): 777–86.
[https://doi.org/10.1016/S0531-5565\(03\)00108-6](https://doi.org/10.1016/S0531-5565(03)00108-6).
- Klingberg, Franco, Grace Chau, Marielle Walraven, Stellar Boo, Anne Koehler, Melissa L. Chow, Abby L. Olsen, et al. 2018. "The Fibronectin ED-A Domain Enhances Recruitment of Latent TGF- β -Binding Protein-1 to the Fibroblast Matrix." *Journal of Cell Science* 131 (5): 1–12. <https://doi.org/10.1242/jcs.201293>.
- Komiyama, Masatoshi, Kintoku Ito, and Yutaka Shimada. 1987. "Origin and Development of the Epicardium in the Mouse Embryo." *Anatomy and Embryology* 176 (2): 183–89.
<https://doi.org/10.1007/BF00310051>.

- Konstandin, Mathias H., Mirko Völkers, Brett Collins, Pearl Quijada, Mercedes Quintana, Andrea De La Torre, Lucy Ormachea, et al. 2013. "Fibronectin Contributes to Pathological Cardiac Hypertrophy but Not Physiological Growth." *Basic Research in Cardiology* 108 (5). <https://doi.org/10.1007/s00395-013-0375-8>.
- Kratsios, Paschalis, Catarina Catela, Ekaterina Salimova, Marion Huth, Valeria Berno, Nadia Rosenthal, and Foteini Mourkioti. 2010. "Distinct Roles for Cell-Autonomous Notch Signaling in Cardiomyocytes of the Embryonic and Adult Heart." *Circulation Research* 106 (3): 559–72. <https://doi.org/10.1161/CIRCRESAHA.109.203034>.
- Krause, Diane S., Neil D. Theise, Michael I. Collector, Octavian Henegariu, Sonya Hwang, Rebekah Gardner, Sara Neutzel, and Saul J. Sharkis. 2001. "Multi-Organ, Multi-Lineage Engraftment by a Single Bone Marrow-Derived Stem Cell." *Cell* 105 (3): 369–77. [https://doi.org/10.1016/S0092-8674\(01\)00328-2](https://doi.org/10.1016/S0092-8674(01)00328-2).
- Krishnamani, Rajan, David Denofrio, and Marvin A. Konstam. 2010. "Emerging Ventricular Assist Devices for Long-Term Cardiac Support." *Nature Reviews Cardiology* 7 (2): 71–76. <https://doi.org/10.1038/nrcardio.2009.222>.
- Laake, L W van, R Passier, P A Doevendans, and C L Mummery. 2008. "Human Embryonic Stem Cell-Derived Cardiomyocytes and Cardiac Repair in Rodents." *Circ Res* 102 (9): 1008–10. <https://doi.org/10.1161/circresaha.108.175505>.
- Laake, Linda W. van, Robert Passier, Jantine Monshouwer-Kloots, Arie J. Verkleij, Daniel J. Lips, Christian Freund, Krista den Ouden, et al. 2007. "Human Embryonic Stem Cell-Derived Cardiomyocytes Survive and Mature in the Mouse Heart and Transiently Improve Function after Myocardial Infarction." *Stem Cell Res* 1 (1): 9–24. <https://doi.org/10.1016/j.scr.2007.06.001>.
- Laflamme, M A, K Y Chen, A V Naumova, V Muskheli, J A Fugate, S K Dupras, H Reinecke, et al. 2007. "Cardiomyocytes Derived from Human Embryonic Stem Cells in Pro-Survival Factors Enhance Function of Infarcted Rat Hearts." *Nat Biotechnol* 25 (9): 1015–24. <https://doi.org/10.1038/nbt1327>.
- Laflamme, Michael A., Kent Y. Chen, Anna V. Naumova, Veronica Muskheli, James A. Fugate, Sarah K. Dupras, Hans Reinecke, et al. 2007. "Cardiomyocytes Derived from Human Embryonic Stem Cells in Pro-Survival Factors Enhance Function of Infarcted Rat Hearts." *Nature Biotechnology* 25 (9): 1015–24. <https://doi.org/10.1038/nbt1327>.
- Laflamme, Michael A., Joseph Gold, Chunhui Xu, Mohammad Hassanipour, Elen Rosler,

- Shailaja Police, Veronica Muskheli, and Charles E. Murry. 2005. "Formation of Human Myocardium in the Rat Heart from Human Embryonic Stem Cells." *American Journal of Pathology* 167 (3): 663–71. [https://doi.org/10.1016/S0002-9440\(10\)62041-X](https://doi.org/10.1016/S0002-9440(10)62041-X).
- Laflamme, Michael A., and Charles E. Murry. 2011. "Heart Regeneration." *Nature*. <https://doi.org/10.1038/nature10147>.
- Lai, Shih Lei, Rubén Marín-Juez, Pedro Luís Moura, Carsten Kuenne, Jason Kuan Han Lai, Ayele Taddese Tsedeke, Stefan Guenther, Mario Looso, and Didier Y.R. Stainier. 2017. "Reciprocal Analyses in Zebrafish and Medaka Reveal That Harnessing the Immune Response Promotes Cardiac Regeneration." *ELife* 6: 1–20. <https://doi.org/10.7554/eLife.25605>.
- Lalu, Manoj M., Sasha Mazzarello, Jennifer Zlepzig, Yuan Yi (Ryan) Dong, Joshua Montroy, Lauralyn McIntyre, P. J. Devereaux, et al. 2018. "Safety and Efficacy of Adult Stem Cell Therapy for Acute Myocardial Infarction and Ischemic Heart Failure (SafeCell Heart): A Systematic Review and Meta-Analysis." *Stem Cells Translational Medicine* 7 (12): 857–66. <https://doi.org/10.1002/sctm.18-0120>.
- Lam, Nicholas T., and Hesham A. Sadek. 2018. "Neonatal Heart Regeneration." *Circulation* 138 (4): 412–23. <https://doi.org/10.1161/CIRCULATIONAHA.118.033648>.
- Lamouille, Samy, Jian Xu, and Rik Derynck. 2014. "Molecular Mechanisms of Epithelial-Mesenchymal Transition." *Nature Reviews Molecular Cell Biology* 15 (3): 178–96. <https://doi.org/10.1038/nrm3758>.
- Leor, J, S Gerecht, S Cohen, L Miller, R Holbova, A Ziskind, M Shachar, M S Feinberg, E Guetta, and J Itskovitz-Eldor. 2007. "Human Embryonic Stem Cell Transplantation to Repair the Infarcted Myocardium." *Heart* 93 (10): 1278–84. <https://doi.org/10.1136/hrt.2006.093161>.
- Lepilina, Alexandra, Ashley N. Coon, Kazu Kikuchi, Jennifer E. Holdway, Richard W. Roberts, C. Geoffrey Burns, and Kenneth D. Poss. 2006. "A Dynamic Epicardial Injury Response Supports Progenitor Cell Activity during Zebrafish Heart Regeneration." *Cell* 127 (3): 607–19. <https://doi.org/10.1016/j.cell.2006.08.052>.
- Lescroart, Fabienne, Samira Chabab, Xionghui Lin, Steffen Rulands, Catherine Paulissen, Annie Rodolosse, Herbert Auer, et al. 2014. "Early Lineage Restriction in Temporally Distinct Populations of Mesp1 Progenitors during Mammalian Heart Development." *Nature Cell Biology* 16 (9): 829–40. <https://doi.org/10.1038/ncb3024>.

- Li, Ren Ke, Zhi Qiang Jia, Richard D. Weisel, Donald A.G. Mickle, Ji Zhang, Molly K. Mohabeer, Vivek Rao, and Joan Ivanov. 1996. "Cardiomyocyte Transplantation Improves Heart Function." *Annals of Thoracic Surgery* 62 (3): 654–61. [https://doi.org/10.1016/S0003-4975\(96\)00389-X](https://doi.org/10.1016/S0003-4975(96)00389-X).
- Li, Ren Ke, Donald A.G. Mickle, Richard D. Weisel, Vivek Rao, and Zhi Qiang Jia. 2001. "Optimal Time for Cardiomyocyte Transplantation to Maximize Myocardial Function after Left Ventricular Injury." *Annals of Thoracic Surgery* 72 (6): 1957–63. [https://doi.org/10.1016/S0003-4975\(01\)03216-7](https://doi.org/10.1016/S0003-4975(01)03216-7).
- Li, Yi Yan, Lingjuan He, Xiuzhen Huang, Shirin Issa Bhaloo, Huan Zhao, Shaohua Zhang, Wenjuan Pu, et al. 2018. "Genetic Lineage Tracing of Nonmyocyte Population by Dual Recombinases." *Circulation* 138 (8): 793–805. <https://doi.org/10.1161/CIRCULATIONAHA.118.034250>.
- Liang, Xingqun, Gang Wang, Lizhu Lin, Jennifer Lowe, Qingquan Zhang, Lei Bu, Yihan Chen, Ju Chen, Yunfu Sun, and Sylvia M. Evans. 2013. "HCN4 Dynamically Marks the First Heart Field and Conduction System Precursors." *Circulation Research* 113 (4): 399–407. <https://doi.org/10.1161/CIRCRESAHA.113.301588>.
- Lie-Venema, Heleen, Nynke M.S. Van Den Akker, Noortje A.M. Bax, Elizabeth M. Winter, Saskia Maas, Tuija Kekarainen, Rob C. Hoeben, Marco C. DeRuiter, Robert E. Poelmann, and Adriana C. Gittenberger-De Groot. 2007. "Origin, Fate, and Function of Epicardium-Derived Cells (EPCDs) in Normal and Abnormal Cardiac Development." *TheScientificWorldJournal* 7: 1777–98. <https://doi.org/10.1100/tsw.2007.294>.
- Lim, Gregory B. 2020. "Complexity and Plasticity of Cardiac Cellular Composition." *Nature Reviews Cardiology* 17 (12): 759. <https://doi.org/10.1038/s41569-020-00464-6>.
- Lin, Zhiqiang, and William T. Pu. 2014. "Harnessing Hippo in the Heart: Hippo/Yap Signaling and Applications to Heart Regeneration and Rejuvenation." *Stem Cell Research* 13 (3): 571–81. <https://doi.org/10.1016/j.scr.2014.04.010>.
- Ling, Yunfei, Sandeep Bhushan, Qiang Fan, and Menglin Tang. 2016. "Midterm Outcome after Surgical Correction of Anomalous Left Coronary Artery from the Pulmonary Artery." *Journal of Cardiothoracic Surgery* 11 (1): 7–11. <https://doi.org/10.1186/s13019-016-0535-7>.
- Linke, Axel, Patrick Müller, Daria Nurzynska, Claudia Casarsa, Daniele Torella, Angelo Nascimbene, Clotilde Castaldo, et al. 2005. "Stem Cells in the Dog Heart Are Self-

- Renewing, Clonogenic, and Multipotent and Regenerate Infarcted Myocardium, Improving Cardiac Function.” *Proceedings of the National Academy of Sciences of the United States of America* 102 (25): 8966–71. <https://doi.org/10.1073/pnas.0502678102>.
- Litviňuková, Monika, Carlos Talavera-López, Henrike Maatz, Daniel Reichart, Catherine L. Worth, Eric L. Lindberg, Masatoshi Kanda, et al. 2020. “Cells of the Adult Human Heart.” *Nature* 588 (7838): 466–72. <https://doi.org/10.1038/s41586-020-2797-4>.
- Liu, Jiandong, and Didier Y.R. Stainier. 2010. “Tbx5 and Bmp Signaling Are Essential for Proepicardium Specification in Zebrafish.” *Circulation Research* 106 (12): 1818–28. <https://doi.org/10.1161/CIRCRESAHA.110.217950>.
- Liu, Pentao, Maki Wakamiya, Martin J. Shea, Urs Albrecht, Richard R. Behringer, and Allan Bradley. 1999. “Requirement for Wnt3 in Vertebrate Axis Formation.” *Nature Genetics* 22 (4): 361–65. <https://doi.org/10.1038/11932>.
- Liu, Yen Wen, Billy Chen, Xiulan Yang, James A. Fugate, Faith A. Kalucki, Akiko Futakuchi-Tsuchida, Larry Couture, et al. 2018. “Human Embryonic Stem Cell-Derived Cardiomyocytes Restore Function in Infarcted Hearts of Non-Human Primates.” *Nature Biotechnology* 36 (7): 597–605. <https://doi.org/10.1038/nbt.4162>.
- Lund, Lars H., Leah B. Edwards, Anne I. Dipchand, Samuel Goldfarb, Anna Y. Kucheryavaya, Bronwyn J. Levvey, Bruno Meiser, Joseph W. Rossano, Roger D. Yusen, and Josef Stehlik. 2016. “The Registry of the International Society for Heart and Lung Transplantation: Thirty-Third Adult Heart Transplantation Report—2016; Focus Theme: Primary Diagnostic Indications for Transplant.” *Journal of Heart and Lung Transplantation* 35 (10): 1158–69. <https://doi.org/10.1016/j.healun.2016.08.017>.
- Lupu, Irina Elena, Andia N. Redpath, and Nicola Smart. 2020. “Spatiotemporal Analysis Reveals Overlap of Key Proepicardial Markers in the Developing Murine Heart.” *Stem Cell Reports* 14 (5): 770–87. <https://doi.org/10.1016/j.stemcr.2020.04.002>.
- Maass, Martina, Benjamin Krausgrill, Simon Eschrig, Tobias Kaluschke, Katja Urban, Gabriel Peinkofer, Tobias G. Plenge, et al. 2017. “Intramyocardially Transplanted Neonatal Cardiomyocytes (NCMs) Show Structural and Electrophysiological Maturation and Integration and Dose-Dependently Stabilize Function of Infarcted Rat Hearts.” *Cell Transplantation* 26 (1): 157–70. <https://doi.org/10.3727/096368916X692870>.
- Madden, Lauran R., Derek J. Mortisen, Eric M. Sussman, Sarah K. Dupras, James A. Fugate, Janet L. Cuy, Kip D. Hauch, Michael A. Laflamme, Charles E. Murry, and

- Buddy D. Ratner. 2010. "Proangiogenic Scaffolds as Functional Templates for Cardiac Tissue Engineering." *Proceedings of the National Academy of Sciences of the United States of America* 107 (34): 15211–16. <https://doi.org/10.1073/pnas.1006442107>.
- Magnusson, Magnus K., and Deane F. Mosher. 1998. "Fibronectin: Structure, Assembly, and Cardiovascular Implications." *Arteriosclerosis, Thrombosis, and Vascular Biology* 18 (9): 1363–70. <https://doi.org/10.1161/01.ATV.18.9.1363>.
- Maliken, Bryan D., Onur Kanisicak, Jason Karch, Hadi Khalil, Xing Fu, Justin G. Boyer, Vikram Prasad, Yi Zheng, and Jeffery D. Molkentin. 2018. "Gata4-Dependent Differentiation of c-Kit+-Derived Endothelial Cells Underlies Artefactual Cardiomyocyte Regeneration in the Heart." *Circulation* 138 (10): 1012–24. <https://doi.org/10.1161/CIRCULATIONAHA.118.033703>.
- Manasek, F. J. 1969. "Embryonic Development of the Heart. II. Formation of the Epicardium." *Journal of Embryology and Experimental Morphology* 22 (3): 333–48.
- Maric-Bilkan, Christine, Arthur P. Arnold, Doris A. Taylor, Melinda Dwinell, Susan E. Howlett, Nanette Wenger, Jane F. Reckelhoff, et al. 2016. "Report of the National Heart, Lung, and Blood Institute Working Group on Sex Differences Research in Cardiovascular Disease: Scientific Questions and Challenges." *Hypertension* 67 (5): 802–7. <https://doi.org/10.1161/HYPERTENSIONAHA.115.06967>.
- Masters, Megan, and Paul R. Riley. 2014. "The Epicardium Signals the Way towards Heart Regeneration." *Stem Cell Research*. Elsevier. <https://doi.org/10.1016/j.scr.2014.04.007>.
- Matsuda, Mitsuhiro, Hanako Hayashi, Jordi Garcia-Ojalvo, Kumiko Yoshioka-Kobayashi, Ryoichiro Kageyama, Yoshihiro Yamanaka, Makoto Ikeya, Junya Toguchida, Cantas Alev, and Miki Ebisuya. 2020. "Species-Specific Segmentation Clock Periods Are Due to Differential Biochemical Reaction Speeds." *Science (New York, N.Y.)* 369 (6510): 1450–55. <https://doi.org/10.1126/science.aba7668>.
- Mattapally, Saidulu, Kevin M. Pawlik, Vladimir G. Fast, Esther Zumaquero, Frances E. Lund, Troy D. Randall, Tim M. Townes, and Jianyi Zhang. 2018. "Human Leukocyte Antigen Class I and II Knockout Human Induced Pluripotent Stem Cell–Derived Cells: Universal Donor for Cell Therapy." *Journal of the American Heart Association* 7 (23): 1–13. <https://doi.org/10.1161/JAHA.118.010239>.
- McDonald, J. A., B. J. Quade, T. J. Broekelmann, R. LaChance, K. Forsman, E. Hasegawa, and S. Akiyama. 1987. "Fibronectin's Cell-Adhesive Domain and an Amino-Terminal

Matrix Assembly Domain Participate in Its Assembly into Fibroblast Pericellular Matrix.” *Journal of Biological Chemistry* 262 (7): 2957–67. [https://doi.org/10.1016/s0021-9258\(18\)61453-x](https://doi.org/10.1016/s0021-9258(18)61453-x).

McMurray, John J.V., Stamatis Adamopoulos, Stefan D. Anker, Angelo Auricchio, Michael Böhm, Kenneth Dickstein, Volkmar Falk, et al. 2012. “ESC Guidelines for the Diagnosis and Treatment of Acute and Chronic Heart Failure 2012: The Task Force for the Diagnosis and Treatment of Acute and Chronic Heart Failure 2012 of the European Society of Cardiology. Developed in Collaboration with the Heart.” *European Heart Journal* 33 (14): 1787–1847. <https://doi.org/10.1093/eurheartj/ehs104>.

Mehra, Mandeep R., Charles E. Canter, Margaret M. Hannan, Marc J. Semigran, Patricia A. Uber, David A. Baran, Lara Danziger-Isakov, et al. 2016. “The 2016 International Society for Heart Lung Transplantation Listing Criteria for Heart Transplantation: A 10-Year Update.” *Journal of Heart and Lung Transplantation* 35 (1): 1–23. <https://doi.org/10.1016/j.healun.2015.10.023>.

Mehra, Mandeep R., Nir Uriel, Yoshifumi Naka, Joseph C. Cleveland, Melana Yuzefpolskaya, Christopher T. Salerno, Mary N. Walsh, et al. 2019. “A Fully Magnetically Levitated Left Ventricular Assist Device — Final Report.” *New England Journal of Medicine* 380 (17): 1618–27. <https://doi.org/10.1056/nejmoa1900486>.

Menasché, Philippe, Ottavio Alfieri, Stefan Janssens, William McKenna, Hermann Reichenspurner, Ludovic Trinquart, Jean Thomas Vilquin, et al. 2008. “The Myoblast Autologous Grafting in Ischemic Cardiomyopathy (MAGIC) Trial: First Randomized Placebo-Controlled Study of Myoblast Transplantation.” *Circulation* 117 (9): 1189–1200. <https://doi.org/10.1161/CIRCULATIONAHA.107.734103>.

Menasché, Philippe, Albert A Hagège, Marcio Scorsin, Bruno Pouzet, Michel Desnos, Denis Duboc, and Ketty Schwartz. 2001. “Myoblast Transplantation for Heart Failure Increased Mitochondrial Toxicity with Ribavirin in HIV / HCV Coinfection.” *Lancet* 357: 279–80.

Menasché, Philippe, Valérie Vanneaux, Albert Hagège, Alain Bel, Bernard Cholley, Isabelle Cacciapuoti, Alexandre Parouchev, et al. 2015. “Human Embryonic Stem Cell-Derived Cardiac Progenitors for Severe Heart Failure Treatment: First Clinical Case Report.” *European Heart Journal* 36 (30): 2011–17. <https://doi.org/10.1093/eurheartj/ehv189>.

Menasché, Philippe, Valérie Vanneaux, Albert Hagège, Alain Bel, Bernard Cholley, Alexandre Parouchev, Isabelle Cacciapuoti, et al. 2018. “Transplantation of Human

- Embryonic Stem Cell–Derived Cardiovascular Progenitors for Severe Ischemic Left Ventricular Dysfunction.” *Journal of the American College of Cardiology* 71 (4): 429–38.
<https://doi.org/10.1016/j.jacc.2017.11.047>.
- Mercer, Sarah E., Shannon J. Odelberg, and Hans Georg Simon. 2013. “A Dynamic Spatiotemporal Extracellular Matrix Facilitates Epicardial-Mediated Vertebrate Heart Regeneration.” *Developmental Biology* 382 (2): 457–69.
<https://doi.org/10.1016/j.ydbio.2013.08.002>.
- Merki, Esther, Monica Zamora, Angel Raya, Yasuhiko Kawakami, Jianming Wang, Xiaoxue Zhang, John Burch, et al. 2005. “Epicardial Retinoid X Receptor α Is Required for Myocardial Growth and Coronary Artery Formation.” *Proceedings of the National Academy of Sciences of the United States of America* 102 (51): 18455–60.
<https://doi.org/10.1073/pnas.0504343102>.
- Merkl, Claudia, Anja Saalfrank, Nathalie Riesen, Ralf Kühn, Anna Pertek, Stefan Eser, Markus Sebastian Hardt, et al. 2013. “Efficient Generation of Rat Induced Pluripotent Stem Cells Using a Non-Viral Inducible Vector.” *PLoS ONE* 8 (1).
<https://doi.org/10.1371/journal.pone.0055170>.
- Messer, Simon, Sendi Cernic, Aravinda Page, Marius Berman, Pradeep Kaul, Simon Colah, Jason Ali, et al. 2020. “A 5-Year Single-Center Early Experience of Heart Transplantation from Donation after Circulatory-Determined Death Donors.” *Journal of Heart and Lung Transplantation* 39 (12): 1463–75.
<https://doi.org/10.1016/j.healun.2020.10.001>.
- Mikawa, T., and D. A. Fischman. 1992. “Retroviral Analysis of Cardiac Morphogenesis: Discontinuous Formation of Coronary Vessels.” *Proceedings of the National Academy of Sciences of the United States of America* 89 (20): 9504–8.
<https://doi.org/10.1073/pnas.89.20.9504>.
- Mikawa, Takashi, and Robert G. Gourdie. 1996. “Pericardial Mesoderm Generates a Population of Coronary Smooth Muscle Cells Migrating into the Heart along with Ingrowth of the Epicardial Organ.” *Developmental Biology* 174 (2): 221–32.
<https://doi.org/10.1006/dbio.1996.0068>.
- Milani-Nejad, Nima, and Paul M L Janssen. 2013. “Small and Large Animal Models in Cardiac Contraction Research: Advantages and Disadvantages.”
<https://doi.org/10.1016/j.pharmthera.2013.10.007>.

- Mittal, Ashok, Maria Pulina, Shuan Yu Hou, and Sophie Astrof. 2010. "Fibronectin and Integrin Alpha 5 Play Essential Roles in the Development of the Cardiac Neural Crest." *Mechanisms of Development* 127 (9–12): 472–84.
<https://doi.org/10.1016/j.mod.2010.08.005>.
- . 2013. "Fibronectin and Integrin Alpha 5 Play Requisite Roles in Cardiac Morphogenesis." *Developmental Biology* 381 (1): 73–82.
<https://doi.org/10.1016/j.ydbio.2013.06.010>.
- Moerkamp, Asja T, Kirsten Lodder, Tessa Van Herwaarden, Esther Dronkers, Calinda K E Dingenouts, Fredrik C Tengström, Thomas J Van Brakel, Marie-José Goumans, and Anke M Smits. n.d. "Human Fetal and Adult Epicardial-Derived Cells: A Novel Model to Study Their Activation." <https://doi.org/10.1186/s13287-016-0434-9>.
- Montolio, Marta, Noèlia Téllez, Montserrat Biarnés, Joan Soler, and Eduard Montanya. 2005. "Short-Term Culture with the Caspase Inhibitor z-VAD.Fmk Reduces Beta Cell Apoptosis in Transplanted Islets and Improves the Metabolic Outcome of the Graft." *Cell Transplantation* 14 (1): 59–65. <https://doi.org/10.3727/000000005783983269>.
- Morgan, Mark R., Martin J. Humphries, and Mark D. Bass. 2007. "Synergistic Control of Cell Adhesion by Integrins and Syndecans." *Nature Reviews Molecular Cell Biology* 8 (12): 957–69. <https://doi.org/10.1038/nrm2289>.
- Moyes, Kara White, Christopher G. Sip, Willimark Obenza, Emily Yang, Cody Horst, Robert E. Welikson, Stephen D. Hauschka, Albert Folch, and Michael A. Laflamme. 2013. "Human Embryonic Stem Cell-Derived Cardiomyocytes Migrate in Response to Gradients of Fibronectin and Wnt5a." *Stem Cells and Development* 22 (16): 2315–25.
<https://doi.org/10.1089/scd.2012.0586>.
- Müller-Ehmsen, Jochen, Kirk L. Peterson, Larry Kedes, Peter Whittaker, Joan S. Dow, Tiffany I. Long, Peter W. Laird, and Robert A. Kloner. 2002. "Rebuilding a Damaged Heart: Long-Term Survival of Transplanted Neonatal Rat Cardiomyocytes after Myocardial Infarction and Effect on Cardiac Function." *Circulation* 105 (14): 1720–26.
<https://doi.org/10.1161/01.CIR.0000013782.76324.92>.
- Müller-Ehmsen, Jochen, Peter Whittaker, Robert A. Kloner, Joan S. Dow, Tsuyoshi Sakoda, Tiffany I. Long, Peter W. Laird, and Larry Kedes. 2002. "Survival and Development of Neonatal Rat Cardiomyocytes Transplanted into Adult Myocardium." *Journal of Molecular and Cellular Cardiology* 34 (2): 107–16.
<https://doi.org/10.1006/jmcc.2001.1491>.

- Mummery, Christine L, Jianhua Zhang, Elizabeth Ng, David A Elliott, Andrew G Elefanty, and Timothy J Kamp. 2012. "Differentiation of Human ES and IPS Cells to Cardiomyocytes: A Methods Overview." *Circulation Research* 111 (July 2012): 344–58. <https://doi.org/10.1161/CIRCRESAHA.110.227512>. Differentiation.
- Münch, Juliane, Dimitrios Grivas, Álvaro González-Rajal, Rebeca Torregrosa-Carrión, and José Luis de la Pompa. 2017. "Notch Signalling Restricts Inflammation and Serpine1 Expression in the Dynamic Endocardium of the Regenerating Zebrafish Heart." *Development (Cambridge)* 144 (8): 1425–40. <https://doi.org/10.1242/dev.143362>.
- Muraoka, Naoto, and Masaki Ieda. 2014. "Direct Reprogramming of Fibroblasts into Myocytes to Reverse Fibrosis." *Annual Review of Physiology* 76: 21–37. <https://doi.org/10.1146/annurev-physiol-021113-170301>.
- Murata, Kozue, Masaya Ikegawa, Kenji Minatoya, and Hidetoshi Masumoto. 2020. "Strategies for Immune Regulation in IPS Cell-Based Cardiac Regenerative Medicine." *Inflammation and Regeneration* 40 (1). <https://doi.org/10.1186/s41232-020-00145-4>.
- Murry, Charles E., and W. Robb MacLellan. 2020. "Stem Cells and the Heart - The Road Ahead." *Science* 367 (6480): 854–55. <https://doi.org/10.1126/science.aaz3650>.
- Murry, Charles E., Mark H. Soonpaa, Hans Reinecke, Hidehiro Nakajima, Hisako O. Nakajima, Michael Rubart, Kishore B.S. Pasumarthi, et al. 2004. "Haematopoietic Stem Cells Do Not Transdifferentiate into Cardiac Myocytes in Myocardial Infarcts." *Nature* 428 (6983): 664–68. <https://doi.org/10.1038/nature02446>.
- Naghavi, Mohsen, Amanuel Alemu Abajobir, Cristiana Abbafati, Kaja M. Abbas, Foad Abd-Allah, Semaw Ferede Abera, Victor Aboyans, et al. 2017. "Global, Regional, and National Age-Sex Specific Mortality for 264 Causes of Death, 1980-2016: A Systematic Analysis for the Global Burden of Disease Study 2016." *The Lancet* 390 (10100): 1151–1210. [https://doi.org/10.1016/S0140-6736\(17\)32152-9](https://doi.org/10.1016/S0140-6736(17)32152-9).
- Nakagawa, Takashi, Shigeomi Shimizu, Tetsuya Watanabe, Osamu Yamaguchi, Kinya Otsu, Hirotaka Yamagata, Hidenori Inohara, Takeshi Kubo, and Yoshihide Tsujimoto. 2005. "Cyclophilin D-Dependent Mitochondrial Permeability Transition Regulates Some Necrotic but Not Apoptotic Cell Death." *Nature* 434 (7033): 652–58. <https://doi.org/10.1038/nature03317>.
- Nesbitt, Tresa, Aubrey Lemley, Jeff Davis, Michael J. Yost, Richard L. Goodwin, and Jay D. Potts. 2006. "Epicardial Development in the Rat: A New Perspective." *Microscopy and*

Microanalysis 12 (5): 390–98. <https://doi.org/10.1017/S1431927606060533>.

Nosedá, Michela, and Michael D. Schneider. 2009. "Fibroblasts Inform the Heart: Control of Cardiomyocyte Cycling and Size by Age-Dependent Paracrine Signals." *Developmental Cell* 16 (2): 161–62. <https://doi.org/10.1016/j.devcel.2009.01.020>.

Nowbar, Alexandra N, Michael Mielewczik, Maria Karavassilis, Hakim-Moulay Dehbi, Matthew J Shun-Shin, Siana Jones, James P Howard, Graham D Cole, Darrel P Francis, and DAMASCENE writing group. 2014. "Discrepancies in Autologous Bone Marrow Stem Cell Trials and Enhancement of Ejection Fraction (DAMASCENE): Weighted Regression and Meta-Analysis." *BMJ (Clinical Research Ed.)* 348 (7109): g2688. <https://doi.org/10.1136/bmj.g2688>.

Nygren, Jens M., Stefan Jovinge, Martin Breitbach, Petter Säwén, Wilhelm Röhl, Jürgen Hescheler, Jalal Taneera, Bernd K. Fleischmann, and Sten Eirik W. Jacobsen. 2004. "Bone Marrow-Derived Hematopoietic Cells Generate Cardiomyocytes at a Low Frequency through Cell Fusion, but Not Transdifferentiation." *Nature Medicine* 10 (5): 494–501. <https://doi.org/10.1038/nm1040>.

Ostrominski, John W, Ravi Chandra Yada, Noriko Sato, Michael Klein, Ksenia Blinova, Dakshesh Patel, Racquel Valadez, et al. 2020. "CRISPR/Cas9-Mediated Introduction of the Sodium/Iodide Symporter Gene Enables Noninvasive in Vivo Tracking of Induced Pluripotent Stem Cell-Derived Cardiomyocytes." *STEM CELLS Transl Med* 9: 1203–17. <https://doi.org/10.1002/sctm.20-0019>.

Pachori, Alok S., Laura Custer, Don Hansen, Shannon Clapp, Erica Kempa, and John Klingensmith. 2010. "Bone Morphogenetic Protein 4 Mediates Myocardial Ischemic Injury through JNK-Dependent Signaling Pathway." *Journal of Molecular and Cellular Cardiology* 48 (6): 1255–65. <https://doi.org/10.1016/j.yjmcc.2010.01.010>.

Paik, David T., Meena Rai, Sergey Ryzhov, Lehanna N. Sanders, Omonigho Aisagbonhi, Mitchell J. Funke, Igor Feoktistov, and Antonis K. Hatzopoulos. 2015. "Wnt10b Gain-of-Function Improves Cardiac Repair by Arteriole Formation and Attenuation of Fibrosis." *Circulation Research* 117 (9): 804–16. <https://doi.org/10.1161/CIRCRESAHA.115.306886>.

Palpant, Nathan J., Peter Hofsteen, Lil Pabon, Hans Reinecke, and Charles E. Murry. 2015. "Cardiac Development in Zebrafish and Human Embryonic Stem Cells Is Inhibited by Exposure to Tobacco Cigarettes and Ecigarettes." *PLoS ONE* 10 (5): 1–19. <https://doi.org/10.1371/journal.pone.0126259>.

- Pankov, Roumen, and Kenneth M. Yamada. 2002. "Fibronectin at a Glance." *Journal of Cell Science* 115 (20): 3861–63. <https://doi.org/10.1242/jcs.00059>.
- Patten, Richard D., and Monica R. Hall-Porter. 2009. "Small Animal Models of Heart Failure Development of Novel Therapies, Past and Present." *Circulation: Heart Failure* 2 (2): 138–44. <https://doi.org/10.1161/CIRCHEARTFAILURE.108.839761>.
- Patterson, Michaela, Lindsey Barske, Ben Van Handel, Christoph D. Rau, Peiheng Gan, Avneesh Sharma, Shan Parikh, et al. 2017. "Frequency of Mononuclear Diploid Cardiomyocytes Underlies Natural Variation in Heart Regeneration." *Nature Genetics* 49 (9): 1346–53. <https://doi.org/10.1038/ng.3929>.
- Pérez-Pomares, José M., Aimée Phelps, Martina Sedmerova, and Andy Wessels. 2003. "Epicardial-like Cells on the Distal Arterial End of the Cardiac Outflow Tract Do Not Derive from the Proepicardium but Are Derivatives of the Cephalic Pericardium." *Developmental Dynamics* 227 (1): 56–68. <https://doi.org/10.1002/dvdy.10284>.
- Perez-Pomares, José María, Rita Carmona, Mauricio González-Iriarte, Gerardo Atencia, Andy Wessels, and Ramon Muñoz-Chapuli. 2002. "Origin of Coronary Endothelial Cells from Epicardial Mesothelium in Avian Embryos." *International Journal of Developmental Biology* 46 (8): 1005–13. <https://doi.org/10.1387/ijdb.12533024>.
- Pérez-Pomares, José María, David Macías, Lina García-Garrido, and Ramón Muñoz-Chápuli. 1998. "The Origin of the Subepicardial Mesenchyme in the Avian Embryo: An Immunohistochemical and Quail-Chick Chimera Study." *Developmental Biology* 200 (1): 57–68. <https://doi.org/10.1006/dbio.1998.8949>.
- Pfeffer, J. M., M. A. Pfeffer, P. J. Fletcher, and E. Braunwald. 1991. "Progressive Ventricular Remodeling in Rat with Myocardial Infarction." *American Journal of Physiology - Heart and Circulatory Physiology* 260 (5 29-5). <https://doi.org/10.1152/ajpheart.1991.260.5.h1406>.
- Pierschbacher, Michael D., and Erkki Ruoslahti. 1984. "Cell Attachment Activity of Fibronectin Can Be Duplicated by Small Synthetic Fragments of the Molecule." *Nature* 309: 30–33.
- Porrello, Enzo R., Ahmed I. Mahmoud, Emma Simpson, Brett A. Johnson, David Grinsfelder, Diana Canseco, Pradeep P. Mammen, Beverly A. Rothermel, Eric N. Olson, and Hesham A. Sadek. 2013. "Regulation of Neonatal and Adult Mammalian Heart Regeneration by the MiR-15 Family." *Proceedings of the National Academy of Sciences*

of the United States of America 110 (1): 187–92.

<https://doi.org/10.1073/pnas.1208863110>.

Porrello, Enzo R, Ahmed I Mahmoud, Emma Simpson, Joseph A Hill, James A Richardson, Eric N Olson, and Hesham A Sadek. 2011. “Transient Regenerative Potential of the Neonatal Mouse Heart.” *Science* 331: 1078–80.

<https://doi.org/10.1126/science.1200708>.

Poss, Kenneth D., Lindsay G. Wilson, and Mark T. Keating. 2002. “Heart Regeneration in Zebrafish.” *Science* 298 (5601): 2188–90. <https://doi.org/10.1126/science.1077857>.

Pouly, Julia, Patrick Bruneval, Chantal Mandet, Suzanne Proksch, Séverine Peyrard, Catherine Amrein, Véronique Bousseaux, et al. 2008. “Cardiac Stem Cells in the Real World.” *Journal of Thoracic and Cardiovascular Surgery* 135 (3): 673–78.

<https://doi.org/10.1016/j.jtcvs.2007.10.024>.

Priller, Josef, Derek A. Persons, Francisco F. Klett, Gerd Kempermann, Georg W. Kreutzberg, and Ulrich Dirnagl. 2001. “Neogenesis of Cerebellar Purkinje Neurons from Gene-Marked Bone Marrow Cells in Vivo.” *Journal of Cell Biology* 155 (5): 733–38.

<https://doi.org/10.1083/jcb.200105103>.

Ptaszek, Leon M., Moussa Mansour, Jeremy N. Ruskin, and Kenneth R. Chien. 2012.

“Towards Regenerative Therapy for Cardiac Disease.” *The Lancet* 379 (9819): 933–42.

[https://doi.org/10.1016/S0140-6736\(12\)60075-0](https://doi.org/10.1016/S0140-6736(12)60075-0).

Pulina, Maria V., Shuan Yu Hou, Ashok Mittal, Dorthe Julich, Charlie A. Whittaker, Scott A. Holley, Richard O. Hynes, and Sophie Astrof. 2011. “Essential Roles of Fibronectin in the Development of the Left-Right Embryonic Body Plan.” *Developmental Biology* 354 (2): 208–20. <https://doi.org/10.1016/j.ydbio.2011.03.026>.

Qian, Li, Yu Huang, C Ian Spencer, Amy Foley, Vasanth Vedantham, Simon J Conway, Jidong Fu, et al. 2012. “HHS Public Access” 485 (7400): 593–98.

<https://doi.org/10.1038/nature11044>.In.

Ramjee, Vimal, Deqiang Li, Lauren J. Manderfield, Feiyan Liu, Kurt A. Engleka, Haig Aghajanian, Christopher B. Rodell, et al. 2017. “Epicardial YAP/TAZ Orchestrate an Immunosuppressive Response Following Myocardial Infarction.” *Journal of Clinical Investigation* 127 (3): 899–911. <https://doi.org/10.1172/JCI88759>.

Ran, F Ann, Patrick D. Hsu, Jason Wright, Vineeta Agarwala, David A Scott, and Feng Zhang. 2013. “Genome Engineering Using the CRISPR-Cas9 System.” *Nature*

- Protocols* 8 (11): 2281–2308. <https://doi.org/10.1038/nprot.2013.143>.Genome.
- Rayon, Teresa, Despina Stamataki, Ruben Perez-Carrasco, Lorena Garcia-Perez, Christopher Barrington, Manuela Melchionda, Katherine Exelby, et al. 2020. “Species-Specific Pace of Development Is Associated with Differences in Protein Stability.” *Science (New York, N.Y.)* 369 (6510). <https://doi.org/10.1126/science.aba7667>.
- Redd, Meredith A., Nicole Zeinstra, Wan Qin, Wei Wei, Amy Martinson, Yuliang Wang, Ruikang K. Wang, Charles E. Murry, and Ying Zheng. 2019. “Patterned Human Microvascular Grafts Enable Rapid Vascularization and Increase Perfusion in Infarcted Rat Hearts.” *Nature Communications* 10 (1). <https://doi.org/10.1038/s41467-019-08388-7>.
- Regitz-Zagrosek, Vera, Sabine Oertelt-Prigione, Ute Seeland, and Roland Hetzer. 2010. “Sex and Gender Differences in Myocardial Hypertrophy and Heart Failure.” *Circulation Journal Official Journal of the Japanese Circulation Society* 74. <https://doi.org/10.1253/circj.CJ-10-0196>.
- Reinecke, Hans, Veronica Poppa, and Charles E. Murry. 2002. “Skeletal Muscle Stem Cells Do Not Transdifferentiate into Cardiomyocytes after Cardiac Grafting.” *Journal of Molecular and Cellular Cardiology* 34 (2): 241–49. <https://doi.org/10.1006/jmcc.2001.1507>.
- Reinecke, Hans, Ming Zhang, Trudy Bartosek, and Charles E Murry. 1999. “Survival, Integration, and Differentiation of Cardiomyocyte Grafts.” *Circulation*, no. 1.
- Riegler, J, M Tiburcy, A Ebert, E Tzatzalos, U Raaz, O J Abilez, Q Shen, et al. 2015. “Human Engineered Heart Muscles Engraft and Survive Long Term in a Rodent Myocardial Infarction Model.” *Circ Res* 117 (8): 720–30. <https://doi.org/10.1161/circresaha.115.306985>.
- Riehle, Christian, and Johann Bauersachs. 2019. “Small Animal Models of Heart Failure.” *Cardiovascular Research* 115 (13): 1838–49. <https://doi.org/10.1093/cvr/cvz161>.
- Riley, Paul R., and Nicola Smart. 2011. “Vascularizing the Heart.” *Cardiovascular Research* 91 (2): 260–68. <https://doi.org/10.1093/cvr/cvr035>.
- Risebro, Catherine A., Joaquim Miguel Vieira, Linda Klotz, and Paul R. Riley. 2015. “Characterisation of the Human Embryonic and Foetal Epicardium during Heart Development.” *Development (Cambridge)* 142 (21): 3630–36. <https://doi.org/10.1242/dev.127621>.

- Rivera-Pérez, Jaime A., and Terry Magnuson. 2005. "Primitive Streak Formation in Mice Is Preceded by Localized Activation of Brachyury and Wnt3." *Developmental Biology* 288 (2): 363–71. <https://doi.org/10.1016/j.ydbio.2005.09.012>.
- Robertson, Elizabeth J. 2014. "Dose-Dependent Nodal/Smad Signals Pattern the Early Mouse Embryo." *Seminars in Cell and Developmental Biology* 32: 73–79. <https://doi.org/10.1016/j.semcd.2014.03.028>.
- Robey, Thomas E, Mark K Saiget, Hans Reinecke, and Charles E Murry. 2009. "Systems Approaches to Preventing Transplanted Cell Death in Cardiac Repair" 45 (4): 567–81. <https://doi.org/10.1016/j.yjmcc.2008.03.009>.
- Roell, Wilhelm, Thorsten Lewalter, Philipp Sasse, Yvonne N. Tallini, Bum Rak Choi, Martin Breitbach, Robert Doran, et al. 2007. "Engraftment of Connexin 43-Expressing Cells Prevents Post-Infarct Arrhythmia." *Nature* 450 (7171): 819–24. <https://doi.org/10.1038/nature06321>.
- Rolstad, Bent. 2001. "The Athymic Nude Rat: An Animal Experimental Model to Reveal Novel Aspects of Innate Immune Responses?" *Immunological Reviews* 184 (1): 136–44. <https://doi.org/10.1034/j.1600-065x.2001.1840113.x>.
- Romagnuolo, Rocco, Hassan Masoudpour, Andreu Porta-Sánchez, Beiping Qiang, Jennifer Barry, Andrew Laskary, Xiuling Qi, et al. 2019. "Human Embryonic Stem Cell-Derived Cardiomyocytes Regenerate the Infarcted Pig Heart but Induce Ventricular Tachyarrhythmias." *Stem Cell Reports* 12 (5): 967–81. <https://doi.org/10.1016/j.stemcr.2019.04.005>.
- Ronaldson-Bouchard, Kacey, Stephen P. Ma, Keith Yeager, Timothy Chen, Loujin Jin Song, Dario Sirabella, Kumi Morikawa, et al. 2018. "Advanced Maturation of Human Cardiac Tissue Grown from Pluripotent Stem Cells." *Nature* 556 (7700): 239–43. <https://doi.org/10.1038/s41586-018-0016-3>.
- Rose, Eric A., Alan J. Gelijns, Annetine C. Moskowitz, Walter Heitjan, Daniel F. Stevenson, Lynne W. Dembitsky, James W. Long, Deborah Ascheim, Anita Tierney, Ronald Levitan, Paul Meier, and John Watson. 2001. "Long-Term Use of a Left Ventricular Assist Device." *The New England Journal of Medicine* 345 (20): 1435–43.
- Roth, Gregory A., Mohammad H. Forouzanfar, Andrew E. Moran, Ryan Barber, Grant Nguyen, Valery L. Feigin, Mohsen Naghavi, George A. Mensah, and Christopher J.L. Murray. 2015. "Demographic and Epidemiologic Drivers of Global Cardiovascular

- Mortality." *New England Journal of Medicine* 372 (14): 1333–41.
<https://doi.org/10.1056/nejmoa1406656>.
- Rudat, Carsten, and Andreas Kispert. 2012. "Wt1 and Epicardial Fate Mapping." *Circulation Research* 111 (2): 165–69. <https://doi.org/10.1161/CIRCRESAHA.112.273946>.
- Rui, Liu, Nie Yu, Lian Hong, He Feng, Han Chunyong, Meng Jian, Zheng Zhe, et al. 2014. "Extending the Time Window of Mammalian Heart Regeneration by Thymosin Beta 4." *Journal of Cellular and Molecular Medicine* 18 (12): 2417–24.
<https://doi.org/10.1111/jcmm.12421>.
- Russell, Jamie L., Sean C. Goetsch, Nicholas R. Gaiano, Joseph A. Hill, Eric N. Olson, and Jay W. Schneider. 2011. "A Dynamic Notch Injury Response Activates Epicardium and Contributes to Fibrosis Repair." *Circulation Research* 108 (1): 51–59.
<https://doi.org/10.1161/CIRCRESAHA.110.233262>.
- Sakakibara, Yutaka, Tambara Keiichi, Lu Fanglin, Nishina Takeshi, and Masashi Komeda. 2002. "Cardiomyocyte Transplantation Does Not Reverse Cardiac Remodeling in Rats With Chronic Myocardial Infarction" 4975 (02): 25–30.
- Sanganalmath, Santosh K., and Roberto Bolli. 2013. "Cell Therapy for Heart Failure: A Comprehensive Overview of Experimental and Clinical Studies, Current Challenges, and Future Directions." *Circulation Research* 113 (6): 810–34.
<https://doi.org/10.1161/CIRCRESAHA.113.300219>.
- Savarese, Gianluigi, and Lars H Lund. 2017. "Global Public Health Burden of Heart Failure" 3 (1): 7–11. <https://doi.org/10.15420/cfr.2016:25:2>.
- Schlaepfer, David D., and Tony Hunter. 1998. "Integrin Signalling and Tyrosine Phosphorylation: Just the FAKs?" *Trends in Cell Biology*. Elsevier Ltd.
[https://doi.org/10.1016/S0962-8924\(97\)01172-0](https://doi.org/10.1016/S0962-8924(97)01172-0).
- Schwarzbauer, Jean E. 1991. "Fibronectin: From Gene to Protein." *Current Opinion in Cell Biology* 3 (5): 786–91. [https://doi.org/10.1016/0955-0674\(91\)90051-Y](https://doi.org/10.1016/0955-0674(91)90051-Y).
- Schwarzbauer, Jean E., and Douglas W. DeSimone. 2011. "Fibronectins, Their Fibrillogenesis, and in Vivo Functions." *Cold Spring Harbor Perspectives in Biology* 3 (7): 1–19. <https://doi.org/10.1101/cshperspect.a005041>.
- Sechler, Jan L., Anne Marie Cumiskey, Deana M. Gazzola, and Jean E. Schwarzbauer. 2000. "A Novel Non-Independent Fibronectin Assembly Pathway Initiated by A4β1

- Integrin Binding to the Alternatively Spliced V Region.” *Journal of Cell Science* 113 (8): 1491–98.
- Senyo, Samuel E., Matthew L. Steinhauser, Christie L. Pizzimenti, Vicky K. Yang, Lei Cai, Mei Wang, Ting-Di Wu, Jean-Luc Guerquin-Kern, Claude P Lechene, and Richard T Lee. 2013. “Mammalian Heart Renewed by Preexisting Cardiomyocytes.” *Nature* 493 (7432): 433–36. <https://doi.org/10.1038/nature11682>.Mammalian.
- Serini, Guido, Patricia Ropraz, Antoine Geinoz, Laura Borsi, Luciano Zardi, and Giulio Gabbiani. 1998. “The Fibronectin Domain ED-A Is Crucial for Myofibroblastic Phenotype Induction by Transforming Growth Factor- β 1.” *Journal of Cell Biology* 142 (3): 873–81.
- Serluca, Fabrizio C. 2008. “Development of the Proepicardial Organ in the Zebrafish.” *Developmental Biology* 315 (1): 18–27. <https://doi.org/10.1016/j.ydbio.2007.10.007>.
- Shah, Ajay M, and Douglas L Mann. 2011. “Heart Failure 1 In Search of New Therapeutic Targets and Strategies for Heart Failure: Recent Advances in Basic Science.” *Lancet*. Vol. 378. [https://doi.org/10.1016/S0140-6736\(11\)60894-5](https://doi.org/10.1016/S0140-6736(11)60894-5).
- Shah, Kevin S., Michelle M. Kittleson, and Jon A. Kobashigawa. 2019. “Updates on Heart Transplantation.” *Current Heart Failure Reports* 16 (5): 150–56. <https://doi.org/10.1007/s11897-019-00432-3>.
- Shiba, Yuji, Sarah Fernandes, Wei-zhong Zhu, Dominic Filice, Veronica Muskheli, Benjamin Van Biber, Todd Dardas, John L Mignone, Atsushi Izawa, and Ramy Hanna. 2013. “hESC-Derived Cardiomyocytes Electrically Couple and Suppress Arrhythmias in Injured Hearts.” *Nature* 489 (7415): 322–25. <https://doi.org/10.1038/nature11317>.hESC-Derived.
- Shiba, Yuji, Dominic Filice, Sarah Fernandes, Elina Minami, Sarah K. Dupras, Benjamin Van Biber, Peter Trinh, et al. 2014. “Electrical Integration of Human Embryonic Stem Cell-Derived Cardiomyocytes in a Guinea Pig Chronic Infarct Model.” *Journal of Cardiovascular Pharmacology and Therapeutics* 19 (4): 368–81. <https://doi.org/10.1177/1074248413520344>.
- Shiba, Yuji, Toshihito Gomibuchi, Tatsuichiro Seto, Yuko Wada, Hajime Ichimura, Yuki Tanaka, Tatsuki Ogasawara, et al. 2016. “Allogeneic Transplantation of IPS Cell-Derived Cardiomyocytes Regenerates Primate Hearts.” *Nature* 538 (7625): 388–91. <https://doi.org/10.1038/nature19815>.

- Singh, Purva, Cara Carraher, and Jean E. Schwarzbauer. 2010. "Assembly of Fibronectin Extracellular Matrix." *Annual Review of Cell and Developmental Biology* 26: 397–419. <https://doi.org/10.1146/annurev-cellbio-100109-104020>.
- Slaughter, M.S. 2018. "Advanced Heart Failure Treated with Continuous-Flow Left Ventricular Assist Device." *50 Studies Every Intensivist Should Know*, 95–101. <https://doi.org/10.1093/med/9780190467654.003.0016>.
- Smart, Nicola, Karina N. Dubé, and Paul R. Riley. 2009. "Coronary Vessel Development and Insight towards Neovascular Therapy." *International Journal of Experimental Pathology*. <https://doi.org/10.1111/j.1365-2613.2009.00646.x>.
- Smart, Nicola, and Paul R. Riley. 2012. "The Epicardium as a Candidate for Heart Regeneration." *Future Cardiology* 8 (1): 53–69. <https://doi.org/10.2217/fca.11.87>.
- Smart, Nicolas, Catherine A Risebro, Athalie A D Melville, Kelvin Moses, Robert J Schwartz, K R Chien, and Paul R Riley. 2007. "Thymosin Beta4 Induces Adult Epicardial Progenitor Mobilization and Neovascularization." *Nature* 445 (7124): 177–82. <https://doi.org/10.1038/nature05383>.
- Smits, Anke M., Esther Dronkers, and Marie José Goumans. 2018. "The Epicardium as a Source of Multipotent Adult Cardiac Progenitor Cells: Their Origin, Role and Fate." *Pharmacological Research* 127: 129–40. <https://doi.org/10.1016/j.phrs.2017.07.020>.
- Song, Kunhua, Young-Jae Nam, Xiang Luo, Xiaoxia Qi, Wei Tan, Guo N Huang, Asha Acharya, et al. 2012. "Heart Repair by Reprogramming Non-Myocytes with Cardiac Transcription Factors Accession Number for Microarray Data Microarray Data Were Deposited in the Gene Expression Omnibus Database (Accession Number GSE37057). HHS Public Access" 485 (7400): 599–604. <https://doi.org/10.1038/nature11139.Heart>.
- Soonpaa, Mark H., Kyung Keun Kim, Laura Pajak, Michael Franklin, and Loren J. Field. 1996. "Cardiomyocyte DNA Synthesis and Binucleation during Murine Development." *American Journal of Physiology - Heart and Circulatory Physiology* 271 (5 40-5). <https://doi.org/10.1152/ajpheart.1996.271.5.h2183>.
- Später, Daniela, Monika K. Abramczuk, Kristina Buac, Lior Zangi, Maxine W. Stachel, Jonathan Clarke, Makoto Sahara, Andreas Ludwig, and Kenneth R. Chien. 2013. "A HCN4+ Cardiomyogenic Progenitor Derived from the First Heart Field and Human Pluripotent Stem Cells." *Nature Cell Biology* 15 (9): 1098–1106. <https://doi.org/10.1038/ncb2824>.

- Squiers, Galen T, Micheal A McLellan, Alexei Ilinykh, Jane Branca, Nadia A Rosenthal, and Alexander R Pinto. 2020. "Cardiac Cellularity Is Dependent upon Biological Sex and Is Regulated by Gonadal Hormones." *Cardiovascular Research*, 1–11.
<https://doi.org/10.1093/cvr/cvaa265>.
- Srivastava, Deepak, and Eric N Olson. 2000. "Development" 407 (September): 221–26.
- Stehlik, Josef, Jon Kobashigawa, Sharon A. Hunt, Hermann Reichenspurner, and James K. Kirklin. 2018. "Honoring 50 Years of Clinical Heart Transplantation in Circulation: In-Depth State-of-the-Art Review." *Circulation* 137 (1): 71–87.
<https://doi.org/10.1161/CIRCULATIONAHA.117.029753>.
- Stoehr, Andrea, Christiane Neuber, Christina Baldauf, Ingra Vollert, Felix W. Friedrich, Frederik Flenner, Lucie Carrier, et al. 2014. "Automated Analysis of Contractile Force and Ca²⁺ Transients in Engineered Heart Tissue." *American Journal of Physiology - Heart and Circulatory Physiology* 306 (9): 1353–63.
<https://doi.org/10.1152/ajpheart.00705.2013>.
- Strauer, Bodo E., Michael Brehm, Tobias Zeus, Matthias Köstering, Anna Hernandez, Rüdiger V. Sorg, Gesine Kögler, and Peter Wernet. 2002. "Repair of Infarcted Myocardium by Autologous Intracoronary Mononuclear Bone Marrow Cell Transplantation in Humans." *Circulation* 106 (15): 1913–18.
<https://doi.org/10.1161/01.CIR.0000034046.87607.1C>.
- Sucov, Henry M., Ying Gu, Simmy Thomas, Peng Li, and Mohammad Pashmforoush. 2009. "Epicardial Control of Myocardial Proliferation and Morphogenesis." *Pediatric Cardiology* 30 (5): 617–25. <https://doi.org/10.1007/s00246-009-9391-8>.
- Sultana, Nishat, Lu Zhang, Jianyun Yan, Jiqui Chen, Weibin Cai, Shegufta Razzaque, Dongtak Jeong, et al. 2015. "Resident C-Kit⁺ Cells in the Heart Are Not Cardiac Stem Cells." *Nature Communications* 6: 1–10. <https://doi.org/10.1038/ncomms9701>.
- Sun, Xin, Sophia Malandraki-Miller, Tahnee Kennedy, Elad Bassat, Konstantinos Klaourakis, Jia Zhao, Elisabetta Gamen, et al. 2020. "The Extracellular Matrix Protein Agrin Is Essential for Epicardial Epithelial-to-Mesenchymal Transition during Heart Development." *BioRxiv*, January, 2020.09.25.313742.
<https://doi.org/10.1101/2020.09.25.313742>.
- Takahashi, Kazutoshi, and Shinya Yamanaka. 2006. "Induction of Pluripotent Stem Cells from Mouse Embryonic and Adult Fibroblast Cultures by Defined Factors." *Cell* 126 (4):

663–76. <https://doi.org/10.1016/j.cell.2006.07.024>.

Tallquist, Michelle D., and Jeffery D. Molkentin. 2017. “Redefining the Identity of Cardiac Fibroblasts.” *Nature Reviews Cardiology* 14 (8): 484–91. <https://doi.org/10.1038/nrcardio.2017.57>.

Taylor, Doris A., B. Zane Atkins, Pinata Hungspreugs, Thomas R. Jones, Mary C. Reedy, Kelley A. Hutcheson, Donald D. Glower, and William E. Kraus. 1998. “Regenerating Functional Myocardium: Improved Performance after Skeletal Myoblast Transplantation.” *Nature Medicine* 4 (8): 929–33. <https://doi.org/10.1038/nm0898-929>.

Thygesen, Kristian, Joseph S. Alpert, and Harvey D. White. 2007. “Universal Definition of Myocardial Infarction.” *Circulation* 116 (22): 2634–53. <https://doi.org/10.1161/CIRCULATIONAHA.107.187397>.

Tiburcy, Malte, James E. Hudson, Paul Balfanz, Susanne F. Schlick, Tim Meyer, Mei Ling Chang Liao, Elif Levent, et al. 2017. “Defined Engineered Human Myocardium with Advanced Maturation for Applications in Heart Failure Modelling and Repair.” *Circulation* 135 (19): 1832–47. <https://doi.org/10.1161/CIRCULATIONAHA.116.024145>.

Tomasini-Johansson, Bianca R., Nicole R. Kaufman, Martin G. Ensenberger, Vered Ozeri, Emanuel Hanski, and Deane F. Mosher. 2001. “A 49-Residue Peptide from Adhesin F1 of *Streptococcus Pyogenes* Inhibits Fibronectin Matrix Assembly.” *Journal of Biological Chemistry* 276 (26): 23430–39. <https://doi.org/10.1074/jbc.M103467200>.

Tompkins, Bryon A., Wayne Balkan, Johannes Winkler, Mariann Gyöngyösi, Georg Goliash, Francisco Fernández-Avilés, and Joshua M. Hare. 2018. “Preclinical Studies of Stem Cell Therapy for Heart Disease.” *Circulation Research* 122 (7): 1006–20. <https://doi.org/10.1161/CIRCRESAHA.117.312486>.

Trinh, Le A., and Didier Y.R. Stainier. 2004. “Fibronectin Regulates Epithelial Organization during Myocardial Migration in Zebrafish.” *Developmental Cell* 6 (3): 371–82. [https://doi.org/10.1016/S1534-5807\(04\)00063-2](https://doi.org/10.1016/S1534-5807(04)00063-2).

Tulloch, Nathaniel L., Veronica Muskheli, Maria V. Razumova, F. Steven Korte, Michael Regnier, Kip D. Hauch, Lil Pabon, Hans Reinecke, and Charles E. Murry. 2011. “Growth of Engineered Human Myocardium with Mechanical Loading and Vascular Coculture.” *Circulation Research* 109 (1): 47–59. <https://doi.org/10.1161/CIRCRESAHA.110.237206>.

Vagnozzi, Ronald J., Jeffery D. Molkentin, and Steven R. Houser. 2018. “New Myocyte

Formation in the Adult Heart Endogenous Sources and Therapeutic Implications.”

Circulation Research 123 (2): 159–76.

<https://doi.org/10.1161/CIRCRESAHA.118.311208>.

Vagnozzi, Ronald J, Marjorie Maillet, Michelle A Sargent, Hadi Khalil, Anne Katrine, Jennifer A Schwaneckamp, Allen J York, Vincent Huang, Sakthivel Sadayappan, and Jeffery D Molkentin. 2020. “An Acute Immune Response Underlies the Benefit of Cardiac Stem Cell Therapy” *577* (7790): 405–9. <https://doi.org/10.1038/s41586-019-1802-2>.An.

Valiente-Alandi, Iñigo, Sarah J. Potter, Ane M. Salvador, Allison E. Schafer, Tobias Schips, Francisco Carrillo-Salinas, Aaron M. Gibson, et al. 2018. “Inhibiting Fibronectin Attenuates Fibrosis and Improves Cardiac Function in a Model of Heart Failure.” *Circulation* 138 (12): 1236–52. <https://doi.org/10.1161/CIRCULATIONAHA.118.034609>.

Virani, Salim S., Alvaro Alonso, Emelia J. Benjamin, Marcio S. Bittencourt, Clifton W. Callaway, April P. Carson, Alanna M. Chamberlain, et al. 2020. *Heart Disease and Stroke Statistics—2020 Update: A Report from the American Heart Association*. *Circulation*. <https://doi.org/10.1161/CIR.0000000000000757>.

Volz, Katharina S, Andrew H Jacobs, Heidi I Chen, Aruna Poduri, Andrew S McKay, Daniel P Riordan, Natalie Kofler, Jan Kitajewski, Irving Weissman, and Kristy Red-Horse. 2015. “Pericytes Are Progenitors for Coronary Artery Smooth Muscle.” *ELife* 4: 1–22. <https://doi.org/10.7554/elife.10036>.

Vunjak Novakovic, Gordana, Thomas Eschenhagen, and Christine Mummery. 2014. “Myocardial Tissue Engineering: In Vitro Models.” *Cold Spring Harbor Perspectives in Medicine* 4 (3): 1–16. <https://doi.org/10.1101/cshperspect.a014076>.

Wang, Jihu, Jingli Cao, Amy L. Dickson, and Kenneth D. Poss. 2015. “Epicardial Regeneration Is Guided by Cardiac Outflow Tract and Hedgehog Signalling.” *Nature* 522 (7555): 226–30. <https://doi.org/10.1038/nature14325>.

Wang, Jihu, Ravi Karra, Amy L. Dickson, and Kenneth D. Poss. 2013. “Fibronectin Is Deposited by Injury-Activated Epicardial Cells and Is Necessary for Zebrafish Heart Regeneration.” *Developmental Biology* 382 (2): 427–35. <https://doi.org/10.1016/j.ydbio.2013.08.012>.

Wang, Jihu, Daniela Panáková, Kazu Kikuchi, Jennifer E. Holdway, Matthew Gemberling, James S. Burris, Sumeet Pal Singh, et al. 2011. “The Regenerative Capacity of Zebrafish Reverses Cardiac Failure Caused by Genetic Cardiomyocyte Depletion.”

- Development* 138 (16): 3421–30. <https://doi.org/10.1242/dev.068601>.
- Wang, Zhaoning, Miao Cui, Akansha M. Shah, Wei Tan, Ning Liu, Rhonda Bassel-Duby, and Eric N. Olson. 2020. “Cell-Type-Specific Gene Regulatory Networks Underlying Murine Neonatal Heart Regeneration at Single-Cell Resolution.” *Cell Reports* 33 (10): 108472. <https://doi.org/10.1016/j.celrep.2020.108472>.
- Weeke-Klimp, Alida, Noortje A.M. Bax, Anna Rita Bellu, Elizabeth M. Winter, Johannes Vrolijk, Josée Plantinga, Saskia Maas, et al. 2010. “Epicardium-Derived Cells Enhance Proliferation, Cellular Maturation and Alignment of Cardiomyocytes.” *Journal of Molecular and Cellular Cardiology* 49 (4): 606–16. <https://doi.org/10.1016/j.yjmcc.2010.07.007>.
- Wei, Ke, Vahid Serpooshan, Cecilia Hurtado, Marta Diez-Cunado, Mingming Zhao, Sonomi Maruyama, Wenhong Zhu, et al. 2015. “Epicardial FSTL1 Reconstitution Regenerates the Adult Mammalian Heart.” *Nature* 525 (7570): 479–85. <https://doi.org/10.1038/nature15372>.
- Wickström, Sara A., Korana Radovanac, and Reinhard Fässler. 2011. “Genetic Analyses of Integrin Signaling.” *Cold Spring Harbor Perspectives in Biology* 3 (2): 1–22. <https://doi.org/10.1101/cshperspect.a005116>.
- Wijk, Bram van, Quinn D. Gunst, Antoon F.M. Moorman, and Maurice J.B. van den Hoff. 2012. “Cardiac Regeneration from Activated Epicardium.” *PLoS ONE* 7 (9). <https://doi.org/10.1371/journal.pone.0044692>.
- Winnier, G., M. Blessing, P. A. Labosky, and B. L.M. Hogan. 1995. “Bone Morphogenetic Protein-4 Is Required for Mesoderm Formation and Patterning in the Mouse.” *Genes and Development* 9 (17): 2105–16. <https://doi.org/10.1101/gad.9.17.2105>.
- Winter, E. M., R. W. Grauss, B. Hogers, J. Van Tuyn, R. Van Der Geest, H. Lie-Venema, R. Vicente Steijn, et al. 2007. “Preservation of Left Ventricular Function and Attenuation of Remodeling after Transplantation of Human Epicardium-Derived Cells into the Infarcted Mouse Heart.” *Circulation* 116 (8): 917–27. <https://doi.org/10.1161/CIRCULATIONAHA.106.668178>.
- Winter, Elizabeth M., Angelique A.M. Van Oorschot, Bianca Hogers, Linda M. Van Der Graaf, Pieter A. Doevendans, Robert E. Poelmann, Douwe E. Atsma, Adriana C.Gittenberger De Groot, and Marie Jose Goumans. 2009. “A New Direction for Cardiac Regeneration Therapy: Application of Synergistically Acting Epicardium-

- Derived Cells and Cardiomyocyte Progenitor Cells." *Circulation: Heart Failure* 2 (6): 643–53. <https://doi.org/10.1161/CIRCHEARTFAILURE.108.843722>.
- Wollert, K C Meyer G P Lotz J Ringes-Lichtenberg S Lippolt P Breidenbach C Fichtner S Korte T Hornig B Messinger D Lubomir A Hertenstein B Ganser A Drexler H. 2004. "Randomised Controlled Trial of Intracoronary Autologous Bone Marrow Cell Transfer After Myocardial Infarction." *Lancet*, 141–48.
- Woods, Anne, and John R. Couchman. 1998. "Syndecans: Synergistic Activators of Cell Adhesion." *Trends in Cell Biology*. Elsevier Current Trends. [https://doi.org/10.1016/S0962-8924\(98\)01244-6](https://doi.org/10.1016/S0962-8924(98)01244-6).
- Wu, Chi Chung, Fabian Kruse, Mohankrishna Dalvoy Vasudevarao, Jan Philipp Junker, David C. Zebrowski, Kristin Fischer, Emily S. Noël, et al. 2016. "Spatially Resolved Genome-Wide Transcriptional Profiling Identifies BMP Signaling as Essential Regulator of Zebrafish Cardiomyocyte Regeneration." *Developmental Cell* 36 (1): 36–49. <https://doi.org/10.1016/j.devcel.2015.12.010>.
- Wu, Mingfu, Christopher L. Smith, James A. Hall, Ivy Lee, Kate Luby-Phelps, and Michelle D. Tallquist. 2010. "Epicardial Spindle Orientation Controls Cell Entry into the Myocardium." *Developmental Cell* 19 (1): 114–25. <https://doi.org/10.1016/j.devcel.2010.06.011>.
- Wu, San Pin, Xiu Rong Dong, Jenna N. Regan, Chang Su, and Mark W. Majesky. 2013. "Tbx18 Regulates Development of the Epicardium and Coronary Vessels." *Developmental Biology* 383 (2): 307–20. <https://doi.org/10.1016/j.ydbio.2013.08.019>.
- Xiao, Yang, Matthew C. Hill, Min Zhang, Thomas J. Martin, Yuka Morikawa, Suyu Wang, Alexander R. Moise, Joshua D. Wythe, and James F. Martin. 2018. "Hippo Signaling Plays an Essential Role in Cell State Transitions during Cardiac Fibroblast Development." *Developmental Cell* 45 (2): 153-169.e6. <https://doi.org/10.1016/j.devcel.2018.03.019>.
- Xin, Mei, Eric N. Olson, and Rhonda Bassel-Duby. 2013. "Mending Broken Hearts: Cardiac Development as a Basis for Adult Heart Regeneration and Repair." *Nature Reviews Molecular Cell Biology* 14 (8): 529–41. <https://doi.org/10.1038/nrm3619>.
- Xiong, Qiang, Katherine L Hill, Qinglu Li, Piradeep Suntharalingam, Abdul Mansoor, Xiaohong Wang, Mohammad Nurulqadr Jameel, et al. 2011. "TRANSLATIONAL AND CLINICAL RESEARCH A Fibrin Patch-Based Enhanced Delivery of Human Embryonic

Stem Cell-Derived Vascular Cell Transplantation in a Porcine Model of Postinfarction Left Ventricular Remodeling.” *STEM CELLS* 29: 367–75.
<https://doi.org/10.1002/stem.580>.

Yancy, Clyde W., Mariell Jessup, Biykem Bozkurt, Javed Butler, Donald E. Casey, Monica M. Colvin, Mark H. Drazner, et al. 2017. *2017 ACC/AHA/HFSA Focused Update of the 2013 ACCF/AHA Guideline for the Management of Heart Failure: A Report of the American College of Cardiology/American Heart Association Task Force on Clinical Practice Guidelines and the Heart Failure Society of Amer. Circulation*. Vol. 136.
<https://doi.org/10.1161/CIR.0000000000000509>.

Yang, Xiulan, Lil Pabon, and Charles E. Murry. 2014. “Engineering Adolescence: Maturation of Human Pluripotent Stem Cell-Derived Cardiomyocytes.” *Circulation Research* 114 (3): 511–23. <https://doi.org/10.1161/CIRCRESAHA.114.300558>.

Ye, Lei, Ying Hua Chang, Qiang Xiong, Pengyuan Zhang, Liying Zhang, Porur Somasundaram, Mike Lepley, et al. 2014. “Cardiac Repair in a Porcine Model of Acute Myocardial Infarction with Human Induced Pluripotent Stem Cell-Derived Cardiovascular Cells.” *Cell Stem Cell* 15 (6): 750–61.
<https://doi.org/10.1016/j.stem.2014.11.009>.

Yoshida, Yoshinori, and Shinya Yamanaka. 2017. “Induced Pluripotent Stem Cells 10 Years Later.” *Circulation Research* 120 (12): 1958–68.
<https://doi.org/10.1161/CIRCRESAHA.117.311080>.

Young, Jennifer L., and Adam J. Engler. 2011. “Hydrogels with Time-Dependent Material Properties Enhance Cardiomyocyte Differentiation in Vitro.” *Biomaterials* 32 (4): 1002–9. <https://doi.org/10.1016/j.biomaterials.2010.10.020>.

Zannad, Faiez, Pedro Ferreira, Stuart J Pocock, Stefan D Anker, Javed Butler, Gerasimos Filippatos, Martina Brueckmann, et al. 2020. “SGLT2 Inhibitors in Patients with Heart Failure with Reduced Ejection Fraction: A Meta-Analysis of the EMPEROR-Reduced and DAPA-HF Trials.” *The Lancet* 396: 819–29. [https://doi.org/10.1016/S0140-6736\(20\)31824-9](https://doi.org/10.1016/S0140-6736(20)31824-9).

Zaruba, Marc-Michael, Mark Soonpaa, Sean Reuter, and Loren J. Field. 2010. “Cardiomyogenic Potential of C-Kit⁺ –Expressing Cells Derived From Neonatal and Adult Mouse Hearts.” *Circulation* 121 (18): 1992–2000.
<https://doi.org/10.1161/CIRCULATIONAHA.109.909093>.

- Zhang, Boyang, Miles Montgomery, M. Dean Chamberlain, Shinichiro Ogawa, Anastasia Korolj, Aric Pahnke, Laura A. Wells, et al. 2016. "Biodegradable Scaffold with Built-in Vasculature for Organ-on-a-Chip Engineering and Direct Surgical Anastomosis." *Nature Materials* 15 (6): 669–78. <https://doi.org/10.1038/nmat4570>.
- Zhang, Jianyi, Wuqiang Zhu, Milica Radisic, and Gordana Vunjak-Novakovic. 2018. "Can We Engineer a Human Cardiac Patch for Therapy?" *Circulation Research* 123 (2): 244–65. <https://doi.org/10.1161/CIRCRESAHA.118.311213>.
- Zhang, Ming, Danielle Methot, Veronica Poppa, Yasushi Fujio, Kenneth Walsh, and Charles E. Murry. 2001. "Cardiomyocyte Grafting for Cardiac Repair: Graft Cell Death and Anti-Death Strategies." *Journal of Molecular and Cellular Cardiology* 33 (5): 907–21. <https://doi.org/10.1006/jmcc.2001.1367>.
- Zhao, Long, Asya L. Borikova, Raz Ben-Yair, Burcu Guner-Ataman, Calum A. MacRae, Richard T. Lee, C. Geoffrey Burns, and Caroline E. Burns. 2014. "Notch Signaling Regulates Cardiomyocyte Proliferation during Zebrafish Heart Regeneration." *Proceedings of the National Academy of Sciences of the United States of America* 111 (4): 1403–8. <https://doi.org/10.1073/pnas.1311705111>.
- Zhao, Tieqiang, Wenyuan Zhao, Yuanjian Chen, Robert A. Ahokas, and Yao Sun. 2011. "Acidic and Basic Fibroblast Growth Factors Involved in Cardiac Angiogenesis Following Infarction." *International Journal of Cardiology* 152 (3): 307–13. <https://doi.org/10.1016/j.ijcard.2010.07.024>.
- Zhao, Yuanbiao, Pilar Londono, Yingqiong Cao, Emily J Sharpe, Catherine Proenza, Rebecca O'rourke, Kenneth L Jones, et al. 2015. "ARTICLE High-Efficiency Reprogramming of Fibroblasts into Cardiomyocytes Requires Suppression of pro-Fibrotic Signalling." *Nature Communications*. <https://doi.org/10.1038/ncomms9243>.
- Zheng, Dejin, Xiaofang Wang, and Ren He Xu. 2016. "Concise Review: One Stone for Multiple Birds: Generating Universally Compatible Human Embryonic Stem Cells." *Stem Cells*. <https://doi.org/10.1002/stem.2407>.
- Zhou, Bin, Alexander Von Gise, Qing Ma, José Rivera-Feliciano, and William T. Pu. 2008. "Nkx2.5- and Isl1-Expressing Cardiac Progenitors Contribute to Proepicardium." *Biochem Biophys Res Commun* 375: 450–53. <https://doi.org/10.1016/j.bbrc.2008.08.044>.
- Zhou, Bin, Leah B. Honor, Huamei He, Ma Qing, Jin Hee Oh, Catherine Butterfield, Rwei

- Zeng Lin, et al. 2011. "Adult Mouse Epicardium Modulates Myocardial Injury by Secreting Paracrine Factors." *Journal of Clinical Investigation* 121 (5): 1894–1904. <https://doi.org/10.1172/JCI45529>.
- Zhou, Bin, Qing Ma, Satish Rajagopal, Sean M. Wu, Ibrahim Domian, José Rivera-Feliciano, Dawei Jiang, et al. 2008. "Epicardial Progenitors Contribute to the Cardiomyocyte Lineage in the Developing Heart." *Nature* 454 (7200): 109–13. <https://doi.org/10.1038/nature07060>.
- Zhu, Keyang, Qiang Wu, Cheng Ni, Peng Zhang, Zhiwei Zhong, Yan Wu, Yingchao Wang, et al. 2018. "Lack of Remuscularization Following Transplantation of Human Embryonic Stem Cell-Derived Cardiovascular Progenitor Cells in Infarcted Nonhuman Primates." *Circulation Research* 122 (7): 958–69. <https://doi.org/10.1161/CIRCRESAHA.117.311578>.
- Zimmermann, W. H., K. Schneiderbanger, P. Schubert, M. Didié, F. Münzel, J. F. Heubach, S. Kostin, W. L. Neuhuber, and T. Eschenhagen. 2002. "Tissue Engineering of a Differentiated Cardiac Muscle Construct." *Circulation Research* 90 (2): 223–30. <https://doi.org/10.1161/hh0202.103644>.
- Zimmermann, Wolfram Hubertus, Ivan Melnychenko, Gerald Wasmeier, Michael Didié, Hiroshi Naito, Uwe Nixdorff, Andreas Hess, et al. 2006. "Engineered Heart Tissue Grafts Improve Systolic and Diastolic Function in Infarcted Rat Hearts." *Nature Medicine* 12 (4): 452–58. <https://doi.org/10.1038/nm1394>.
- Zogbi, Camila, Ana E.T. Saturi de Carvalho, Juliana S. Nakamuta, Viviane de M. Caceres, Silvana Prando, Maria C.P. Giorgi, Carlos E. Rochitte, Jose C. Meneghetti, and Jose E. Krieger. 2014. "Early Postnatal Rat Ventricle Resection Leads to Long-Term Preserved Cardiac Function despite Tissue Hypoperfusion." *Physiological Reports* 2 (8): 1–11. <https://doi.org/10.14814/phy2.12115>.
- Zvibel, Isabel, Françoise Smets, and Humberto Soriano. 2002. "Anoikis: Roadblock to Cell Transplantation?" *Cell Transplantation*. Vol. 11. www.cognizantcommunication.com.
- Zymek, Pawel, Marcin Bujak, Khaled Chatila, Anna Cieslak, Geeta Thakker, Mark L. Entman, and Nikolaos G. Frangogiannis. 2006. "The Role of Platelet-Derived Growth Factor Signaling in Healing Myocardial Infarcts." *Journal of the American College of Cardiology* 48 (11): 2315–23. <https://doi.org/10.1016/j.jacc.2006.07.060>.